



**HAL**  
open science

# Serum bikunin, a biomarker of inborn errors of proteoglycan biosynthesis and Golgi homeostasis

Walid Haouari

► **To cite this version:**

Walid Haouari. Serum bikunin, a biomarker of inborn errors of proteoglycan biosynthesis and Golgi homeostasis. Biochemistry, Molecular Biology. Université Paris-Saclay, 2021. English. NNT: 2021UPASQ047 . tel-03621944

**HAL Id: tel-03621944**

**<https://theses.hal.science/tel-03621944>**

Submitted on 28 Mar 2022

**HAL** is a multi-disciplinary open access archive for the deposit and dissemination of scientific research documents, whether they are published or not. The documents may come from teaching and research institutions in France or abroad, or from public or private research centers.

L'archive ouverte pluridisciplinaire **HAL**, est destinée au dépôt et à la diffusion de documents scientifiques de niveau recherche, publiés ou non, émanant des établissements d'enseignement et de recherche français ou étrangers, des laboratoires publics ou privés.

# Serum bikunin: a biomarker of inborn errors of proteoglycan biosynthesis and Golgi homeostasis

*La bikunine, un biomarqueur des troubles innés de la synthèse des protéoglycanes et de l'homéostasie de l'appareil de Golgi*

## Thèse de doctorat de l'université Paris-Saclay

École doctorale n° 569 : Innovation thérapeutique : du fondamental à l'appliqué (ITFA)  
Spécialité de doctorat : physiologie, physiopathologie  
Graduate School : Santé et médicaments. Référent : Faculté de pharmacie

Thèse préparée dans l'unité de recherche : **UMR-S 1193 – Physiopathogénèse et traitement des maladies du foie (Université Paris-Saclay, Inserm)**, sous la direction de **Christian POÛS**, professeur des universités et praticien hospitalier, le co-encadrement de **Arnaud BRUNEEL**, maître de conférences et praticien hospitalier.

Thèse soutenue à Paris-Saclay, le 14 décembre 2021, par

**Walid Haouari**

## Composition du Jury

<b>Dulce PAPY-GARCIA</b> Professeure des universités - Université Paris-Est Créteil Val de Marne Directrice de recherche - Gly-CRRET	Présidente
<b>Romain VIVES</b> Directeur de recherche - Institut de biologie structurale (SAGAG-Vivés). Université Grenoble Alpes	Rapporteur & Examinateur
<b>Sylvie FOURNEL-GIGLEUX</b> Directrice de recherche - INSERM UMR7365 CNRS - Université de Lorraine (IMoPA)	Rapporteuse & Examinatrice
<b>Caroline MICHOT</b> Praticienne hospitalière - Hôpital Necker, CRMR maladies osseuses constitutionnelles. Université Paris Descartes	Examinatrice
<b>Christian POÛS</b> Professeur des universités - Université Paris-Saclay Directeur de recherche - INSERM UMR 1193 Praticien hospitalier - Hôpital Antoine Béchère, service de biochimie-hormonologie	Directeur de thèse
<b>Arnaud BRUNEEL</b> Maître de conférences des universités - Université Paris-Saclay Enseignant-chercheur - INSERM UMR 1193 Praticien hospitalier - Hôpital Bichat, service de biochimie métabolique et nutrition	Co-encadrant de thèse

*« Le meilleur travail n'est pas celui qui te coûtera  
le plus, mais celui que tu réussiras le mieux. »*

*Jean-Paul Sartre*





# Remerciements

*Je tiens tout d'abord à remercier mon encadrant, Docteur Arnaud Bruneel. Merci de m'avoir permis de travailler avec vous sur ce beau projet et merci pour votre aide à la rédaction de ce manuscrit. Merci pour toutes nos discussions et réflexions communes qui ont constamment nourri et fait progresser ce travail. Merci pour votre bonne humeur, votre sincérité et votre pédagogie qui ont été une grande source de motivation pour moi. Merci pour tous vos conseils très avisés qui ont fait de moi quelqu'un de meilleur. Ce fût un immense plaisir et j'espère que notre Bikunine sera toujours entre de bonnes mains, elle le sera en tous cas avec vous.*

*Un grand merci à mon directeur de thèse, Professeur Christian Poüs, pour son accueil dans ce laboratoire, merci de m'avoir offert l'opportunité d'y réaliser mon stage de Master 2 puis ma thèse de doctorat. Merci également de m'avoir fait bénéficier de votre grande expérience et vos immenses connaissances.*

*Je remercie Docteur Sylvie Fournel-Gigleux et Docteur Romain Vivès pour avoir accepté d'être membres du jury de ma thèse et d'être les rapporteurs de ce manuscrit. Merci pour votre précieuse analyse de ce travail et votre avis favorable à ma soutenance. Je remercie également Professeur Dulce Papy-Garcia pour avoir évalué positivement l'avancement de mon travail lors du comité de mi-thèse et merci d'avoir accepté de faire partie du jury final en tant qu'examinatrice. Je remercie également Docteur Caroline Michot pour avoir accepté de lire ce manuscrit et d'être membre du jury final en qualité d'examinatrice.*

*Je tiens également à adresser mes remerciements au Professeur Valérie Cormier-Daire qui est à l'origine de ce projet de recherche et qui nous a permis d'analyser les sérums de patients*

*atteints de troubles des protéoglycanes. Merci également au Professeur François Foulquier pour son implication dans ce travail notamment dans les troubles de l'homéostasie golgienne. Je remercie également le Docteur Stéphanie Nicolaj et Guillaume Ruellou pour leur contribution à ce projet notamment dans le cadre des analyses en spectrométrie de masse.*

*Je remercie très chaleureusement tous les enseignants-chercheurs, thésards, post-docs et professeurs du laboratoire : Antoine Pilon, Elise Jacquin, Daniel Perdiz, Béatrice Benoit, Anita Baillet, Najet Charef, Joelle Salameh, Samra Lounis, Dalal Douaihy, Maya Talantikite, Phillippe Billiald et Bruno Baudin. Merci pour votre gentillesse, pour nos discussions et vos réponses à mes questions, je suis vraiment très heureux d'avoir fait partie de cette équipe. Je vous souhaite beaucoup de bonheur et bon courage pour la suite à Saclay !*

*Je remercie très chaleureusement Isabelle Cantaloube et Ameetha Ratier pour leur précieuse aide technique. Merci pour votre gentillesse et votre disponibilité ainsi que tous vos conseils et toutes nos discussions. En fait, merci meufs et désolé 😊. Je remercie également les adjoints techniques du laboratoire Bamba et Sara, merci pour votre gentillesse et votre soutien, je vous souhaite bon courage pour la suite.*

*Je remercie également ma co-thésarde Samra Lounis, merci pour ton aide et ta contribution précieuses à ce travail. Merci pour ta joie de vivre (et pour tous les gâteaux :p ). Tous mes vœux de réussite pour la fin de ta thèse !*

*Merci aux stagiaires qui ont contribué à ce travail, Alexandre Raynor et Sahra, Muhamad, merci pour votre implication et votre bonne humeur. Bon courage pour la suite !*

*Je tiens à remercier Docteur Béatrice Benoit pour avoir accepté d'être le garant technique pour l'organisation de la visioconférence de ma soutenance de thèse.*

*Merci à mes parents qui, malgré l'éloignement, m'ont soutenu et pensé à moi tous les jours. Je vous remercie de m'avoir donné la chance de faire ces études de pharmacie. Merci pour tout votre amour. Merci à mes petits frères Anis et Samy et ma petite sœur Célia ... d'exister, je vous aime très fort et j'espère que vous allez réussir (comme moi !) dans vos études et vos vies.*

*Merci à mon épouse Margot. Merci pour ton soutien sans faille pendant ma thèse et pour tes corrections de mes fautes d'orthographe. Merci pour ton amour, je t'aime BBD 'Am. Merci à ma belle-famille Thierry, Pascale, Julia et Mamie-Miche pour tous les moments passés ensemble et les vacances, merci pour vos encouragements pendant la rédaction de ce manuscrit.*

*Merci à tous mes amis Amine, Djamil, Nadir, Lotfi, Nazim, Oussama, Mehdi, Camille, Vincent, Elo, Adrien, Cécile et Mona. Merci pour votre amitié sincère et votre soutien pendant ma thèse.*



# Table of contents

List of abbreviations.....	11
List of figures .....	15
General Introduction .....	17
Chapter 1: Proteoglycans .....	23
I.1. Introduction .....	25
I.2. Biosynthesis of proteoglycans .....	26
I.2.1. Formation of the tetrasaccharide linkage region .....	26
I.2.2. Elongation and modifications of the GAG chains.....	27
I.2.3 Substrate synthesis and supply for proteoglycan biosynthesis.....	30
I.2.4 Transport and sorting of the proteoglycans .....	33
I.2.5 Degradation of proteoglycans.....	34
I.2.6 Importance of the Golgi homeostasis for proteoglycan biosynthesis.....	34
I.2.7 Classification, distribution, and roles of proteoglycans.....	37
Table 1. Overview of some proteoglycans and their pathophysiological involvements.....	38
I-3 Proteoglycan inherited metabolic diseases (PG-IMD).....	41
Table 2. Proteoglycan inherited metabolic diseases: Classification and clinical aspects .....	42
I.3.1 Linkeropathies .....	47
I.3.2 GAG elongation defects .....	48
I.3.3 GAG sulfation defects .....	50

I.3.4 Defects in sugar transporters .....	52
I.3.5 Proteoglycan defects linked to impaired Golgi homeostasis.....	53
I-3-6 Mucopolysaccharidoses .....	55
I-4 Screening of proteoglycan inherited metabolic diseases.....	56
I-4-1 Current laboratory tools and examples of applications.....	56
I-4-2 Potential diagnostic value of serum bikunin.....	60
Chapter 2: Bikunin proteoglycan isoforms .....	61
II.1 Introduction .....	63
II.2. Bikunin proteoglycans: Genes, expression, and regulation .....	63
II.2.1. AMBP gene .....	63
II.2.2. ITIH1, ITIH2 and ITIH3 genes .....	64
II.3. Synthesis, structure, and post-translational modifications of bikunin core protein .....	66
II.3.1. From AMBP precursor to inter- $\alpha$ -trypsin inhibitor.....	66
II.3.2. Polypeptide structure and modifications of bikunin core protein .....	67
II.4. Bikunin CS chain elongation and modifications.....	69
II.4.1. Synthesis of the linkage region and CS elongation.....	69
II.4.2. Modifications of the bikunin-linked CS chain .....	70
II.5. The Heavy Chains proteins (HCs) .....	71
II.5.1. Biosynthesis and post-translational modifications of the HCs.....	71
II.5.2. Linkage of the HCs to the AMBP precursor via the CS chain.....	72
II-6- Roles of bikunin isoforms.....	76

Chapter 3: Bikunin analyses in PG-IMD and CDG with impaired Golgi homeostasis .....	79
III-1 Introduction .....	81
III-2 Publication 1 : Letter to the Editor - Serum bikunin is a biomarker of linkeropathies .....	83
III-2-1 Summary of the letter to the Editor .....	85
III-2-2 Concluding remarks and perspectives .....	91
III-3 Publication 2: Original article - Serum bikunin isoforms in congenital disorders of glycosylation and linkeropathies .....	93
III-3-1 Article presentation .....	95
III-3-2 Complementary results (unpublished).....	117
III-3-2-1 Complementary Western blot and 2-DE analyses .....	117
III-3-2-2 Mass spectrometry analysis of linkeropathy-associated Bkn abnormal forms .....	120
III-3-2-3 Bkn analyses in sulfation defects .....	127
III-3-2-4 Application of Bkn analysis to dried blood spots (DBS).....	129
III-4 Publication 3: Original article - SLC37A4-CDG: New biochemical insights for an emerging congenital disorder of glycosylation with major coagulopathy .....	131
III-4-1 Article presentation .....	133
III-5 Publication 4 : Revue - Inherited Proteoglycan Biosynthesis Defects - Current Laboratory Tools and Bikunin as a Promising Blood Biomarker.....	139
III-5-1 Presentation of the review .....	141
III-6 Bikunin analyses in HepG2 cells with Golgi homeostasis defects.....	161

III-6-1 Effects of Bafilomycin A1-mediated Golgi pH defects on bikunin profile ..	163
III-6-2 Bikunin analysis in manganese homeostasis defects .....	172
General conclusion .....	175
Bibliography .....	181
Material & Methods .....	231
Mass spectrometry analyses.....	233
Gel collection procedure .....	233
Protein In-Gel Digestion .....	233
Liquid Chromatography - Tandem Mass Spectrometry (LC-MS/MS).....	234
Mass spectrum and data processing parameters .....	235
2-DE analysis of chondroitinase treated serum samples.....	235
Hemoglobin depletion from dried blood spots for Bkn analysis (Manufacturer protocol).....	236
Bkn analyses in HepG2.....	237
Cell culture and treatments .....	237
Western blot analysis .....	237
Immunofluorescence.....	238
<i>Résumé en français</i> .....	239



## List of abbreviations

2-DE: two-dimensional electrophoresis

aa: amino acid

A1MG:  $\alpha$ 1-microglobulin

AMBIP:  $\alpha$ 1-microglobulin-bikunin-precursor

$\beta$ 3Gal-T6:  $\beta$ -3 galactosyltransferase 6

$\beta$ 4Gal-T7:  $\beta$ -4 galactosyltransferase 7

Baf A1: bafilomycin A1

BFA: brefeldin A

Bkn: bikunin

C4ST: chondroitin-4-sulfotransferase

C6ST-1: chondroitin-4-sulfotransferase

CANT1: calcium activated nucleotidase 1

CHST: chondroitin sulfotransferase

CDG: congenital disorder(s) of glycosylation

chABC: chondroitinase ABC

ChPF: chondroitin polymerizing factor

ChSy: chondroitin synthase

COG: conserved oligomeric Golgi

COP: coated protein complex

CS: chondroitin sulfate

CSGalNAcT: chondroitin sulfate GalNAc transferase

D4ST: dermatan-4-sulfotransferase

DBS: dried blood spot

DS: dermatan Sulfate

DSE: dermatan sulfate epimerase

ECM: extracellular matrix

EDS: Ehlers-Danlos syndrome

ER: endoplasmic reticulum

ERGIC: endoplasmic reticulum Golgi intermediate compartment

EXT: exostosin

EXTL: exostosin-like

FAM20B: family with sequence similarity member 20B

GAG: glycosaminoglycan

Gal: galactose

Gal6ST: galactose-6-sulfotransferase

GalNAc: *N*-acetyl galactosamine

GalNAcT: *N*-acetyl galactosamine transferase

GlcA: glucuronic Acid

GlcAT-I:  $\beta$ -3 glucuronyltransferase 1

GlcNAc: *N*-acetylglucosamine

GlcNAc6ST: *N*-acetylglucosamine-6-Sulfotransferase

GlcNAcT: *N*-acetylglucosamine transferase

GlcNS: sulfoglucosamine

GORAB: Rab-6 interacting protein

HA: hyaluronan

HC: heavy chain

HMES: hereditary multiple exostosis syndrome

HPLC: high-performance liquid chromatography

HS: heparan Sulfate

IAIP: inter- $\alpha$ -trypsin inhibitor proteins

IdoA: iduronic Acid

IMPAD1: inositol monophosphatase domain-containing-1

ITI: inter- $\alpha$ -trypsin inhibitor

KS: keratan sulfate

NDST: *N*-deacetylase/*N*-sulfotransferase

NST: nucleotide-sugar transporter

PAP: phospho-adenosine phosphate

PAPS: phosphoadenosine phosphosulfate

PAPST: phosphoadenosine phosphosulfate transferase

PG: proteoglycan

PG-IMD: proteoglycan inherited metabolic diseases

PGP: protein-glycosaminoglycan-protein

P $\alpha$ I: pro- $\alpha$ -trypsin inhibitor

SHAP-HA: serum-derived hyaluronan-associated proteins-HA complex

SLC35: solute carrier 35 family

TGN: *trans*-Golgi Network

TMEM165: transmembrane protein 165

U2ST: uronic acid-2-Sulfotransferase

UTI: urinary-trypsin inhibitor

UDP/UMP: uridine di/monophosphate

Xyl: xylose

XYLP: xylose phosphatase

XylIT-1/2: xylosyltransferase-1/2



## List of figures

Figure 1: Protein glycosylation types .....	20
Figure 2: Glycosaminoglycan chain types and corresponding disaccharides .....	25
Figure 3: Biosynthesis and modifications of the tetrasaccharide linkage region .....	27
Figure 4: Biosynthesis and modifications of proteoglycans .....	30
Figure 5: Substrate supply for proteoglycan biosynthesis .....	32
Figure 6: Molecular actors involved in Golgi homeostasis .....	36
Figure 7: Schematic of current PG-IMD diagnosis strategy .....	58
Figure 8: Schematic of AMBP gene and its 5' promoter region containing HNF, IL-6 and TNF binding sites .....	64
Figure 9: Schematic of an ITIH gene and its 5' promoter regions containing HNF and IL-6 binding sites .....	65
Figure 10: Biosynthesis of inter- $\alpha$ -trypsin inhibitor (ITI) from the AMBP gene to the mature proteoglycan .....	67
Figure 11: Bikunin core protein structure and modifications .....	69
Figure 12: Schematic structure of heavy chain precursor Pro HC and N-terminal cleavage .....	71
Figure 13: Heavy chain proteins glycosylation pattern .....	72
Figure 14: Structure of the Asp-GalNAc link between heavy chains and the chondroitin sulfate chain of bikunin. From Fries et al. 2003 (316) .....	72
Figure 15: HC biosynthesis and coupling with the CS chain of bikunin .....	74
Figure 16: Schematic structure of bikunin isoforms .....	75
Figure 17: Schematic overview of bikunin isoforms roles during inflammation .....	77
Figure 18: Western blot analysis of heavy and light Bkn forms in CDG with proton pump deficiencies (2 ATP6V1F-CDG and one ATP6AP1-CDG) .....	118
Figure 19: Complemental analyses of Bkn light forms in TMEM165-CDG and ChSy-1 deficiency .....	119

Figure 20: 2-DE based purification of Bkn-hexasaccharide from chABC treated control serum	122
Figure 21: HPLC/MS analysis of 2-DE purified hexasaccharide-Bkn from chABC treated serum	124
Figure 22: 2-DE based purification of B4GALT7-associated abnormal Bkn light forms	124
Figure 23: HPLC/MS analysis of 2-DE purified B4GALT7 deficient patient serum	127
Figure 24: Western blot and 2-DE of serum Bkn light forms in SLC35B2 and IMPAD1 deficient patients	128
Figure 25: Hemoglobin depletion of blood extracts from DBS followed by Western blot analysis of Bkn isoforms	130
Figure 26: Heterozygous c.1267C>T mutation causes half mislocalization of the ER SLC37A4 glucose-6-phosphate transporter to other cellular compartments	134
Figure 27: Western blot profile of secreted Bkn isoforms from HepG2 cells	164
Figure 28: Immunofluorescence analysis of LysoTracker in control and Baf A1-treated HepG2	165
Figure 29: Assessment of BFA-induced Golgi-to-ER retrograde trafficking in control and Baf A1-treated HepG2	166
Figure 30: Western blot analysis of transferrin and orosomucoid in Baf A1-treated HepG2	167
Figure 31: Western blot profile of Bkn in supernatant and lysate of Baf A1-treated HepG2	169
Figure 32: Immunofluorescence analysis of Bkn in Baf A1-treated HepG2	171
Figure 33: High Mn <sup>2+</sup> concentrations in cell culture medium result in TMEM165 degradation in HEK293 cells (Figure from Potelle et al. 2017) (342)	172
Figure 34: Western blot analysis of Bkn in MnCl <sub>2</sub> -treated HepG2 compared to TMEM165 deficient patient	174
Figure 35: Bikunin, a biological Swiss Army knife	180

# General Introduction





Glycosylation is a cellular multistep process consisting of sequential enzymatic transfer of various monosaccharides to proteins, lipids, and as recently reported, to small noncoding RNA molecules (1,2). For proteins, glycosylation is a post-translational modification corresponding to the branching of polysaccharidic chains known as “glycans” on specific amino acids (aa). These glycosidic structures contribute to maturation, folding, functionalization and addressing of proteins. Schematically, there are two major types of protein glycosylation that can be distinguished according to the nature of the glycan-protein binding (**Figure 1**). In *N*-linked glycosylation, an initial *N*-acetyl-glucosamine (GlcNAc) monosaccharide binds an asparagine (Asn) of the protein while *O*-glycosylation includes various initiating monosaccharides including *N*-acetyl-galactosamine (GalNAc), xylose (Xyl), mannose (Man) and fucose linked to the hydroxyl group of a serine (Ser) or a threonine (Thr).

In this Ph.D. thesis work, we mostly focused on Xyl-type *O*-glycosylation which primes the elongation of glycosaminoglycan (GAG) chains on certain proteins thereby forming the so-called proteoglycans (PG) (**Figure 1**). In humans, PG are present in extracellular matrices (ECM) of virtually all organs and tissues where they play important physiological roles. They confer lubricant properties of synovial fluid in joints, they provide elasticity to skin and they regulate immunity and cell proliferation (3).

Glycosylation takes place in the endoplasmic reticulum (ER) and the Golgi apparatus. In these cellular organelles formed by a dynamic set of membranes and vesicles, a complex network of glycosyltransferases, nucleotide-phosphate monosaccharide transporters, as well as key proteins regulating the ionic environment and the vesicular trafficking (i.e., ER/Golgi homeostasis) orchestrate glycosylation reactions. In humans, inherited gene deficiencies affecting this process result in impaired protein glycosylation and are known as congenital disorders of glycosylation or CDG. These rare and mainly autosomal recessive diseases can

manifest by a plethora of clinical phenotypes including asymptomatic forms, mild, severe, or lethal diseases (4).

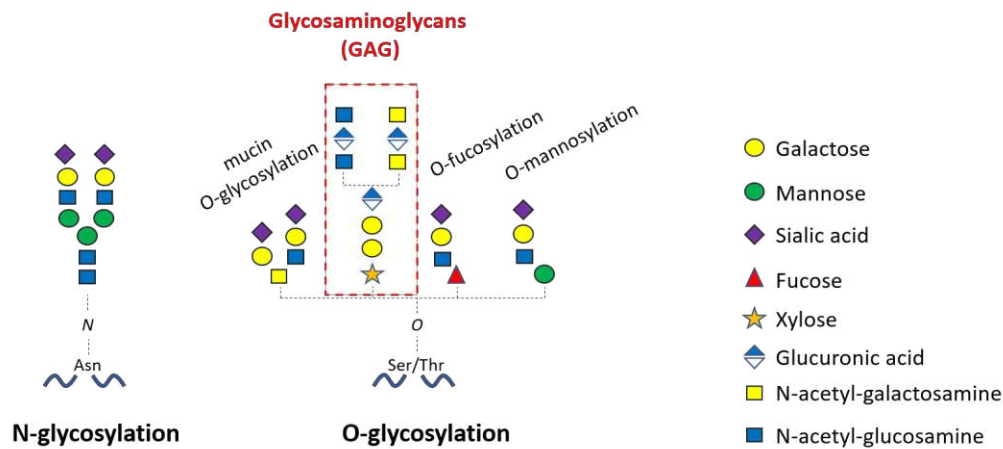


**Figure 1: Protein glycosylation types**

*N*-glycans consists of biantennary structures GlcNAc-*N*-linked to Asn and terminated by sialic acids. Four *O*-glycosylation subtypes exist with variable initiating linkage and sugar combination. Xyl-*O*-linked GAG are highlighted since they constitute the main thread of our work.

The genesis of the work presented herein arises from our collaboration with clinicians of Necker hospital (Paris - France) who manage patients with inborn diseases due to defective PG biosynthesis. The so-called PG inherited metabolic diseases (PG-IMD) are due to mutations in genes coding proteins directly involved in GAG elongation such as glycosyltransferases and nucleotide-phosphate monosaccharide transporters, or proteins regulating the Golgi homeostasis such as ionic transporters and vesicular tethering factors. PG-IMD are incurable diseases and life-threatening for affected individuals and their families. Clinical manifestations include severe osteoarticular abnormalities associated to multiorgan deficiencies such as neurological disorders, cardiac defects, and cutaneous abnormalities. Clinicians and biologists often struggle to easily identify the pathogenic gene deficiency because of unspecific symptomatology, hardly accessible biological tests, and lack of convenient biomarkers. In this context, we focused on developing the analysis of a PG present in the blood at high concentration, that could serve as a new biomarker for the screening and diagnosis of PG-IMD.

This PG is called Bikunin (Bkn) and the analyses we developed were mainly based on its immunodetection [i.e., Western blot and two-dimensional electrophoresis (2-DE)] from blood samples (serum/plasma/dried blood spot) of affected individuals. We mostly showed that Bkn profiles can efficiently orient towards some PG-IMD-causative gene deficiencies thereby significantly facilitating the diagnosis of these diseases.

Additionally, we found that Bkn isoforms biosynthesis was impaired in some patients with CDG due to genetic deficiencies affecting the Golgi homeostasis and characterized by *N*- and mucin-type *O*-glycosylation defects. As the diagnosis of these diseases already benefits from established screening techniques, we showed that Bkn isoforms profile could be an interesting additional biomarker highlighting further insights into their pathophysiology.

Lastly, we used a model of HepG2 cell lines with chemically-induced Golgi homeostasis impairments (i.e., ionic and vesicular trafficking disturbances) and we showed alterations of Bkn biosynthesis. This indicated interesting potentials of Bkn as an *in vitro* marker of Golgi homeostasis defects.

My work resulted in the publication of one letter (4<sup>th</sup> author), two articles (first author) and one review (first author) which are presented in this manuscript. Moreover, other still-unpublished results including Bkn analyses in samples from various affected individuals and in HepG2 cells are described. Altogether, our data show that Bkn is a promising biomarker that can facilitate the screening and diagnosis of genetic deficiencies leading to PG-IMD and of glycosylation disorders due to impaired Golgi homeostasis.



# Chapter 1: Proteoglycans



## I.1. Introduction

Proteoglycans (PGs) are macromolecules composed of a core protein linked to one or more highly sulfated glycosaminoglycan (GAG) chains such as chondroitin sulfate (CS), dermatan sulfate (DS), heparan sulfate (HS), heparin or keratan sulfate (KS) (**Figure 2**). The PG biosynthesis occurs in many cell types into the ER and the Golgi apparatus and involves the interplay between numerous molecular actors along the secretory pathway. Except for KS PGs, the GAG chain elongation is initiated by the formation of a tetrasaccharide linkage region consisting in glucuronic acid-galactose-galactose-xylose (GlcA-Gal-Gal-Xyl) linked to a serine (Ser) residue of the core protein. The following GAG synthesis is carried out by the enzymatic addition of  $n$ -repeated disaccharide motifs consisting of (GlcA-GalNAc) for CS, (GlcA-GlcNAc) for HS and (GlcNAc-Gal) for KS. Furthermore, many modifications occur on the tetrasaccharide linker and the GAG chain such as sulfation, phosphorylation, or epimerization, the latter giving rise to DS (IdoA-GalNAc) $_n$  and heparin (IdoA-GlcN) $_n$  (**Figure 2**) (5).

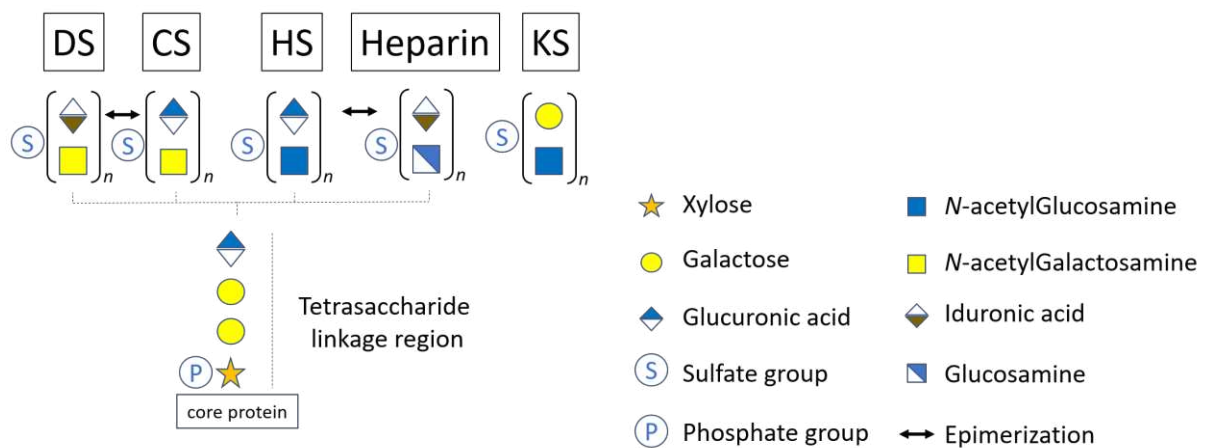


**Figure 2: Glycosaminoglycan chain types and corresponding disaccharides**

Once synthesized, PGs are addressed to intracellular granules, plasma membrane, extracellular matrices or blood circulation and are involved in many biological processes (6). Their negative charges conferred by sulfate groups provide hydrophilic and viscoelastic properties to the extracellular matrices (ECMs). Moreover, *via* numerous interactions with other

ECM components (e.g., hyaluronan and collagen), PGs play important roles in the ECM assembly and participate to the architecture of bones, joints, tendons, skin, and cartilage. PGs can also act as signaling molecules interacting with chemokines, cytokines, and growth factors for the regulation of immune response, skeletal development or cell proliferation/adhesion in wound healing and cancer (6,7).

PG-inherited metabolic diseases (PG-IMD) result from mutations in genes involved in the biosynthesis, modifications, transport, and degradation of PGs or involved in the regulation of Golgi homeostasis. Given the major physiological roles of PGs, their alteration can result in multiple and severe damages. Thus, PG-IMD are characterized by multiorgan alterations including marked osteoarticular malformations, neurological troubles, cardiac defects, cutaneous diseases, tooth abnormalities and deafness (8–10).

## **I.2. Biosynthesis of proteoglycans**

### **I.2.1. Formation of the tetrasaccharide linkage region**

The aa sequence of the core protein has a critical influence on the initiation of the PG biosynthesis. Indeed, the GAG elongation takes place on a Ser preceded by acidic aa and followed by glycine (Gly) or alanine (Ala) residues (11–14). The GAG chain is initiated by a Ser-*O*-xylosylation catalyzed by a xylosyltransferase (XylIT-1 or XylIT-2) (15). This reaction starts in the exit sites of the ER or in ER/Golgi intermediate compartments (ERGIC) and is achieved in the *cis*-Golgi (16,17). The two following reactions, also occurring in the *cis*-Golgi, correspond to the sequential addition of two Gal residues by the galactosyltransferases  $\beta$ 4GalT7 and  $\beta$ 3GalT6, respectively (18,19). Afterwards, a GlcA is added by the glucuronyltransferase GlcAT-I in the *medial*-Golgi (20). The resulting (GlcA-Gal-Gal-Xyl-*O*-Ser) tetrasaccharide linker is common to CS, DS and HS GAG chains (**Figure 3**). In KS PGs, three kinds of linkage regions exist leading to three KS types. The core protein is linked to a GlcNAc in KS-I, a Gal



in KS-II and a mannose in KS-III (21).

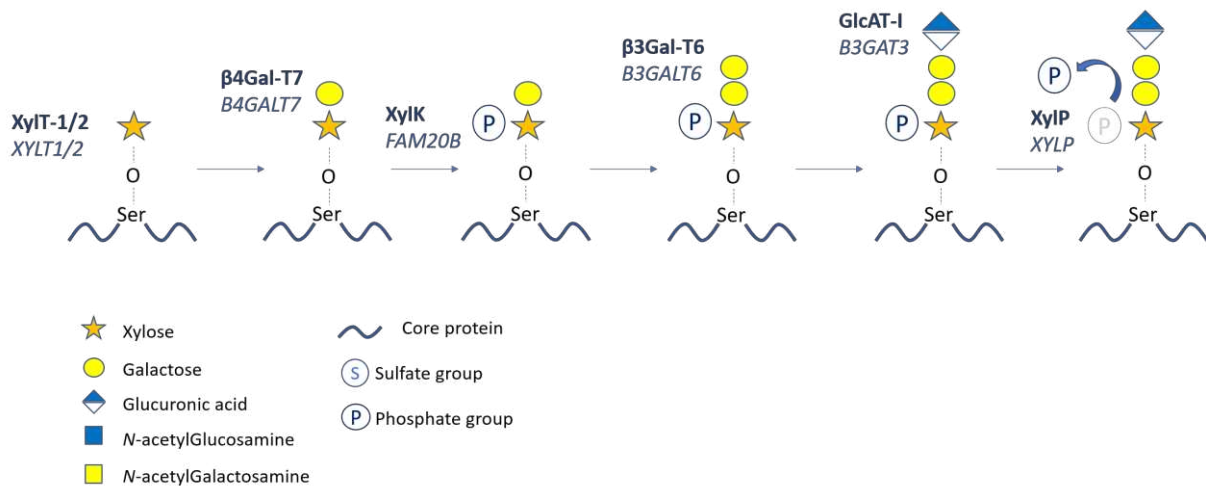


**Figure 3: Biosynthesis and modifications of the tetrasaccharide linkage region**

The successive steps of the initiating tetrasaccharide biosynthesis and modifications are represented with the corresponding enzymes and their encoding genes. A transient phosphorylation of the xylose is thought to occur after the first Gal addition and is removed before the first aminosugar transfer. Enzyme abbreviations: XylT: Xylosyltransferase;  $\beta$ 4GAL-T7:  $\beta$ -4-galactosyltransferase7; XylK: Xylose kinase; FAM20B: Family with sequence similarity 20B;  $\beta$ 3GAL-T6:  $\beta$ -3-galactosyltransferase6; GlcAT-I: Glucuronosyltransferase I; XYLP: xylose phosphatase.

During the linker formation (**Figure 3**), the Xyl residue is 2-*O* phosphorylated by the “Family sequence similarity 20B” kinase (FAM20B also named XylK) probably after the addition of the first Gal (22). It has been shown that Xyl phosphorylation enhances substrate recognition by  $\beta$ 3Gal-T6 and GlcAT-I for the addition of the second Gal and the following GlcA, respectively (23,24). This Xyl phosphorylation is transient since the addition of the first amino sugar (i.e., GalNAc for CS or GlcNAc for HS) of the GAG chain is accompanied by the removal of the phosphate by XylP phosphatase (25,26). Additionally, a sulfation catalyzed by chondroitin-6-*O* sulfotransferase (C6ST1) could occur on both Gal residues of the linkage region in CSPGs and DSPGs but not in HSPGs and has regulatory roles (27–29). It has been shown that sulfation of the first Gal significantly enhances GlcAT-I activity (24).

### I.2.2. Elongation and modifications of the GAG chains

The orientation of the GAG elongation towards HS or CS chain is determined by the aa

sequence of the core protein. Neighboring the Ser/Thr which links the initiating xylose, the presence of repetitive Ser-Gly motifs together with acidic aa and Trp residues promote HS elongation. For CS elongation, the presence of Ser-Gly motifs preceded by acidic aa is also required (5,14,30,31). Sulfation of the linkage region may also orient the GAG elongation. Indeed, the observed systematic absence of sulfate in HS linkage region could suggest that this modification may be a signal for CS/DS GAG biosynthesis (27). In addition, the activity of the *N*-acetylgalactosaminyltransferase-1 (GalNAcT-1), which adds the first GalNAc of the CS/DS chain, is significantly increased when the first or second Gal is sulfated in comparison to unsulfated counterparts (32).

After the formation of the tetrasaccharide linker, the GAG elongation begins with the addition of the first amino sugar (i.e., GalNAc for CS/DS or GlcNAc for HS/heparin) (**Figure 3 and Figure 4**). Thereafter, the elongation involves successive enzymatic additions of *n*-repeated disaccharides motifs. For CSPGs, the *N*-acetylgalactosaminyl-transferases CSGalNAcT-1 or CSGalNAcT-2 transfer a GalNAc to the terminal GlcA of the linkage region (33). The following polymerization of the [GlcA-GalNAc]<sub>*n*</sub> backbone is ensured by a CS synthase complex (ChSy) composed of six enzymes namely ChSy-1, ChSy-2, ChSy-3, Chondroitin polymerizing factor (ChPF), CSGalNAcT-1 and CSGalNAcT-2 (34–37) (**Figure 4**) (For review see (38)). It is unclear whether the biosynthesis of CS chains requires all these enzymes or the combination of some of them, but it has been demonstrated that in vitro CS polymerization is achieved when any two of ChSy-1, 2, 3 or ChPF were incubated with the acceptor substrate  $\alpha$ -thrombomodulin (37).

The HS elongation begins with a GlcNAc transfer to the linkage region, a reaction being catalyzed either by EXTL2 or EXTL3, two members of the exostosin family. The following [GlcA-GlcNAc]<sub>*n*</sub> polymerization is ensured by EXTL1, having a GlcNAcT activity, and a heterodimeric complex formed by EXT1 and EXT2, having both GlcAT and GlcNAcT

activities (39–41) (**Figure 4**) [For review see (42)].

Regarding the 3 KS GAG-type chains, they consist of a sulfated [GlcNAc–Gal]<sub>n</sub> (polylactosamine) backbone synthesized by various enzymes (43–45).

Numerous modifications including sulfation and epimerization occur on the disaccharide motifs of the GAG chains (**Figure 4**). For CS chains, chondroitin-4 sulfotransferases (C4ST)-1,2 and 3 as well as C6ST-1 and 2 mediate the sulfation of various GalNAc residues (46–49). GlcA residues could also be sulfated by uronic acid-2-sulfotransferase (U2ST) (50). Furthermore, varying proportions of GlcA residues of the CS chains could be converted to IdoA by the DS-epimerases (DSE)-1 and -2 to form DS chains (51,52). Sulfations occur on both GalNAc and IdoA residues via D4ST1 (CHST14) and U2ST, respectively (50,53) (**Figure 4**).

For HSPGs, series of modifications occur within various sections of 3-6 adjacent disaccharides forming the so-called “S-domains”. In these domains, GlcNAc residues undergo N-deacetylation and subsequent N-sulfations leading to the formation of sulfoglucosamine (GlcNS) units. This reaction is catalyzed by bifunctional enzymes named GlcNAc N-deacetylase/N-sulfotransferases (NDSTs) (54,55). Moreover, GlcA residues adjacent to GlcNS are converted to IdoA, a reaction catalyzed by C5 epimerase (56). Various sulfation reactions occur on HS GAG chains: (i) the single isoform 2-OST catalyzes the transfer of sulfate groups upon IdoA and GlcA residues to form IdoA2S and GlcA2S (57), (ii) GlcNAc and GlcNS residues are 6-O sulfated by 6-OST which is represented by three isoforms (58), and (iii) seven isoforms of 3-OST catalyze the 3-O sulfation of GlcN units (59). Heparin GAG chains are extensively modified and contain 50-90 % of S-domains. In contrast, HS are less modified and have 30-55 % of S-domains (56).

For KSPGs, sulfations can occur on both GalNAc and Gal residues and are catalyzed by Gal6ST (CHST1) and GlcNAc6ST (CHST5 and/or CHST6) (60,61) (**Figure4**).

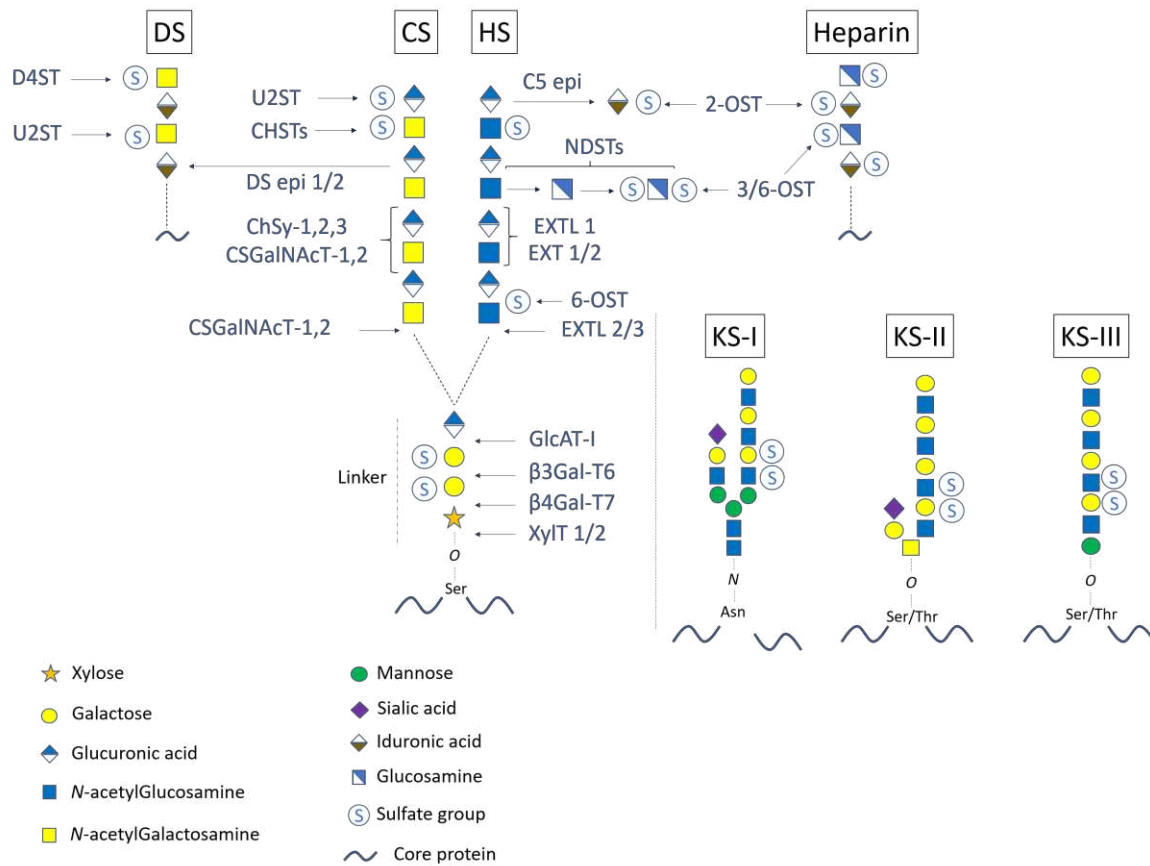


**Figure 4: Biosynthesis and modifications of proteoglycans**

Upon the core protein-linked tetrasaccharide linkage region (i.e., GlcA-Gal-Gal-Xyl), the GAG chain polymerization starts with the transfer of a first amino sugar (i.e., GalNAc for CS and GlcNAc for HS) and continues with the addition of repetitive [GlcA-GalNAc] for CS and [GlcA-GlcNAc] for HS. Epimerization from CS to DS (i.e., [IdoA-GalNAc] backbone) could occur. The GAG chains are also modified by sulfate groups. HS and heparin GAG chains undergo series of modifications including N-deacetylation and subsequent N-sulfation as well as various sulfation types and GlcA to IdoA epimerization. Each pathway involves specific glycosyltransferases, sulfotransferases, and epimerases. For KS GAG chain elongation, there is three types of initiations leading to KS-I, KS-II and KS-III GAG chains which are composed of a polylactosamine backbone [GlcNAc-Gal]. Enzyme abbreviations: XylT: Xylosyltransferase;  $\beta$ 4Gal-T7:  $\beta$ -4-galactosyltransferase7;  $\beta$ 3Gal-T6:  $\beta$ -3-galactosyltransferase6; GlcAT-I:  $\beta$ -3-glucuronyltransferase3; CSGalNAcT: N-acetylgalactosaminyltransferase; ChSy: chondroitin synthase complex; CHST: chondroitin sulfotransferase; DS epi: dermatan sulfate epimerase; U2ST: uronic acid-2-sulfotransferase; D4ST: dermatan-4-sulfotransferase; EXT: exostosin family protein; EXTL: exostosin-like; NDST: N-deacetylase/N-sulfotransferase; OST: heparan O-sulfotransferase; C5 epi: GlcNAc C5 epimerase.

### 1.2.3 Substrate synthesis and supply for proteoglycan biosynthesis

The donor substrates used by the glycosyltransferases during the GAG elongation correspond to “activated” uridine-diphosphate (UDP)-sugars. Their synthesis occur in the cytosol and involves numerous metabolic pathways leading first to the formation of sugar-1-

phosphate (e.g., Gal-1-P, GalNAc-1-P) and a process frequently called “activation” catalyzed by specific UDP-sugar pyrophosphorylases (USPase) that transfer the uridine group of uridine-triphosphate (UTP) to sugar-1-phosphate thus producing UDP-sugar and inorganic pyrophosphate (PPi) (62–64) (**Figure 5**). UDP-sugars are then translocated to the lumen of the Golgi through transmembrane nucleotide-sugar transporters (NSTs). At least 31 NSTs belonging to the solute carrier 35 family (SLC35) have been described (65,66). Glycosylation reactions release free UDP molecules, which are further converted by nucleotidases such as calcium activated nucleotidase-1 (CANT1) to uridine-monophosphate (UMP) (67–69), the latter being exported to the cytosol by NSTs to the benefit of new UDP-sugar molecules (**Figure 5**).

For sulfation reactions, sulfotransferases use the sulfate donor 3'-phosphoadenosine 5'-phosphosulfate (PAPS). The biosynthesis of PAPS occurs in the cytosol and is mediated by PAPS synthases (PAPSS 1 and 2) that catalyze the transfer of phospho-adenosine-phosphate (PAP) to inorganic sulfate ( $\text{SO}_4^{2-}$ ) (70). The activated PAPS molecules are then translocated into the Golgi lumen. Two PAPS transporters have been identified and named SLC35B2 and SLC35B3 (71,72). GAG sulfation reactions release free PAP that is hydrolyzed by inositol-monophosphatase-1 (IMPAD1) into adenosine-monophosphate (AMP) and inorganic phosphate (Pi) (73) (**Figure 5**).

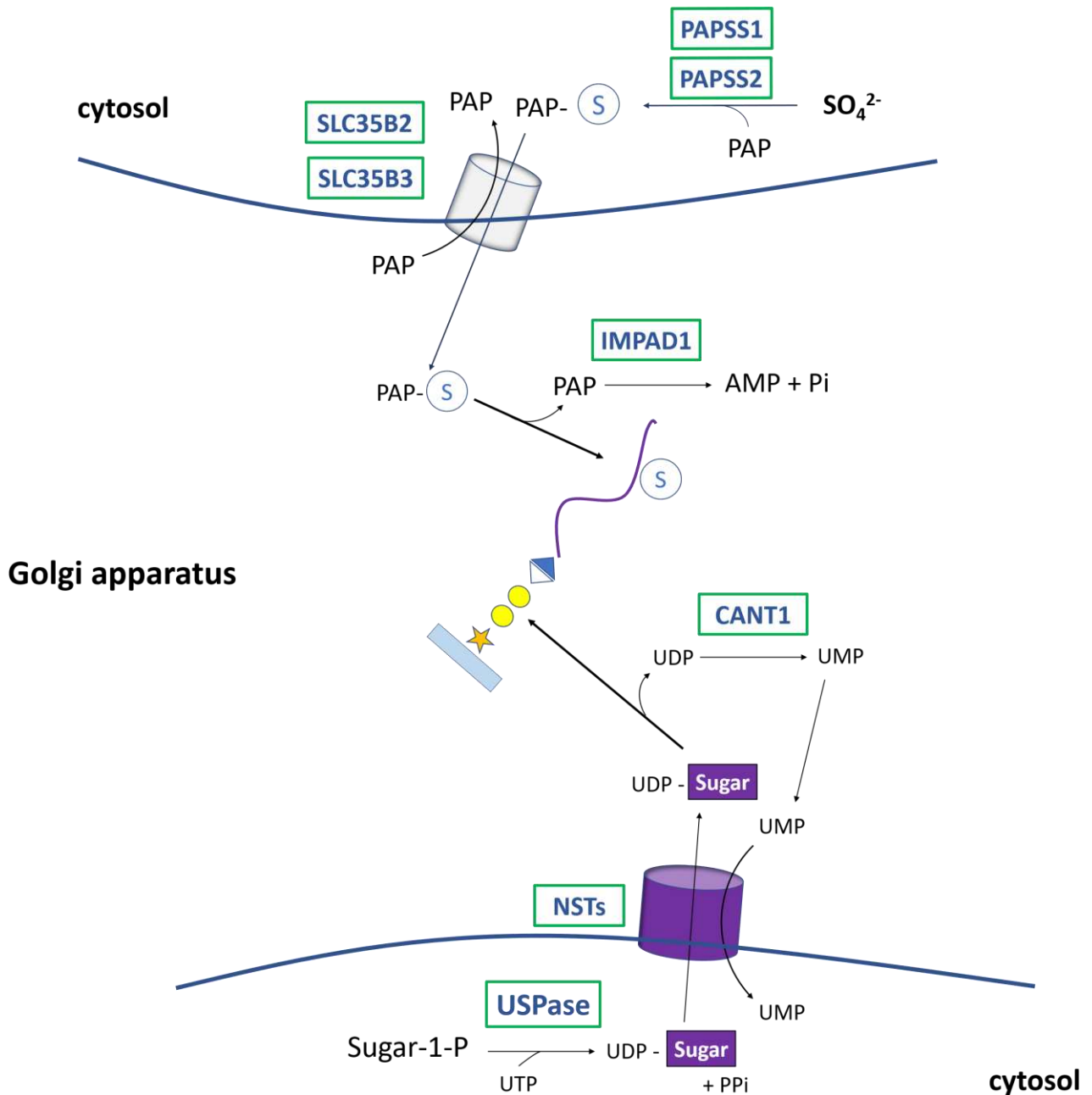


### Figure 5: Substrate supply for proteoglycan biosynthesis

UDP-sugars are synthesized by USPases from phosphosugars and UTP in the cytosol and are imported in the Golgi apparatus through specific NSTs. Glycosylation reactions release UDP which is converted to UMP and exchanged with new UDP-sugar by NSTs. Activated PAPS originate from PAPSS-catalyzed PAP transfer to  $\text{SO}_4^{2-}$  in the cytosol. PAPS Golgi intake is ensured by SLC35B2 and SLC35B3. GAG sulfation releases free PAP that is hydrolyzed to AMP and Pi by IMPAD1. Abbreviations: AMP: adenosine-monophosphate; CANT1: calcium activated nucleotidase-1; IMPAD1: inositol monophosphatase domain-containing-1; NSTs: nucleotide-sugar transporters; PAP: phosphoadenosine phosphate; PAPS: 3'-phosphoadenosine 5'-phosphosulfate; PAPSS: PAPS synthase; Pi: inorganic phosphate; SLC35: solute carrier 35; UDP: uridine-diphosphate; USPase: UDP-sugar pyrophosphorylase; UMP: uridine-monophosphate; UTP: uridine-triphosphate.

## I.2.4 Transport and sorting of the proteoglycans

Newly synthesized PGs are sorted and packaged into cargo vesicles at the *trans* face of the Golgi apparatus and the *trans*-Golgi network (TGN) for being exported to their destination through an anterograde vesicular trafficking. GAG chains play crucial role in the orientation of the PG vesicular transport towards. In polarized cells such as MDCK and CaCo-2, the CS chain promotes the addressing of CSPGs to the apical cell side while HS chain favors the basolateral sorting of HSPGs (74–76). Furthermore, in non-polarized cells (HeLa), it has been shown that the introduction of a CS chain in the amyloid-precursor protein and the asialoglycoprotein receptor H1 induced the acceleration of their transport from the TGN to the cell surface (77,78). The vesicular transport of PGs targeted to intracellular compartments is also GAG-dependent. The CS chain is necessary for packaging the PG serglycin into intracellular zymogen granules of pancreatic acinar cells (79). Although the underlying mechanisms are unclear, it is possible that GAG-specific cargo receptors should be present in the TGN membrane, facilitating the transport of PGs in a similar manner than the lectin-mediated sorting of some *N*-glycosylated proteins (80). Moreover, it has been shown in rat hepatocytes that HSPGs were transported by vesicles different than those transporting albumin, apolipoprotein E and fibrinogen suggesting that HSPG-transporting cargoes are different than the constitutive secretory vesicles (81). Additionally, the physical properties and the important size of the GAG chains may induce steric hindrances avoiding their entry into small coated vesicles. Thus, as for pro-collagen 1, the transport of PG into the bulky vesicles emerging from the large TGN tubular domain may be favored (82). Consistently, a recent “organelle zone” theory which segregates a PG specific pathway from other glycosylation-types pathways has been described (83–85).

### **I.2.5 Degradation of proteoglycans**

The PGs catabolism is essential to prevent their accumulation in cells and ECMs. This process occurs mostly in the lysosomes and involves the action of specific glycosidases and sulfatases. The hydrolysis of the GAG chains releases free monosaccharides that will be used for new GAG elongation reactions (86). Genetic defects leading to deficiencies in the enzymes involved in the PG degradation are called mucopolysaccharidoses (MPS). They are characterized by GAG accumulation resulting in multiple cellular and tissue damages (87). In this work, MPS are not extensively described since we rather focus on PG biosynthesis defects.

### **I.2.6 Importance of the Golgi homeostasis for proteoglycan biosynthesis**

The Golgi homeostasis consists of the luminal ionic environment and the balance between anterograde and retrograde vesicular trafficking (**Figure 6**) (88). Correct Golgi homeostasis is essential for allowing each biosynthetic enzyme and substrate transporter to function within adequate milieu and at the right localization among the successive Golgi subcompartments. Several studies, briefly summarized here, have reported important alterations of the PG biosynthesis upon Golgi homeostasis defects in mammalian cultured cells (89).

Regarding the vesicular trafficking, coat protein complexes (COP1 and COP2), tethering factors such as the conserved oligomeric complex (COG), and associated Rab-GTPases, regulate vesicular movements in a coordinated manner (**Figure 6**) (90–92). This has an impact on the localization of PG biosynthetic enzymes. While glycosyltransferases involved in the initiating linker formation localize in the early *cis*- and *medial*-Golgi, those involved in GAG elongation and sulfation reside rather in the late *trans*-Golgi/TGN (93). Brefeldin A (BFA) is a fungal compound that disturbs COP assembling which reversibly blocks anterograde trafficking and leads to ER redistribution of *cis*-, *medial*- and *trans*-Golgi resident proteins, without affecting that of the TGN. In BFA-treated human melanoma cells, CS chain elongation and



sulfation were abolished, while linker formation was not altered indicating a BFA-induced segregation of CS elongation and sulfation enzymes from that of linker formation (94). This emphasizes the importance of the harmonious distribution of each glycosyltransferase for successful PG biosynthesis. Otherwise, treatment of rat chondrosarcoma cells with cyclofenil - a compound that have been shown to disturb the Golgi membrane organization - resulted in alteration of CS chain elongation (95).

Besides anterograde/retrograde trafficking balance, each organelle of the secretory pathway presents a specific range of luminal pH that becomes progressively more acidic from the ER (7.2-7.5) to the Golgi (6.0-6.7), the TGN (5.9), reaching 5.5 in the late secretory vesicles and 4.5 in lysosomes (96,97) (**Figure 6**). This pH gradient is crucial for PG metabolism since glycosyltransferases' activity as well as PG vesicular transport and lysosomal degradation are pH dependents (98–100). The Golgi pH regulation is mediated by the vacuolar H<sup>+</sup>-ATPase proton pump (V-ATPase) (101) (**Figure 6**) and other transmembrane channels such as the Golgi pH regulator (GPHR) (102). Concerning the V-ATPase, it consists of a membrane protein complex formed by eight subunits (A-H) distributed in two sectors (V0 and V1) (101). Pathogenic variants in genes encoding the subunits ATP6V0A2, ATP6AP1 and ATP6V1F as well as the assembling factor CCDC115 cause CDG with impaired Golgi homeostasis (103,104,104,105). Exposition of MDCK cells to Bafilomycin A1 (Baf A1), a specific V-ATPase inhibitor, led to aberrant increase of HS chain length and CS sulfation compared to controls together with impaired PG sorting (100). Treatment of human melanoma cells with ammonium chloride, a weak base inducing neutralization of acidic compartments, resulted in defective CSPGs biosynthesis (106).

Additionally, the Golgi intraluminal ionic equilibrium is important for PG metabolism and is ensured by ion transporters such as TMEM165 [i.e., manganese (Mn<sup>2+</sup>) transporter] and

SPCA1/2 [i.e., calcium ( $\text{Ca}^{2+}$ ) channel] (Figure 6). The catalytic activity of several glycosyltransferases requires the presence, at correct concentrations, of  $\text{Mn}^{2+}$  as cofactor, as it has been shown for B4GALT7 (107,108). In cartilage from  $\text{Mn}^{2+}$ -deficient chicks, PG content was decreased compared to controls and skeletal defects were observed (108).  $\text{Ca}^{2+}$  homeostasis is also important in the PG synthesis and sorting (99). It has been shown that PG levels were reduced in rabbit articular chondrocytes upon treatment with the calcium ionophore A23187 which increases cytosolic  $\text{Ca}^{2+}$  levels (109). Moreover, in rat parathyroid cells, PG sorting and secretion were impaired under increased extracellular  $\text{Ca}^{2+}$  concentration (110).

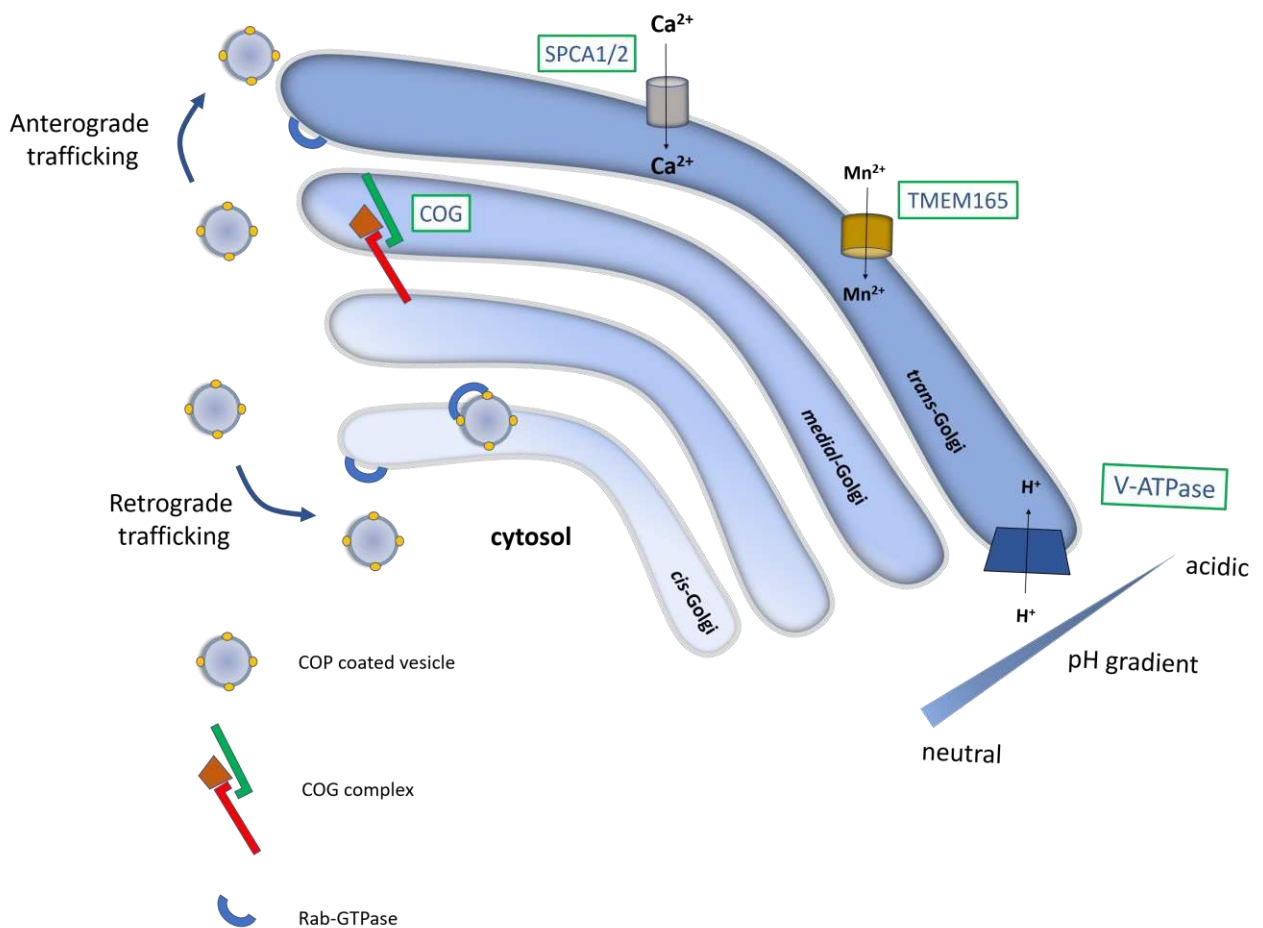


**Figure 6: Molecular actors involved in Golgi homeostasis**

Golgi pH regulation by V-ATPase proton pump ensures a *cis* to *trans* increasing  $\text{H}^+$  concentration resulting in a pH gradient. Ionic homeostasis also requires correct  $\text{Mn}^{2+}$  and  $\text{Ca}^{2+}$  concentrations, these are regulated by TMEM165 and SPCA1/2 transporters respectively. Anterograde and retrograde trafficking involve vesicular movements orchestrated by COP-coated vesicles, COG vesicular tethering complex and Rab-GTPases. Abbreviations: COG: conserved oligomeric Golgi; COP: coat protein complex; SPCA1/2: secretory pathway  $\text{Ca}^{2+}$ -ATPase pump type-1/2; TMEM165: transmembrane protein type-165.

### **I-2-7 Classification, distribution, and roles of proteoglycans**

PGs can be classified into four classes (**Table 1**) according to their cellular localization. The unique known intracellular PG is serglycin, which carries a heparin chain or a CS chain according to the cell type. It is involved in the storage of histamine and proteases into secretory granules in mast cells and macrophages for their delivery during inflammatory response (111). The second class of PGs includes those embedded into the cell plasma membrane such as syndecans and glypicans. In numerous cell types including leucocytes and epithelial cells, their extracellular domain binds several ligands such as the vascular endothelial growth factor (VEGF) and inflammatory cytokines. This leads to various signal transduction pathways regulating leukocyte recruitment, angiogenesis, cell proliferation, and differentiation (112–115). They also interact with ECM components such as collagens, hyaluronan, and fibronectin to form the ECM network (116). Otherwise, the cytoplasmic domain of cell surface PGs interacts with the cytoskeleton, thereby participating in cell motility (117).

Pericellular PGs (the third class) are linked to the cell surface through adhesion molecules such as integrins and constitute a supportive matrix allowing interactions with the cellular microenvironment. For example, perlecan is a ubiquitous HSPG located in the basement membranes, which is involved in healing and angiogenesis during wound repair by interacting with collagen IV and VEGF, respectively (118).

The fourth class of PGs comprises the extracellular PGs that are composed of hyaluronan- and lectin-binding PGs (hyalectans) and the small leucin-rich proteoglycans (SLRPs). Aggrecan is a hyalectan that carries several CS, DS, and KS GAG chains and is the main PG of cartilage. It forms bulky aggregates with hyaluronan, collagen fibrils, and with other PGs to generate a hydrated gel underlying the viscoelastic consistence and the resistance of cartilage (119). Biglycan is a CS/DS PG of the SLRPs family that is ubiquitously found in ECMs. Among the wide range of its physiological functions, biglycan is involved in bone formation by regulating

osteoblast differentiation through interaction with the bone morphogenic protein (BMP) (120). Decorin, an SLRP carrying a DS chain, promotes assembly of collagen fibers in skin, tendons, bone and cornea during wound healing (121,122). Decorin also forms complexes with growth factors such as TGF- $\beta$  and TNF- $\alpha$  to modulate their interaction with the corresponding receptors which regulates intracellular signaling pathways involved in bone morphogenesis and skeletal muscle differentiation (123,124). In blood and urine, the inter- $\alpha$ -trypsin inhibitor proteins (IAIPs) are liver-expressed SLRPs carrying a unique short CS chain branched on the core protein Bkn. Their roles are described below in a dedicated section. Another circulating PG called endocan is a DSPG secreted by endothelial cells that inhibits leucocyte migration and adhesion to inflamed tissues as well as angiogenesis and cell proliferation during wound healing and tumor progression (125) (**Table 1**).

**Table 1. Overview of some proteoglycans and their pathophysiological involvements.**

<b>Location</b>	<b>Designation</b>	<b>Type of GAG chain</b>	<b>Roles</b>
Intracellular	<b>Serglycin (SG)</b>	Heparin/CS	Formation of intracellular storage granules in mast cells (111).
Cell surface	<b>Syndecans</b>	HS/CS	Regulation of vascular development and wound healing (112). Regulation of chondrocyte proliferation during skeletogenesis (126)

	<b>Glypicans</b>	HS	Regulation of Wnt, FGF and Hedgehog signaling pathways during growth, development and cancer (114,115).
Extracellular matrices	<b>Aggrecan</b>	CS/DS/KS	Resistance to compression of cartilage in joints (119). Structure of brain ECM and involvement in neuronal plasticity (127).
	<b>Fibromodulin</b>	KS	Regulation of collagen fibrillogenesis, muscle cell growth, cellular reprogramming, and angiogenesis (128).
	<b>Decorin</b>	DS	Promotes collagen fibrillogenesis in skin, tendons, bone and cornea during wound healing (129). Involved in bone morphogenesis and skeletal muscle differentiation (123,124). Inhibits various tyrosine kinase receptors (130).
	<b>Biglycan</b>	CS/DS	Promotes collagen fibrillogenesis (131) and promotes osteoblast differentiation and bone maturation (120).
	<b>Collagen XVIII</b>	HS	Structural component of the basement membranes of vascular and epithelial cells. Inhibits

angiogenesis and Wnt signalling (132).

**Collagen XII**

CS

Regulation of bone morphogenesis and regeneration (133,134).  
Regulation of tendon formation and mechanical properties (135).

**Perlecan**

HS/CS/KS

Tissue organisation and ECM stabilization. Participation to mechanical properties of cartilage, protection of vascular endothelium, regulation of lipid clearance (136).

---

Blood

**Endocan**

DS

Regulation of cell adhesion, migration, proliferation, and angiogenesis in cancer and wound healing (125).

**Inter- $\alpha$ -trypsin inhibitor family**

CS

Stabilization of extracellular matrices, anti-plasmin activity, inhibition of complement activation and protection against kidney stone formation (137).

**PG-100**

CS

Macrophage-derived PG involved in inhibition of atherosclerosis formation by trapping of low-density lipoprotein (138). Growth factor activity triggering differentiation of bone marrow cells (139).

---

### I-3 Proteoglycan inherited metabolic diseases (PG-IMD)

The inborn pathologies resulting from abnormal PG biosynthesis, transport or degradation lead mostly to skeletal and connective tissue disorders. Overall, the clinical phenotypes show various overlapping skeletal and articular features including skeletal dysplasia, joint dislocations, recurrent fractures and dysmorphisms. Additional troubles such as neurological disorders, growth retardations, cutaneous pathologies, tooth abnormalities, deafness, ocular disorders could expand the clinical presentation and make the clinical diagnosis difficult (8–10). PG-IMD can be classified according to the defective step of PG biosynthesis (**Table 2**). Therefore, one can distinguish those caused by impaired tetrasaccharide linker formation (linkeropathies), GAG elongation, GAG sulfation, substrate supply, and by defects in Golgi homeostasis (including Golgi vesicular trafficking and ionic environment) (**Table 2**). Importantly, it appears that no clinical characteristic could differentiate a PG-IMD subgroup from another one. Here we recapitulate some biochemical analyzes performed in patients' samples and/or cellular and animal models which allowed identification of PG metabolism defects and helped to determine genotype/phenotype correlations.

**Table 2. Proteoglycan inherited metabolic diseases: Classification and clinical aspects.**

<b>PG defect subgroup</b>	<b>Mutated gene</b>	<b>Associated disorder and clinical features</b>
<b>Defects of the tetrasaccharide linkage region</b> (Linkeropathies)	<b><i>XYLT1</i></b> Initiating xylose transfer to the core protein (Xyl $\beta$ 1- <i>O</i> -Ser).	<b>Desbuquois dysplasia type 2</b> (MIM - 615777): Short long bones, joint laxity and dislocations, advanced carpal/tarsal ossification, chondrodysplasia, growth retardation (142).
	<b><i>XYLT2</i></b> Initiating xylose transfer to the core protein (Xyl $\beta$ 1- <i>O</i> -Ser).	<b>Spondyloocular syndrome</b> (MIM - 605822): Osteopenia/osteoporosis, cataract, deafness, heart defects (143).
	<b><i>B4GALT7</i></b> Transfer of the first galactose of the linkage (Gal $\beta$ 1-3Gal $\beta$ 1-4Xyl $\beta$ 1- <i>O</i> -Ser).	<b>Ehlers-Danlos syndrome (EDS) spondylodysplastic type 1</b> (MIM - 130070): Joint laxity, hyperelastic skin, short stature, hypotonia, poor wound healing (18).
	<b><i>B3GALT6</i></b> Transfer of the second galactose of the linkage region (Gal $\beta$ 1-3Gal $\beta$ 1-4Xyl $\beta$ 1- <i>O</i> -Ser).	<b>EDS spondylosyplastic 2</b> (MIM – 615349) and <b>Spondyloepymetaphyseal dysplasia with joint laxity</b> (MIM – 271640): Recurrent bone fractures, epimetaphyseal dysplasia, joint laxity and dislocations, cutaneous hyperlaxity, scoliosis, intellectual disabilities, poor wound healing, hypotonia (144).
	<b><i>B3GAT3</i></b> Transfer of the terminating glucuronic acid of the linkage region (GlcA $\beta$ 1-3Gal $\beta$ 1-3Gal $\beta$ 1-4Xyl $\beta$ 1- <i>O</i> -Ser).	<b>Larsen-like syndrome</b> (MIM – 245600): Short stature, joint laxity and dislocations, scoliosis, cutis laxa, heart defects (145).
	<b><i>FAM20B</i></b> Phosphorylation of the xylose after the first galactose addition (Gal-Xyl(2- <i>O</i> -phosphate)- <i>O</i> -Ser ).	<b>Desbuquois dysplasia</b> (MIM - 615777) with lethal neonatal short limb dysplasia (146).



---

**GAG elongation  
defects**

***CSGALNACT1***

First GalNAc transfer to the linkage region: initiation of CS elongation.

**Mild skeletal dysplasia with advanced bone age** (unreferenced):

Skeletal dysplasia, short stature, advanced bone age, facial dysmorphism, joint laxity, monkey wrench appearance of the femur, Bell's palsy, neuropathies (147).

***CHSY1***

[GlcA-GalNAc] polymerization: CS GAG elongation

**Temtamy preaxial brachydactyly syndrome** (MIM - 605282):

Characteristic digits shortening, facial dysmorphism, deafness, growth and mental retardation (148).

***EXTL3***

First GlcNAc transfer to the linkage region: Initiation of HS elongation.

**Neuro-immuno-skeletal dysplasia syndrome** (MIM - 617425):

Severe immunodeficiency associated to skeletal dysplasia, developmental delay and intellectual disability (149).

***EXT1/EXT2***

[GlcA-GlcNAc] polymerization: HS GAG elongation

**Hereditary multiple exostosis syndrome** (MIM - 133700/133701):

Benign osteoarticular tumors called exostosis or osteochondromas leading to skeletal dysmorphisms (150,151).

***DSE-1***

GlcA epimerization to IdoA: CS conversion to DS

**EDS musculocontractural type 2** (MIM - 615539):

Characteristic craniofacial deformities (large fontanel, hypertelorism, blue sclerae...), skin hyperextensibility, muscle hypoplasia, contractures and hypotonia (152).

---

**GAG sulfation  
defects**

***SLC26A2***

Cell-surface inorganic sulfate transporter

**Achondrogenesis type 1B** (MIM - 600972):

Micromelia, flat face, short trunk, fetal/perinatal lethality (153).

**Atelosteogenesis type 2** (MIM - 256050):

Limb shortening, cleft palate, characteristic facial dysmorphisms, 'hitchhiker' thumbs, possible fetal/perinatal lethality (154).

	<b>Diastrophic dysplasia</b> (MIM - 222600): Short and thick long bones, joint dysplasia, scoliosis, ‘hitchhiker’ thumbs, club feet, cleft palate, cysts on the external ear (155).
	<b>Recessive multiple epiphyseal dysplasia type 4</b> (MIM - 226900): Flat epiphyses, hips arthritis, double layered-patella, clubfoot, brachydactyly, joint pain.
<b>CHST3</b> Sulfation of GalNAc residues in the CS chains	<b>Spondyloepiphyseal dysplasia with joint laxity (SEDJL) CHST3 type</b> (MIM - 143095): Kyphosis/scoliosis, Club feet, knees and hips dislocations, short stature (156).
<b>CHST6</b> Sulfation of GlcNAc residues in KS chains	<b>Macular corneal dystrophy</b> (MIM - 217800): Corneal opacity and thinning, photophobia, tearing, progressive vision loss (157).
<b>CHST12*, CHST13*</b> Sulfation of GalNAc residues on the CS chain	<b>Kashin-Beck disease*</b> Joint pain, deformities and limited joint mobility in fingers, shoulders, ankles, knees, wrists, toes. Bone damage and short stature (158).
<b>UST*</b> Sulfation of GlcA/IdoA residue in CS/DS chains	<i>*Unestablished causality</i>
<b>CHST14 (D4ST1)</b> Sulfation of GalNAc residues on the DS chains	<b>EDS musculocontractural type 1</b> (MIM - 601776): Muscle hypotonia, facial dysmorphisms, joint dislocation, skin hyperlaxity, club feet, bruising (159,160).

**PAPSS2**

Synthesis of sulfate donors (PAPS)

**IMPAD1**

Hydrolysis of PAP released from sulfation reactions

**Spondyloepimetaphyseal dysplasia**

**Pakistani type** (MIM - 612847):

Short stature, scoliosis, osteoarthritis, mild brachydactyly (161).

**Brachyolmia** (MIM - 271530):

Short stature, short trunk, platyspondyly, vertebral deformities, calcification of costal cartilage, and hormonal disturbances (162,163).

**Chondrodysplasia with joint dislocations, gPAPP type** (MIM - 614078):

Short stature, chondrodysplasia with brachydactyly, joint dislocations, micrognathia, cleft palate and facial dysmorphism (73).

**Catel-Manzke syndrome** (MIM – 616145):

Growth retardation, cleft palate with micrognathia, isolated knee hyperlaxity, abnormally shaped phalanges and carpal synostosis (164).

---

**Defects in UDP-sugar synthesis and transport**

**SLC35D1**

Transport of UDP-GlcA, UDP-GalNAc, UDP-GlcNAc, UDP-Gal, and UDP-Xyl in the ER.

**SLC35A3**

UDP-GlcNAc transport in the Golgi apparatus

**Schneckenbecken dysplasia** (MIM - 269250):

Lethal chondrodysplasia, snail-like pelvis, flattened hypoplastic vertebral bodies, short ribs, short and wide fibulae, short and broad long bones with a dumbbell-like appearance, and precocious ossification of the tarsus (165,166).

**SLC35A3-CDG - Autism spectrum disorder-epilepsy-arthrogryposis syndrome** (MIM - 615553):

Arthrogryposis, retromicrognathia, hypotonia, delayed psychomotor development, autism, seizures, microcephaly, and intellectual disability (167).

<p style="text-align: center;"><b><i>SLC35A2</i></b></p> <p>UDP-Gal transport in the Golgi apparatus</p>	<p><b>SLC35A2-CDG</b> (MIM - 3000896):</p> <p>Epilepsy, delayed psychomotor development, hypotonia, skeletal abnormalities, facial dysmorphism, inverted nipples, vision and hearing abnormalities, cardiac diseases (168,169).</p>
<p style="text-align: center;"><b>CANT1</b></p> <p style="text-align: center;">(Calcium activated nucleotidase)</p> <p style="text-align: center;">ER/Golgi protein involved in the hydrolysis of the UDP released after the glycosylation reactions</p>	<p><b>Desbuquois dysplasia type 1</b> (MIM - 613165):</p> <p>Severe growth retardation, joint laxity, short extremities, scoliosis, short-long bones with metaphyseal splay, 'Swedish key' appearance of the proximal femur and advanced carpal and tarsal ossification (170–174).</p>

**Defects linked to impaired Golgi homeostasis**

<p style="text-align: center;"><b><i>TMEM165</i></b></p> <p style="text-align: center;">Golgi localized Ca<sup>2+</sup> - Mn<sup>2+</sup> / H<sup>+</sup> antiporter</p>	<p><b>TMEM165-CDG</b> (MIM:614727):</p> <p>Psychomotor and growth retardation, facial dysmorphism, skeletal dysplasia with osteoporosis, scoliosis (175).</p>
<p style="text-align: center;"><b><i>COG4</i></b></p> <p style="text-align: center;">(Conserved oligomeric Golgi - subunit 4)</p> <p style="text-align: center;">Tethering complex involved in the retrograde trafficking from the Golgi apparatus to the ER</p>	<p><b>Saul Wilson syndrome</b> (MIM:606976):</p> <p>Short stature, characteristic craniofacial dysmorphisms, prominent forehead, cataract, microencephaly, clubfoot, brachydactyly, irregularities of the vertebral bodies (176).</p>
<p style="text-align: center;"><b><i>SLC10A7</i></b></p> <p style="text-align: center;">Ca<sup>2+</sup> influx regulation across intracellular membranes</p>	<p><b>Skeletal dysplasia and amelogenesis imperfecta</b> (unreferenced):</p> <p>Short stature, microretrognathia, dislocations, monkey wrench appearance of the femora, short-long bones, advanced carpal and tarsal ossification, tooth abnormalities (177,178).</p>
<p style="text-align: center;"><b><i>GORAB</i></b></p> <p style="text-align: center;"><i>Trans</i>-Golgi protein involved in retrograde trafficking</p>	<p><b>Geroderma osteodysplastica</b> (MIM:231070):</p> <p>Lax and wrinkled skin, osteoporosis with spontaneous fractures, short stature, joint dislocations, and intellectual disabilities (179).</p>

### I.3.1 Linkeropathies

Patients with *XYLT1* gene pathogenic variants mainly display severe short stature, altered carpal and tarsal ossification and joint hyperlaxity (142,180). In patient's fibroblasts, the observed XylT decreased activity and/or mislocalization were associated to important decreases of the CS and DS amounts compared to controls. Analysis of decorin in fibroblasts' supernatant showed presence of abnormal DS-free core protein in patients (142,181). Otherwise, *XYLT2* gene mutations have been found in affected individuals presenting skeletal dysplasia, osteoporosis, cataract, deafness, and heart defects with patient's fibroblasts showing decreased XylT activity and CS/HS levels (182–186). The distinct clinical phenotypes between *XYLT1* and *XYLT2*-linkeropathies could be partially explained by differences in the tissue expression of these two homologous enzymes (185).

*B4GALT7* and *B3GALT6* gene deficiencies result in subtypes of “Ehlers-Danlos syndrome” (EDS), a group of connective tissue disorders associated to many organ defects. In *B4GALT7* and *B3GALT6* linkeropathies, patients present joint hypermobility, cutaneous abnormalities, poor wound healing, and visceral dysfunctions (18,144,187–190). Accordingly, fibroblasts from *B4GALT7* mutated patients showed decreased  $\beta 4\text{GalT7}$  activity leading to the presence of core proteins linked solely to a Xyl residue. Consistently, strong reduction of CS and DSPGs levels were observed together with HS sulfation defects associated to defective ECM organization and cell proliferation (191–193). In fibroblasts from  $\beta 3\text{GalT6}$ -deficient patients, CS, DS and HS production was significantly decreased compared to controls (144). In *b3galt6*-deficient zebrafish extracts, the presence of biglycan with a non-canonical linkage region GlcA-Gal-Xyl together with overall decrease of CS, DS and HS were highlighted. Furthermore, *b3galt6*-deficient zebrafish displayed a skeletal phenotype that mimics that observed in patients with EDS linked to *B3GALT6* deficiency (194). *B3GALT6* linkeropathy could also manifest by a syndrome different from EDS and known as Spondyloepimetaphyseal dysplasia with joint

laxity type 1 (SEMDJL1). Interestingly, PG analyses in patients' fibroblasts and lymphoblastoid cells showed different results than in patients' fibroblasts with EDS. Indeed, CS and DS amounts were higher than controls while HS levels were decreased (195,196).

*B3GAT3*-related linkeropathy manifests by the so-called Larsen-like syndrome which displays short stature, joint laxity, and scoliosis (145,197,198). Dramatic decreases of *B3GAT3* mRNA level and enzymatic activity were shown in patients' fibroblasts together with a loss of GlcAT-I Golgi localization (145). Additionally, decreased CS, DS and HS levels were shown in patients' fibroblasts and lymphoblastoid cells indicating an overall PG biosynthesis defect (145,198,199).

Recently, heterozygous variants in *FAM20B* (i.e., kinase that phosphorylates Xyl residue of the linker) were identified in two newborns with a lethal neonatal dysplasia (146). Mutant *fam20b* mice displayed reduced cartilage HS and DS amounts compared to wild types. Moreover, abnormal chondrocyte differentiation and impaired bone maturation was described demonstrating the crucial role of *FAM20B* for the connective tissue and skeletal development (200).

### **I.3.2 GAG elongation defects**

CSGalNAcT-1 catalyzes the transfer of a GalNAc residue to the linker region and is then fundamental for the synthesis of CS and DS chains of PGs. Mutations in *CSGALNACT1* gene have been identified in patients presenting skeletal dysplasia, joint dislocations, and neuropathies (147,201). In fibroblasts from patients, the observed decreased GalNAc transferase activity results in the lack of CS/DS chains elongation on core proteins (201). Moreover, significant reductions of CS levels in cartilage and brain were found in *csgalnact-1* KO mice together with ECM alterations. While such material was not available in patients,

these observations in murine models could partially explain the articular and neurological disorders related to *CSGalNAcT-1* mutations (202).

ChSy-1 enzyme has both GlcA and GalNAc transferase activity and is then a major actor of the CS polymerization (34). Several pathogenic variants in *CHSY-1* gene have been reported in patients presenting facial dysmorphism, hand deformities, tooth abnormalities, hearing loss and growth and mental retardations (148,203,204). Immunohistochemistry on patients' skin fibroblasts showed lower CS levels when compared to controls (203). Moreover, *chsy-1* KO zebrafish displayed neural, skeletal and vestibular malformations (148).

Exostosin (EXT) family members are responsible for the HS elongation. Pathogenic mutations in *EXTL3* coding for EXTL3 (GlcNAcT-1) involved in the first step of HS elongation, have been reported in various patients displaying the “neuro-immuno-skeletal dysplasia syndrome” (*NISDS*) (149,205). Besides several skeletal and intellectual disabilities, the patients present severe immunodeficiency. Induced pluripotent stem cells from *EXTL3*-mutated individuals showed alterations of the hematopoietic progenitor cells differentiation corroborating the frequently observed lymphopenia (149). A total absence of EXTL3 was shown in patient's T cells and fibroblasts showed a loss of EXTL3 Golgi localization together with alterations of HS chain elongation and sulfation (149,206). The second major pathology resulting from EXT defects is the “Hereditary multiple exostosis syndrome”(HMES) due to mutations in *EXT1* or *EXT2* genes coding for the enzymes catalyzing the HS chain elongation (150,151,207). HMES is the most frequent skeletal genetic disorder with a prevalence estimated at 1:50,000. The symptoms are restricted to skeletal malformations characterized by benign osteoarticular tumors localized at the end of long bones and called “exostosis” or “osteochondromas”. Quantification of HS-related disaccharides levels in plasma showed half reduction compared to controls (208). Biopsies of osteochondromas from *HMES* patients with *EXT1* variants showed

decreased biosynthesis and increased degradation of HS compared to controls. The pathogenesis of *HMES* could be linked to an imbalance of the HSPGs-regulated anti- and pro-chondrogenic signaling pathways leading to the formation of osteochondromas (209,210). *HMES* associated osteochondroma can worsen and lead to malignant secondary peripheral chondrosarcoma (211).

The CS to DS chain conversion results from GlcA to IdoA epimerization catalyzed by the Golgi-resident enzymes DS-epi1 and DS-epi2. Mutations in *DSE-1* have been described in patients presenting an EDS subtype characterized by muscular abnormalities (212,213). In patients' fibroblasts, defective DS-epi1 activity was associated to decreased DS and increased CS chains' levels (212). Interestingly, DS-epi2 isoform was not able to rescue the defective epimerization, at least in fibroblasts. Moreover, increased CS biosynthesis did not prevent the observed muscular abnormalities. Accordingly, DSPG are crucial components for muscle regeneration since they stimulate growth factor-mediated myoblast proliferation (214).

### **I.3.3 GAG sulfation defects**

The physicochemical properties of PGs and their interaction with ECMs components are mostly related to the negative charges provided by the sulfate groups on the GAG chains (215). Pathogenic variants in genes involved in GAG sulfation could lead to major alterations of the connective tissues resulting in mild to severe osteoarticular syndromes. Various mutations in the *CHST3* gene coding for C6ST1 have been found in a wide spectrum of osteoarticular diseases sharing severe joint dislocations. Biochemical studies on *CHST3* mutated patient's fibroblasts showed total absence of C6ST activity and major hyposulfation of the [GlcA-GalNAc] disaccharide motifs (157,216,217).

Mutations in *D4ST1* (also named *CHST14*) lead to alterations of DS sulfation (218). As for *DSE-1* mutated patients, the resulting syndrome is the musculo-contractural-EDS



(160,219,220). Analysis of GAGs from patients' fibroblasts showed decreased DS levels while CS levels were increased compared to controls (219). Indeed, the absence of IdoA sulfation allows its reverse epimerization to GlcA and then the DS to CS chain reconversion (160).

Mutations in the *SLC26A2* gene, a cell-surface inorganic sulfate transporter mostly present in cartilage, have been identified in various pathological conditions with severe chondrodysplasias (e.g., achondrogenesis type 1B) (153–155,221). GAG sulfation in cartilage samples from patients showed important hyposulfation. Accordingly, uptake assays in cultured patient's fibroblasts showed decreased sulfate incorporation (222).

Defective *SLC35B2*, a Golgi localized PAPS transporter was found in two affected individuals with a phenotype sharing chondrodysplasia, bone dislocations and psychomotor delay. The analysis of patient's cultured fibroblasts showed hyposulfated secreted CS chains (article under submission).

Mutations in the *PAPSS2* gene lead to osteoarticular phenotypes mostly affecting the spine (161,162). Some clinical phenotypes with mild skeletal abnormalities are characterized by severe hormonal disturbances linked to unsulfation of dehydroepiandrosterone (DHEA). Indeed, unsulfated DHEA is a precursor of androgen synthesis while its sulfated counterpart is inactive. Thereby, *PAPSS2* patients showed increased androgen levels responsible for hormonal disturbance (163,223). CS quantification in cartilage extracts from *papss2*-deficient mice showed significantly reduced levels compared to controls (224).

The sulfate transfer reaction from PAPS to the sugar moieties produces a phosphoadenosine-phosphate (PAP) molecule that is hydrolyzed to adenosine monophosphate (AMP) by a Golgi-resident PAP phosphatase named *IMPAD1* (inositol monophosphatase domain-containing 1). A defective PAP hydrolysis caused by mutations in *IMPAD1* leads to PAP accumulation in the Golgi apparatus which results in sulfotransferases' inhibition by negative feedback. *IMPAD1* mutated patients present a chondrodysplasia with joint dislocations

(73,164). In mice, *Impad1* inactivation resulted in CS and HS chain sulfation defects associated to chondrodysplasia (225,226).

### **I.3.4 Defects in sugar transporters**

*SLC35D1* gene encodes for a UDP-sugars transporter expressed in the ER. It has been shown in vitro that SLC35D1 could transport UDP-GlcA, UDP-GalNAc, UDP-GlcNAc, UDP-Gal, and UDP-Xyl (166,227). Despite its ER expression, SLC35D1 seems to play important roles in the GAG elongation, a process occurring in the GA. Several pathogenic variants have been identified resulting in a lethal skeletal dysplasia characterized by malformations of the pelvis (166,228,229). Dramatic decreases of UDP-sugar transport activity were described in vitro using microsomes preparations (227) and defective CS chain biosynthesis was shown in cartilage from *Slc35d1*<sup>-/-</sup> mice (166). Given the ability of SLC35D1 to transport UDP-Xyl, the observed PG biosynthesis alterations in SLC35D1 defects could be due to a lack of UDP-Xyl supply for the initiation of the GAG elongation in the ER, despite the presence of the main UDP-Xyl transporter i.e., SLC35B4.

SLC35A3 is a Golgi-resident UDP-GlcNAc transporter. Pathogenic variants in *SLC35A3* have been described in patients presenting skeletal malformations, autism, and epilepsy (167,230,231). In patients' fibroblasts, UDP-GlcNAc transport across the Golgi membrane is significantly reduced compared to controls. The observed defective *N*-glycosylation in patients' serum and fibroblasts led to classify *SLC35A3* inherited deficiency among the group of congenital disorders of glycosylation (CDG). *slc35a3*<sup>-/-</sup> MDCK cells presented significant reductions of both UDP-GlcNAc and UDP-Gal transport together with dramatic decreases of KS biosynthesis compared to wild-types. In contrast, CS and HS levels were normal suggesting residual SLC35A3 activity with a preferential substrate supply towards CS and HS biosynthesis (232).

SLC35A2 deficiencies are also classified among CDG given the observed *N*-glycosylation defects in patients (233). The clinical spectrum is wide and unspecific, including neurological, skeletal and multivisceral abnormalities (168,234). In mutant MDCK cells defective for UDP-Gal transport, KS levels were strongly decreased while CS and HS amounts were normal compared to wild-types (235,236). As for *SLC35A3* defects, the residual SLC35A2 activity could allow UDP-Gal supply with a preferential use for CS and HS biosynthesis.

### **I.3.5 Proteoglycan defects linked to impaired Golgi homeostasis**

The Conserved oligomeric Golgi (COG) complex is an octameric tethering complex involved in the retrograde trafficking within the Golgi apparatus (91,237). Although COG mutations are mostly encountered in CDG, Ferreira and al described 14 patients with Saul Wilson syndrome (a rare skeletal dysplasia) harboring recurrent heterozygous de-novo *COG4* mutation with normal *N*- and mucin-type *O*-glycosylation (176). However, the analysis of patients' fibroblasts showed significant PG alterations while mutant zebrafishes had defective PG secretion. In fibroblasts, *COG4* levels were normal, however, qualitative defect within the protein structure was highlighted. This was associated with an alteration of the Golgi morphology together with acceleration of the retrograde trafficking and delayed anterograde transport. It is likely that these Golgi trafficking alterations were responsible for the mislocalization of the enzymes involved in the PG biosynthesis but not that of *N*- and mucin-type *O*-glycosylation. A possible explanation would be that the lobe of the COG complex that has been shown to be involved in *N*- and *O*-glycosylation is unaltered in the heterozygous condition with de-novo *COG4* mutation (238).

Golgin-Rab-6 (GORAB) is a *trans*-Golgi protein involved in the retrograde trafficking via its interaction with small GTPases and the vesicular COP-1 coat protein (239). Pathogenic variants in GORAB encoding gene have been described in patients presenting a Cutis laxa-like

syndrome characterized by a loss of skin elasticity and osteoporosis (179,240,241). In *gorab*-KO mice, a defective decorin-DS biosynthesis was observed in the skin and bone tissues, together with ECM alterations (242). Given the major role of DSPGs in the elastic properties of the skin as well as their involvement in bone remodeling, it is likely that the observed DS defects are in line with the clinical phenotype of *GORAB* mutated patients.

Transmembrane protein 165 (TMEM165) is a Golgi localized  $\text{Ca}^{2+}$  -  $\text{Mn}^{2+}$  /  $\text{H}^{+}$  antiporter (243). It plays crucial roles in the maintenance of Golgi pH,  $\text{Ca}^{2+}$  and  $\text{Mn}^{2+}$  homeostasis. Marked glycosylation defects, consistent with a CDG, were shown in *TMEM165* mutated individuals presenting severe bone and cartilage dysplasia with osteoporosis (244). Recently, it has been shown that the glycosylation defects due to TMEM165 deficiency mostly result from decreased  $\text{Mn}^{2+}$  levels in the Golgi (245). In a *tmem165*-deficient zebrafish model, a significant loss of CSPGs was demonstrated in cartilage from embryos, together with decreased total protein glycosylation. Interestingly, the observed alterations of the craniofacial cartilage development, the reduced chondrocyte and osteoblast differentiation and the glycosylation abnormalities mirrored the human TMEM165-CDG phenotype (246).

Calcium activated nucleotidase 1 (CANT1) is an ER/Golgi protein involved in the hydrolysis of the UDP released after the glycosylation reactions. The produced UMP is exchanged, *via* an antiport channel, for a cytosolic UDP-sugar that will be used for a new glycosylation reaction (174). Numerous *CANTI* gene variants have been described in individuals sharing chondrodysplasias with multiple joint dislocations and uncontrolled ossification (“Desbuquois type 1” syndrome DBQD (170,172–174,247–249). Patients’ fibroblasts showed enlarged ER cisternae and decreased PG levels compared to controls. *CANTI*<sup>R302H/R302H</sup> (a mutation described in human) and *CANTI* KO mice displayed similar skeletal features than those observed in DBQD1 patients. Chondrocytes from these mice

showed enlarged ER cisternae, defective GAG elongation, increased sulfation, and reduced PG secretion. CANT1 deficiency may lead to blockade in the secretory route resulting in delayed PG processing and secretion with overexposure of the nascent GAG chains to sulfotransferases.

SLC10A7 is a transmembrane protein expressed at the plasma membrane and the ER. It is involved in intracellular  $\text{Ca}^{2+}$  homeostasis as a negative regulator of  $\text{Ca}^{2+}$  entry in the cytosol and ER lumen. Indeed, *SLC10A7 KO* HAP1 cells showed increased ER and cytosolic  $\text{Ca}^{2+}$  entry while *SLC10A7* overexpression in HEK293 cells reduced these  $\text{Ca}^{2+}$  influx (250). Moreover, increased  $\text{Ca}^{2+}$  influx was observed in fibroblasts from *SLC10A7* mutated patients compared to controls (178). Clinically, *SLC10A7* mutations have been associated with skeletal dysplasia with multiple joint dislocations and tooth abnormalities (177). In patients' fibroblasts, although normal total GAG levels, the HS proportion was significantly reduced indicating a defective HS biosynthesis, possibly counterbalanced by an increased CS biosynthesis. Moreover, the observed Golgi morphology impairments together with the alterations of the  $\text{Ca}^{2+}$ -dependent vesicular trafficking could be responsible of impaired PG transport and secretion (251).

### **I-3-6 Mucopolysaccharidoses**

PG catabolism occurs in lysosomes and involves sequential action of several glycosidases and sulfatases which progressively depolymerize the GAG chains into free monosaccharides. Degradation of core proteins also occurs and is ensured by lysosomal proteases such as metalloproteinases and cathepsins (86). Genetic defects leading to malfunction of these enzymes lead to incomplete degradation and deleterious GAG accumulation in organs. The resulting MPS syndromes manifest by skeletal dysplasia, articular damages, facial dysmorphism, short stature and corneal opacities. Patient can also present neuropathies, developmental delay, cardiac diseases, ocular defects and skin lesions (For review, see ref (87).

## **I-4 Screening of proteoglycan inherited metabolic diseases**

### **I-4-1 Current laboratory tools and examples of applications**

The low incidence of PG-IMD and their unspecific clinical signs make a diagnosis only based on a clinical approach difficult. As shown in **Figure 7**, the screening strategy benefits from the development of next-generation sequencing techniques (gene panels, whole exome/genome sequencing) classically applied to DNA from blood-derived lymphocytes for the early identification of potentially causative gene variants. However, to ascertain their pathogenicity and perform an accurate diagnosis, the implementation of tedious biochemical assays is often required. In most cases, invasive skin biopsies are performed and addressed to specialized laboratories where the overall PG content of fibroblasts is evaluated and compared to controls. The most common strategy involves fibroblasts cell culture in the presence of radiolabeled substrates ( $^{35}\text{S}$  and  $^3\text{H}$ -radiolabelled sugars) that enter the cells and are incorporated into the GAG chains of PGs. After elimination of unlabeled radioactive substrate, liquid scintillation counting is employed to quantify labeled GAGs in cell culture media or lysates (**Figure 7**). For example, this technique allowed the detection of decreased PG biosynthesis in XylT-1 and CANT1-deficient patient fibroblasts (142,174).

The quantification of fibroblasts' PG content by immune-based techniques is also possible using antibodies and/or lectins recognizing the GAG chains. Enzyme-linked immunosorbent assay using anti-CS/DS antibodies showed reduced absorbance in CSGalNAcT-1-deficient patient fibroblasts (252). Flow cytometry using anti-CS and -HS antibodies showed a significant decrease in cell surface CS and HSPG in patients with B3GAT3 linkeropathy (145). More accurate analyses allowing the determination of GAG disaccharide composition and sulfation degree could be performed using high-performance liquid chromatography (HPLC) and mass spectrometry (MS) following specific enzymatic treatments (**Figure 7**). Indeed, the disaccharide units of CS/DS, HS/heparin, and KS GAG chains are obtained by treating the cell lysates with chondroitinase, heparitinase, and keratanase (i.e., GAG lyases), respectively. HPLC analysis of chondroitinase-treated fibroblast lysates from DSE-deficient patients showed decreased amounts of [IdoA–GalNAc] disaccharide (i.e., the DS backbone) compared to controls (152). HPLC–MS coupling highlighted reduced [IdoA–GalNAc4-*O*-sulfate] levels in chondroitinase-treated cell fractions from D4ST1-deficient patients compared to controls (159). Otherwise, specific PGs from skin fibroblasts such as decorin and biglycan can be used as markers, using antibody-based Western blot techniques, to highlight defective GAG chain synthesis, as it has been performed for a patient with B4GALT7 and B3GALT6 linkeropathies (144,192).

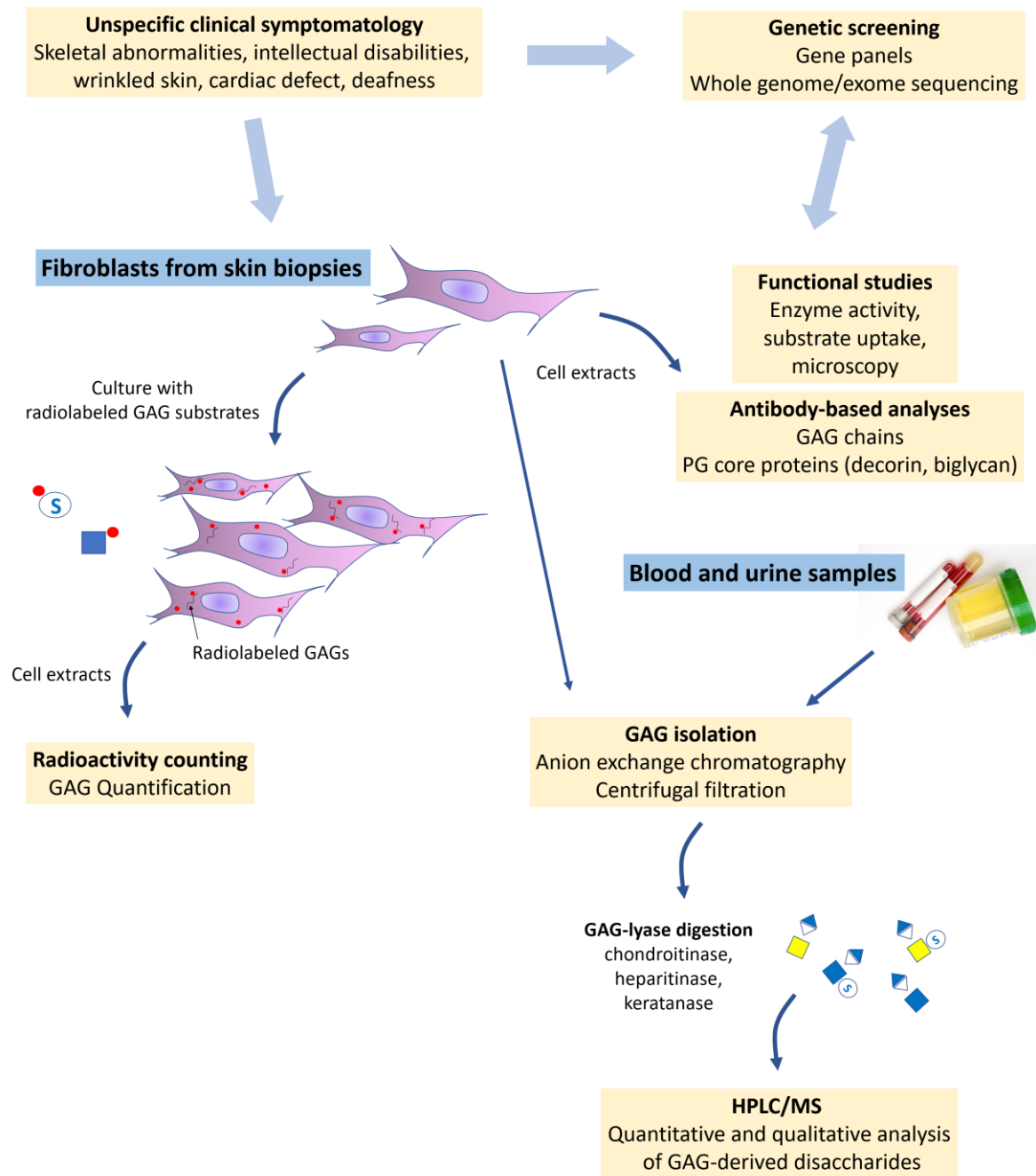


**Figure 7: Schematic of current PG-IMD diagnosis strategy**

Once PG defect is suspected clinically, genetic screening and GAG assessment are performed using patients' samples. Whole genome/exome sequencing allows the identification of possibly pathogenic variants in PG metabolism-associated genes. Fibroblasts from skin biopsies are cultured with radiolabeled substrates and the measured radioactivity in cell extracts reflects PG biosynthesis capacities. Fibroblasts are also used for functional analyses measuring the activity of the suspected defective enzyme or transporter, while microscopy could detect protein mislocalization and/or abnormal Golgi morphology. Antibody-based techniques such as Western blot and flow cytometry are useful for highlighting impaired PG biosynthesis by targeting GAG chains and PG core proteins such as decorin and biglycan. As from blood and urine, GAGs could be assessed by analyzing purified and enzymatically released disaccharides using HPLC/MS. Altogether, these laboratory analyses either orient towards a genetic deficiency or confirm the causality of the suspected gene variant.



Fibroblasts are also convenient cells for functional biochemical analyses to highlight loss of function resulting from the suspected gene variant. Indeed, decreased enzymatic activities were shown for XylT-2 (143),  $\beta$ 4GalT7 (192), and GlcAT-I (145) in patients' fibroblasts. In the case of defective UDP-sugar transporters, substrate uptake assays can be performed as shown in SLC35A3 mutated patient fibroblasts with reduced UDP-GlcNAc transport (167). Additionally, observations of the Golgi apparatus using electron and/or fluorescence microscopy can highlight morphological alterations, impaired anterograde/retrograde trafficking balance, and the mislocalization of enzymes and transporters involved in PG biosynthesis such as in COG4 deficiency (176) (**Figure 7**). Less commonly, blood and urine can be used to quantify total GAG levels. Purification steps involving anion exchange chromatography and desalting allow the isolation of GAGs, which are further digested using GAG lyases (**Figure 7**). GAG disaccharide composition and sulfation degree can then be analyzed using HPLC or MS as it has been performed for patients with EXT1 and EXT2 deficiency where HS-related disaccharide plasma levels were decreased compared to controls (208). Blood and urine samples can also be already treated with GAG lyases and applied to a centrifugal filter before analyzing GAG disaccharide containing filtrate by HPLC/MS. This technique showed decreased HS serum levels in EXTL3-deficient cases (206), while major hyposulfation of CS chains was detected in urine from one *CHST3*-mutated patient (156). Regarding PG degradation defects (i.e., MPS), their biochemical diagnosis is mostly based on a colorimetric method using dimethyl-methylene blue, which switches to purple when mixed with urine samples containing increased GAG concentrations. Qualitative GAG analyses from blood and urine are also performed using HPLC/MS to determine the defective GAG catabolic step (253).

The above biochemical techniques are time-consuming and often require complex technical handling and expensive material. Skin biopsies are invasive, especially for young

children. Moreover, in vitro primary culture of skin fibroblasts can trigger phenotype changes and bias or affect the reproducibility of the results. Additionally, cell cultures are vulnerable to microbial and mycoplasma contaminations and thus need skilled personnel able to ensure cautious handling for long-term cell viability. Blood and urine constitute more affordable biological material with easy sampling and storage. However, the complexity of blood composition and the presence of high amounts of salts in urine can hinder the following HPLC and/or MS analyses of the PG and/or GAG content. Therefore, some preliminary purification and desalting steps are frequently required (208).

#### **I-4-2 Potential diagnostic value of serum bikunin**

Regarding the current lack of rapid and simple routine analyses for the screening/diagnosis of PG biosynthesis defects, the discovery and development of new blood and/or urine biomarkers are mandatory. In this context we focused on the development of a biochemical test based on the analysis of a blood biomarker. We searched for a circulating PG that could be affected during PG-IMD and our attention was drawn to a family of CS-type PG having a common core protein called bikunin (Bkn) and present in the blood at high levels. We therefore purchased an antibody directed toward the core protein Bkn to analyze its electrophoretic profiles using classical Western blot and two-dimensional electrophoresis (2-DE) in patients by comparison to representative healthy individuals.

In the following sections, we describe the biosynthesis, the structure, and roles of Bkn. Afterwards we present the work undertaken to evaluate the reliability of serum Bkn as a convenient blood biomarker of PG-IMD. The main results are presented as published articles. Additionally, we provide still unpublished supplementary data.

## Chapter 2:

# Bikunin proteoglycan isoforms



## II.1 Introduction

Bikunin (Bkn) is a protein mainly synthesized by the liver (254,255). Besides its presence in the free state in serum, Bkn constitutes the core protein of a group of original CS PGs known as the inter- $\alpha$ -trypsin inhibitor proteins (IAIP) (256,257). This group contains three isoforms i.e., one light form called Urinary-trypsin inhibitor (UTI) corresponding to Bkn linked to a CS chain (Bkn-CS), and two heavy forms named Pro- $\alpha$ -trypsin inhibitor (PaI) and Inter- $\alpha$ -trypsin inhibitor (ITI) where the CS chain is esterified by respectively one or two glycoproteins named “heavy chains” proteins (HCs). The biosynthesis of PaI and ITI then involves separate biosynthetic pathways for the core protein and the HCs before their linkage *via* the CS chain (258).

Bikunin isoforms are secreted by hepatocytes into the blood in high amounts. ITI and PaI, consisting of 98% of blood Bkn isoforms, have concentrations ranging from 25 to 700 mg/L while UTI and free Bkn do not exceed 4 mg/L in healthy individuals (259,260). In urine, UTI, is present at levels ranging from 2 to 10 mg/L (261). However, these serum and urine levels could be markedly changed in various pathological situations such as in sepsis and cancer (262,263).

## II.2. Bikunin proteoglycans: Genes, expression, and regulation

### II.2.1. AMBP gene

The Bkn core protein is encoded by the  $\alpha$ 1-microglobulin-bikunin-precursor (*AMBP*) gene located in the chromosome 9 q32-33 (**Figure 8**) (264). This gene also codes for  $\alpha$ 1-microglobulin (A1MG), a serum protein belonging to the lipocalin family (265). A1MG and Bkn gene-coding regions are separated by a large intronic sequence (7kb) suggesting that *AMBP* results from the fusion of two ancestral genes (266). This fusion led to a very conserved

sequence between human, fishes, pig and rodents (267). The *AMBP* gene is composed of 10 exons and 9 introns (268). *A1MG* is encoded by exons 1 to 6 and *Bkn* by exons 7 to 10. The initiation of the transcription is modulated by *cis*-regulatory elements (269). In addition, many transcription factors are recruited to bind enhancing sequences modulating the tissue-gene expression. In this respect, the 5' flanking region contains a strong liver-specific enhancer with binding sites for hepatocyte nuclear factors (HNF 1-4) (**Figure 8**). Thus, *AMBP* is mostly expressed by the liver (270). However, a local production of *Bkn* isoforms has also been observed in chondrocytes, lung, pancreas, kidney, brain, stomach, epidermis and testis (271–274). In pathology, abnormal expression could be found in other tissues such as kidney in the context of calcium-oxalate stone formation (urolithiasis) (275). In vitro experiments showed an increase of HNF-4 mediated *AMBP* expression in pig kidney epithelial (LLC-PK1) cells under oxalate exposure (276). Moreover, the presence of a binding sites for inflammatory cytokines interleukine-6 (IL-6) and tumor necrosis factor (TNF) in the promoter region suggests modulation of *AMBP* expression during inflammation (268).

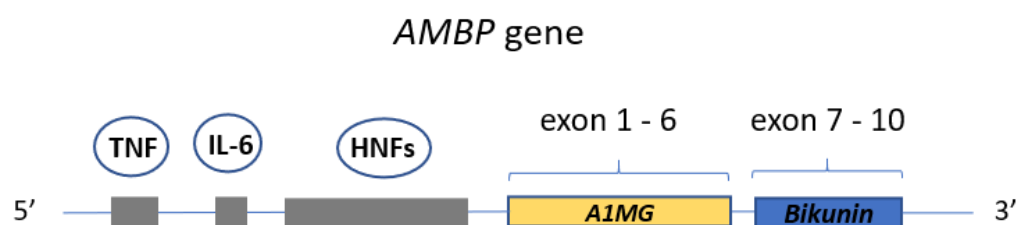


**Figure 8: Schematic of *AMBP* gene and its 5' promoter region containing HNF, IL-6 and TNF binding sites**

### II.2.2. *ITIH1*, *ITIH2* and *ITIH3* genes

There are three HC proteins i.e., HC1, HC2 and HC3 encoded by *ITIH1*, *ITIH2* and *ITIH3* respectively. While *ITIH1* and *ITIH3* genes are located in close proximity on chromosome 3p21.1-21.2, *ITIH2* is located on chromosome 10p14-15 (277,278). The three *ITIHs* genes share high sequence homologies indicating the occurrence of ancient duplications from a common

ancestor gene (279,280). The promoter region contains binding sites for HNFs triggering liver expression (281,282) (**Figure 9**).

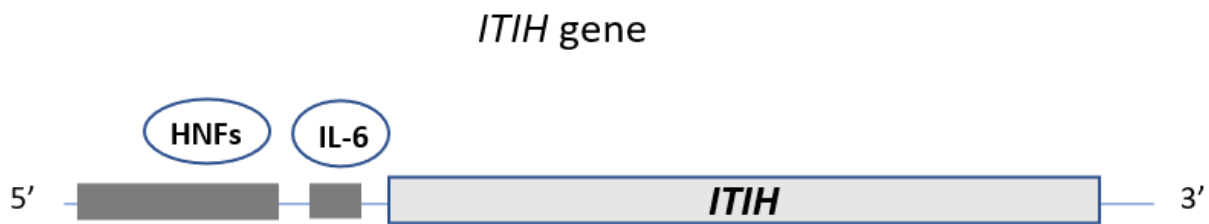


**Figure 9: Schematic of an *ITIH* gene and its 5' promoter regions containing HNF and IL-6 binding sites**

A synchronous increase of the liver expression of *ITIHs* and *AMBP* genes during the first week of life has been shown in mouse (283). The *ITIHs* genes are also expressed in other tissues such as lung, skin and cartilage (273). Furthermore, their promoter regions contain IL-6 binding sites, which could act as both activators and inhibitors of the gene expression during inflammatory episodes. Indeed, while *ITIH2* is down-regulated during inflammation, *ITIH3* is up-regulated and *ITIH1* is not affected (284). Considering that the three genes originate from a same ancestor, this differential behavior is quite surprising and deserves to be better understood. Otherwise, it has been shown that the *ITIHs genes* expression was down-regulated in various cancers suggesting that they could be putative tumor suppressor genes (263).

## II.3. Synthesis, structure, and post-translational modifications of bikunin core protein

### II.3.1. From AMBP precursor to inter- $\alpha$ -trypsin inhibitor

In liver cells, the transcription and translation of the *AMBP* gene generate the AMBP precursor protein containing a signal peptide of 19 aa followed by A1MG and Bkn protein sequences separated by a tetrapeptide (Arg-Ala-Arg-Arg) (**Figure 10**) (285). The Bkn sequence of the uncleaved AMBP precursor protein then subsequently undergoes different post-translational modifications including *N*-glycosylation on Asn45, CS elongation on Ser10 followed by CS-HC esterification (**Figure 10 and Figure 11**) (255). Toledo and al (286) also suggested a mucin type *O*-glycosylation site on Thr17.

These reactions sequentially occur in the ER and Golgi compartments along the secretory pathway (**Figure 10**). When the modified AMBP precursor reaches the TGN and the secretory vesicles, A1MG and Bkn proteins are separated through a furin-like cleavage reaction at the C-terminal end of the connecting tetrapeptide (287) (**Figure 10**). From that step, A1MG and Bkn proteins will continue their maturation and will be separately secreted (288). To date, no functional or structural relationship between A1MG and Bkn was clearly established. Recently, it has been suggested that the A1MG part of the AMBP precursor participates in the maturation of Bkn with A1MG possibly acting as a chaperone involved in the formation of correct disulfide bridges and folding of Bkn (289).



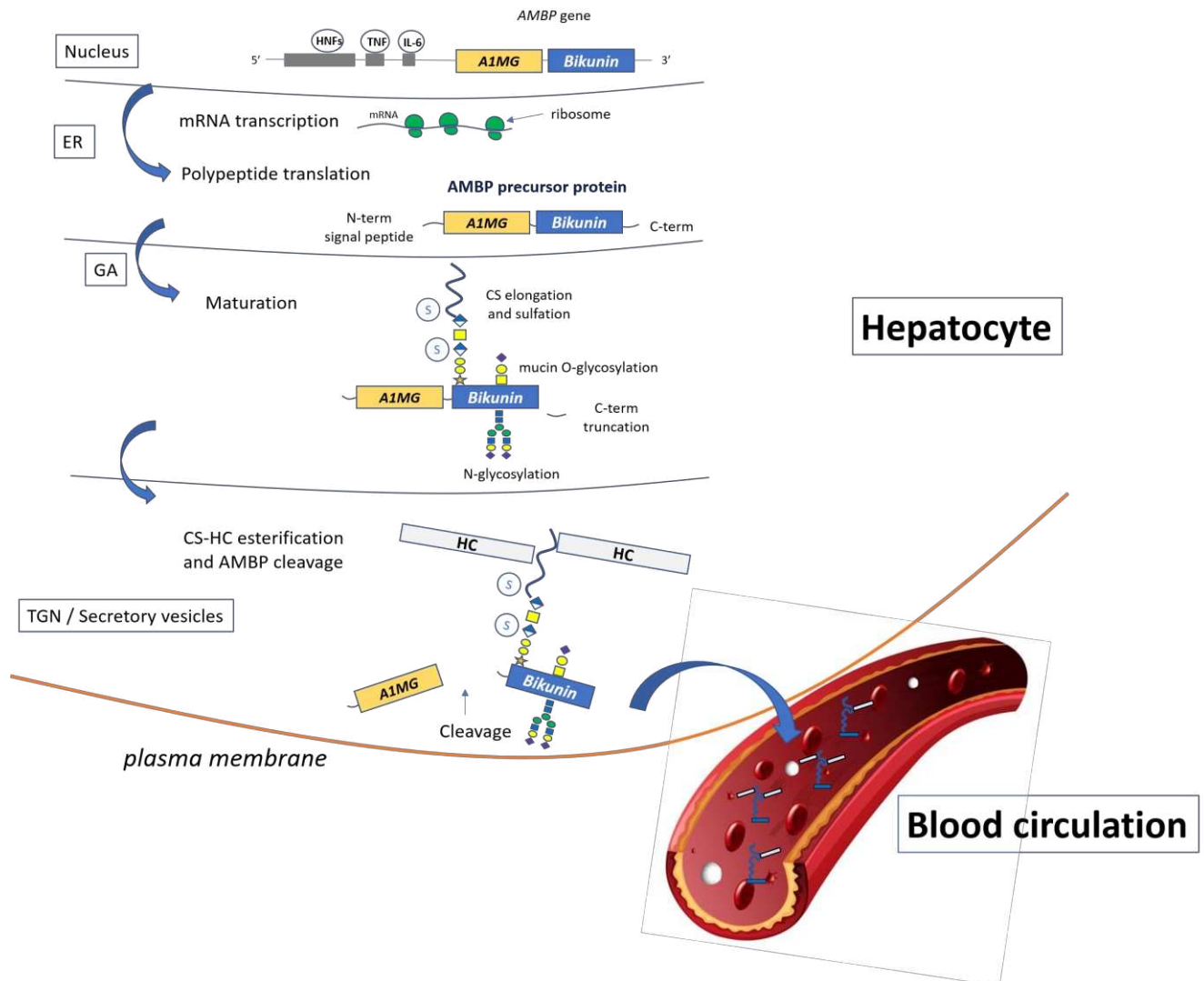


**Figure 10: Biosynthesis of inter- $\alpha$ -trypsin inhibitor (ITI) from the AMBP gene to the mature proteoglycan**

The DNA to mRNA transcription of the *AMBP* gene is regulated by transcription factors including HNFs, TNF and IL-6. The translation in the ER gives rise to the AMBP precursor protein that is transported to the Golgi and undergoes the CS elongation and *N*-glycosylation. In the TGN, Bkn-CS is esterified by one or two HC glycoproteins, followed by the A1MG release by furin-like mediated cleavage reaction. The mature ITI is then transported through secretory vesicles to the plasma membrane for secretion.

### II.3.2. Polypeptide structure and modifications of bikunin core protein

The Bkn part of the translated AMBP precursor polypeptide chain consists in 143 aa (290). The aa content of the polypeptide chain is a determinant signal for the following post-translational modifications and for the functions of the Bkn core protein. The Ser10 is preceded by acidic aa and followed by Gly residues (**Figure 11**). This promotes the initiating O-xylosylation and CS chain elongation. Another consensus aa sequence in the Bkn polypeptide

is the Asn-X-Thr involved in *N*-glycosylation. Thus, the amide group of the Asn45 is linked to the first GlcNAc of a typical biantennary *N*-glycan chain with contradictory findings concerning its terminal sialylation level. Indeed, whereas various sialylation degrees (i.e., 2, 1 and 0 terminal sialic acid) has been first highlighted (291), a 100% bi-sialylated *N*-glycan chain has been suggested otherwise (292). The Bkn polypeptide is also subjected to folding with the formation of three disulfide bridges during the biosynthetic pathway (**Figure 11**).

The inhibitory activity of Bkn PGs towards proteases such as trypsin or leucocyte elastase is assigned to the two “Kunitz” domains (KD) of the core protein. The interactions of the KD with trypsin have been studied using crystallography which exhibited Met36 and Arg92 as protease recognition sites (293). The Bkn core protein also exerts an inhibitory activity toward calcium oxalate (CaOx) stone formation in urinary tracts (294). It has been suggested that the positively charged Arg88, Arg92, Lys104 and Lys106 could bind the oxalate anions therefore preventing the formation of CaOx crystals.



inflammatory diseases, the CS chain size could increase proportionally to the inflammation severity and reach up to 27 disaccharide motifs (301).

#### **II.4.2. Modifications of the bikunin-linked CS chain**

As mentioned above (I-2-1), the first Xyl carried by Bkn should undergo transient 2-O-phosphorylation (after the addition of the first Gal) with the phosphate removal before the [GlcA-GalNAc] polymerization. Therefore, this modification is expected to be absent in the secreted isoforms of Bkn PGs. However, a Xyl phosphorylation has been reported at weak intensity in Bkn-CS from human urine together with the presence of fucosylated Xyl (302). This modified Xyl could potentially have a biological relevance in urine since neither Xyl phosphorylation nor fucosylation have been detected in serum Bkn. Always according to these authors, in both serum and urine, the first Gal of the linkage region could bear a sialic acid, but its biological relevance has not been clarified. Concerning the second Gal, a sulfate is present on C-4 position and is uniformly detectable in serum and urinary Bkn (303,304). However, it has not been established whether this sulfation occurs during or after the biosynthesis of the linkage region. Sugumaran and al. (305) showed, using microsomal preparations from mouse mastocytoma cells, that the CS chain is sulfated while it is still actively growing and stated that sulfotransferases are in proximity with the polymerizing glycosyltransferases in the Golgi membrane. Besides Gal sulfation, sulfate groups are C-4-branched on various GalNAc residues of the Bkn CS chain with sulfation pattern being organized in a cluster of 4 to 7 sulfated GalNAc nearby the linkage region (*i.e.*, the proximal end) (298,306,307). In contrast, the remaining GalNAc and GlcA residues composing the distal end of the Bkn CS chain do not carry any modification. This unsulfated end constitutes the domain for the following HC ester linkages.

## II.5. The Heavy Chains proteins (HCs)

### II.5.1. Biosynthesis and post-translational modifications of the HCs

The transcription and translation of the *ITIH* genes result in the formation of precursor polypeptides called proHCs (**Figure 12**). They consist of a N-terminal pro-peptide followed by the future mature polypeptide and a large C-terminal extension (CTX). The size of these segments is variable according to the HC (308). A cleavage between a Pro and Arg residue occurs in the ER, via the action of a furin transiting from the Golgi, to release the N-term pro-peptide (**Figure 12**) (309).

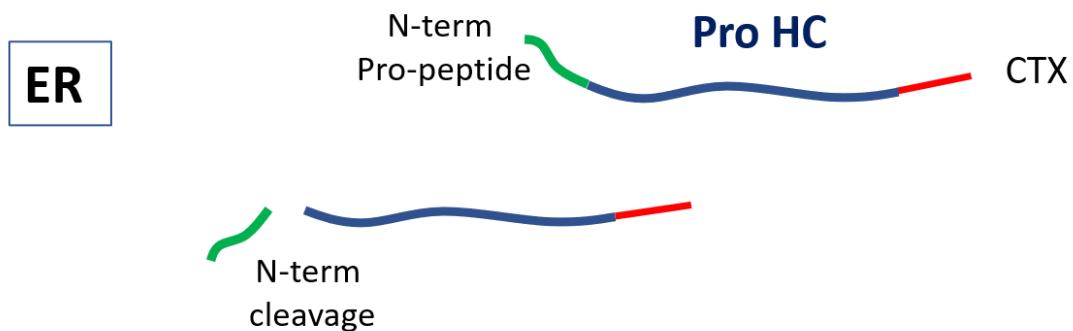


**Figure 12: Schematic structure of heavy chain precursor Pro HC and N-terminal cleavage**

During their transit from the ER to the *medial/trans*-Golgi, the proHCs undergo glycosylation reactions with different patterns according to the HC (**Figure 13**). HC1 is modified by a bi-antennary *N*-glycan and a mucin core 1 *O*-glycan while HC2 displays one *N*-glycan and a cluster of four mucin core 1 *O*-glycans at the C-term region. HC3 is modified by two *N*-glycans (310,311). Additionally, the proHCs are folded through the formation of disulfide bridges (312) (**Figure 13**). Glycosylated proHCs are then transported with their CTX until the *trans*-Golgi/TGN compartments. The CTX removal is then mediated through the more acidic pH of these compartments which triggers an autocatalytic cleavage via an intramolecular reaction between an Asp and a Pro (313).

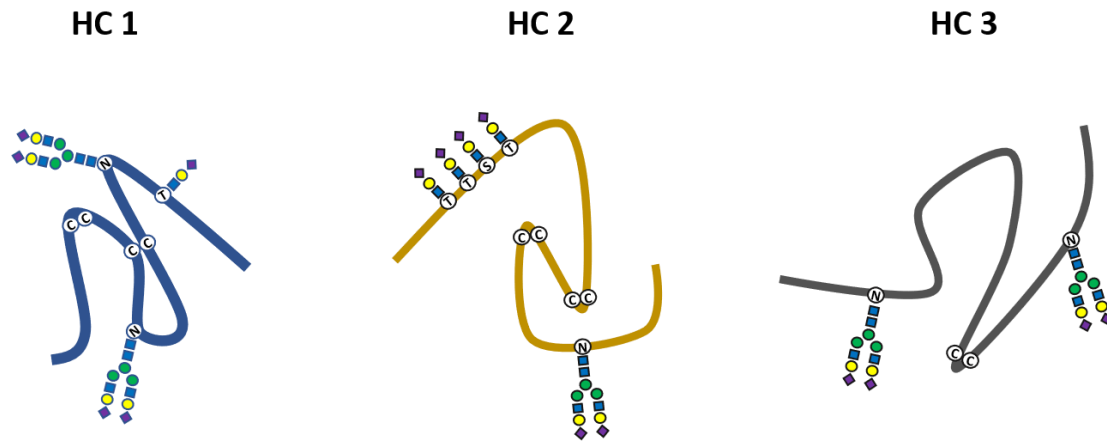


**Figure 13: Heavy chain proteins glycosylation pattern**

### II.5.2. Linkage of the HCs to the AMBP precursor via the CS chain

The coupling between HCs and the AMBP precursor through the CS chain takes place into the *trans*-Golgi/TGN and corresponds to an unusual post-translational modification called “protein-GAG-protein (PGP)” cross-link (314). It consists of an esterification reaction occurring between the Asp exposed after the CTX cleavage and the C-6 of a GalNAc residue of the CS chain at the unsulfated region (**Figure 14 and Figure 15**) (315).

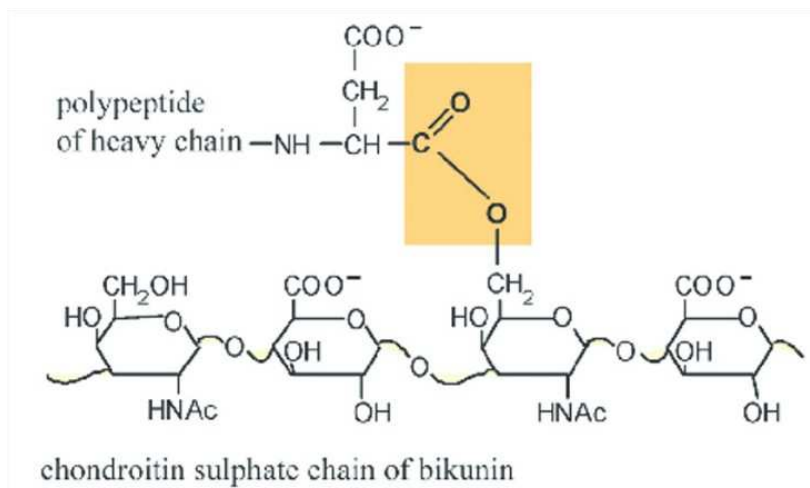


**Figure 14: Structure of the Asp-GalNAc link between heavy chains and the chondroitin sulfate chain of bikunin.** From Fries et al. 2003 (316)

After the C-terminal cleavage of the proHCs, the CTX remains associated to the mature HCs through an unclear interaction that is required for the following esterification reaction(s) with the CS chain (**Figure 15**). In COS-1 cells, Kaczmarczyk and al (258) showed that mutation of the His<sup>649</sup> close to the CTX cleavage site of proHC3 compromised the HC-CS coupling reaction. Given that this His is comprised into a conserved sequence in the three proHCs, it could be required for the PGP cross linkage. The authors suggested that the opposite charges of the His and the CS chain at the *trans*-Golgi pH may promote an initial HC-CS interaction before the esterification reaction itself and the complete release of the CTX. The HC-CS esterification takes place while AMBP precursor is not yet cleaved. However, it has been shown that the HC linkage is efficient even upon a free CS chain suggesting that neither A1MG, nor Bkn polypeptide are necessary for the HC-CS esterification (258). Therefore, the determining factors of the HC-CS esterification may be strictly afforded to the HCs, the CS chain, and the environment of the *trans*-Golgi (i.e., unsulfated GalNAc of the CS chain, conserved sequence at the cleavage site of the proHCs and acidic pH of the *trans*-Golgi/TGN).

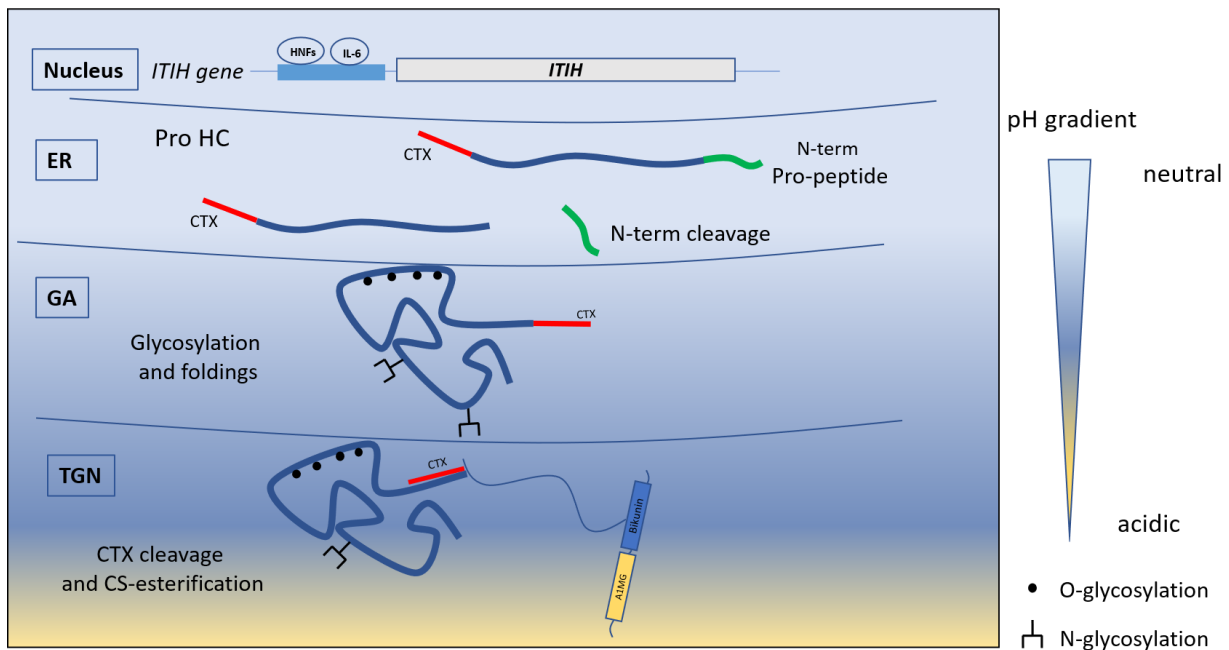


### Figure 15: HC biosynthesis and coupling with the CS chain of bikunin

*ITIHs* genes transcription is under the control of HNFs and IL-6 transcription factors. The mRNA translation gives rise to precursor proteins (i.e., proHCs) carrying N-term pro-peptide and C-term extension. HC maturation includes N-term cleavage in the ER, glycosylation and folding in the Golgi and CTX cleavage together with ester linkage to Bkn-CS in the TGN.

The formation of ITI occurs when both HC1 and HC2 are linked to the CS chain (Figure 16). It has been shown that in all ITI molecules, HC2 is positioned towards the reducing (proximal) end of the CS chain while HC1 is positioned towards the non-reducing (distal) end (292). Additionally, HC1 and HC2 are positioned very close to each other, even at adjacent GalNAc residues (286). The linkage of HC3 to the CS chain gives rise to P $\alpha$ I, and no form containing HC1 and HC3, or HC2 and HC3 has been detected. The mechanisms of these CS-HC cross linkages remain unclear although the heterogeneity in the CS chain size and sulfation pattern, as well as in the HCs polypeptide sequences, could play a role.





## II-6- Roles of bikunin isoforms

During pathophysiological processes inducing increases of the vascular permeability such as inflammation and ovulation, ITI and P $\alpha$ I are extravasated to the ECMs and their HCs are transferred to hyaluronan (HA) (**Figure 17**) (317–319). This reaction is mediated by the inflammation-associated protein TSG6 and involves two successive reactions (320). A first esterification occurs between the C-term Asp of the HC and TSG6 leading to a TSG6-HC intermediate. Afterwards, HC is attached to HA through an ester bond between its C-term Asp and a GlcNAc residue of HA (**Figure 17**).

The resulting HC-HA complexes, also called SHAP-HA (serum-derived hyaluronan-associated proteins-HA complex) associate with each other to form a SHAP-HA rich matrix (321–323). The latter results in a range of protective such as inhibition of ECM degradation of joints during osteoarthritis (324), sequestration and inactivation of leucocytes during sepsis (325), and protection of oocytes and amniotic membrane during ovulation and fetal development, respectively (318). Additionally, HC transfer to HA releases Bkn-CS which mediates anti-protease activity through Bkn core protein kunitz domains, thereby contributing to the tissue protection through the inhibition of inflammation-associated proteases (326) (**Figure 17**). Otherwise, the HCs have been shown to promote wound healing after injury by promoting binding of HA to vitronectin, an ECM glycoprotein promoting cell adhesion and migration (327). Moreover, HCs were found to have inhibitory activity towards the complement activation, thereby attenuating inflammation (328). Finally, as already mentioned (I-3-2) the Bkn core protein is known for its protective effects against kidney stones through inhibition of calcium oxalate crystallization.

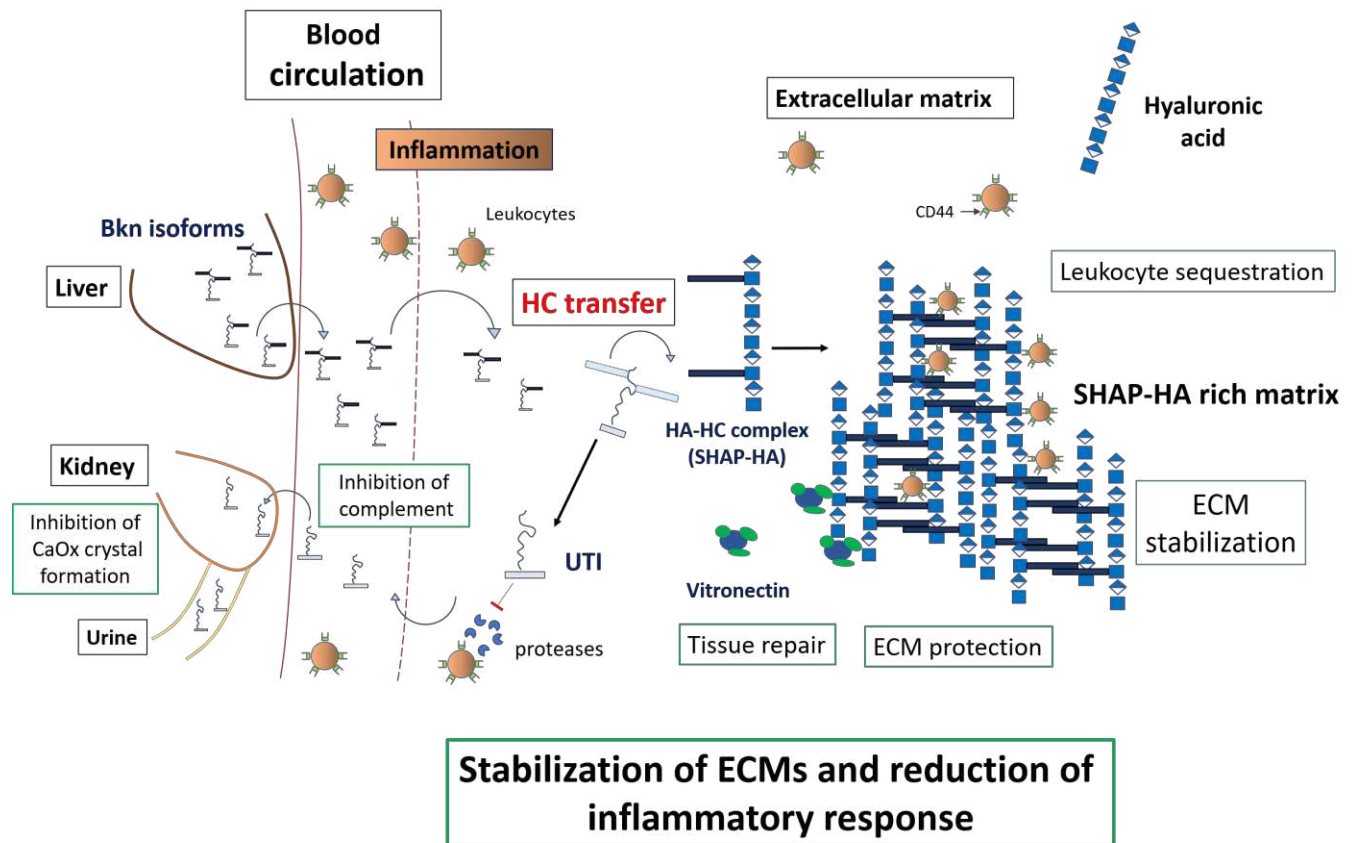


**Figure 17: Schematic overview of bikunin isoforms roles during inflammation**

Following inflammatory stimuli, the circulating heavy Bkn isoforms are extravasated to the ECM where they transfer their HC to HA which forms the SHAP-HA complexes. This leads to protective effects against ECM degradation. The SHAP-HA rich matrix has a high affinity for leukocytes which results in their sequestration and inactivation. Binding of the HCs to vitronectin promotes cell adhesion and migration for tissue repair. The transfer of the HCs to HA and vitronectin releases the UTI that inhibits leukocytes proteases through the Bkn core protein. Bkn isoforms in the intravascular compartment also inhibit the complement cascade triggered during inflammation. In the kidney, Bkn core protein has an inhibitory activity towards crystal calcium oxalate (CaOx) formation which protects against urolithiasis.



## Chapter 3:

# Bikunin analyses in PG-IMD and CDG with impaired Golgi homeostasis



### III-1 Introduction

In this chapter, we present serum Bkn analyses we performed in the blood samples from various affected individuals presenting with PG-IMD and CDG with impaired Golgi homeostasis. The first results have been published through a letter to the editor entitled “Serum bikunin is a biomarker of linkeropathies” in *Clinica Chimica Acta* (2018). We showed that simple Western blot analysis of Bkn-CS allows the rapid screening of linkeropathies by highlighting defective linker formation through the presence of abnormal Bkn light forms.

Secondly, we used two-dimensional electrophoresis (2-DE) to better characterize the encountered abnormal Bkn light forms in linkeropathies and highlighted potential signature patterns. The results have been published through an original article entitled “Serum bikunin isoforms in congenital disorders of glycosylation and linkeropathies” in *Journal of inherited metabolic diseases* (2020). In this article, we also present Bkn isoforms analysis in patients presenting with CDG due to impaired Golgi V-ATPase (i.e., ATP6V0A2-CDG, CCDC115-CDG and ATP6AP1-CDG), manganese transporter (i.e., TMEM165-CDG) and defective sugar transporters (i.e., SLC35A2- and SLC35A3-CDG). We showed specific abnormal patterns suggesting potential of Bkn as an additional biomarker of these inherited glycosylation-related diseases.

The third presented original article, published in *Clinica Chimica Acta* (2021), includes serum Bkn analysis in the diagnosis pathway of a recently characterized CDG resulting from defective glucose-6-phosphate transporter (i.e., SLC37A4-CDG). Consistently with previously demonstrated Golgi acidification defects in this CDG, we showed impaired Western blot profiles of Bkn isoforms with potential screening interests.

The last presented publication is a review recently published in the journal *Genes* (2021) and entitled “Inherited proteoglycan biosynthesis defects – Current laboratory tools and bikunin as a promising blood biomarker”. We herein provide an updated short review on the molecular pathways of PG biosynthesis, the pathophysiology of PG-IMD, the current screening strategies, and the benefits of serum Bkn as a promising biomarker.

This chapter also includes yet unpublished results. Mass spectrometry examination of serum Bkn in linkeropathy patients allowed to better characterize observed Bkn abnormal forms. Indeed, we developed a 2-DE-based purification of serum Bkn followed by tryptic digestion and HPLC/MS/MS analyses. Otherwise, in PG-IMD related to GAG sulfation inherited defects (e.g., SLC35B2 and IMPAD1 deficiencies), we showed that 2-DE analysis of chondroitinase-treated serum could present screening interests. Lastly, we developed Bkn analysis from hemoglobin-depleted samples from dried blood spots, with encouraging results for future applications in the screening of PG-IMD.



## III-2 Publication 1

### Letter to the Editor

#### Serum bikunin is a biomarker of linkeropathies

Bruneel A, Dubail J, Roseau C, Prada P, **Haouari W**, Huber C, Dupré T, Poüs

C, Cormier-Daire V, Seta N

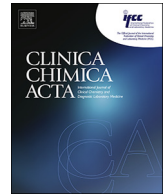
Clin Chim Acta. 2018, 485:178-180. doi: 10.1016/j.cca.2018.06.044.



### III-2-1 Summary of the letter to the Editor

This letter represents our initiating work and has been the “springboard” of our project since we showed, for the first time, the high potential of Bkn analysis for the screening of PG biosynthesis defects. In this short article, we briefly introduce the biosynthesis of PGs by focusing on the involvement of *XYLT1/2*, *B4GALT7*, *B3GALT6* and *B3GAT3* for the formation of the tetrasaccharide linkage region. Then, we highlight the problematic of linkeropathies at the clinical and diagnosis level, pointing out the severity of the skeletal manifestations and the difficulties of their screening. In this way, we promote Bkn as a serious biomarker candidate given its relevant structure and the possibility of a convenient Western blot analysis in patients’ serum. In support of these arguments, we provide the result of a Western blot analysis in the serum from linkeropathy patients as well as one individual with a pathogenic variant in ChSy-1 encoding gene. The analysis also included one CDG patient with defective PMM2 (phosphomannomutase 2) which is an enzyme involved in an early step of *N*-glycosylation process, one SLC35A2-CDG case, and one affected individual with mutation in the sulfate transporter encoding gene *SLC35B2*.





## Letter to the editor

## Serum bikunin is a biomarker of linkeropathies



## ARTICLE INFO

## Keywords:

Bikunin  
Biomarker  
CDG  
Glycosaminoglycans  
Linkeropathies  
Proteoglycans

Proteoglycans (PGs) are major components of extracellular matrices (ECM) and cell surfaces playing pivotal roles in cell interactions, cellular proliferation, ECM organization, cancer metastasis and immune responses. They are composed of a core protein linked to a glycosaminoglycan (GAG) chain starting by the common tetrasaccharide Xylose-Galactose-Galactose-Glucuronic Acid (Xyl-Gal-Gal-GlcA) further elongated by sulfated repeating disaccharide motif. Depending on this motif, chondroitin sulfate (CS), heparan sulfate and dermatan sulfate can be differentiated. Inherited defects in genes encoding for enzymes successively involved in the synthesis of the common tetrasaccharide linker, i.e., xylosyltransferases (XYLT1 or XYLT2), galactosyltransferases (B4GALT7 and B3GALT6) and glucuronyltransferase (B3GAT3), have been grouped as “linkeropathies” diseases. The clinical symptoms of linkeropathies are rather heterogeneous and notably share short stature, chondrodysplasia with multiple joint dislocations, fractures, developmental retardation and hypotonia [1]. When considering the very low prevalence of these diseases and the current absence of convenient blood screening test, there is a need for biomarkers of linkeropathies orientating their diagnosis and avoiding difficult and time-consuming biochemical/genetic investigations.

Our purpose was to evaluate the potentials of serum bikunin as a biomarker of linkeropathies. Bikunin is a circulating liver PG corresponding to a CS GAG chain (15 +/- 3 GlcNAc-GlcA sulfated disaccharide units) linked to a core protein, namely the free bikunin protein (fBkn; ~20 kDa), via the tetrasaccharide linker. Furthermore, as a unique feature of serum bikunin, the CS chain is mostly (> 98%) esterified by 1 or 2 glycoprotein(s) called “heavy chains” (HC). The main reported role of HC-linked bikunin isoforms would be, once extravasated from the blood, to exchange HC with hyaluronic acid notably leading to ECM stabilization [2]. Given the availability of an efficient polyclonal antibody (see figure legend for technical details), we

undertook the Western-blot detection of fBkn (~20 kDa) and of Bkn-CS (~35 kDa) in 20-fold diluted sera from patients with mutations in *XYLT1*, *B4GALT7*, *B3GALT6* and *B3GAT3* as well as with mutations in *CHSY1* (encoding chondroitin sulfate synthase 1) [3], *PMM2* (phosphomannomutase 2), a sulfate transporter encoding gene (unpublished data) and *SLC35A2* (Golgi galactose transporter) [4].

As shown Fig.1, Western-blot duplicate analysis of one representative control serum showed one large and marked band (35 +/- 2 kDa) corresponding to bikunin linked to heterogeneous CS chain (Bkn-CS) as well as one minority band at 22 kDa corresponding to light free bikunin (fBkn). The analysis of 12 control sera further showed that Bkn-CS Mw landmarks ranged between 30 kDa and 45 kDa (Supplementary file). Profile of the serum from *XYLT1* mutated patient appeared similar to controls. By contrast, those from other patients with linkeropathies (*B4GALT7*, *B3GALT6* and *B3GAT3*) showed marked % increase of light bikunin forms with average Mw rising from ~23 kDa to ~25 kDa. Since *XYLT1* is not expressed in the liver [5], normal profile was not surprising in the related mutated case. For other linkeropathies, it should be suggested that observed abnormal accumulating light forms of bikunin from *B4GALT7*, *B3GALT6* and *B3GAT3* mutated patients mainly respectively correspond to Bkn-Xyl, Bkn-Xyl-Gal and Bkn-Xyl-Gal-Gal, in agreement with the stepwise action of related enzymes in the tetrasaccharide linker biosynthesis. For the patient with mutations in the *CHSY1* gene encoding for the dual enzyme adding GalNAc-GlcA disaccharide units, the band corresponding to Bkn-CS showed, despite faint staining, decreased average Mw (~31 +/- 2 kDa). Thus, this result is in accordance with a defect in the CS chain elongation. Furthermore, the accumulating bikunin light form of this sample appeared similar to the one of *B3GAT3* mutated patient, suggesting an associated defect in the GlcA addition at the end of the tetrasaccharide linker. As expected given to the small size of sulfate moieties, no abnormality

**Abbreviations:** B3GALT6, Beta-1,3-galactosyltransferase 6; B4GALT7, Beta-1,4-galactosyltransferase 7; B3GAT3, Beta-1,3-glucuronyltransferase 3; Bkn-CS, Bikunin linked to chondroitin sulfate chain; CDG, Congenital disorder of glycosylation; CHSY1, Chondroitin sulfate synthase 1; CS, Chondroitin sulfate; ECM, Extracellular matrix; fBkn, Free bikunin; GAG, Glycosaminoglycan; Gal, Galactose; GlcA, Glucuronic acid; GalNAc, N-Acetylgalactosamine; PG, Proteoglycans; PMM2, Phosphomannomutase 2; Xyl, Xylose; XYLT, Xylosyltransferase

<https://doi.org/10.1016/j.cca.2018.06.044>

Received 27 June 2018; Received in revised form 27 June 2018; Accepted 28 June 2018  
Available online 30 June 2018

0009-8981/ © 2018 Elsevier B.V. All rights reserved.

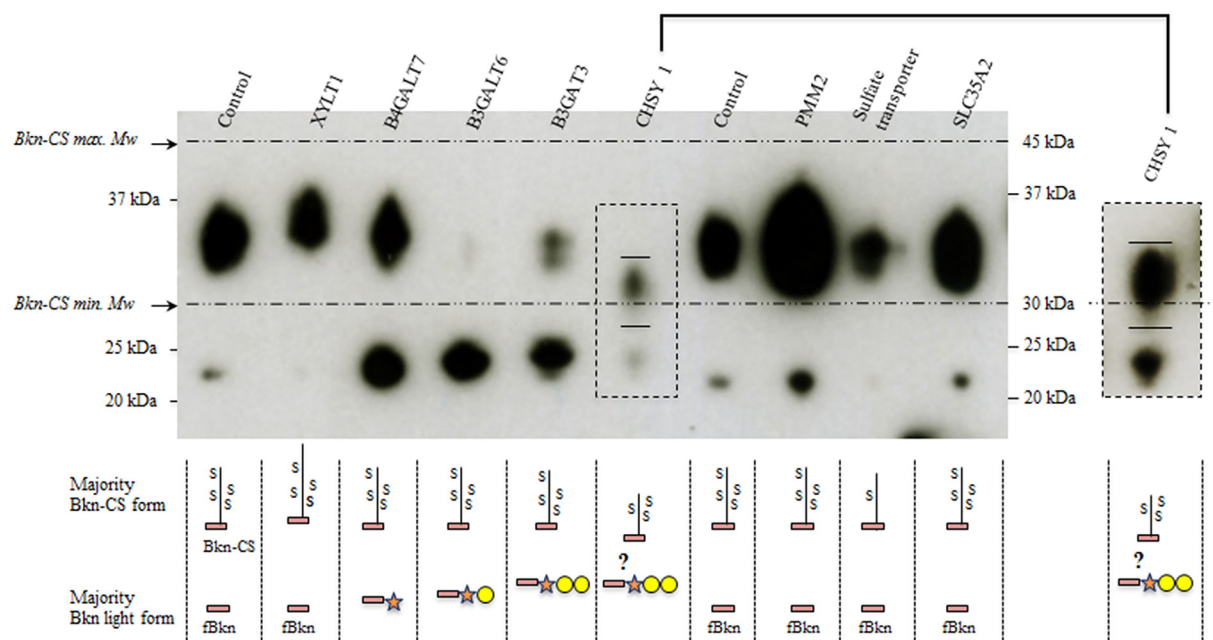


**Fig. 1.** Western-blot analysis of serum bikunin from patients with linkeropathies.

Serum bikunin from following samples (20-fold diluted in water) were analyzed: control, *XYLT1*, *B4GALT7*, *B3GALT6*, *B3GAT3*, *CHSY1*, *PMM2*, sulfate transporter encoding gene and *SLC35A2* mutated patients. PAGE (8  $\mu$ L/well) was conducted using Nu-PAGE 4–12% bis-tris gels as recommended (Novex). After transfer on nitrocellulose (1 h, 100 V) and sheet cutting ( $M_w < 50$  kDa), ECL film revelation was conducted after incubation with rabbit anti-bikunin primary antibodies (Millipore; 1/5000 v/v in TTBS-5% milk) and secondary HRP-linked anti-rabbit antibodies (Cell Signaling technologies; 1/5000 v/v). An additional profile of the *CHSY1* serum (10-fold diluted) is presented (right) for better interpretation. Horizontal dot lines delimitate Bkn-CS  $M_w$  normal range. For each pattern, suspected majority Bkn-CS and light forms are schematized; rectangle, free bikunin (fBkn); line, CS chain; star, xylose; circles: galactose; S, sulfate.

could be evidenced in Bkn-CS from the patient with sulfate transporter encoding gene mutations. Serum of patient with *PMM2* mutations (*PMM2*-CDG), typically associated with partial absence of N-glycans on glycoproteins [6], did not show qualitative bikunin abnormality (even though in higher concentration) in agreement with the specific involvement of phosphomannomutase 2 in GDP-mannose biosynthesis. Although 2 galactose residues are incorporated in the linker tetrasaccharide, bikunin analysis of the *SLC35A2* mutated patient did not show galactosylation defects by contrast with N-glycans and mucin O-glycans abnormalities described elsewhere [7]. This could suggest either insufficient sensitivity of the bikunin analysis in this case or a preferential flux of residual galactose entering into the Golgi towards the synthesis of the PGs tetrasaccharide linker region.

In summary, we showed that, with exception of *XYLT1* mutations, marked % increase of bikunin light form could be specifically associated to linkeropathies with the ability to discriminate between causative mutations. Furthermore, potentially associated  $M_w$  decrease of Bkn-CS could further specifically orientate towards defect in CS GAG chain elongation. Although needing a stronger validation with additional (but very rare) samples, presented results are tightly consistent with related enzymatic defects already heavily suggesting the high potential of bikunin as a specific, simple and useful biomarker of linkeropathies.

## Funding

This work was supported by grant ANR-15RAR3-0004-06 under the frame of E-RARE-3, the ERA-Net for Research on Rare Diseases; it was also supported by the European Union's Horizon 2020 research and innovation program under the ERA-NET cofund action N° 643578.

## Appendix A. Supplementary data

Western-blot analysis of serum bikunin from 12 control patients. Here, serum samples were more concentrated (i.e., 10-fold diluted sera) than in Fig. 1 in order to better determine Bkn-CS  $M_w$  normal range (defined by horizontal dot lines). Supplementary data to this article can be found online at <https://doi.org/10.1016/j.cca.2018.06.044>.

## References

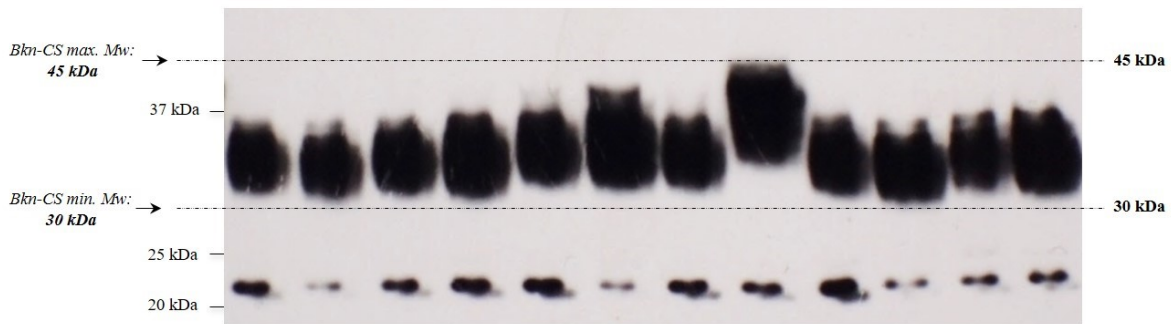
- [1] F. Taylan, O. Makitie, Abnormal proteoglycan synthesis due to gene defects causes skeletal diseases with overlapping phenotypes, *Horm. Metab. Res.* 48 (2016) 745–754.
- [2] L. Zhuo, M. Yoneda, M. Zhao, W. Yingsung, N. Yoshida, Y. Kitagawa, K. Kawamura, T. Suzuki, K. Kimata, Defect in SHAP-hyaluronan complex causes severe female infertility. A study by inactivation of the bikunin gene in mice, *J. Biol. Chem.* 276 (2001) 7693–7696.
- [3] E. Ramza, C. Huber, N. Levin, G. Baujat, C. Bole-Feysot, P. Nitschke, C. Masson, Y. Alanay, Y. A-Gazali, P. Bitoun, O. Boute, P. Campeau, C. Coubes, M. McEntagart, N. Elcioglu,

- L. Faivre, A. Gezirici, D. Johnson, E. Mihci, B.G. Nur, L. Perrin, C. Quelin, P. Terhal, B. Tuysuz, V. Cormier-Daire, Chondrodysplasia with multiple dislocations: comprehensive study of a serie of 30 cases, *Clin. Genet.* 91 (2017) 868–880.
- [4] A. Bruneel, S. Cholet, V. Drouin-Garraud, M.L. Jacquemont, A. Cano, A. Mégarbané, C. Ruel, D. Cheillan, T. Dupré, S. Vuillaumier-Barrot, N. Seta, F. Fenaille, Complementarity of electrophoretic, mass spectrometric and gene sequencing techniques for the diagnosis and characterization of congenital disorders of glycosylation, *Electrophoresis* (Jun 5, 2018), <http://dx.doi.org/10.1002/elps.201800021> (Epub ahead of print).
- [5] C. Roch, J. Kuhn, K. Kleesiek, C. Gotting, Differences in gene expression of human xylosyltransferases and determination of acceptor specificities for various proteoglycans, *Biochem. Biophys. Res. Commun.* 391 (2010) 685–691.
- [6] H. Carchon, E. Van Schaftingen, G. Matthijs, J. Jaeken, Carbohydrate-deficient glycoprotein syndrome type IA (phosphomannomutase-deficiency), *Biochim. Biophys. Acta* 1455 (1999) 155–165.
- [7] B. Xia, W. Zhang, X. Li, R. Jiang, T. Harper, R. Liu, R.D. Cummings, M. He, Serum N-glycan and O-glycan analysis by mass spectrometry for diagnosis of congenital disorders of glycosylation, *Anal. Biochem.* 442 (2013) 178–185.

Arnaud Bruneel<sup>a,b,\*</sup>, Johanne Dubail<sup>c</sup>, Charles Roseau<sup>b</sup>, Pierre Prada<sup>a</sup>,  
Walid Haouari<sup>b</sup>, Céline Huber<sup>c</sup>, Thierry Dupré<sup>a</sup>, Christian Pouïs<sup>b</sup>,  
Valérie Cormier-Daire<sup>c</sup>, Nathalie Seta<sup>a,d</sup>  
<sup>a</sup> *Biochimie Métabolique et Cellulaire, AP-HP, Hôpital Bichat-Claude  
Bernard, Paris, France*  
<sup>b</sup> *INSERM UMR1193 "Mécanismes cellulaires et moléculaires de  
l'adaptation au stress et cancérogène", Université Paris-Sud, Châtenay-  
Malabry, France*  
<sup>c</sup> *Département de Génétique, INSERM UMR1163, Université Paris  
Descartes-Sorbonne Paris Cité, Institut Imagine, AP-HP, Hôpital Necker  
Enfants Malades, Paris, France*  
<sup>d</sup> *Paris Descartes University, France*  
E-mail address: arnaud.bruneel@aphp.fr

\* Corresponding author at: Hôpital Bichat, Biochimie Métabolique et Cellulaire, 46 rue Henri Huchard, 75018 Paris, France.

## Supplementary file



**Supporting file: Western-blot analysis of serum bikunin from 12 control patients**

Here, samples were more concentrated (i.e., 10-fold diluted sera) than in Figure 1 in order to better determine Bkn-CS Mw normal range (defined by horizontal dot lines).



### III-2-2 Concluding remarks and perspectives

In this work, we showed very promising results concerning the potential of serum Bkn analysis to rapidly detect defective PG biosynthesis and, therefore, to screen PG-IMD. Indeed, using a simple and convenient western-blot method in serum from affected individuals, we showed signature profiles in B4GALT7, B3GALT6 and B3GAT3 linkeropathies (i.e., increasing free Bkn MW) as well as in ChSy-1 deficiency (i.e., decreased Bkn-CS MW). The observed profiles indicated the presence of immature Bkn light forms resulting from defective linker formation. Part of the following work aims to identify these abnormal structures to evaluate the reliability of Bkn as a biomarker of linkeropathies. Otherwise, since we found no abnormalities for the individual with mutated *XYLT1* (a gene not expressed by the liver), this work outlined an important limitation consisting of an application of Bkn analysis restricted to PG-IMD arising from liver-expressed defective genes.



## III-3 Publication 2

### Original article

# Serum bikunin isoforms in congenital disorders of glycosylation and linkeropathies

**Haouari W**, Dubail J, Lounis-Ouaras S, Prada P, Bennani R, Roseau C, Huber  
C, Afenjar A, Colin E, Vuillaumier-Barrot S, Seta N, Foulquier F, Poüs C,  
Cormier-Daire V, Bruneel A.

J Inherit Metab Dis. 2020, 43(6):1349-1359. doi: 10.1002/jimd.12291.



### III-3-1 Article presentation


In this original article, we present results of Bkn analysis in various patients displaying PG-IMD and CDG with impaired Golgi homeostasis. We present Western blot profile of all Bkn isoforms in various CDG with impaired Golgi homeostasis including defective V-ATPase proton pump subunits (i.e., ATP6V0A2-CDG, ATP6AP1-CDG, CCDC115-CDG), tethering factors involved in retrograde trafficking (COG5-CDG and COG7-CDG) and manganese transporter (TMEM165-CDG). Individuals with pathogenic variants in UDP-Gal and UDP-GlcNAc transporters (SLC35A2-CDG and SLC35A3-CDG respectively) were also analyzed.

Moreover, in the previously analyzed samples from linkeropathy patients, we provide additional data consisting of 2-DE profiles of abnormal Bkn light forms as well as Western blot of Bkn heavy forms (ITI and P $\alpha$ I). We also performed 2-DE on phosphatase alkaline (ALP)-treated samples that allowed characterization of the phosphorylation state of linkeropathy-associated abnormal forms.

Following this article, we present unpublished data consisting of (i) Western blot of serum Bkn in patients with defective ATP6V1F (subunit of the Golgi V-ATPase) and 2-DE analyses in samples from TMEM165-CDG and ChSy-1 deficiency, (ii) mass spectrometry analyses in B4GALT7-deficient patient to precisely identify the encountered abnormal Bkn light forms (iii) Western blot and 2-DE of serum Bkn in patients with PG-IMD due to sulfation defects (SLC35B2 and IMPAD1 deficiencies), and (iv) the development of Bkn analysis from dried blood spots (DBS).



# Serum bikunin isoforms in congenital disorders of glycosylation and linkeropathies

Walid Haouari<sup>1</sup> | Johanne Dubail<sup>2</sup> | Samra Lounis-Ouaras<sup>1,3</sup> | Pierre Prada<sup>4</sup> | Rizk Bennani<sup>4</sup> | Charles Roseau<sup>1</sup> | Céline Huber<sup>2</sup> | Alexandra Afenjar<sup>5</sup> | Estelle Colin<sup>6,7</sup> | Sandrine Vuillaumier-Barrot<sup>4</sup> | Nathalie Seta<sup>4,8</sup> | François Foulquier<sup>9</sup> | Christian Poüs<sup>1,3</sup> | Valérie Cormier-Daire<sup>2</sup> | Arnaud Bruneel<sup>1,4</sup> 

<sup>1</sup>INSERM UMR1193, Université Paris-Saclay, Châtenay-Malabry, France

<sup>2</sup>Department of Clinical Genetics and Reference Centre for Constitutional Bone Diseases, INSERM U1163, Université de Paris, Imagine Institute, Necker-Enfants Malades Hospital, AP-HP, Paris, France

<sup>3</sup>AP-HP, Biochimie-Hormonologie, Hôpital Antoine Bécclère, Clamart, France

<sup>4</sup>AP-HP, Biochimie Métabolique et Cellulaire, Hôpital Bichat-Claude Bernard, Paris, France

<sup>5</sup>Département de Génétique et Embryologie Médicale, Sorbonne Universités, Centre de Référence Malformations et Maladies Congénitales du Cervelet et Déficiences Intellectuelles de Causes Rares, Hôpital Trousseau, AP-HP, Paris, France

<sup>6</sup>Department of Biochemistry and Genetics, University Hospital, Angers, France

<sup>7</sup>MitoLab Team, Institut MitoVasc, UMR CNRS6015, INSERM U1083, Angers, France

<sup>8</sup>Université de Paris, Paris, France

<sup>9</sup>Université de Lille, CNRS, UMR 8576 – UGSF - Unité de Glycobiologie Structurale et Fonctionnelle, Lille, France

## Correspondence

Arnaud Bruneel, INSERM UMR1193, "Mécanismes Cellulaires et Moléculaires de l'Adaptation au Stress et Cancérogenèse," Faculté de Pharmacie de Châtenay-Malabry, Tour D4, 1er étage, 5 rue Jean Baptiste Clément, 92220 Châtenay-Malabry, France.  
Email: arnaud.bruneel@aphp.fr

**Communicating Editor:** Ron A Wevers

## Funding information

Agence Nationale de la Recherche, Grant/Award Number: 15RAR3-0004-06; European Union's Horizon 2020 Research and Innovation Program, Grant/Award Number: 643578

## Abstract

Bikunin (Bkn) isoforms are serum chondroitin sulfate (CS) proteoglycans synthesized by the liver. They include two light forms, that is, the Bkn core protein and the Bkn linked to the CS chain (urinary trypsin inhibitor [UTI]), and two heavy forms, that is, pro- $\alpha$ -trypsin inhibitor and inter- $\alpha$ -trypsin inhibitor, corresponding to UTI esterified by one or two heavy chains glycoproteins, respectively. We previously showed that the Western-blot analysis of the light forms could allow the fast and easy detection of patients with linkeropathy, deficient in enzymes involved in the synthesis of the initial common tetrasaccharide linker of glycosaminoglycans. Here, we analyzed all serum Bkn isoforms in a context of congenital disorders of glycosylation (CDG) and showed very specific abnormal patterns suggesting potential interests for their screening and diagnosis. In particular, genetic deficiencies in V-ATPase

**Abbreviations:** Alb, albumin; ALP, alkaline phosphatase; ApoC-III, apolipoprotein C-III; B3GALT6, beta-1,3-galactosyltransferase 6; B3GAT3, beta-1,3-glucuronyltransferase 3; B4GALT7, beta-1,4-galactosyltransferase 7; Bkn, bikunin; Bkn-CS, bikunin linked to chondroitin sulfate chain; CDG, congenital disorder(s) of glycosylation; COG, conserved oligomeric Golgi complex; CS, chondroitin sulfate; ER, endoplasmic reticulum; GAG, glycosaminoglycan; Gal, galactose; GlcA, glucuronic acid; GlcNAc, N-acetylglucosamine; HC, heavy chain protein; ITI, inter- $\alpha$ -trypsin inhibitor; Mn<sup>2+</sup>, manganese; PG, proteoglycans; PTMs, posttranslational modifications; P $\alpha$ I, pro- $\alpha$ -trypsin inhibitor; SLC35A2, solute carrier family 35 member A2; SLC35A3, solute carrier family 35 member A3; TBS, Tris buffer saline; TMEM165, transmembrane protein 165; Trf, transferrin; TTBS, TBS with 0.1% Tween; UTI, urinary trypsin inhibitor; Xyl, xylose.

(ATP6V0A2-CDG, CCDC115-CDG, ATP6AP1-CDG), in Golgi manganese homeostasis (TMEM165-CDG) and in the *N*-acetyl-glucosamine Golgi transport (SLC35A3-CDG) all share specific abnormal Bkn patterns. Furthermore, for each studied linkeropathy, we show that the light abnormal Bkn could be further in-depth characterized by two-dimensional electrophoresis. Moreover, besides being interesting as a specific biomarker of both CDG and linkeropathies, Bkn isoforms' analyses can provide new insights into the pathophysiology of the aforementioned diseases.

#### KEYWORDS

bikunin, CDG, GAG tetrasaccharide, inter- $\alpha$ -trypsin inhibitor, linkeropathies, SLC35A3, TMEM165

## 1 | INTRODUCTION

Bikunin (Bkn) isoforms are serum proteoglycans of liver origin bearing a chondroitin sulfate (CS) chain mainly esterified by one or two glycoproteins named “heavy chains” (HCs). Three major serum isoforms have been extensively described: the inter- $\alpha$ -trypsin inhibitor (ITI) and the pro- $\alpha$ -trypsin inhibitor (P $\alpha$ I), carrying respectively two and one HC, as well as the urinary trypsin inhibitor (UTI), which corresponds to Bkn linked to the CS chain.<sup>1</sup> In addition, we showed that free Bkn (ie, the core protein) could be detected at low level in serum<sup>2</sup> (Figure 1A).

UTI (Bkn-CS) results from the linkage of one xylose (Xyl) residue to the Ser10 of Bkn followed by the sequential action of enzymes catalyzing the biosynthesis of the PG common tetrasaccharide linker (GlcA-Gal-Gal-Xyl-O-Ser) and the elongation of a short CS chain consisting of  $15 \pm 3$  (GlcA-GalNAc) sulfated disaccharide motifs. The tetrasaccharide linker synthesis starts in the endoplasmic reticulum (ER) lumen while the elongation occurs in the Golgi compartment. This requires specific glycoenzymes, nucleotide sugars, and an activated form of sulfate as substrates.<sup>3,4</sup> Once the Bkn CS chain is elongated and sulfated, it covalently binds one or two HC(s) leading to P $\alpha$ I and ITI, respectively (heavy Bkn isoforms) (Figure 1B). Noticeably, the ester linkages between the HCs and the CS chain occur in the *trans*-Golgi after a pH-dependent C-terminal autocatalytic cleavage of HC precursors.<sup>5</sup> Besides the linkage and the elongation of the CS chain, the core protein Bkn and HCs precursors are *N*-glycosylated, *O*-glycosylated and undergo proteolytic cleavage in the ER and the Golgi. Thus, with the reported CS chain phosphorylation, sulfation, and sialylation, a large range of posttranslational modifications (PTMs) can be found on serum Bkn isoforms<sup>3,6-9</sup> (Figure 1B).

In pathophysiology, under stimuli such as inflammation or ovulation, circulating ITI and P $\alpha$ I can be extravasated from the blood, playing an important role in the stabilization of the extracellular matrices through the exchange of HCs with hyaluronic acid.<sup>10,11</sup> Moreover, the Bkn core protein has been shown to inhibit inflammation-associated proteases such as trypsin, elastase, and plasmin in pancreatitis, septic shock and rheumatoid arthritis.<sup>12,13</sup> In some cancers, Bkn has been shown to inhibit cell proliferation, thus attenuating tumor invasion.<sup>14</sup> Finally, Bkn isoforms exert inhibitory activity toward calcium oxalate crystal formation and therefore has protective effects against kidney stones and urolithiasis.<sup>15</sup>

In linkeropathies, that is, rare skeletal/osteoarticular genetic diseases affecting the biosynthesis of the common initial tetrasaccharide (-GlcA-Gal-Gal-Xyl-O-Ser-) of protein-linked glycosaminoglycans (GAG), we previously showed high levels of abnormal serum Bkn light forms suggesting a potential interest for screening purposes.<sup>2</sup>

In this work, we performed Western-blot analysis of all serum Bkn isoforms from patients with various congenital disorders of glycosylation (CDG) including defects in the V-ATPase Golgi protons pump (ATP6V0A2-CDG, CCDC115-CDG, and ATP6AP1-CDG), in manganese (Mn<sup>2+</sup>) homeostasis (TMEM165-CDG), in tethering factors (conserved oligomeric Golgi complex [COG]-CDG) and in activated sugar transporters (SLC35A2-CDG and SLC35A3-CDG). We focused on these CDG because we anticipated the presence of abnormal Bkn isoforms, linked to impaired Golgi homeostasis (V-ATPase deficiencies, TMEM165-CDG, COG-CDG), and/or associated with GAG biosynthesis defects leading to skeletal clinical phenotypes (TMEM165-CDG, SLC35A2-CDG, and SLC35A3-CDG). Furthermore, we carried out the characterization of abnormal Bkn light forms in linkeropathies by using two-dimensional electrophoresis (2-DE).



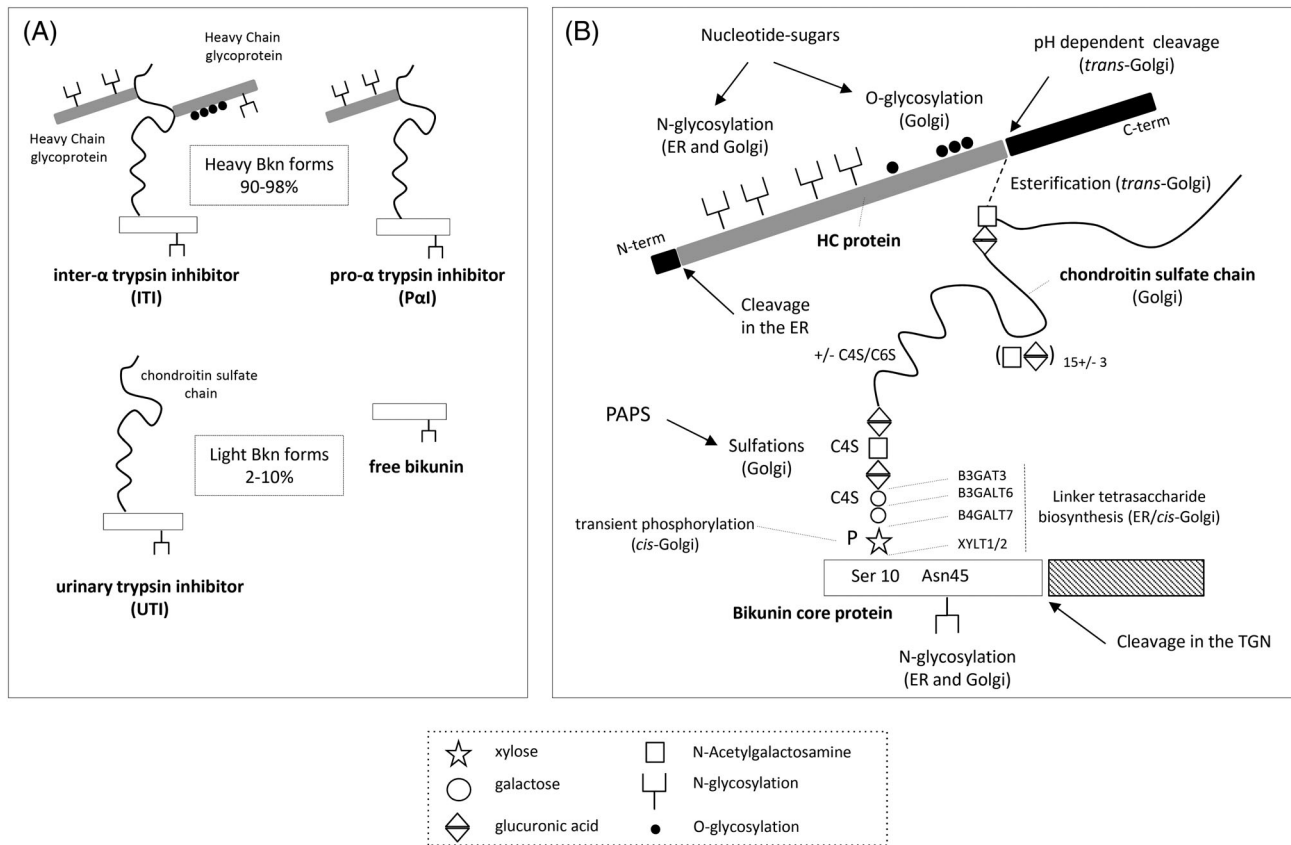


**FIGURE 1** Schematic summary of known bikunin (Bkn) isoforms posttranslational modifications (PTMs). **A**, Structure details of the circulating Bkn isoforms consisting of inter- $\alpha$ -trypsin inhibitor (ITI) and pro- $\alpha$ -trypsin inhibitor (P $\alpha$ I) (the major fraction), and urinary trypsin inhibitor (UTI) (bikunin linked to chondroitin sulfate chain [Bkn-CS]) and free Bkn (the minor fraction). **B**, Ser10 of the core protein is xylosylated in the endoplasmic reticulum (ER). The CS chain is initiated (GlcA-Gal-Gal-Xyl- tetrasaccharide) and elongated (GlcA-GalNAc- disaccharide repeats) in the Golgi. A transient phosphorylation of the Xyl is required for the second Gal linkage. Sulfation reactions in the Golgi require 3'-phosphoadenosine 5'-phosphosulfate (PAPS) as donor substrate. Esterification reactions between the heavy chain (HC) C-terminal Asp and one GalNAc of the CS chain occur in the *trans*-Golgi in association with the pH-dependent C-terminal autocatalytic cleavage of the HC proteins precursors. Very unusually, the N-terminal cleavage of the HC precursors occurs in the ER. *N*-glycosylation is initiated in the ER and continues in the Golgi. Mucin core1 *O*-glycosylation occurs only in the Golgi. The glycosyltransferases involved in the biosynthesis of *N*-glycans, *O*-glycans, and of the CS chain need nucleotide-sugars as donor substrates. The C-terminal cleavage of the core protein precursor occurs in the *trans*-Golgi network just before its secretion into the blood. C4S/C6S: sulfated C-4/C-6; TGN: *trans*-Golgi network

## 2 | MATERIALS AND METHODS

### 2.1 | Serum/plasma samples

All blood samples were collected in agreement with the ethical policy of each institution. It should be underlined that, for some samples we tested, we could not determine whether they were anticoagulated (plasma) or not (sera).

Control samples originated from CDG-negative pediatric patients ( $n = 16$ ), obese adults waiting for bariatric surgery ( $n = 11$ ; cohort of Louis-Mourier Hospital; Dr S. Ledoux) and adult individuals with various pathologies ( $n = 9$ ) including liver diseases ( $n = 6$ ) such as cirrhosis, fibrosis and hepatitis (Antoine Bécélère Hospital). Samples from patients with morbid obesity and liver diseases were tested since these conditions were shown to be frequently

associated with secondary glycosylation abnormalities. Serum/plasma samples from CDG patients, mainly detected and diagnosed in our laboratory, were selected as follows: 3 ATP6V0A2-CDG (ATP6V0A2#1 to ATP6V0A2#3), 3 CCDC115-CDG (CCDC115#1 to CCDC115#3), 2 ATP6AP1-CDG (ATP6AP1#1 and ATP6AP1#2), 2 TMEM165-CDG (TMEM165#1 and TMEM165#2) (from Dr F. Foulquier and Prof J. Jaeken), 5 COG-CDG (2 COG5-CDG: COG5#1 and COG5#2; 3 COG7-CDG: COG7#1 to COG7#3), one SLC35A2-CDG and one SLC35A3-CDG. Clinical data and identified gene variants of studied CDG patients are available in Supp. File 1.

Samples from patients with linkeropathy (Prof V. Cormier-Daire) originated from individuals deficient in B4GALT7 (two unrelated individuals), B3GALT6 (one individual), and B3GAT3 (one individual). Detailed gene

variants were as follows: *B4GALT7* (a) and *B4GALT7* (b): ex.5 c.808C > T p.Arg270Cys (same missense mutation); *B3GALT6*: ex.1 c.353del p.Asp118Alafs\*160-ex.1 c.653A > T p.Tyr218Phe (missense mutation); *B3GAT3*: ex3. c.461C > T p.Thr139Met (missense mutation). Brief clinical data of studied linkeropathy patients are available in Supp. File 1.

## 2.2 | Albumin level measurement

Albumin (Alb) levels of all the samples were determined (VISTA 1500 from Siemens) and measured values were used as loading controls in order to check for possible quantitative discrepancies with presented Western-blot visual results.

## 2.3 | Western-blot of Bkn isoforms

For the Western-blot analysis, sera/plasma were either diluted 1/10 (for UTI and free Bkn) or 1/250 (for ITI and P $\alpha$ I) in water. These dilutions were considered as “optimal” based on our previous work<sup>2</sup> and on the prior analysis of various sera and corresponding plasma sequentially diluted within 1/10 to 1/4000 (Supp. Figure S1).

Total of 20  $\mu$ L of the diluted sera/plasma was mixed with Laemmli sample buffer (4X concentrate) and heated at 100°C for 10 minutes. Polyacrylamide gel electrophoresis, with 10  $\mu$ L of treated sample loaded per well for all patients, was conducted using Nu-PAGE 4% to 12% bis-tris gels (ThermoFisher; cat. # NP0336BOX), as recommended by the manufacturer. After transfer to nitrocellulose (70 minutes, 100 V), heavy (ITI and P $\alpha$ I) and light Bkn isoforms (UTI and free Bkn) were detected after incubation with rabbit anti-Bikunin (CP6) polyclonal antibody (Merck-Millipore, cat. # ABT1346; 1/5000 in TTBS-5% milk for 90 minutes). Concerning this commercial primary antibody, the manufacturer indicates that “human ITI, P $\alpha$ I, bikunin-CS (UTI), and bikunin were specifically detected using a representative lot of this antibody.” HRP-linked anti-rabbit secondary antibodies (Cell Signaling Technologies; cat. # 7074) were used (1/5000 in TTBS-5% milk). Finally, ECL revelation was conducted using Clarity Western ECL Substrate (cat. # 170-5060) and ChemiDoc XRS+ camera from Bio-Rad. Signal measurements (after background subtraction) of Bkn isoforms and relative quantitation of ITI and P $\alpha$ I were performed using ImageJ software.

## 2.4 | Two-dimensional electrophoresis

2-DE of proteins from 5  $\mu$ L of crude serum/plasma from patients with linkeropathy was conducted using ZOOM

strip pH 4 to 7 (ThermoFisher; cat. # ZM0012) for the first dimension and 4% to 12% Nu-PAGE bis-tris gel (ThermoFisher; cat. # NP0330BOX) for the second dimension, as recommended by the manufacturer. After 2-DE, separated proteins were transferred (90 minutes, 100 V) to nitrocellulose sheets and the abnormal serum Bkn light forms were detected using Clarity Western ECL Substrate (Bio-Rad) and ECL HyperFilm from GE Healthcare (cat. # 28906843). Film-based revelation was here preferred because of its higher sensitivity toward the detection of abnormal Bkn light forms compared with our camera system.

For the study of the phosphorylation state of Bkn abnormal light forms, samples were treated with commercial alkaline phosphatase (ALP) as recommended by the manufacturer (Roche; cat. # 10713023001). Briefly, samples (8  $\mu$ L) were treated overnight at 37°C with a mixture of ALP (1  $\mu$ L) and ALP buffer (1  $\mu$ L) and were then analyzed by 2-DE as described above.

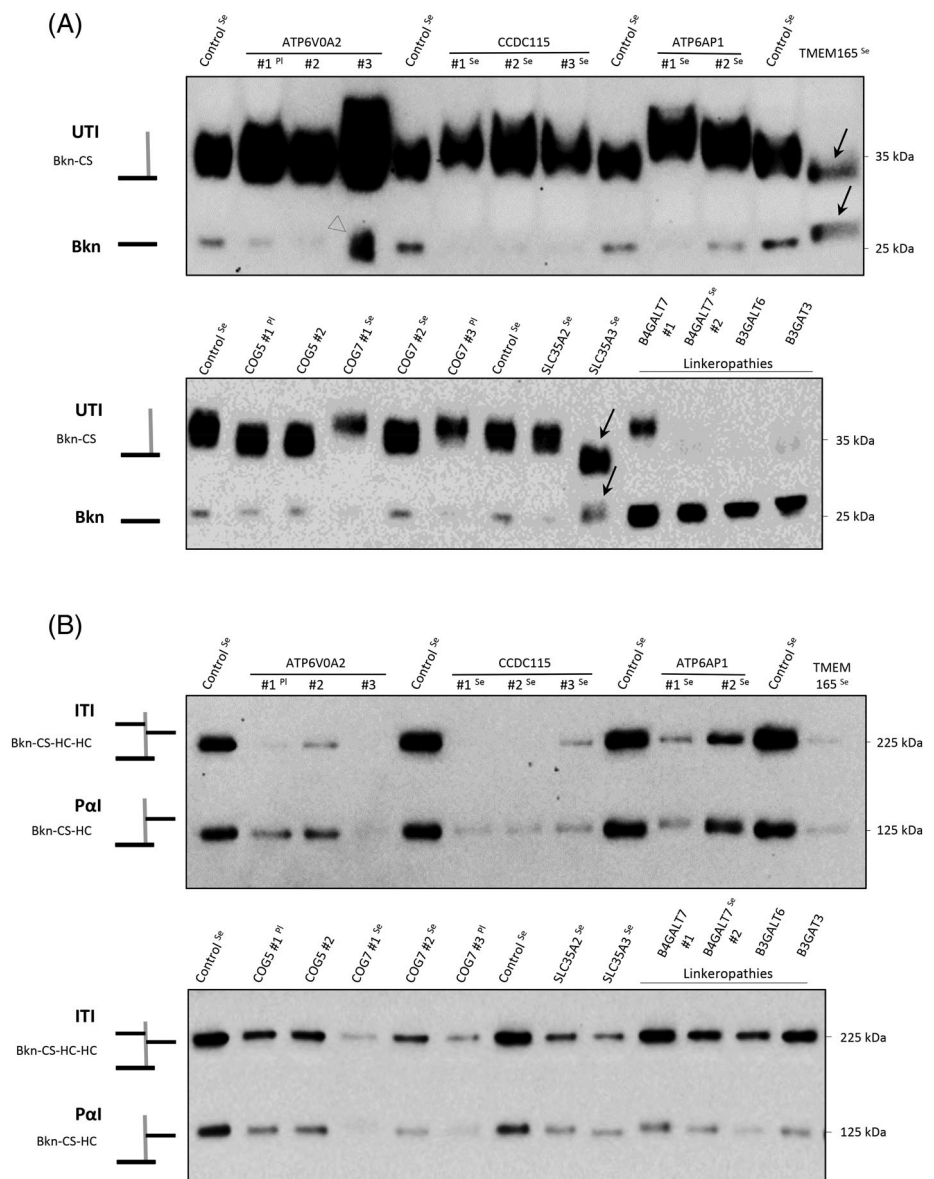
## 3 | RESULTS

### 3.1 | Western-blot of bikunin isoforms in CDG and linkeropathies

Western-blot patterns of all Bkn isoforms from one representative control, various type 2 CDG (CDG-II), and linkeropathy samples are shown in Figure 2A (free Bkn and UTI) and Figure 2B (P $\alpha$ I and ITI). As previously described,<sup>2</sup> the Bkn patterns from the 10-fold diluted control serum (Figure 2A) presented a small band at 25 kDa consistent with free Bkn and a  $\sim$ 35 kDa marked and large band corresponding to UTI, that is, Bkn linked to the variable-sized CS chain (Bkn-CS). Using a 250-fold diluted serum, the heavy Bkn isoforms could be seen (Figure 2B) as two bands at 125 and 225 kDa corresponding, respectively, to P $\alpha$ I (Bkn-CS-HC) and ITI (Bkn-CS-2HC). Also, ITI levels in controls (Figure 2B; Supp. Figure S2) were systematically higher than those of P $\alpha$ I.

In CDG with Golgi proton pump defects (ATP6V0A2-CDG, CCDC115-CDG and ATP6AP1-CDG), the free Bkn corresponding band at 25 kDa was either absent (2/3 ATP6V0A2-CDG; 3/3 CCDC115-CDG; 1/2 ATP6AP1-CDG) or found in small amounts (other cases) compared to control. The apparently abnormal and large free Bkn band observed in one ATP6V0A2-CDG patient (Figure 2A, arrowhead) was likely due to an important level of free Bkn leading to signal saturation. The UTI protein band was similar to that of the control in 2/3 ATP6V0A2-CDG cases and shared a mildly higher molecular weight (MW) in other proton pump-related CDG cases (Figure 2A). However, the corresponding MW

**FIGURE 2** Western-blot profiles of all bikunin (Bkn) isoforms in various congenital disorder(s) of glycosylation type 2 (CDG-II) and linkeropathies. Western-blot of Bkn light forms, **A**, and heavy forms, **B**, from CDG with defects in: protons pump deficiencies (ATP6V0A2-CDG; CCDC115-CDG; ATP6AP1-CDG), Mn<sup>2+</sup> homeostasis (TMEM165-CDG), retrograde Golgi trafficking (conserved oligomeric Golgi complex [COG]-CDG), sugar transporters (SLC35A2-CDG and SLC35A3-CDG) and in linkeropathies. Se, serum; Pl, plasma. Arrows indicate the major observed abnormalities



values remain included within normal values we determined previously.<sup>2</sup> Concerning the heavy forms, the overall signal levels of ITI and PαI were dramatically decreased compared to control with exception of one ATP6AP1-CDG sample showing a discrete reduced signal. To exclude any visual discrepancies related to possible major protein level differences between wells (under the same volume), ITI and PαI signals of each analyzed sample were adjusted with corresponding albumin level value (Suppl. Table S1). Thus, all observed major signal decreases we described were fully corroborated. Moreover, these decreases were systematically associated with an inversion of the ITI/PαI ratio in comparison with various control groups consisting of 16 non-CDG pediatric patients, 11 obese adults, and 6 individuals with liver diseases (Figure 2B; Supp. Figures S2 and S5).

Since we did not know whether some of the samples we tested were plasma or serum, it is important to note

that the impact of the coagulation was tested to avoid potential discrepancies in our conclusions. Indeed, a prior Western-blot analysis was undertaken (Suppl. Figure S1) showing that the signal levels of ITI, PαI, UTI, and free Bkn appeared mildly decreased in serum compared to plasma. Thus, given that the control sample in Figure 2 is a serum, it is very likely that the marked decreased signal levels we describe are not related to the potential plasma nature of the related samples.

In the TMEM165-CDG patient, a genetic defect affecting Golgi Mn<sup>2+</sup> homeostasis, the overall serum Bkn isoforms signal levels were dramatically decreased (Figure 2) and an abnormal ~27 kDa band associated with an abnormally low UTI MW could also be noticed (Figure 2A). Furthermore, the ITI/PαI ratio was also altered (Figure 2B; Supp. Figure S2). An additional TMEM165-CDG serum sample was analyzed during the redaction of this article, showing similar abnormal Bkn profiles (Supp. Figure S3).

In COG-CDG, the free Bkn band appeared similar to that of the control in 2/2 COG5-CDG cases and in 1/3 COG7-CDG, while it was barely detectable in the two remaining COG7-CDG cases (Figure 2A). For ITI and P $\alpha$ I, we observed overall decreased signal levels compared to the control, with particularly low signal observed for 2/3 COG7-CDG cases. In addition, in all COG-CDG cases, the ITI form was predominant with percentages ranging from 74% to 98% (Figure 2B; Supp. Figure S4).

In the SLC35A2-CDG (UDP-Gal transporter deficiency) studied serum, Bkn light forms did not show any abnormality (Figure 2A). Furthermore, the ITI/P $\alpha$ I ratio appeared similar to that of controls in association with a serum level decrease of these two heavy Bkn forms (Figure 2B; Supp. Figure S4). In the serum from the SLC35A3-CDG (UDP-GlcNAc transporter deficiency) individual, an abnormal  $\sim$ 27 kDa band associated with an abnormally low UTI (Bkn-CS) MW could be evidenced (Figure 2A) with an ITI/P $\alpha$ I pattern similar to that of SLC35A2-CDG (Figure 2B; Supp. Figure S4). Finally, in linkeropathy samples, we corroborated the previously reported defects, consisting of abnormal light forms of  $\sim$ 27 kDa and undetectable UTI in 3/4 cases (Figure 2A). Interestingly, the two samples from the patients sharing the same *B4GALT7* variant showed a marked discrepancy in the observed UTI signal. Finally, concerning ITI/P $\alpha$ I levels and ratios, no clear associated defect was noted (Figure 2B; Supp. Figure S4).

In summary, concerning Bkn light forms, marked abnormalities were observed for TMEM165-CDG, SLC35A3-CDG, and all tested linkeropathy individuals. Regarding the two heavy Bkn forms, dramatically decreased signals coupled to inverted ratios were noted for nearly all (except ATP6AP1#2) of the V-ATPase defects and for the two TMEM165-CDG individuals. For 2/3 COG7-CDG individuals, a decreased ITI/P $\alpha$ I signal was observed without associated inverted ratio. Finally, no evident abnormality was found in the heavy Bkn forms of linkeropathy patients.

### 3.1.1 | 2-DE of abnormal bikunin light forms in linkeropathies

Abnormal Bkn light forms in samples from patients with linkeropathy (Figure 3A) were analyzed by 2-DE. As shown in Figure 3B, while the samples from the two patients with *B4GALT7* deficiency (ie, the enzyme involved in the first Gal linkage to -Xyl-O-Bkn) showed very similar patterns with up to three protein spots, those from the patients with a deficiency in the two subsequent enzymes were clearly different from the first ones and

from each other. More precisely, the migration of the observed abnormal major Bkn light forms increasingly shifted toward the anode, according to the defective enzymes, that is, *B4GALT7*, *B3GALT6*, or *B3GAT3*, respectively. In addition, the 2-DE analysis of a mixture of samples (in ratios 1:1:1) from *B4GALT7*-, *B3GALT6*-, and *B3GAT3*-deficient patients corroborated the observed differences of charge and further exhibited increasing MW differences.

In order to evaluate the phosphorylation state of the abnormal Bkn light forms in linkeropathy patients, samples were first treated with ALP prior 2-DE analysis (Figure 3C). For the ALP-treated serum from *B4GALT7*-deficient patient, no difference in the migration was observed. In contrast, for ALP-treated samples from *B3GALT6*- and *B3GAT3*-deficient patients, we observed a cathodic shift of the major Bkn spots consistent with the ALP-mediated loss of a negatively charged phosphate group.

## 4 | DISCUSSION

In patients with Golgi protons pump defects that is, *ATP6V0A2*-CDG, *CCDC115*-CDG, and *ATP6AP1*-CDG, the serum/plasma levels of the Bkn core protein were decreased or undetectable in all except one case of *ATP6V0A2*-CDG. This result does not seem to be specific of the potential pH defect as similar Bkn patterns were also seen in other investigated controls (eg, in Suppl. Figure S1). It is likely that Golgi pH disturbances have no effects on the biosynthesis and/or secretion of the free Bkn core protein. Similarly, no major quantitative or qualitative defects were observed for UTI (Bkn-CS). Thus, this apparent lack of major CS GAG biosynthesis defects in Golgi protons pump-related CDG is in sharp contrast with abnormal *N*- and *O*-glycosylation reported elsewhere.<sup>16-18</sup> Concerning heavy Bkn isoforms, an inversion of the ITI/P $\alpha$ I ratio was observed in these three CDG subtypes compared to control groups. Moreover, the circulating levels of these two heavy forms were dramatically decreased. This has been already observed in individuals with severe acute infection,<sup>19</sup> which was not the case in our investigated patients. Furthermore, these decreases are specific for Bkn isoforms as albumin measurements in the analyzed samples allowed to exclude associated major protein level decreases compared to control.

*ATP6V0A2*-CDG, *CCDC115*-CDG, and *ATP6AP1*-CDG are genetic deficiencies affecting the V-ATPase protons pump, which plays pivotal roles not only in the luminal *trans*-Golgi acidification, but also in vesicular trafficking, fusion of vesicles and protein sorting.<sup>20,21</sup> While *ATP6V0A2* is a subunit of the proton translocator



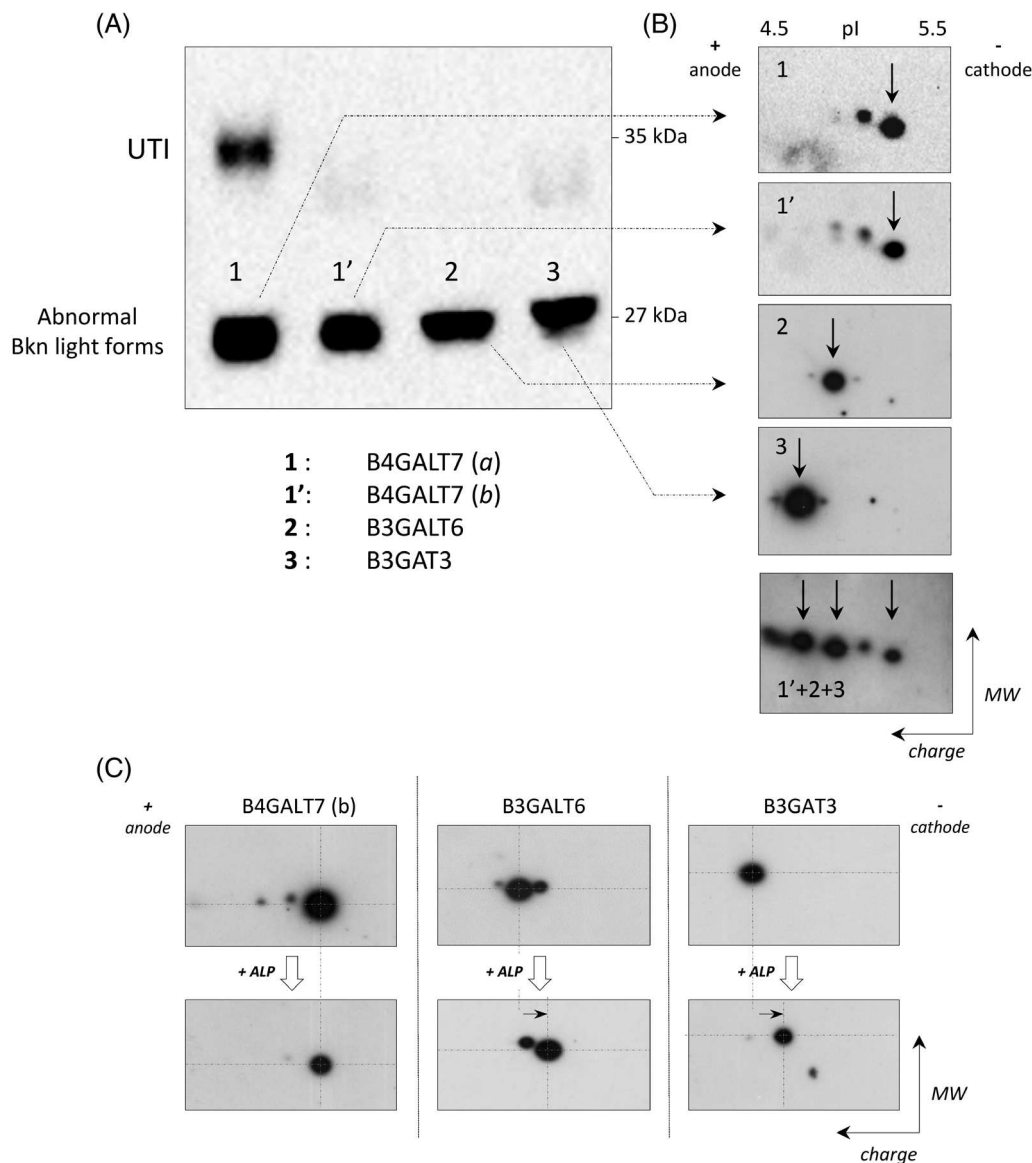


**FIGURE 3** Serum/plasma bikunin electrophoretic profiles in linkeropathies. **A**, Western-blot patterns of abnormal light Bkn forms (~25-27 kDa) in samples from B4GALT7 (1 and 1'), B3GALT6 (2), and B3GAT3 (3) deficient patients. **B**, Corresponding two-dimensional electrophoresis (2-DE) patterns showing an anodic shift of the major Bkn spots (arrows). The 2-DE profile of a mixture (in ratios 1:1:1) of B4GALT7-, B3GALT6-, and B3GAT3-deficient patients' samples (1' + 2 + 3) corroborated the charge differences and evidenced molecular weight (MW) differences. pI: isoelectric point. **C**, 2-DE patterns of abnormal Bkn light forms in B4GALT7-, B3GALT6-, and B3GAT3-deficient patients' samples, before (up) and after (below) alkaline phosphatase (ALP) treatment. Small horizontal arrows indicate the cathodic shift observed for the major spot

V0 domain of the V-ATPase,<sup>16</sup> CCDC115 and ATP6AP1 are assembly factor and accessory subunit of this complex, respectively.<sup>17,22</sup> Thus, as expected, it would appear that the impaired acidification of the *trans*-Golgi associated with these CDG does not affect the Bkn CS chain biosynthesis that essentially takes place in early Golgi compartments. Conversely, the observed ITI/PαI ratio inversion and overall decreased levels suggest that this *trans*-Golgi acidification defect might impair the pH-

dependent protein cleavage of HCs precursors and disturb their ester linkage to the CS chain. Since it has been shown that an increased pH in the *trans*-Golgi could lead to *N*- and *O*-glycosyltransferases mislocalization, inactivation, and interaction defects,<sup>23,24</sup> similar consequences on putative ester transferases responsible for the linkages of HCs to the CS chain could also be evoked and will need to be further addressed. In addition, the vesicular trafficking defects related to V-ATPase deficiencies could

also contribute to the mislocalization of the ester transferases and to a decreased protein secretion.

TMEM165 is a  $\text{Ca}^{2+}$ - $\text{Mn}^{2+}$ / $\text{H}^{+}$  Golgi antiporter playing a pivotal role in the Golgi luminal pH maintenance and in the level of  $\text{Mn}^{2+}$  cations that are important cofactors of specific Golgi-resident glycosylation enzymes.<sup>25,26</sup> In the two presented TMEM165-CDG cases, we report marked defects in the light Bkn forms patterns as well as in ITI/P $\alpha$ I signal levels and ratios (Figure 2). For light Bkn forms, the observed impairments suggest combined defects in the initiation and in the elongation of the CS chain. They could be related to overall enzymatic defects linked to Golgi  $\text{Mn}^{2+}$  deficiency and strongly fit with the major skeletal phenotype of the investigated patients.<sup>27</sup> In this regard, TMEM165-CDG interestingly appears as a genetic disease affecting *N*-glycosylation, *O*-glycosylation, glycolipids, and the CS biosynthesis. Concerning the heavy Bkn forms (ITI and P $\alpha$ I) in TMEM165-CDG, the observed abnormalities are highly comparable to those found in V-ATPase deficiencies. As regarding the similarity of the glycosylation defects between these CDG subtypes,<sup>25</sup> our results are consistent with potential Golgi pH-related PTM alterations, not only affecting the *N*- and *O*-glycosylation, but also the CS-HC esterification. The involvement of the  $\text{Mn}^{2+}$  deficiency in the impairment of esterification and protein sorting could also be suspected and will need further testing.

The multisubunit COG complex is a molecular tethering factor mainly involved in the retrograde trafficking from the *cis*-Golgi to the ER and its impairment was shown to affect *N*- and mucin type *O*-glycosylation mainly through the mislocalization of the related enzymes.<sup>28</sup> In COG-CDG samples, the observed absence of defects in the UTI biosynthesis (Figure 2) suggests COG is not involved in the subcellular localization of the enzymes involved in the CS chain synthesis. Although unexpected, this observation is supported by a recently published “organelle zones” theory, which differentiates in the Golgi a “proteoglycan zone” from a “mucin zone” with variable responses to different stresses.<sup>29</sup> Concerning the observed ITI and P $\alpha$ I decreased levels, they could be explained by HCs glycosylation defects that would decrease the secretion or increase the degradation of heavy Bkn isoforms.

SLC35A2 protein mainly corresponds to UDP-galactose (UDP-Gal) Golgi transporter.<sup>30</sup> Since Gal residue is a key monosaccharide for *N*-glycosylation, SLC35A2 deficiency was expected to be associated with abnormal transferrin (Trf) patterns. However, it has been recently shown in two distinct cohorts that the screening of SLC35A2-CDG could be very challenging with only 35% to 60% of samples sharing Trf *N*-glycosylation abnormalities.<sup>31,32</sup> We previously showed that the SLC35A2-CDG case used in this study harbored markedly abnormal CDG-II Trf pattern.<sup>33</sup> In contrast, the observed normal

light Bkn forms pattern suggests a normal tetrasaccharide linker synthesis despite the presence of two Gal residues in this structure. Thus, this observation could be linked, in this case, to the preferential use of UDP-Gal toward the GAG biosynthesis rather than *N*-glycosylation. Nevertheless, it could be possible that other causal *SLC35A2* gene variants (notably those associated with a skeletal phenotype) could lead to an abnormal light Bkn forms pattern, with potential screening/diagnosis interest. Concerning heavy Bkn forms in the *SLC35A2*-CDG case, the observed decreases of heavy Bkn isoforms in absence of an obvious Golgi homeostasis disturbance could be related to abnormal protein elimination and/or sorting associated with abnormal HCs glycosylation. [Correction added on 12 August 2021, after print and online publication: The two preceding sentences were previously missing and has been added in this version.]

*SLC35A3*-CDG is an inherited deficiency in UDP-*N*-acetylglucosamine (UDP-GlcNAc) Golgi transporter typically associated with *N*-glycosylation abnormalities in agreement with the involvement of GlcNAc moieties in the *N*-glycan core structure.<sup>30,33</sup> Since GlcNAc is lacking in the CS chains, the abnormal Bkn light form and the abnormally low UTI MW (Figure 2) are surprising in the *SLC35A3*-CDG. Nevertheless, they could result from major interaction defects with other Golgi sugar transporters involved in the CS biosynthesis, including *SLC35A2*.<sup>34</sup> Moreover, this alteration in the pattern of serum Bkn light forms suggests overall CS defects in line with the skeletal abnormalities observed in our patient (showing major long bones growth retardation) as well as in other cases described elsewhere.<sup>35,36</sup>

Inherited defects in the enzymes involved in the stepwise synthesis of the common GAG tetrasaccharide linker, that is, xylosyltransferases (XYLT1 or XYLT2), galactosyltransferases (B4GALT7 and B3GALT6), and glucuronyltransferase (B3GAT3), correspond to linkeropathies.<sup>37</sup> In this work, we corroborated previously described high levels of abnormal Bkn light forms in B4GALT7, B3GALT6, and B3GAT3 deficiencies (Figure 2). Furthermore, we showed a quasi-absence of circulating normal UTI in 3/4 samples coupled with unexpectedly normal ITI and P $\alpha$ I signal levels and ratios. Hence, it would appear that missense mutations found in the four cases studied would allow residual UTI biosynthesis, the latter being sufficient for normal HC ester linkages in the *trans*-Golgi. Moreover, it is likely that once mostly used for ITI and/or P $\alpha$ I synthesis, the remaining intracellular stock of normal UTI could be very low in 3/4 patients, finally leading to its severely reduced blood secretion. Concerning the different UTI levels that we observed in the two patients sharing the same B4GALT7 variant, they could be linked to distinct

UTI requirements toward the formation of ITI and PaI according to the patient's condition at the sampling time.

By coupling charge- and MW-based separation (2-DE), we showed that the abnormal Bkn light forms found in linkeropathies were clearly different according to the mutated gene (Figure 3). Since it has been shown that the transient 2-O-phosphorylation of the xylose is required for the B3GALT6-catalyzed linkage of the second galactose,<sup>38,39</sup> the anodic shift observed between the major spots detected in samples from B4GALT7- and B3GALT6-deficient patients could be consistent with the presence of Xyl-O-Bkn in the first case, and Gal-Xyl(2-O-phosphate)-O-Bkn in the second case. Indeed, the cathodic shift induced by phosphatase treatment corroborated the presence of a phosphate in the Bkn linkage region from the B3GALT6-deficient patient, contrary to the B4GALT7-deficient case. In the ALP-treated sample from the B3GAT3-deficient patient, a cathodic shift was also observed. Thus, since the second Gal residue of the UTI tetrasaccharide linker has been shown to be systematically sulfated,<sup>3,40</sup> the observed shift between B3GALT6- and B3GAT3-deficient patients could correspond to the presence of Gal(4-C-sulfate)-Gal-Xyl(2-O-phosphate)-O-Bkn in the B3GAT3-deficient patient's sample.

Finally, it is likely that the other observed minor spots are linked to other modifications such as *N*-glycosylation,<sup>7</sup> sialylation of the first gal residue, xylose fucosylation<sup>41</sup> or a recently reported non-canonical CS linkage region trisaccharide (GlcA-Gal-Xyl-O).<sup>42</sup>

Although limited to a small number of patients with linkeropathy, our results are consistent with the current knowledge about the early steps of the Bkn-linked CS chain synthesis and highlight the existence of 2-DE signature patterns.

When assessed in their clinical context and summarized in a decisional tree (Figure 4), our results first indicate that the heavy Bkn isoforms electrophoretic profile could be a convenient additional tool in the CDG-II diagnosis pathway, complementing the second-line MS-based glycomic studies and apolipoprotein C-III (apoC-III) analysis (Figure 4A). Second, our findings also reveal that the light Bkn isoforms pattern could be of interest for the screening of TMEM165-CDG, SLC35A3-CDG, and patients with linkeropathies, with probable signature 2-DE patterns for the latter ones (Figure 4B).

## 5 | CONCLUSIONS

Bikunin isoforms are multifaceted circulating proteoglycans whose the follow-up of the diverse PTMs can be used as biomarkers for the screening and diagnosis of various genetic diseases, including linkeropathies and inherited defects of Golgi ion homeostasis. Further work will now be important to enlarge the analysis of Bkn isoforms to additional CDG/linkeropathy samples. In this way, particular interest will be paid toward (a) other CDG with Golgi homeostasis defects associated with

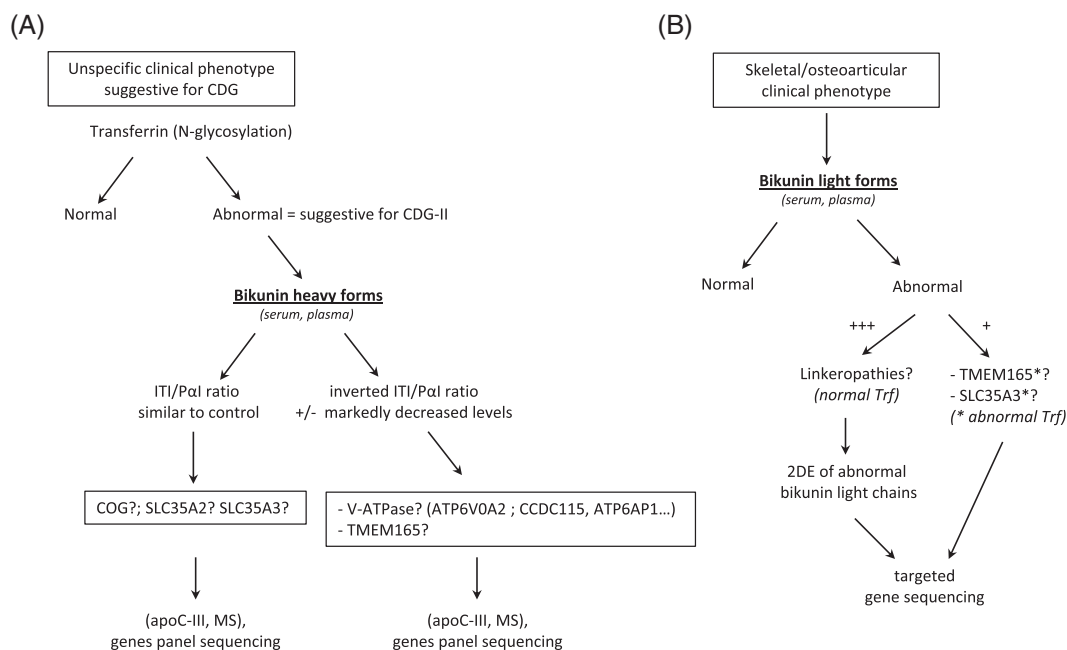


**FIGURE 4** Suggestion of a decisional tree summarizing the main diagnostic orientations given by our bikunin isoforms analysis. **A**, In the diagnosis pathway of congenital disorder(s) of glycosylation type 2 (CDG-II). **B**, In the diagnosis pathway of TMEM165-CDG, SLC35A3-CDG and linkeropathies. ApoC-III, apolipoprotein C-III; MS, mass spectrometry

skeletal phenotypes (eg, SLC10A7-CDG, SLC39A8-CDG, COG4-CDG, etc.) and (b) inherited defects in the elongation of the CS chain (eg, CS synthase deficiencies). Finally, we will also evaluate the potentials of the Bkn isoforms' patterns in the diagnosis of the GAG sulfation defects.

## ACKNOWLEDGMENTS

This work was supported by grant ANR-15RAR3-0004-06 under the frame of E-RARE-3, the ERA-Net for Research on Rare Diseases; it was also supported by the European Union's Horizon 2020 Research and Innovation Program under the ERA-NET cofund action No. 643578. The authors confirm independence from the sponsors; the content of the article has not been influenced by the sponsors.

## CONFLICT OF INTEREST

The authors declare no conflict of interest.

## AUTHOR CONTRIBUTIONS

**Walid Haouari:** PhD student. Performed the majority of the experiments; wrote the article with Arnaud Bruneel. **Johanne Dubail:** Importantly involved in linkeropathy patients diagnosis and samples management. Critical reading of the manuscript. **Samra Lounis-Ouaras:** Performed the experiments relative to controls with liver diseases. Critical reading of the manuscript. **Pierre Prada:** Performed some important 2-DE experiments. **Rizk Bennani:** Performed some very important Western-blotting experiments. **Charles Roseau:** Importantly involved in the development of the Western-blot detection of bikunin isoforms. **Céline Huber:** Molecular diagnosis and clinical management of the linkeropathy patients. **Alexandra Afenjar:** Molecular diagnosis and clinical management of the patient COG5#2. **Estelle Colin:** Molecular diagnosis and clinical management of the patients COG7#1 and COG7#2. **Sandrine Vuillaumier-Barrot:** Molecular diagnosis of patients ATP6V0A2#1, ATP6V0A2#2, CCDC115#1 to #3 and SLC35A2. **Nathalie Seta:** Critical reading of the manuscript; supervision of the work with Arnaud Bruneel. **François Foulquier:** Critical reading of the manuscript and notably the part related to TMEM165-CDG. **Christian Poüs:** Team leader of UMR1193. Critical reading of the paper; supervision of the work with Arnaud Bruneel. **Valérie Cormier-Daireand:** Leader of UMR1163. Significantly contributed to the initiation of this work. Critical reading of the manuscript; recruitment of linkeropathy patients. **Arnaud Bruneel:** Wrote the manuscript with Walid Haouari. Supervision and direction of all the experiments and collaborative works.

## INFORMED CONSENT

All procedures followed were in accordance with the ethical standards of the responsible committee on human experimentation (institutional and national) and with the Helsinki Declaration of 1975, as revised in 2000. Informed consent was obtained from all patients for being included in the study.

## ORCID

Arnaud Bruneel  <https://orcid.org/0000-0001-8411-3309>

## REFERENCES

- Salier JP, Rouet P, Raguenez G, Daveau M. The inter-alpha-inhibitor family: from structure to regulation. *Biochem J*. 1996; 315(Pt 1):1-9.
- Bruneel A, Dubail J, Roseau C, et al. Serum bikunin is a biomarker of linkeropathies. *Clin Chim Acta*. 2018;485:178-180.
- Ly M, Leach FE, Laremore TN, Toida T, Amster IJ, Linhardt RJ. The proteoglycan bikunin has a defined sequence. *Nat Chem Biol*. 2011;7(11):827-833.
- Paganini C, Costantini R, Superti-Furga A, Rossi A. Bone and connective tissue disorders caused by defects in glycosaminoglycan biosynthesis: a panoramic view. *FEBS J*. 2019;286(15):3008-3032.
- Thuveson M, Fries E. The low pH in trans-Golgi triggers autocatalytic cleavage of pre-alpha-inhibitor heavy chain precursor. *J Biol Chem*. 2000;275(40):30996-31000.
- Flahaut C, Capon C, Balduyck M, Ricart G, Sautiere P, Mizon J. Glycosylation pattern of human inter-alpha-inhibitor heavy chains. *Biochem J*. 1998;333(Pt 3):749-756.
- Enghild JJ, Thøgersen IB, Cheng F, Fransson LA, Roepstorff P, Rahbek-Nielsen H. Organization of the inter-alpha-inhibitor heavy chains on the chondroitin sulfate originating from Ser (10) of bikunin: posttranslational modification of IalphaI-derived bikunin. *Biochemistry*. 1999;38(36):11804-11813.
- Thuveson M, Fries E. Intracellular proteolytic processing of the heavy chain of rat pre-alpha-inhibitor. The COOH-terminal propeptide is required for coupling to bikunin. *J Biol Chem*. 1999;274(10):6741-6746.
- Héron A, Bourguignon J, Callé A, et al. Post-translational processing of the inter-alpha-trypsin inhibitor in the human hepatoma HepG2 cell line. *Biochem J*. 1994;302(Pt 2):573-580.
- Zhu L, Zhuo L, Watanabe H, Kimata K. Equivalent involvement of inter-alpha-trypsin inhibitor heavy chain isoforms in forming covalent complexes with hyaluronan. *Connect Tissue Res*. 2008;49(1):48-55.
- Zhuo L, Hascall VC, Kimata K. Inter-alpha-trypsin inhibitor, a covalent protein-glycosaminoglycan-protein complex. *J Biol Chem*. 2004;279(37):38079-38082.
- Pratt CW, Pizzo SV. Mechanism of action of inter-alpha-trypsin inhibitor. *Biochemistry*. 1987;26(10):2855-2863.
- Yingsung W, Zhuo L, Mörgelin M, et al. Molecular heterogeneity of the SHAP-hyaluronan complex isolation and characterization of the complex in synovial fluid from patients with rheumatoid arthritis. *J Biol Chem*. 2003;278(35):32710-32718.
- Kobayashi H, Suzuki M, Hirashima Y, Terao T. The protease inhibitor bikunin, a novel anti-metastatic agent. *J Biol Chem*. 2003;384(5):749-754.



15. Suzuki M, Kobayashi H, Kageyama S, Shibata K, Fujie M, Terao T. Excretion of bikunin and its fragments in the urine of patients with renal stones. *J Urol*. 2001;166(1):268-274.
16. Kornak U, Reynders E, Dimopoulou A, et al. Impaired glycosylation and cutis laxa caused by mutations in the vesicular H<sup>+</sup>-ATPase subunit ATP6V0A2. *Nat Genet*. 2008;40(1):32-34.
17. Jansen JC, Cirak S, van Scherpenzeel M, et al. CCDC115 deficiency causes a disorder of Golgi homeostasis with abnormal protein glycosylation. *Am J Hum Genet*. 2016;98(2):310-321.
18. Jansen EJ, Timal S, Ryan M, et al. ATP6AP1 deficiency causes an immunodeficiency with hepatopathy, cognitive impairment and abnormal protein glycosylation. *Nat Commun*. 2016;7:11600.
19. Daveau M, Rouet P, Scotte M, et al. Human inter-alpha-inhibitor family in inflammation: simultaneous synthesis of positive and negative acute-phase proteins. *Biochem J*. 1993;292(Pt 2):485-492.
20. Forgac M. Vacuolar ATPases: rotary proton pumps in physiology and pathophysiology. *Nat Rev Mol Cell Biol*. 2007;8(11):917-929.
21. Cotter K, Stransky L, McGuire C, Forgac M. Recent insights into the structure, regulation, and function of the V-ATPases. *Trends Biochem Sci*. 2015;40(10):611-622.
22. Jansen EJ, Martens GJM. Novel insights into V-ATPase functioning: distinct roles for its accessory subunits ATP6AP1/Ac45 and ATP6AP2/(pro) renin receptor. *Curr Protein Pept Sci*. 2012;13(2):124-133.
23. Rivinoja A, Hassinen A, Kokkonen N, Kauppila A, Kellokumpu S. Elevated Golgi pH impairs terminal N-glycosylation by inducing mislocalization of Golgi glycosyltransferases. *J Cell Physiol*. 2009;220(1):144-154.
24. Hassinen A, Rivinoja A, Kauppila A, Kellokumpu S. Golgi N-glycosyltransferases form both homo- and heterodimeric enzyme complexes in live cells. *J Biol Chem*. 2010;285(23):17771-17777.
25. Dulary E, Potelle S, Legrand D, Foulquier F. TMEM165 deficiencies in congenital disorders of glycosylation type II (CDG-II): clues and evidences for roles of the protein in Golgi functions and ion homeostasis. *Tissue Cell*. 2017;49(2) Pt A:150-156.
26. Lebretonchel E, Houdou M, Potelle S, et al. Dissection of TMEM165 function in Golgi glycosylation and its Mn<sup>2+</sup> sensitivity. *Biochimie*. 2019;165:123-130.
27. Zeevaert R, de Zegher F, Sturiale L, et al. Bone dysplasia as a key feature in three patients with a novel congenital disorder of glycosylation (CDG) type II due to a deep intronic splice mutation in TMEM165. *JIMD Rep*. 2013;8:145-152.
28. Blackburn JB, D'Souza Z, Lupashin VV. Maintaining order: COG complex controls Golgi trafficking, processing, and sorting. *FEBS Lett*. 2019;593(17):2466-2487.
29. Sasaki K, Yoshida H. Golgi stress response and organelle zones. *FEBS Lett*. 2019;593(17):2330-2340.
30. Hadley B, Maggioni A, Ashikov A, Day CJ, Haselhorst T, Tiralongo J. Structure and function of nucleotide sugar transporters: current progress. *Comput Struct Biotechnol J*. 2014;10(16):23-32.
31. Ng BG, Sosicka P, Agadi S, et al. SLC35A2-CDG: functional characterization, expanded molecular, clinical, and biochemical phenotypes of 30 unreported individuals. *Hum Mutat*. 2019;40(7):908-925.
32. Vals M-A, Ashikov A, Ilves P, et al. Clinical, neuroradiological, and biochemical features of SLC35A2-CDG patients. *J Inher Metab Dis*. 2019;42(3):553-564.
33. Bruneel A, Cholet S, Drouin-Garraud V, et al. Complementarity of electrophoretic, mass spectrometric, and gene sequencing techniques for the diagnosis and characterization of congenital disorders of glycosylation. *Electrophoresis*. 2018;39(24):3123-3132.
34. Maszczak-Seneczko D, Sosicka P, Majkowski M, Olczak T, Olczak M. UDP-N-acetylglucosamine transporter and UDP-galactose transporter form heterologous complexes in the Golgi membrane. *FEBS Lett*. 2012;586(23):4082-4087.
35. Marini C, Hardies K, Pisano T, et al. Recessive mutations in SLC35A3 cause early onset epileptic encephalopathy with skeletal defects. *Am J Med Genet A*. 2017;173(4):1119-1123.
36. Edmondson AC, Bedoukian EC, Deardorff MA, et al. A human case of SLC35A3-related skeletal dysplasia. *Am J Med Genet A*. 2017;173(10):2758-2762.
37. Mizumoto S, Yamada S, Sugahara K. Mutations in biosynthetic enzymes for the protein linker region of chondroitin/dermatan/heparan sulfate cause skeletal and skin dysplasias. *Biomed Res Int*. 2015;2015:861752.
38. Wen J, Xiao J, Rahdar M, et al. Xylose phosphorylation functions as a molecular switch to regulate proteoglycan biosynthesis. *Proc Natl Acad Sci U S A*. 2014;111(44):15723-15728.
39. Koike T, Izumikawa T, Sato B, Kitagawa H. Identification of phosphatase that dephosphorylates xylose in the glycosaminoglycan-protein linkage region of proteoglycans. *J Biol Chem*. 2014;289(10):6695-6708.
40. Yamada S, Oyama M, Yuki Y, Kato K, Sugahara K. The uniform galactose 4-sulfate structure in the carbohydrate-protein linkage region of human urinary trypsin inhibitor. *Eur J Biochem*. 1995;233:687-693.
41. Toledo AG, Nilsson J, Noborn F, Sihlbom C, Larson G. Positive mode LC-MS/MS analysis of chondroitin sulfate modified glycopeptides derived from light and heavy chains of the human inter- $\alpha$ -trypsin inhibitor complex. *Mol Cell Proteomics*. 2015;14(12):3118-3131.
42. Persson A, Nilsson J, Vorontsov E, Noborn F, Larson G. Identification of a non-canonical chondroitin sulfate linkage region trisaccharide. *Glycobiology*. 2019;29(5):366-371.

## SUPPORTING INFORMATION

Additional supporting information may be found online in the Supporting Information section at the end of this article.

**How to cite this article:** Haouari W, Dubail J, Lounis-Ouaras S, et al. Serum bikunin isoforms in congenital disorders of glycosylation and linkeropathies. *J Inher Metab Dis*. 2020;43:1349–1359. <https://doi.org/10.1002/jimd.12291>

# Supplementary files

## Supplementary File 1.

### 1) Brief clinical data and identified gene variants of studied CDG patients.

#### - Patient **ATP6V0A2#1**

Female; currently 27 years old; French origin; non-consanguineous parents; age at diagnosis: 13 years old; CDG type 2 transferrin pattern; abnormal 'apoC-III-1' pattern. **Published.** Brief clinical description, CDG screening tests and identified variant can be found in reference [33] (patient 2).

#### - Patient **ATP6V0A2#2**

Female; currently 11 years old; consanguineous parents (first cousins); Malian origin; samples were addressed in a clinical context of autosomal recessive cutis laxa type II (ARCL-II); large fontanel; microcephaly. Age at diagnosis (abnormal CDG screening): 9 months; CDG type 2 transferrin pattern; abnormal 'apoC-III-1' pattern. Identified variant: c.1724+2T>C (homozygous). **Unpublished.**

#### - Patient **ATP6V0A2#3**

The analyzed sample is a generous gift from Prof Dirk J. Lefeber. CDG type 2 transferrin pattern; abnormal 'apoC-III-1' pattern.

#### - Patients **CCDC115#1** to **CCDC115#3**

Clinical data, glycosylation studies and identified variants of these three unrelated individuals have been **published** in supplementary reference (1) (CCDC115#1 is patient 1; CCDC115#2 is patient 3; CCDC115#3 is patient 2).

#### - Patients **ATP6AP1#1** and **ATP6AP1#2**

Two male siblings; currently 41 years old (ATP6AP1#1) and 43 years old (ATP6AP1#2); French origin; non-consanguineous parents; CDG type 2 transferrin patterns with increase of the 3-sialo glycoform. **Under publication** (identified variants on request).

#### - Patients **TMEM165#1** and **TMEM165#2**

The analyzed samples are generous gifts from Dr F. Foulquier and Prof. J. Jaeken. TMEM165#1 (male) and TMEM165#2 (female; additional sample received during article redaction) are siblings. They have been published in supplementary reference (2) (TMEM165#1 is case 1; TMEM165#2 is case 2).

- Patient **COG5#1**

Male; currently 14 years old; age at diagnosis: 6 years old; French origin; diagnosed after exome sequencing and functional validation with very typical transferrin and ‘apoC-III-0’ patterns. Clinician/geneticist prefers the clinical phenotype and identified *COG5* variants not to be released. **Unpublished.**

- Patient **COG5#2**

Female; currently 8 years old; French origin; samples were addressed in a reported clinical context of psychomotor delay with hypotonia. Age at diagnosis: 4 year-old; CDG type 2 transferrin pattern; ‘apoC-III-0’ pattern. Identified variants: c.2324C>T / c.1508dup. **Unpublished.**

- Patients **COG7#1** and **COG7#2**

Two female siblings; currently 11 years old (COG7#1) and 8 years old (COG7#2); ages at diagnosis: 8 and 5 years old, respectively. Moroccan origin; consanguineous parents (first cousins). Samples were addressed in a clinical context of psychomotor delay, hypotonia, hyperthermia episodes of unknown origin, many infectious episodes, mild hepatomegaly for both patients. Cerebellar atrophy and diffuse ischemic lesions at MRI for COG7#1. CDG type 2 transferrin patterns; ‘apoC-III-0’ patterns. Identified variant: c170-7A>G (homozygous). **Under publication.**

- Patient **COG7#3**

Male; Moroccan origin; consanguineous parents (first cousins). Clinical data, glycosylation studies and identified variant of this patient have been published in supplementary reference (3).

- Patient **SLC35A2**

Female; currently 2 years old; from “La Réunion Island”, France. Age at diagnosis: 5 months. CDG type 2 transferrin pattern. **Published.** Brief clinical presentation, CDG screening tests and identified variant can be found in reference [33] (patient 3).

- Patient **SLC35A3**

Male; French origin; age at diagnosis: 6 months. **Published.** Brief clinical presentation, CDG screening tests and identified variants can be found in reference [33] (patient 4).

**2) Brief clinical data of studied linkeropathy patients:**

	<b>B4GALT7 (a)</b>	<b>B4GALT7 (b)</b>	<b>B3GALT6</b>	<b>B3GAT3</b>
Age at diagnosis	20 years	10 years	2 years	2 years
Gender	female	female	male	male
Other affected	No - La Réunion Island	No - First cousin parents	No	No - First cousin parents
Clinical features	- Dislocation hips and radial head. - Cervical instability - Bifid thumb - Glaucoma - Height<-5 DS	- Multiple dislocations affecting especially the knees - School difficulties - Height<- 4SD; weight < - 3 SD	- Kyphoscoliosis - Dislocation of elbows, <i>pectus carinatum</i> , - Club feet - Height -1SD	- Dislocations of knee and ankle, <i>Genu valgum</i> - Hyperlordosis - Radioulnar synostosis - School difficulties - Height< -3SD
Publication	<b>Published</b> Supp. ref (4)	<b>Unpublished</b>	<b>Unpublished</b>	<b>Published</b> Supp. ref (5) (patient 9)

**3) Supplementary references:**

(1) Girard M, Poujois A, Fabre M, et al. CCDC115-CDG: A new rare and misleading inherited cause of liver disease. *Mol Genet Metab.* 2018;124(3):228-35.

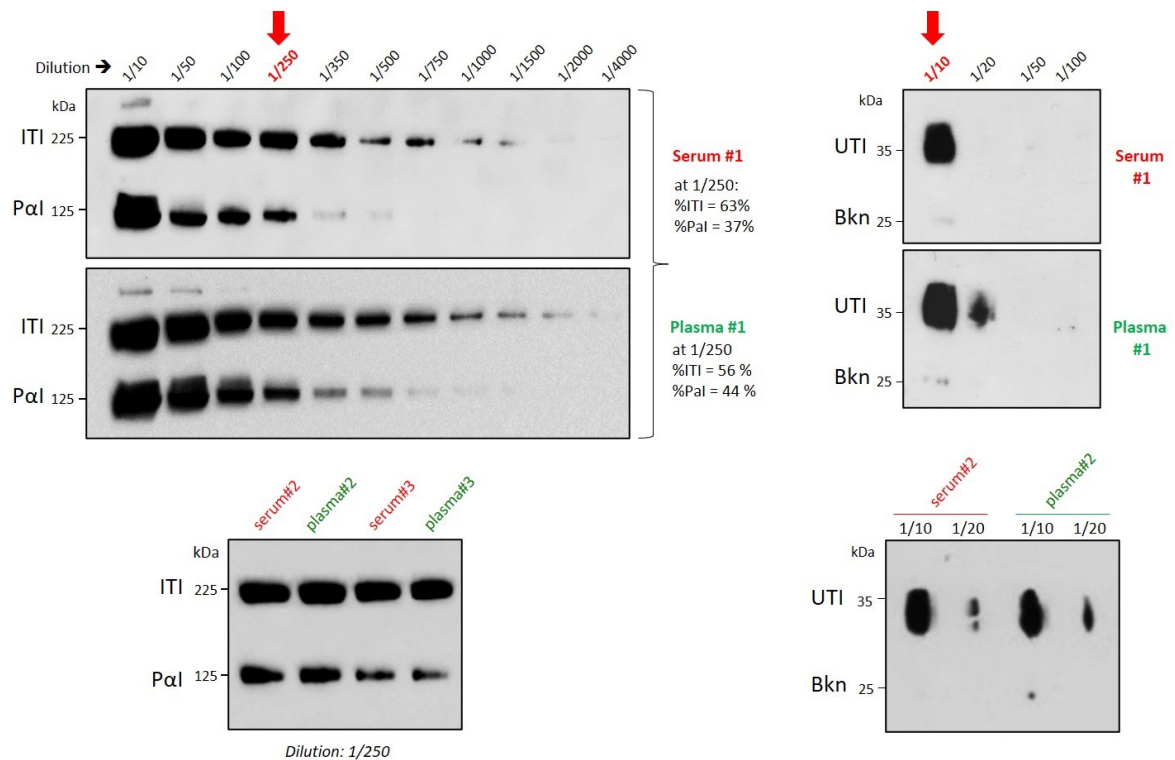
(2) Foulquier, F.; Amyere, M.; Jaeken, J. et al. TMEM165 Deficiency Causes a Congenital Disorder of Glycosylation. *The American Journal of Human Genetics* **2012**, 91 (1), 15–26.

(3) Zeevaert, R.; Foulquier, F.; Cheillan, et al. A New Mutation in COG7 Extends the Spectrum of COG Subunit Deficiencies. *European Journal of Medical Genetics* **2009**, 52 (5), 303–305.

(4) Cartault, F.; Munier, P.; Jacquemont, M.-L. et al. Expanding the Clinical Spectrum of B4GALT7 Deficiency: Homozygous p.R270C Mutation with Founder Effect Causes Larsen of Reunion Island Syndrome. *Eur J Hum Genet* **2015**, 23 (1), 49–53.

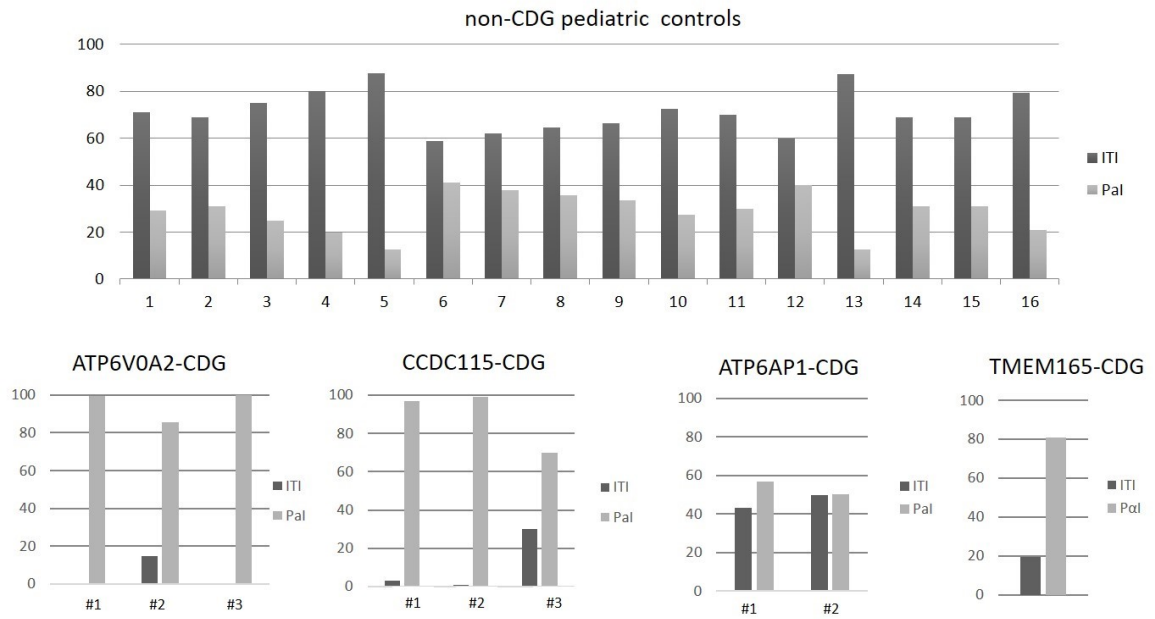
(5) Ranza, E.; Huber, C.; Levin, N. et al. Chondrodysplasia with Multiple Dislocations: Comprehensive Study of a Series of 30 Cases. *Clinical Genetics* **2017**, 91 (6), 868–880.

**Supplementary Fig.S1**



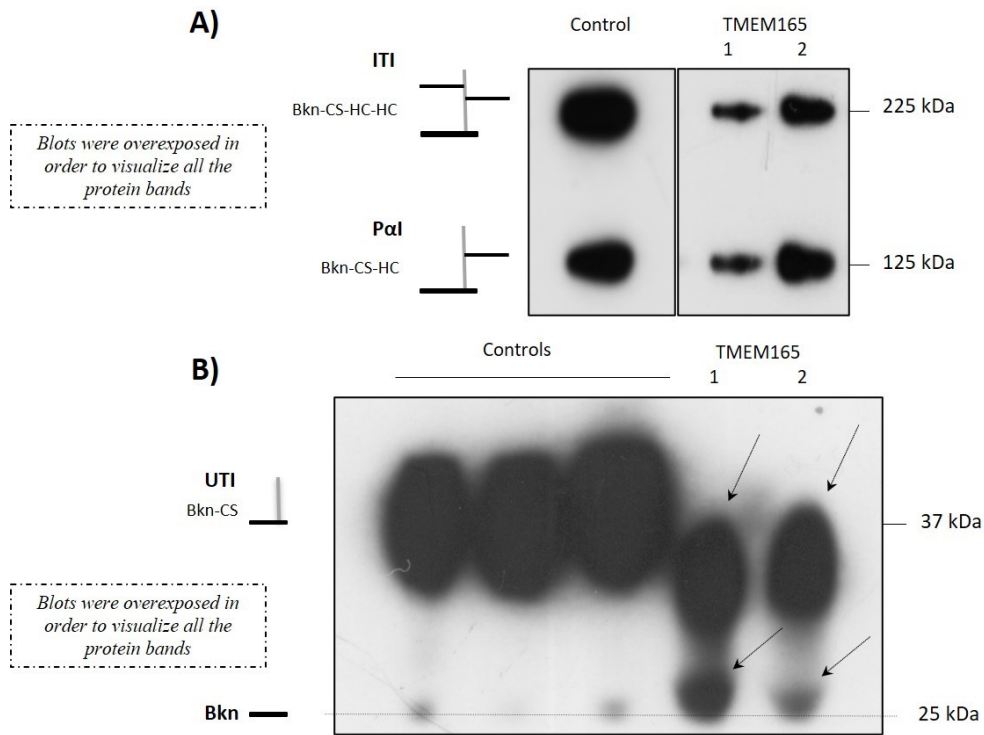
Determination of the optimal sample dilutions (up) and serum/plasma comparizon (below)

## Supplementary Fig.S2



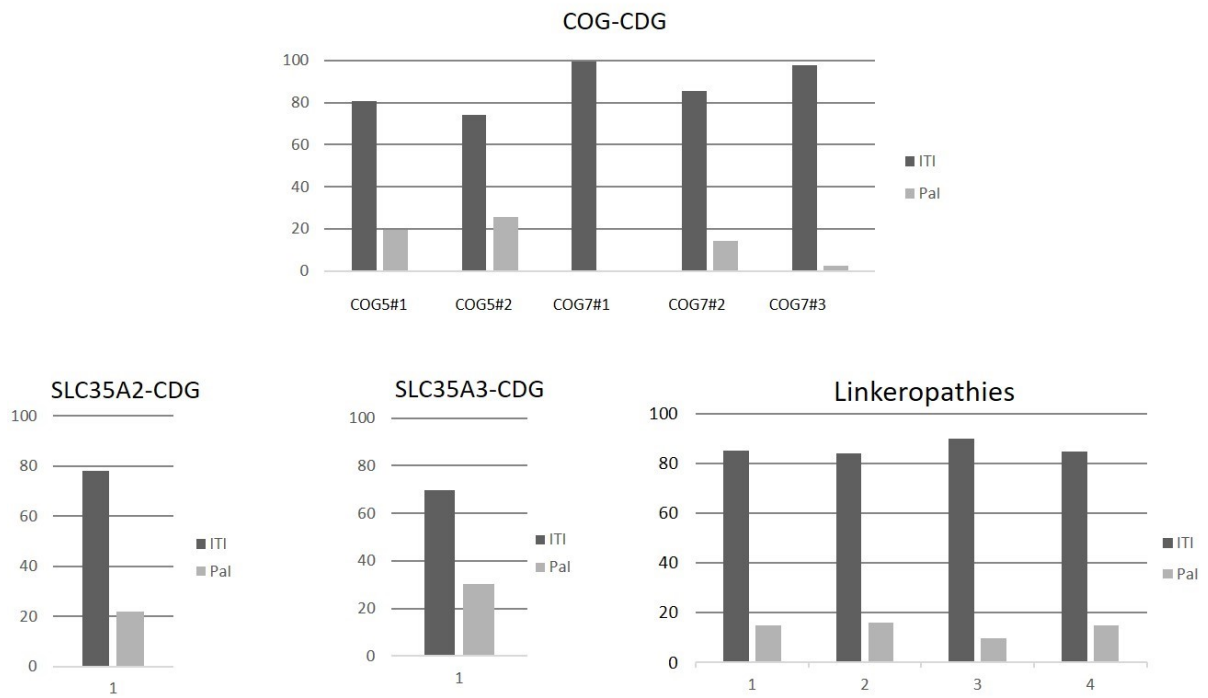
Percentages of ITI and Pal in non-CDG pediatric controls (n=16), ATP6V0A2-CDG (n=3), CCDC115-CDG (n=3), ATP6AP1-CDG (n=2) and TMEM165-CDG (n=1).

**Supplementary Fig.S3**



Western-blot of heavy Bkn isoforms (A) and light Bkn isoforms (B) in the two TMEM165-CDG samples. *TMEM165-CDG #1* is the sample described in the manuscript. *TMEM165 #2* is an additional *TMEM165-CDG* sample. Dotted arrows indicate qualitative abnormalities compared to controls.

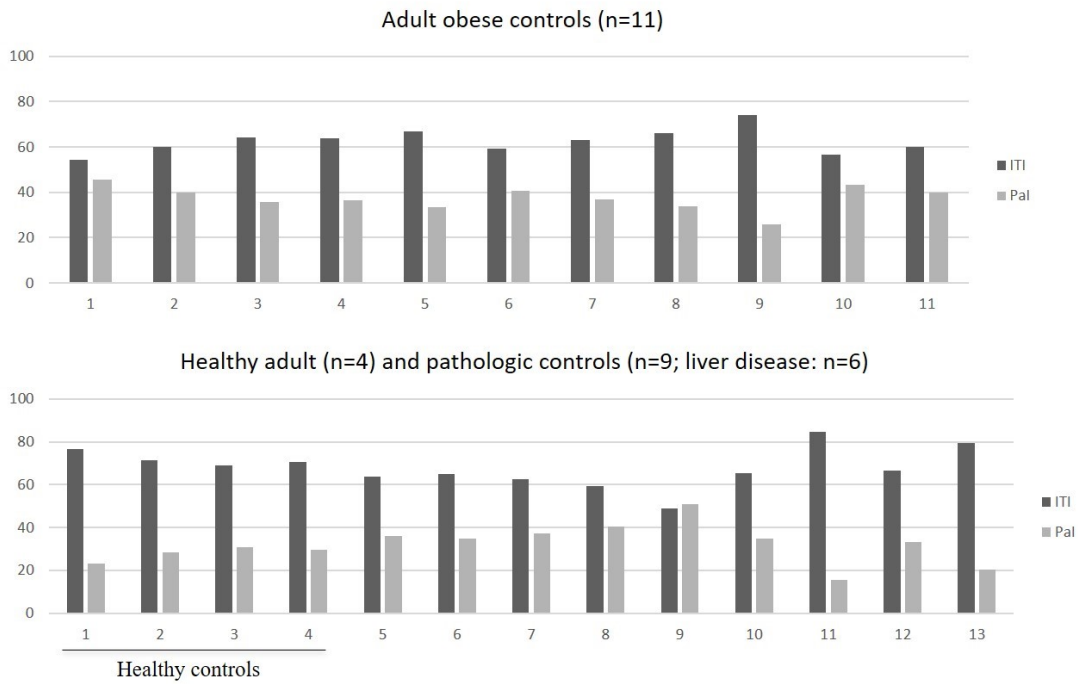
### Supplementary Fig.S4



Percentages of ITI and Pal in COG-CDG (n=5), SLC35A2-CDG (n=1), SLC35A3-CDG (n=1) and linkeropathies (n=4; 1-2: B3GALT7; 3: B4GALT6; 4: B3GAT3).



## Supplementary Fig.S5



Percentages of ITI and PaI in obese patients (n=11), and in healthy (1-4) and pathologic adult patients (5-13)

5: alcoholic cirrhosis + hepatitis C; 6: liver fibrosis (F4); 7: alcoholic cirrhosis ; 8: waldenstrom disease; 9: periumbilical mass + icterus + anemia;  
10: gastric sleeve surgery; 11: hepatitis; 12-13: cirrhosis.

**Supplementary Table1:** ITI and PaI signal levels, albumin values and calculated (ITI + PaI)/Alb ratios for the samples analyzed in **Fig.2**.

<b>Patient</b>	<b>ITI signal</b>	<b>PaI signal</b>	<b>ITI + PaI</b>	<b>Albumin (Alb) (g/L)</b>	<b>(ITI + PaI)/Alb</b>
<b>Control</b>	74653 (mean)	45190 (mean)	119843	<b>43</b>	<b>2787</b>
<b>ATP6V0A2 #1</b>	17157	34204	51361	64.1	801
<b>ATP6V0A2 #2</b>	18150	35477	53627	53.7	999
<b>ATP6V0A2 #3</b>	0	1530	1530	56.6	27
<b>CCDC115 #1</b>	16	1134	1150	46.7	25
<b>CCDC115 #2</b>	0	1173	1173	50.5	23
<b>CCDC115 #3</b>	1651	3360	5011	66.8	75
<b>ATP6AP1 #1</b>	3749	4274	8023	38.5	208
<b>ATP6AP1 #2</b>	28356	30671	59027	63.4	931
<b>TMEM165 #1</b>	94	350	444	40.6	11
<b>COG5 #1</b>	40491	12788	53279	49.5	1076
<b>COG5 #2</b>	49874	17579	67453	58.5	1153
<b>COG7 #1</b>	4332	70	4402	47	94
<b>COG7#2</b>	30018	4950	34968	34.6	1011
<b>COG7#3</b>	8830	647	9477	42.4	224
<b>SLC35A2</b>	25707	8623	34330	63.3	542
<b>SLC35A3</b>	15122	5944	21066	38.6	546
<b>B4GALT7 (a)</b>	90374	15753	106127	66.7	1591
<b>B4GALT7 (b)</b>	54782	7064	61846	59.2	1045
<b>B3GALT6</b>	37344	1130	38474	58.3	660
<b>B3GAT3</b>	72876	8127	81003	47.9	1691

### III-3-2 Complementary results (unpublished)

In this section we provide unpublished data which complements results showed in the previous publications (i.e., CCA letter to the editor and JIMD article). We performed (i) Western blot analysis of heavy and light Bkn isoforms in patients with defective ATP6V1F (2 patients) and ATP6AP1 (one new patient) subunits of the V-ATPase, (ii) 2-DE analysis of abnormal Bkn light forms in TMEM165 and ChSy-1 deficiencies as well as Western blot of Bkn heavy forms in ChSy-1 deficient patient, (iii) mass spectrometry analyses to characterize linkeropathy-associated Bkn light forms, (iv) development of a 2-DE based strategy to detect sulfation defects in patients with defective SLC35B2 and IMPAD1, and (v) development of Bkn analysis from dried blood spots (DBS).

#### III-3-2-1 Complementary Western blot and 2-DE analyses

In two patients with pathogenic variants in *ATP6V1F* (coding a subunit of the Golgi V-ATPase) and an additional patient with mutated *ATP6AP1*, we found dramatically decreased ITI and PaI levels together with abnormal ITI/PaI ratio compared to controls. Moreover, Bkn-CS displayed mildly increased MW compared to controls (**Figure 18**). These profiles were strictly similar to that found in ATP6V0A2, CCDC115 and ATP6AP1 deficiencies. This result reinforced the reliability of Bkn as an additional biomarker for the screening of CDG with impaired V-ATPase.

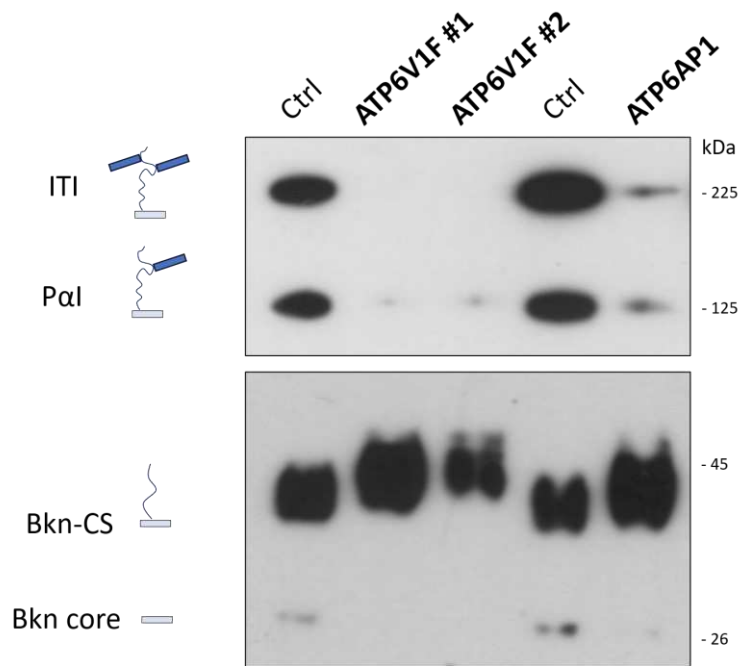


**Figure 18: Western blot analysis of heavy and light Bkn forms in CDG with proton pump deficiencies (2 ATP6V1F-CDG and one ATP6AP1-CDG)**

Western blot analysis of Bkn heavy and light forms in two ATP6V1F and one ATP6AP1 deficient-patients compared to controls

In the sample from one TMEM165 deficient patient, we performed 2-DE analysis of Bkn to characterize the encountered abnormal light forms. In contrast to the homogeneous linkeropathy-associated profiles, we found heterogeneous pattern with four spots indicating the presence of several variably charged immature Bkn light forms (**Figure 19 A**). Combined with the previously described abnormal Western blot pattern, this result suggests that lack of  $Mn^{2+}$  in the Golgi lumen may lead to malfunction of various enzymes involved in the linker formation and the CS chain elongation.

Similarly, 2-DE analysis of serum Bkn from one ChSy-1 deficient patient (i.e., described in *CCA* letter to the editor) showed heterogeneous profile with several spots of different *pI* (**Figure 19 A**). While ChSy-1 has been shown to carry both GlcA and GalNAc transferase activity [32], such a 2-DE profile indicates the presence of multiple abnormal Bkn light forms resulting from enzymatic blockades at several steps of the CS-GAG  $[GlcA-GalNAc]_n$  polymerization.

Regarding the potential influence of such CS chain elongation defects on the following HC esterification, we performed the Western blot analysis of the heavy forms in patient's serum. The result showed a decreased MW compared to control, at least for P $\alpha$ I, indicating the presence of shorter Bkn-CS chains harboring the HC proteins (**Figure 19 B**). This result indicates that, in this ChSy-1 deficient case, CS-HC esterification was not influenced by the associated GAG chain length shortening.

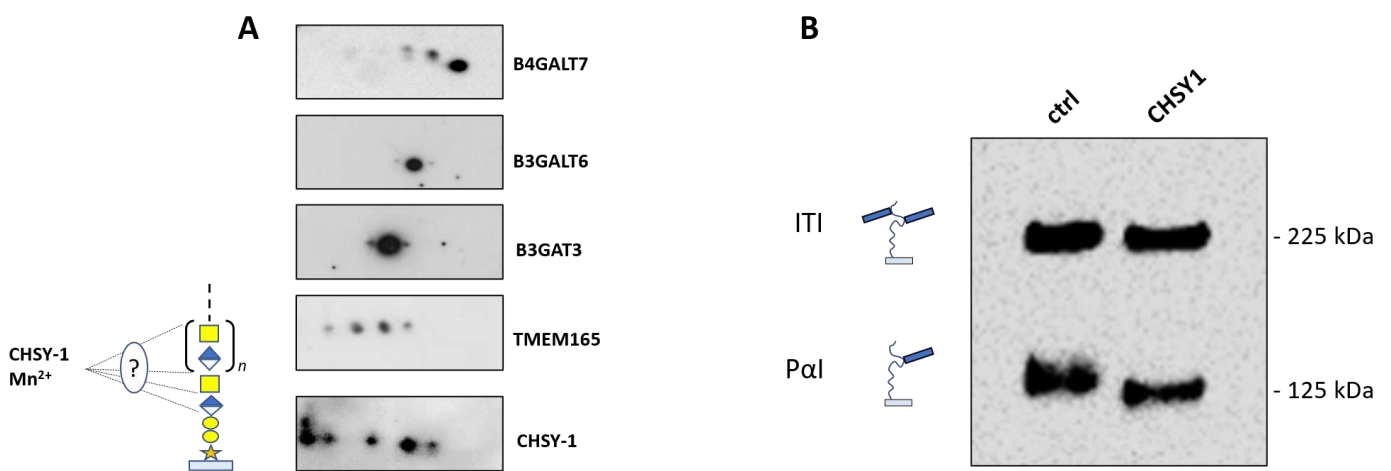


**Figure 19: Complemental analyses of Bkn light forms in TMEM165-CDG and ChSy-1 deficiency**

A) 2-DE profiles of Bkn abnormal light forms in linkeropathies, TMEM165 and ChSy-1 deficiency. Left scheme illustrates the possible involvement of ChSy-1 and Mn<sup>2+</sup> at several steps of CS elongation  
 B) Western blot profile of heavy Bkn forms (ITI and P $\alpha$ I) in ChSy-1 deficient patient compared to one healthy individual

### **III-3-2-2 Mass spectrometry analysis of linkeropathy-associated Bkn abnormal forms**

#### **a. Testing on chondroitinase-treated serum bikunin isoforms**

To develop a mass spectrometry (MS) protocol for identifying linkeropathy-associated Bkn abnormal forms, we first performed testing experiments in a control serum treated by chondroitinase ABC (chABC) which is a CS-GAG degrading enzyme releasing core protein-linked hexasaccharide (GlcA-GalNAc(S)-GlcA-Gal(S)-Gal-Xyl-core protein) (**Figure 20 A**). Since such light Bkn glycoform is theoretically absent from normal serum, it has been used as a model to mimic linkeropathy-associated Bkn abnormal forms in order to develop the HPLC/MS analysis protocol in linkeropathy patients' serum (Material and methods p.231).

Western blot of serum Bkn in chABC treated serum showed a unique band at ~30 kDa that likely corresponds to hexasaccharide-Bkn resulting from the removal of the CS chain from ITI, P $\alpha$ I and Bkn-CS (**Figure 20 B**). Furthermore, 2-DE analysis showed two spots in chABC treated serum that could correspond to bi-sulfated and mono/unsulfated hexasaccharide-Bkn (**Figure 20 B**). Expectedly, such 2-DE pattern was not found in the untreated serum. When bypassing the antibody detection by a colloidal silver blue staining of 2-DE resulting gel, we obtain whole separation pattern of serum proteins (**Figure 20 C**) (329). By comparison with the untreated serum, chABC-treated serum had a staining pattern showing an additional spot that is likely to correspond to +/- sulfated hexasaccharide-Bkn. This spot was manually removed from the gel and digested with trypsin.

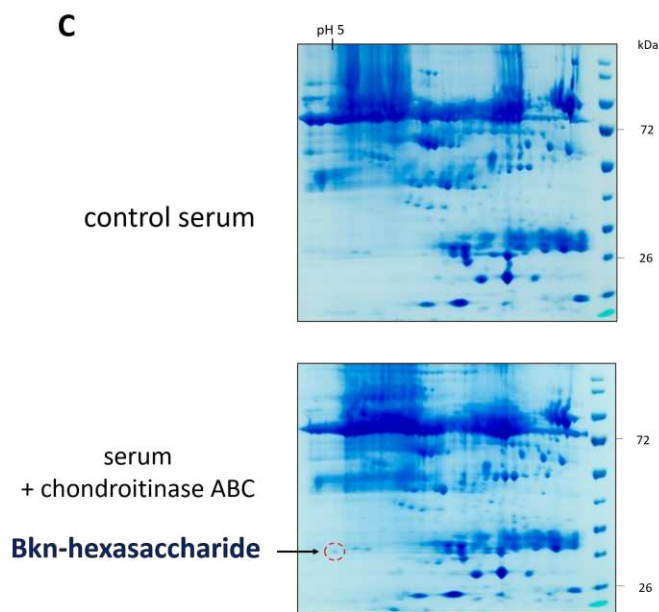
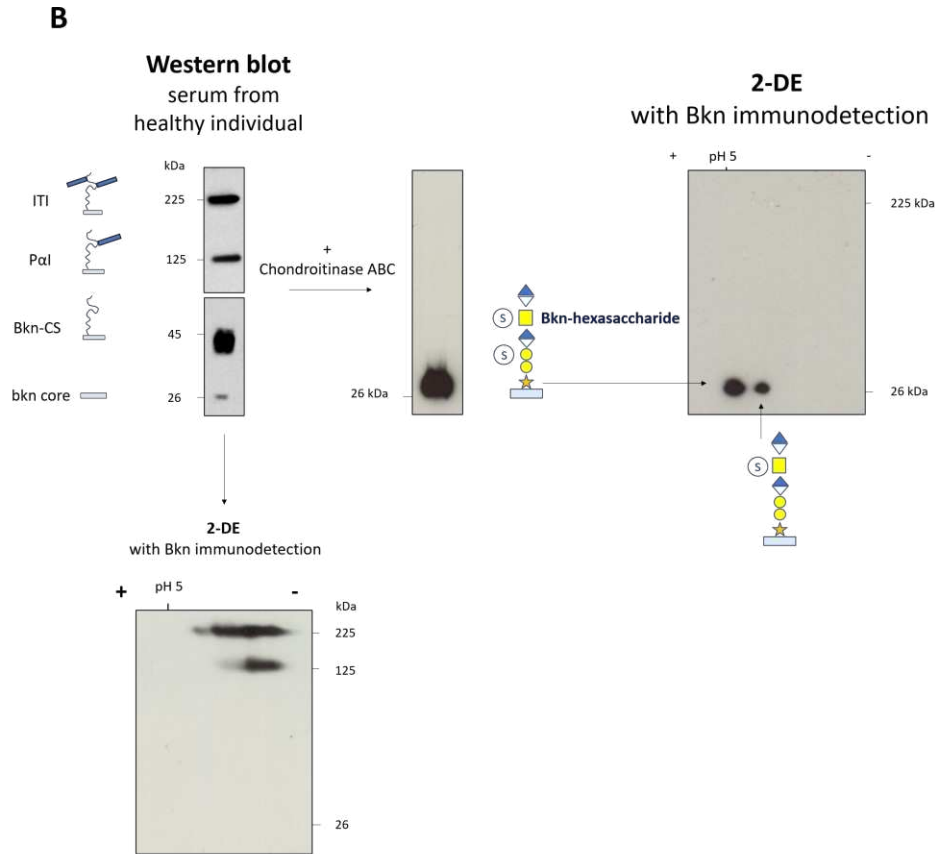
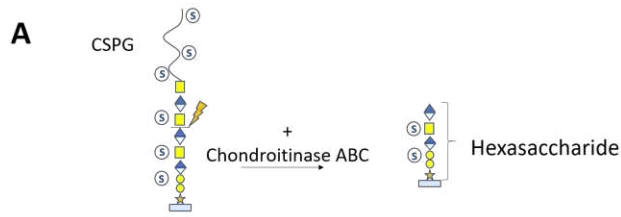


**Figure 20: 2-DE based purification of Bkn-hexasaccharide from chABC treated control serum**

A) ChABC is an enzyme that degrades CS-GAG chains from CSPG which releases hexasaccharide-linked core proteins. B) Serum Bkn isoforms in control serum showing the usual bands (Left) and the profile after chABC digestion (middle). Right panel shows 2-DE profile of chondroitinase-treated serum which exhibits two spots corresponding to Bkn-Hexasaccharide (+/- S). (C) 2-DE gel silver blue staining pattern of chABC-treated serum compared to untreated counterpart. ChABC digestion led to an additional spot (red dotted circle) that could correspond to Bkn-Hexasaccharide.

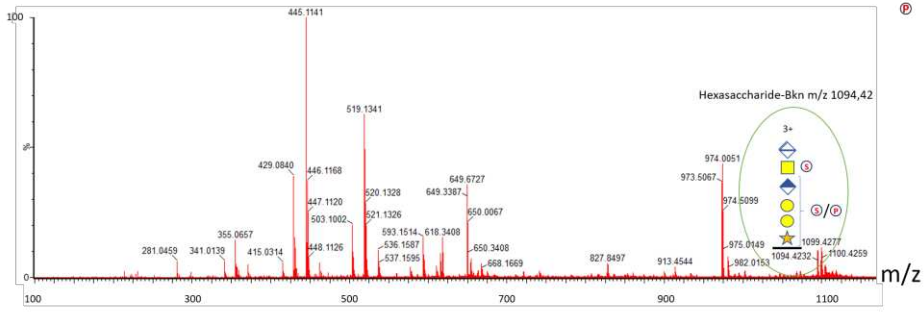
HPLC/MS analysis of the trypsin-digested sample included electrospray ionization (ESI) which generated precursor ion spectrum (MS1) highlighting an  $m/z$  1094.42 (3+) specie corresponding to the tryptic Bkn (AVLPQEEEGSGGGQLVTEVTK) linked to a bi-sulfated hexasaccharide (**Figure 21 A**). Precursor ion fragmentation by collision-induced dissociation (CID) yielded MS2 spectrum containing CS disaccharide units [GlcA-GalNAc] and [GlcA-GalNAc(S)] ( $m/z$  362.10 and 442.05 respectively). Moreover, various hexasaccharide-Bkn fragments corresponding to Xyl-Bkn ( $m/z$  1131.05), Gal-Xyl-Bkn ( $m/z$  1212.07), Gal-Gal-Xyl-Bkn ( $m/z$  1293.10), GlcA-Gal-Gal-Xyl-Bkn ( $m/z$  1381.12) and the tryptic Bkn ( $m/z$  1064.52) were detected (**Figure 21 B**). As showed by  $m/z$  1094.42 isolated chromatogram, the ionic current of this specie was consistently 80x lower in the untreated serum compared to chABC-treated serum (**Figure 21 B**). To make sure that hexasaccharide-bkn is the major Bkn glycoform in chABC-treated serum, we compared its relative abundance with that of other Bkn glycoforms including Xyl-Bkn, Gal-Xyl-Bkn, Gal-Gal-Xyl-Bkn, GlcA-Gal-Gal-Xyl-Bkn. The MS1 spectrum showed a clear minority of linkeropathy-associated Bkn abnormal forms compared to hexasaccharide-Bkn (**Figure 21 D**).

Altogether, these results showed the ability of HPLC/MS (ESI-CID) analysis to efficiently detect Bkn glycoforms from 2-DE purified serum samples. Such strategy has been employed to identify the abnormal Bkn-light forms in linkeropathy patients' serum.

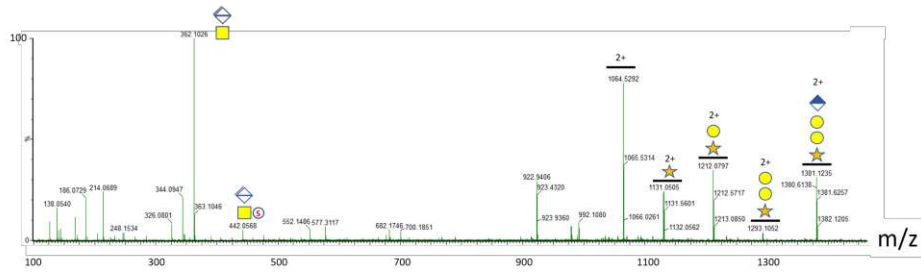


- AVLPQEEGGGGQLVTEVTK 2130 Da
- ★ Xylose 132.04 Da
- Galactose 162.05 Da
- GalNAc 203.08 Da
- ◇ GlcA 176.03 Da
- ◇ Dehydro-GlcA 158 Da (GlcA - H<sub>2</sub>O)
- ⊖ SO<sub>3</sub> 79.96 Da
- ⊕ PO<sub>3</sub> 79.97 Da

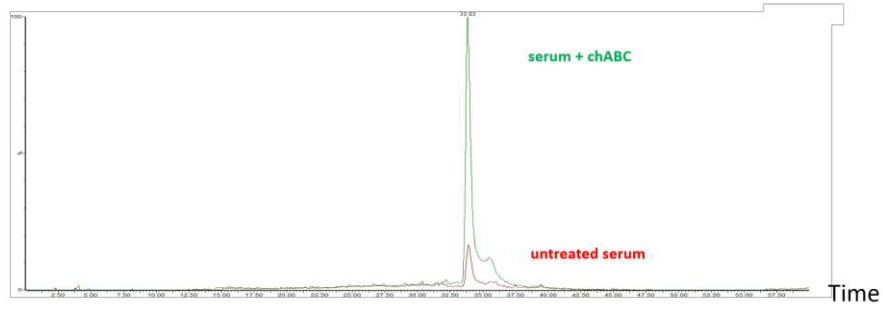
**A MS1 precursor ions spectrum (Serum + chABC)**



**B MS2 fragment spectrum (m/z 1094.4232 precursor ion)**



**C Isolated m/z 1094,42 HPLC chromatogram**



**D MS1 precursor ions spectrum (Serum + chABC) - ZOOM**

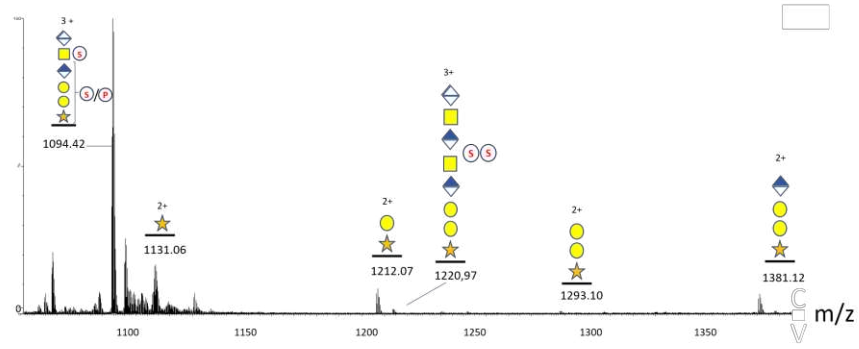


**Figure 21: HPLC/MS analysis of 2-DE purified hexasaccharide-Bkn from chABC treated serum**

A) MS1 precursor ions spectrum of chABC treated serum sample. Hexasaccharide-Bkn was detected at m/z 1094.04. B) MS2 spectrum generated from CID of m/z 1094.04 ion shows the resulting fragments including the basement [GlcA-GalNAc] motif of the CS chain and various compounds of the tetrasaccharide linkage region. (C) HPLC chromatogram associated to m/z 1094.04 precursor ion showing higher levels of hexasaccharide-Bkn in chABC serum compared to untreated counterpart. (D) Zoom on the chABC MS1 spectrum to show relative abundance of hexasaccharide-Bkn compared to linkeropathy-associated Bkn abnormal forms.

**b. Characterization of linkeropathy-associated Bkn abnormal forms.**

As shown in **Figure 22**, we performed 2-DE of B4GALT7 patient's serum followed by colloidal silver blue staining. By overlapping the stained gel with the anti-Bkn Western blot revelation film, we localized and removed the gel area likely to contain the Xyl-Bkn abnormal form (~1 cm<sup>2</sup> spot). A control spot was obtained by removing the same area from 2-DE gel of a control serum. Spots were subjected to trypsin digestion following HPLC/MS analysis (**Figure 22**).

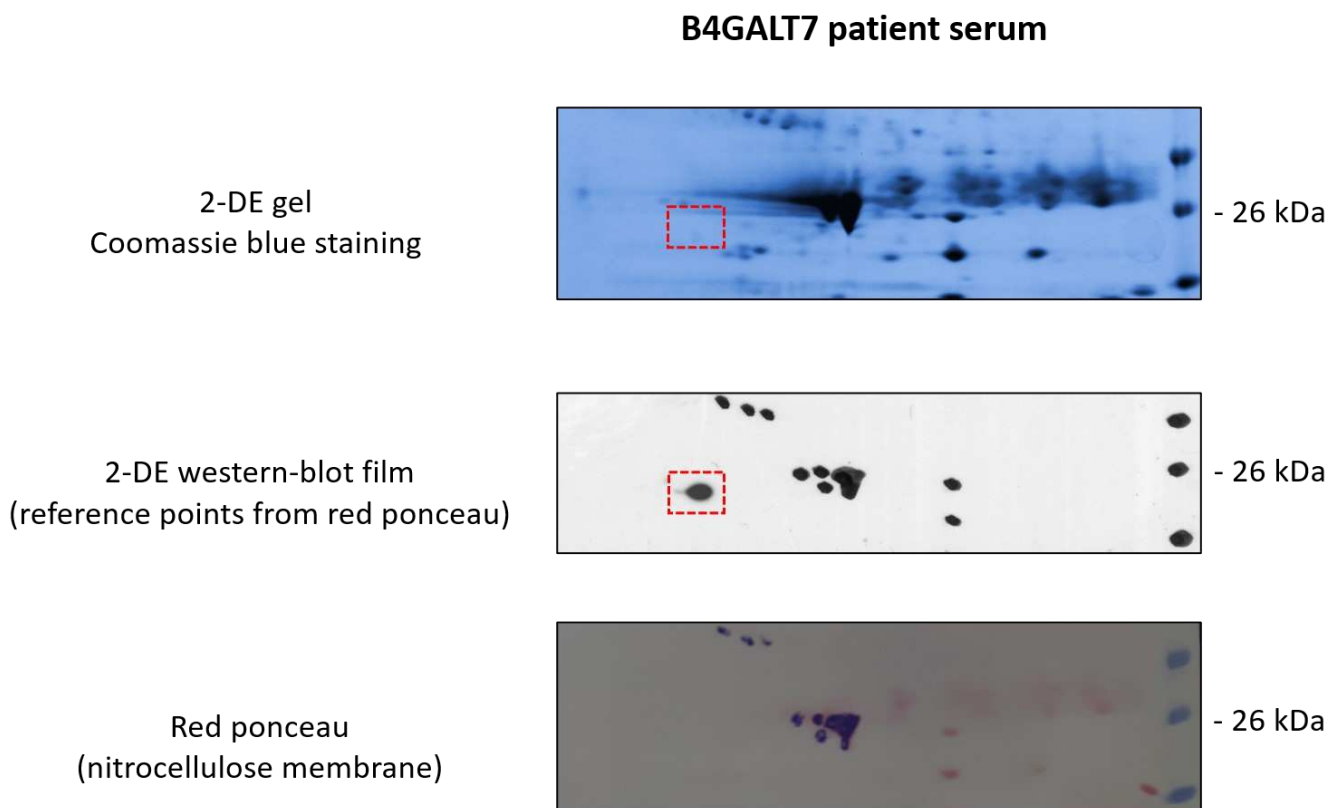


**Figure 22: 2-DE based purification of B4GALT7-associated abnormal Bkn light forms**

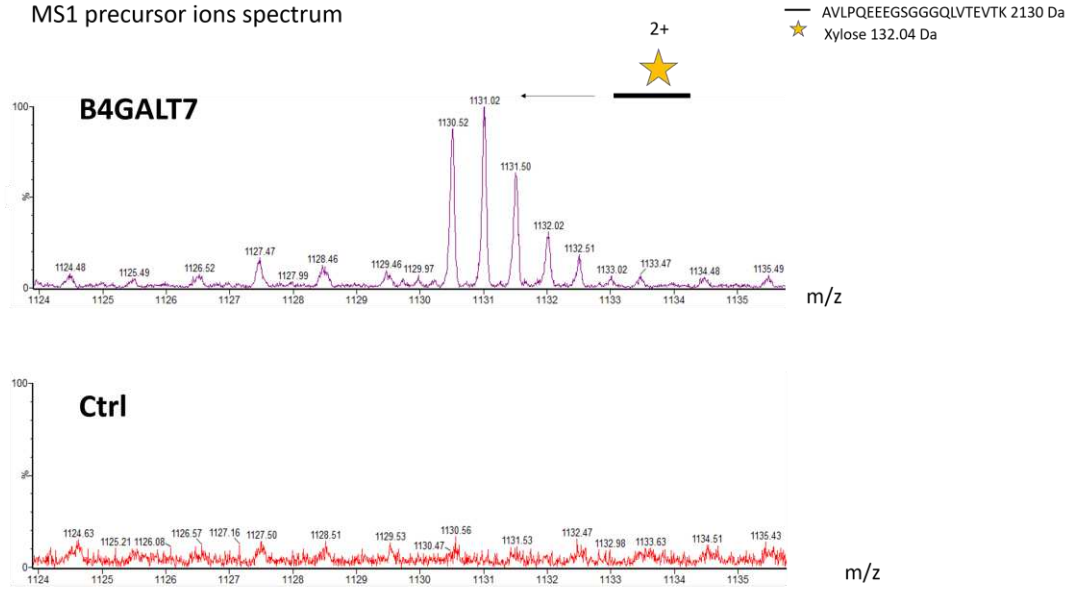
2-DE of B4GALT7 patient serum was performed and gel was stained with Silver blue. Western blot

with anti-Bkn antibodies together with red ponceau staining of nitrocellulose membrane were performed in parallel for accurate localization of the gel area likely to contain target Bkn abnormal form (red square).

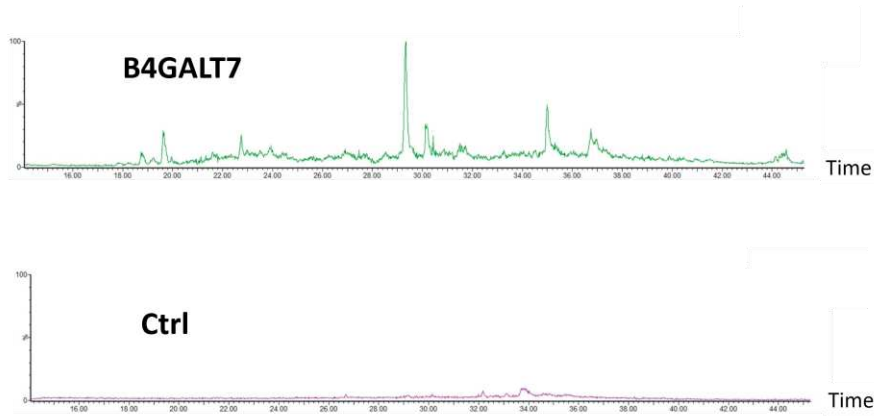
MS1 spectrum clearly showed the presence of Xyl-Bkn specie at  $m/z=1131.02$  in B4GALT7 deficient patient sample by contrast to control (**Figure 23 A**). This result was confirmed by the  $m/z$  1131.02 isolated chromatogram showing a major peak at  $\sim 29$  min retention time for B4GALT7 deficient patient while no signal was observed for the control (**Figure 23 B**). MS 2 fragmentation spectrum of  $m/z$  1131.02 precursor ion consistently yielded the tryptic Bkn (AVLPQEEEGSGGGQLVTEVTK) at  $m/z = 1065.06$  and its fragments  $y_5$  ( $m/z$  577.33),  $y_{18}$  ( $m/z$  922.96) and  $y_{19}$  ( $m/z$  979.49) (**Figure 23 C**).

By showing that B4GALT7 deficiency leads to abnormal blood secretion of the immature Xyl-Bkn, these MS data reinforce the reliability of Bkn analysis by Western blot and 2-DE for screening B4GALT7 linkeropathy. Currently, the analyses are being performed for *B3GALT6* and *B3GAT3* mutated patients.

**A** MS1 precursor ions spectrum



**B** Isolated m/z 1131,02 HPLC chromatogram



**C** MS2 fragment spectrum (m/z 1131.02 precursor ion)

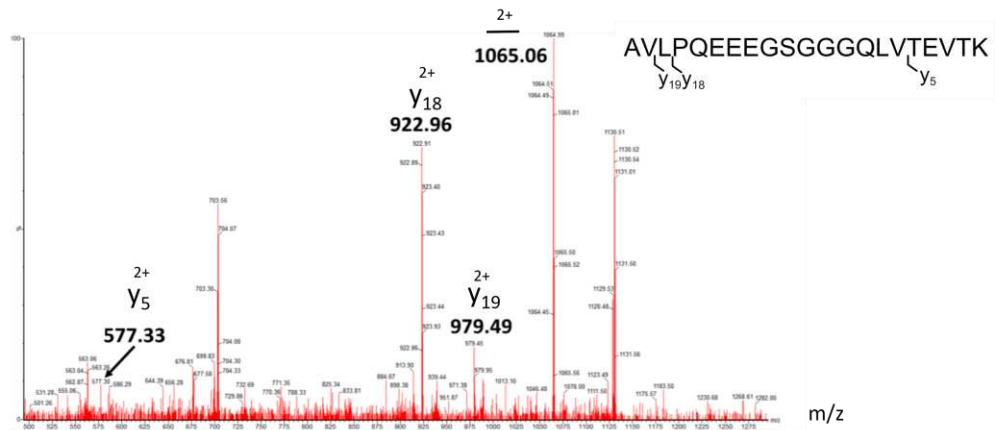


**Figure 23: HPLC/MS analysis of 2-DE purified B4GALT7 deficient patient serum**

A) MS1 spectrum of B4GALT7 deficient patient sample in comparison to control. Xyl-Bkn was highlighted at  $m/z = 1131.02$  within its isotopic massif. This peak is clearly absent in healthy control. B) Isolated  $m/z 1131.02$  chromatogram in B4GALT7 deficient patient compared to control. C) MS2 fragmentation spectrum of  $m/z 1131.02$  precursor ion showing corresponding fragments of tryptic Bkn.

**III-3-2-3 Bkn analyses in sulfation defects**

Western blot analysis of Bkn-CS in patients with PG-IMD due to deficient SLC35B2 (sulfate transporter) and IMPAD1 (hydrolysis of PAP released from sulfation reactions) yielded similar profile than that of controls (**Figure 24 A**). This result was not surprising since sulfate groups have too low molecular weight for generating visible MW variations. To analyze Bkn-CS sulfation, we employed a strategy based on chondroitinase treatment of patients' serum which generates a sulfated hexasaccharide-Bkn (Material and methods p.231). Treated samples are then analyzed by 2-DE. As showed in **Figure 24 B**, 2-DE profiles of chABC-treated control sera displayed two spots corresponding to variably sulfated hexasaccharide-Bkn. Left spot is referred to as the sulfated hexasaccharide-Bkn while right spot is the hyposulfated form. In two chABC-treated SLC35B2 (#1 and #2) and one IMPAD1-deficient patient serum, the ratio sulfated/hyposulfated hexasaccharide-Bkn was decreased compared to chABC-treated control samples (n=8) indicating defective Bkn-CS sulfation (**Figure 24 B**). Although additional analyses are required in additional patients to confirm these results, such data strongly suggest potential value of serum Bkn as a biomarker of GAG sulfation defects.

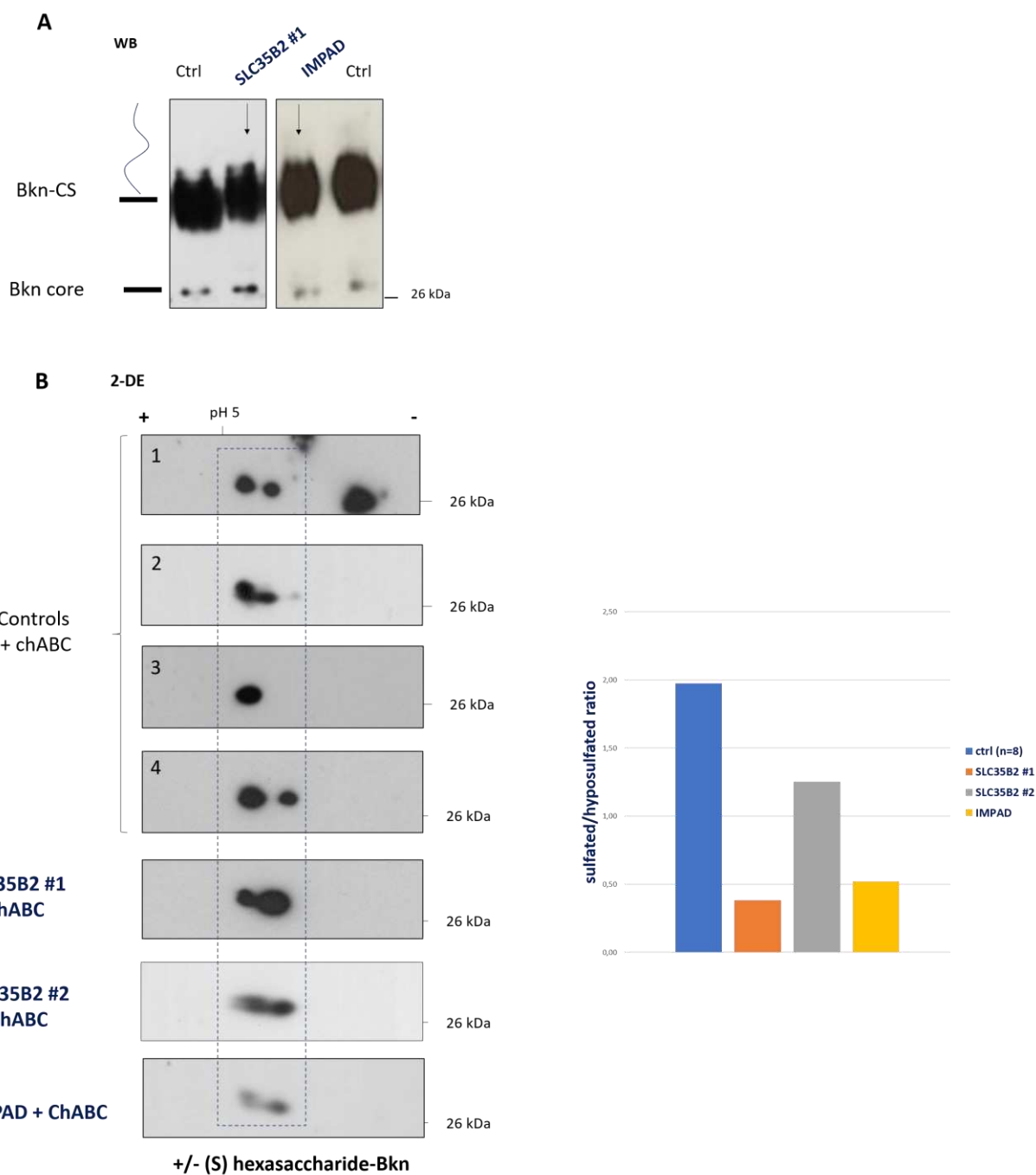


**Figure 24: Western blot and 2-DE of serum Bkn light forms in SLC35B2 and IMPAD1 deficient patients**

A) Western blot analysis of serum Bkn light forms (i.e., Bkn-CS and PaI) in SLC35B2 and IMPAD deficient patients compared to controls. B) left panel, 2-DE of chABC-treated serum from two SLC35B2 and one IMPAD deficient patients compared to controls. Right panel, sulfated/hyposulfated ratios in patients were compared to that of controls.

### III-3-2-4 Application of Bkn analysis to dried blood spots (DBS)

DBS stem from a drop of blood on a Guthrie paper (**Figure 25 A**). They constitute an alternative to vascular blood sampling for several medical applications including neonatal screening of various congenital diseases (330,331). The benefits of DBS include non-invasiveness of the sampling method, low volume of the collected blood, easier conservation and transport, and cost-effective management.

Serum samples from PG-IMD and CDG patients are often limited, therefore, we evaluated the possibility of performing Bkn analysis from DBS. Preliminary experiments showed that Western blot analysis is highly hindered by hemoglobin, the latter having peroxidase activity which creates contaminating signal during chemiluminescence revelation (data not shown). Then, we developed a protocol based on hemoglobin depletion using a commercial kit (Hemovoid™ from Biotech Support Group) prior to Western blot analysis (**Figure 25 A**) (Material and methods p.231).

We analyzed Bkn isoforms by Western blot in three hemoglobin-depleted DBS samples by comparison to serum from healthy individuals. Regarding Bkn light forms, Bkn-CS (35-45 kDa) and free Bkn (26 kDa) profiles in hemoglobin-depleted DBS samples were similar to that in serum, without contaminating hemoglobin signal (**Figure 25 B**). To assess whether the analysis could highlight abnormal Bkn light forms profiles as in linkeropathies, we treated one hemoglobin-depleted DBS sample with chABC to generate hexasaccharide-Bkn and simulate a positive control. ChABC-treatment yielded, consistently, a hexasaccharide-Bkn ~30 kDa band suggesting the ability of this analysis to detect abnormal Bkn profile (**Figure 25 B**). Although this study should be validated by showing abnormal Western blot profiles in patients with PG-IMD, the results are rather encouraging for future utilization in screening these defects.

Surprisingly, heavy forms systematically displayed an abnormal profile consisting of a

reversed ITI/PαI ratio (Figure 25 B). This result suggests a vulnerability of Bkn heavy forms to oxidative properties of hemoglobin within the DBS, which may trigger HC-CS ester linkages breakdown, at least for ITI (332). This would considerably compromise the heavy forms profile interpretation in patients displaying ITI and PαI quantitative and/or qualitative abnormalities such as individuals with Golgi homeostasis defects (Haouari et al. JIMD). We are currently working on determining the cause of such hinderance in heavy forms' profile. If the deleterious effect of oxidative properties of hemoglobin on CS-HC esterification is confirmed, Bkn analyses from DBS should be exclusively intended for the light forms (free Bkn and Bkn-CS) to detect PG defects and not for the screening of CDG with impaired Golgi homeostasis.

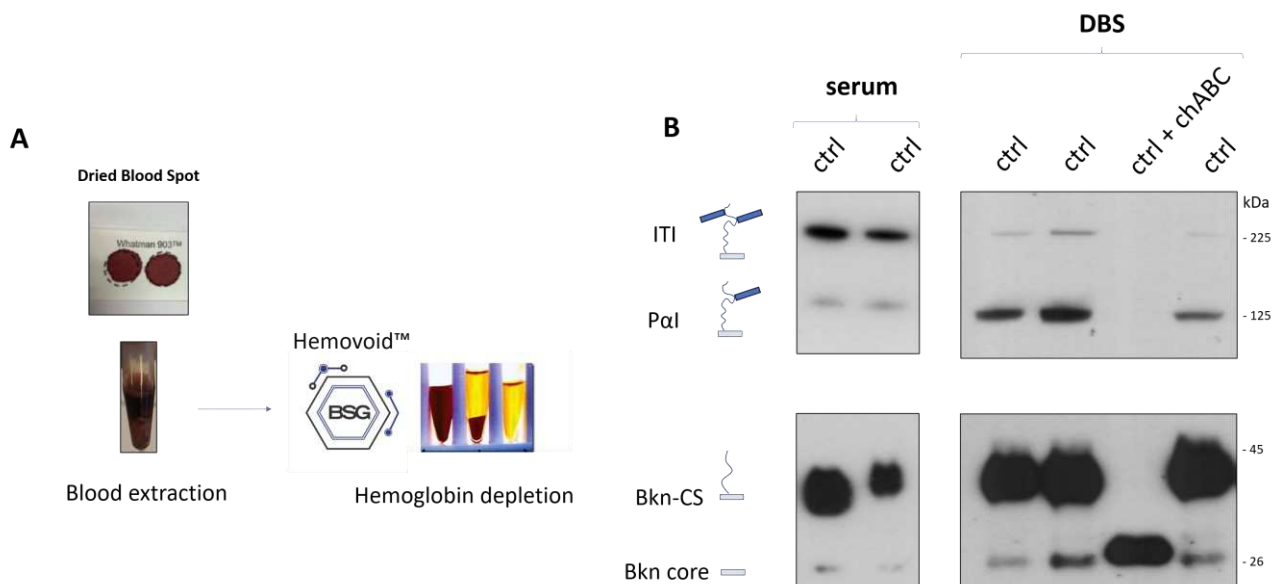


**Figure 25: Hemoglobin depletion of blood extracts from DBS followed by Western blot analysis of Bkn isoforms**

A) Total blood extraction from DBS and hemoglobin depletion using hemovoid™ kit. B) Bkn analysis by Western blot from hemoglobin-depleted blood extracts of three control individuals, one of which being treated by chABC and used as a positive control. Chemiluminescence allowed detection of the four Bkn isoforms (ITI, PαI, Bkn-CS and free Bkn).



## III-4 Publication 3

### Original article

# SLC37A4-CDG: New biochemical insights for an emerging congenital disorder of glycosylation with major coagulopathy

Raynor A\*, **Haouari W**\*, Ng BG, Cholet S, Harroche A, Raulet-Bussian C, Lounis-Ouaras S, Vuillaumier-Barrot S, Pascreau T, Borgel D, Freeze HH, Fenaille F, Bruneel A.

Clin Chim Acta. 2021, 521:104-106. doi: 10.1016/j.cca.2021.07.005.

\*: *first co-authors*



### III-4-1 Article presentation

SLC37A4 is an ER-localized transporter allowing intake of glucose-6-phosphate (G6P) from the cytosol to produce glucose during fasting conditions (gluconeogenesis). A dominantly inherited pathogenic variant (c.1267C>T) leading to partial loss of SLC37A4 ER-retention signal have been described in patients presenting liver diseases and coagulopathy. Hypoglycosylation of plasma *N*- and *O*-glycoproteins have been found, allowing to classify this deficiency among CDG (333,334). Furthermore, Ng et al showed impaired Golgi homeostasis in slc37A4 KO HuH7 cells (altered morphology and decreased luminal pH) (335). While the molecular mechanisms leading to such impairments are not understood, it appears that half of SLC37A4 transporters are mislocalized which leads to abnormal G6P delivery to other undefined cellular compartments than the ER (**Figure 26**).

In six SLC37A4 mutated patients, we analyzed serum Bkn to seek for possible CS elongation or CS-HC esterification abnormalities that could result from Golgi homeostasis defect. The results have been published in an original article which is presented herein.

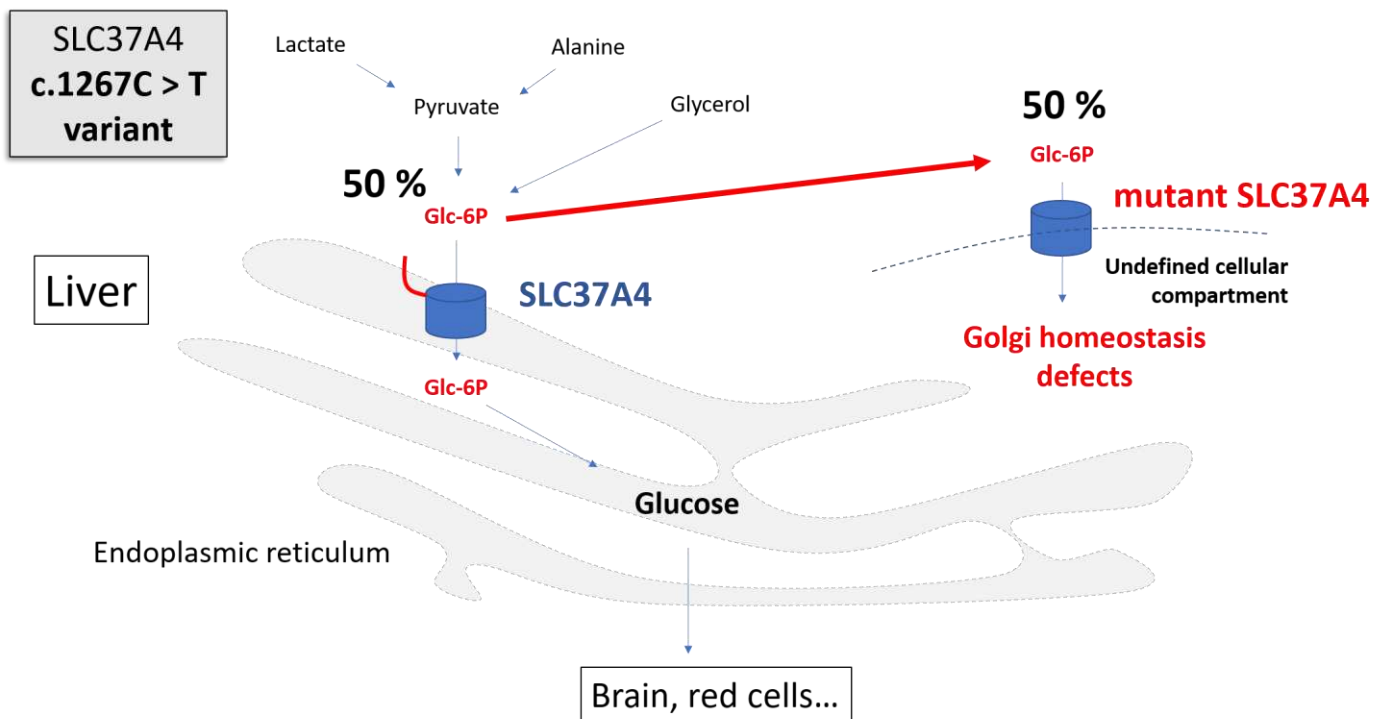


**Figure 26: Heterozygous c.1267C>T mutation causes half mislocalization of the ER SLC37A4 glucose-6-phosphate transporter to other cellular compartments**

During fasting conditions, hepatocytes use the gluconeogenic substrates lactate, alanine, glycerol, and pyruvate to produce G6P. The latter enters the ER through SLC37A4 for being metabolized into glucose that will reach the blood circulation to supply glucose-dependent organs such as brain and red cells. Heterozygous c.1267C>T pathogenic variant induces loss of the SLC37A4 ER retention signal leading to partial (50 %) mislocalization to undefined cellular organelles resulting in impaired homeostasis including abnormal Golgi pH and morphology.



## SLC37A4-CDG: New biochemical insights for an emerging congenital disorder of glycosylation with major coagulopathy

Alexandre Raynor<sup>a,1</sup>, Walid Haouari<sup>b,1</sup>, Bobby G. Ng<sup>c</sup>, Sophie Cholet<sup>d</sup>, Annie Harroche<sup>e</sup>, Celia Raulet-Bussian<sup>a</sup>, Samra Lounis-Ouaras<sup>b</sup>, Sandrine Vuillaumier-Barrot<sup>a</sup>, Tiffany Pascreau<sup>f</sup>, Delphine Borgel<sup>f,g</sup>, Hudson H. Freeze<sup>c</sup>, François Fenaille<sup>d,1</sup>, Arnaud Bruneel<sup>a,b,1,\*</sup>

<sup>a</sup> AP-HP, Biochimie Métabolique et Cellulaire, Hôpital Bichat-Claude Bernard, Paris, France

<sup>b</sup> INSERM UMR1193, Université Paris-Saclay, 92290 Châtenay-Malabry, France

<sup>c</sup> Human Genetics Program, Sanford Burnham Prebys Medical Discovery Institute, La Jolla, CA 92037, USA

<sup>d</sup> Université Paris-Saclay, CEA, INRAE, Département Médicaments et Technologies pour la Santé, MetaboHUB, 91191 Gif sur Yvette, France

<sup>e</sup> AP-HP, Haemophilia Care Centre, Necker Hospital, Paris, France

<sup>f</sup> Laboratoire d'Hématologie Biologique, AP-HP, Hôpital Necker Enfants Malades, 75015 Paris, France

<sup>g</sup> HITH, INSERM UMR-S 1176, Université Paris-Saclay, 94270 Le Kremlin-Bicêtre, France

### ARTICLE INFO

#### Keywords:

Bikunin

CDG

Coagulopathy

SLC37A4

### ABSTRACT

SLC37A4-CDG is an emerging congenital disorder of glycosylation which is characterized by a dominant inheritance and a major coagulopathy originating from the liver. Recent studies took interest in the biochemical alterations found in this CDG and showed that they consisted of multiple glycosylation abnormalities, which result from mislocalization of the endoplasmic reticulum glucose-6-phosphate transporter and associated Golgi homeostasis defects. In this work, we highlight in six affected individuals abnormal patterns for various serum N-glycoproteins and bikunin proteoglycan isoforms, together with specific alterations of the mass spectra of endoglycosidase H-released serum N-glycans. Collectively, these data complement previous findings, help to better delineate SLC37A4-CDG and could present interest in diagnosing this disease.

### 1. Introduction

Heterozygous SLC37A4 deficiency is a recently characterized congenital disorder of glycosylation (SLC37A4-CDG) with, to this day, nine described affected individuals sharing the c.1267C > T (p.R423X) variant [1–3]. In this dominantly inherited metabolic disease, the monoallelic loss of the retrieval motif of the endoplasmic reticulum SLC37A4 glucose-6-phosphate transporter leads to its partial mislocalization, with deleterious impacts on liver Golgi homeostasis (pH and morphology), glycosylation and coagulation factors levels [3]. All affected individuals showed altered N- and mucin-type O-glycosylation profiles, elevated ASAT and decreased F2, F11 and antithrombin (AT) levels. In this context of major coagulopathy, most patients nevertheless

safely benefited from more or less invasive surgery including lip/palate cleft, tongue-tie and heavy cardiac surgeries, under fresh frozen plasma or not [3]. This suggests a preserved balance between pro-coagulant (e.g., F2 and F11) and anti-coagulant factors (e.g., AT), although this must be confirmed in additional patients. Furthermore, given its rather reduced symptomatology and dominant inheritance, SLC37A4-CDG may be widely underdiagnosed.

In this work on six SLC37A4-CDG affected individuals, we expand the previously reported biochemical features by analyzing other relevant serum glycoproteins, including bikunin proteoglycan isoforms, and by performing additional matrix assisted laser desorption/ionization-time of flight mass spectrometry (MALDI-TOF MS) studies of mannosylated and hybrid-type serum N-glycans.

**Abbreviations:** 2-DE, two-dimensional electrophoresis; A1AG,  $\alpha$ 1-acid glycoprotein; AT, antithrombin; ASAT, aspartate aminotransferase; Bkn, bikunin; CDG, congenital disorder(s) of glycosylation; CS, chondroitin sulfate; ECL, electrochemiluminescence; Endo H, endoglycosidase H; 'HC' protein, 'heavy chain' protein; Hpt, haptoglobin; ITI, inter- $\alpha$ -trypsin inhibitor; MALDI-TOF, matrix assisted laser desorption/ionization-time of flight; MS, mass spectrometry; MW, molecular weight;  $\alpha$ I, pro- $\alpha$ -trypsin inhibitor; Trf, transferrin.

\* Corresponding author at: Hôpital Bichat, Biochimie Métabolique et Cellulaire, 46 rue Henri Huchard, 75018 Paris, France.

E-mail address: [arnaud.bruneel@aphp.fr](mailto:arnaud.bruneel@aphp.fr) (A. Bruneel).

<sup>1</sup> These authors equally contributed to this work.

<https://doi.org/10.1016/j.cca.2021.07.005>

Received 8 June 2021; Accepted 5 July 2021

Available online 8 July 2021

0009-8981/© 2021 Elsevier B.V. All rights reserved.

## 2. Materials and methods

### 2.1. Serum samples

Serum samples were obtained from six SLC37A4-CDG affected individuals (P1 to P6) previously reported by Ng et al. [3].

### 2.2. Western blot of serum N-glycoproteins and two-dimensional electrophoresis (2-DE) of haptoglobin

Western blots of three N-glycoproteins, transferrin (Trf), haptoglobin (Hpt) and  $\alpha$ 1-acid-glycoprotein (A1AG), were performed on the six samples. SDS-PAGE was performed (10  $\mu$ L of treated sample per well) using Nu-PAGE 4–12% bis-tris gels (ThermoFisher Scientific). Proteins were transferred onto nitrocellulose, incubated with primary rabbit antibodies (anti-Trf from Siemens, anti-Hpt and anti-A1AG from Dako; 1:3000 v/v in TTBS-5% milk), then with HRP-linked secondary antibodies (GE Healthcare; 1:5000 v/v) and detected using ECL revelation. 2-DE of Hpt was performed as previously described [4].

### 2.3. MALDI-TOF MS of endoglycosidase H-released serum N-glycans

Profiles of mannosylated and hybrid-type serum N-glycans from P1 to P6 were obtained by MALDI-TOF MS following N-glycan cleavage by *endo*- $\beta$ -N-acetylglucosaminidase (Endo H), glycan purification by solid-phase extraction and permethylation, as previously described [5]. Mass spectra were acquired on an UltrafleXtreme instrument (Bruker Daltonics) operating in the positive reflector ion mode using 2,5-dihydroxybenzoic acid as matrix.

### 2.4. Western blots of serum bikunin isoforms

Western blots of serum bikunin (Bkn) isoforms were performed on four controls (C1 to C4) and on the six SLC37A4-CDG affected individuals. For inter- $\alpha$ -trypsin inhibitor (ITI: bikunin-chondroitin sulfate esterified by two HC proteins) and pro- $\alpha$ -trypsin inhibitor (PaI: bikunin-chondroitin sulfate esterified by one HC protein), sera were diluted 1:250 v/v in water. For unesterified Bkn-chondroitin sulfate and free Bkn, sera were diluted 1:10 v/v. SDS-PAGE, protein transfer and immunorevelation were performed as described above, with rabbit anti-bikunin (CP6) antibodies (Merck-Millipore, cat. # ABT1346; 1:5000 v/v in TTBS-5% milk).

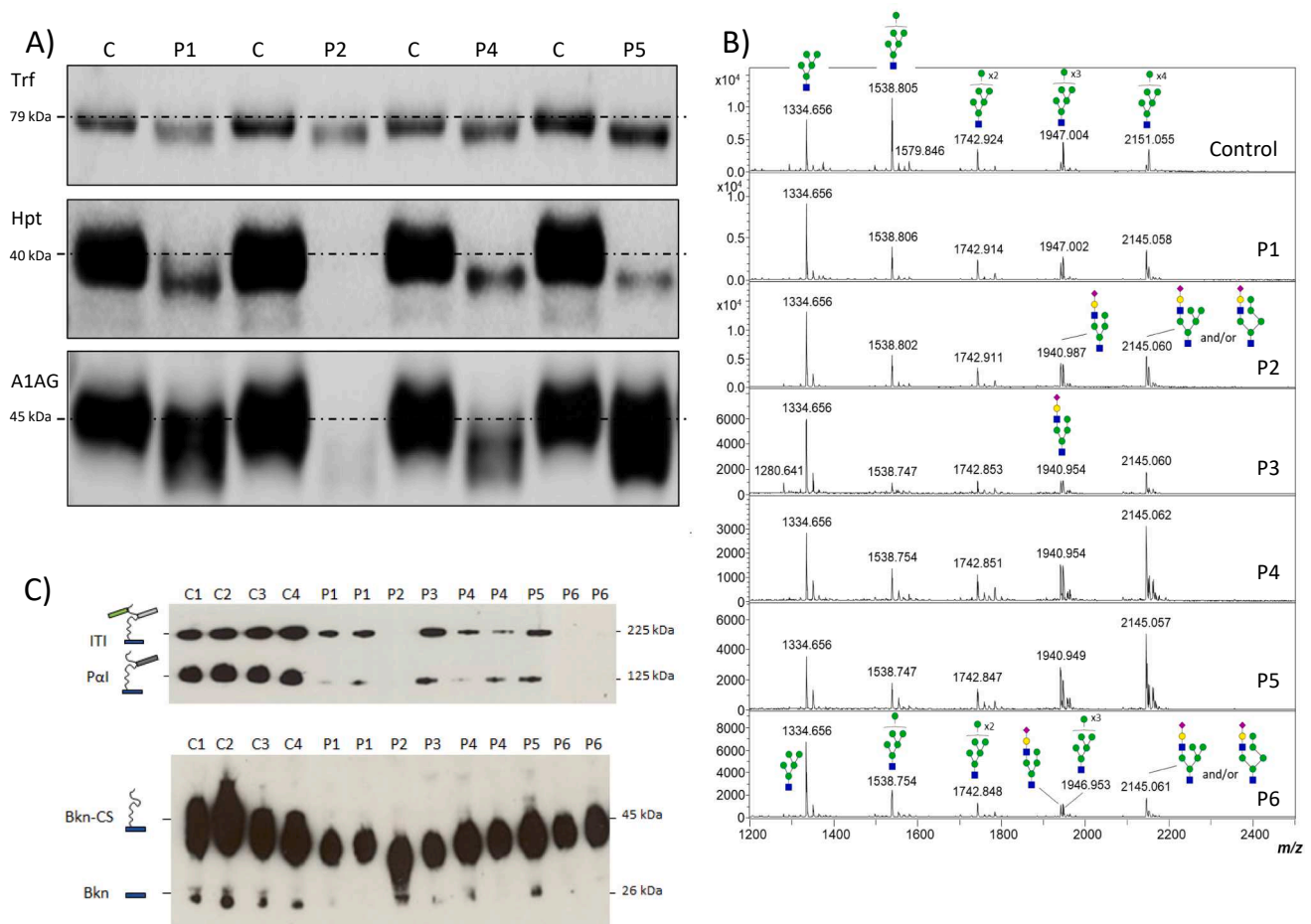


**Fig. 1.** Western blots of three serum N-glycoproteins, MALDI-TOF MS of Endo H-released serum N-glycans and western blots of bikunin isoforms, in SLC37A4-CDG. (A) Illustrative western blots of (from top to bottom) serum transferrin (Trf), haptoglobin (Hpt) and  $\alpha$ 1-acid-glycoprotein (A1AG) in four SLC37A4-CDG affected individuals (P1, P2, P4, P5) and a control (C). Dotted lines refer to normal glycoprotein MW. (B) MALDI-TOF mass spectra of permethylated N-glycans released from serum samples from a healthy subject (control) and six SLC37A4 patients (P1 to P6) following Endo H treatment. Measurements were performed in the positive-ion mode and all ions are present in sodiated form. Green circles, mannose; yellow circles, galactose; blue squares, N-acetyl glucosamine; red triangles, fucose; purple diamonds, sialic acid. (C) Western blots of serum bikunin (Bkn) isoforms in four controls (C1 to C4) and six SLC37A4-CDG affected individuals (P1 to P6). For P1, P4 and P6, two different samples were analyzed. ITI: bikunin (Bkn) linked to a chondroitin sulfate (CS) chain esterified by two HC glycoproteins; PaI: Bkn linked to a CS chain esterified by one HC glycoprotein. Profiles of controls were overexposed in order to be able to visualize ITI and PaI protein bands in some patients.

### 3. Results

#### 3.1. Western blot of N-glycoproteins and 2-DE of Hpt

Representative western blots of Trf, Hpt and A1AG from P1, P2, P4 and P5 are presented in Fig. 1A. For all patients, glycoprotein bands clearly display molecular weight (MW) decreases compared to the control (C). In addition, 2-DE patterns of Hpt glycoforms (Supp. Fig. 1) showed that these MW decreases were combined to a loss of negative charges as they displayed an abnormal tray of protein spots of cathodical migration.

#### 3.2. MALDI-TOF MS profiling of Endo H-released serum N-glycans

MALDI-TOF MS profiles of permethylated Endo H-released total serum N-glycans of the six patients and the control are shown in Fig. 1B. All patients shared a similar pattern, which notably displayed the abnormally prominent high-mannose GlcNAcMan<sub>5</sub> structure at *m/z* 1334.6. Besides, profiles also contained predominant hybrid monosialylated N-glycan species at *m/z* 1940.9 and *m/z* 2145.1.

#### 3.3. Western blot of serum bikunin isoforms

Western blots of serum Bkn isoforms are shown in Fig. 1C. For both ITI and PαI, corresponding protein bands showed severely reduced levels in the affected individuals compared to the controls. For Bkn-chondroitin sulfate (Bkn-CS), patients' patterns were similar to those of the controls with the exception of a lower MW for P2.

### 4. Discussion

To further characterize the biochemical alterations in SLC37A4-CDG, we performed various experiments, consisting of western blots of serum N-glycoproteins and bikunin (Bkn) proteoglycan isoforms, and MALDI-TOF MS analysis of Endo H-released serum N-glycans. First, western blots of serum Trf, Hpt and A1AG showed systematic MW decreases, in line with a major N-glycosylation deficiency (Fig. 1A) as corroborated using 2-DE applied to Hpt (Supp. Fig. 1). Such altered western blot and 2-DE profiles are rather unusual since, in our experience, they are only retrieved in MGAT2-CDG [6] and B4GALT1-CDG [7], two CDG with very severe clinical phenotypes.

Furthermore, we previously showed that SLC37A4-CDG-related N-glycosylation defects consist of the accumulation of high-mannose and hybrid-type N-glycans, together with hyposialylated and hypogalactosylated structures [3]. To specifically highlight probable major mannosidase(s) defect(s), we performed complementary MALDI-TOF MS analysis of Endo H-released high mannose and hybrid-type serum N-glycans. All affected individuals shared a similar pattern (Fig. 1B), which efficiently discriminated them from the healthy subject. Results were even more striking than after peptide-N-glycosidase F treatment [3] and were clearly different from those found in α1-2 mannosidase deficiency (MAN1B1-CDG), as reported elsewhere [5,8].

Lastly, SLC37A4-CDG was shown to be associated with an increased acidification of intraluminal Golgi pH [3]. Since we previously described altered ester linkages of the 'HC' proteins to the chondroitin sulfate (CS) moiety of the bikunin (Bkn) proteoglycan in CDG with Golgi V-ATPase proton pump disruption [9], we analyzed serum Bkn isoforms in the patients. Western blots of the heavy forms of Bkn (ITI and PαI) showed severely reduced levels compared to controls (Fig. 1C). Moreover, profiles of unesterified Bkn-CS were similar to controls with the exception of P2, who presented an abnormally low MW Bkn-CS isoform. In line with

our previous work on Bkn isoforms [9], these patterns were consistent with a Golgi pH defect in all patients while P2 could possibly display an additional defect in the CS chain biosynthesis. Regarding the influence of pH, SLC37A4-CDG-associated Golgi pH decrease seems to have similar deleterious effects on the biosynthesis of Bkn heavy forms to that of a raised pH, as described in CDG with V-ATPase deficiencies [9]. However, the ITI/PαI ratio seems to be in favor of ITI in SLC37A4-CDG, in contrast with V-ATPase deficiencies where PαI was shown to be predominant [3]. Besides corroborating the high sensitivity of the Bkn heavy forms biosynthesis towards Golgi pH, these results suggest that the ITI/PαI ratio can distinguish between excessive decreasing or rising Golgi pH variations.

### 5. Conclusion

In summary, western blots of serum N-glycoproteins, MALDI-TOF MS analysis of Endo H-released N-glycans and western blots of bikunin isoforms highlighted new biochemical features of SLC37A4-CDG that are relevant to better delineate this newly described CDG while also providing seemingly characteristic patterns, with possible diagnostic implications.

### Funding

This work was supported by the European Union's Horizon 2020 research and innovation program under the ERA-NETcofund action n° 643578 (A.B., S.V.B.), the Rocket Fund and R01DK99551 (H.H.F.), the Commissariat à l'Énergie Atomique et aux Énergies Alternatives and the MetaboHUB infrastructure (ANR-11-INBS-0010) (S.C., F.F.).

### Appendix A. Supplementary material

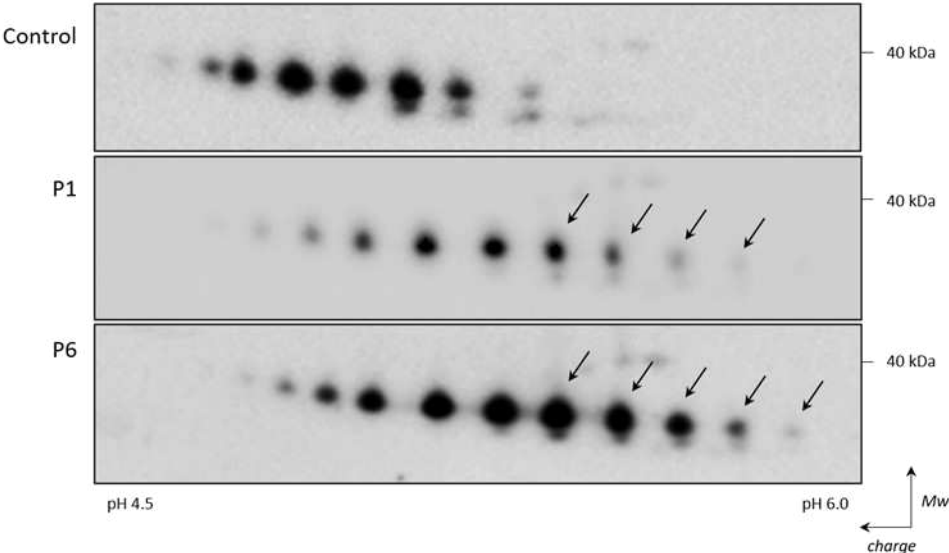
Supplementary data to this article can be found online at <https://doi.org/10.1016/j.cca.2021.07.005>.

### References

- [1] T. Marquardt, V. Bzduch, M. Hogrebe, S. Rust, J. Reunert, M. Grüneberg, et al., SLC37A4-CDG: Mislocalization of the glucose-6-phosphate transporter to the Golgi causes a new congenital disorder of glycosylation, *Mol. Genet. Metab. Rep.* 25 (2020), 100636.
- [2] M.P. Wilson, D. Quelhas, E. Leão-Teles, L. Sturiale, D. Ryman, L. Keldermans, et al., SLC37A4-CDG: Second patient, *JIMD Rep.* 58 (1) (2021) 122–128.
- [3] B.G. Ng, P. Sosicka, F. Fenaille, A. Harroche, S. Vuillaumier-Barrot, M. Porterfield, et al., A mutation in SLC37A4 causes a dominantly inherited congenital disorder of glycosylation characterized by liver dysfunction, *Am. J. Hum. Genet.* S0002-9297 (21) (2021) 00144, <https://doi.org/10.1016/j.ajhg.2021.04.013>.
- [4] A. Bruneel, F. Habarou, T. Stojkovic, G. Plouviez, L. Bougas, F. Guillemet, et al., Two-dimensional electrophoresis highlights haptoglobin beta chain as an additional biomarker of congenital disorders of glycosylation, *Clin. Chim. Acta* 470 (2017) 70–74.
- [5] S. Sakhi, S. Cholet, S. Wehbi, B. Isidor, B. Cogne, S. Vuillaumier-Barrot, et al., MAN1B1-CDG: three new individuals and associated biochemical profiles, *Mol. Genet. Metab. Rep.* 28 (2021), <https://doi.org/10.1016/j.ymgmr.2021.100775>.
- [6] A. Bruneel, S. Cholet, V. Drouin-Garraud, M.L. Jacquemont, A. Cano, A. Mégarbané, et al., Complementarity of electrophoretic, mass spectrometric, and gene sequencing techniques for the diagnosis and characterization of congenital disorders of glycosylation, *Electrophoresis* 39 (24) (2018) 3123–3132.
- [7] A. Bruneel, S. Cholet, N.T. Tran, T.D. Mai, F. Fenaille, CDG biochemical screening: Where do we stand? *Biochim. Biophys. Acta, Gen. Subj.* 1864 (10) (2020), 129652.
- [8] S. Duvet, D. Mouajjah, R. Péanne, G. Matthijs, K. Raymond, J. Jaeken, et al., Use of Endoglycosidase H as a diagnostic tool for MAN1B1-CDG patients, *Electrophoresis* 39 (24) (2018) 3133–3141.
- [9] W. Haouari, J. Dubail, S. Lounis-Ouaras, P. Prada, R. Bennani, C. Roseau, et al., Serum bikunin isoforms in congenital disorders of glycosylation and linkeropathies, *J. Inher. Metab. Dis.* 43 (6) (2020) 1349–1359.

# Supplementary file

Supplemental Figure 1



**Representative 2-DE patterns of haptoglobin (Hpt) glycoforms in two SLC37A4-CDG affected individuals and in a control.** Compared to the control, the affected individuals (P1 and P6) presented an abnormal tray of protein spots of cathodical migration and lower MW (black arrows), corroborating major N-glycosylation defects.



## III-5 Publication 4

### Revue

# Inherited Proteoglycan Biosynthesis Defects – Current Laboratory Tools and Bikunin as a Promising Blood Biomarker

**Walid Haouari**, Johanne Dubail, Christian Poüs, Valérie Cormier-Daire and  
Arnaud Bruneel

*Genes*, **2021**, *12*, 1654. <https://doi.org/10.3390/genes12111654>



### **III-5-1 Presentation of the review**

To some extent, this review is a global picture of our project. In this work we reviewed the current knowledges in the field of PG by describing their intracellular biosynthetic pathways as well as their structure, classification, and physiological roles. Afterwards, we focused on inborn diseases resulting from genetic dysfunctions in the PG biosynthetic machinery (i.e., PG-IMD). We present the different classes of PG biosynthesis defects including linkeropathies, GAG elongation and sulfation defects, and PG-IMD resulting from abnormal Golgi apparatus homeostasis. We outline the technical challenge represented by the current diagnosis strategy and emphasize on the crucial need for new screening biochemical tools. In this context, we promote bikunin as a promising biomarker by underlining our previous results in blood samples from various PG-IMD-affected individuals. We mostly highlight the genetic deficiencies for which Western blot and/or 2-DE have been performed in patients' serum by indicating the obtained result (i.e., normal, or abnormal profile) by reference to our publications and personal data. Moreover, although Bkn analysis have not yet been performed in some PG-IMD, we anticipate the potential resulting profiles according to the nature of the defective genes. We show the advantages of Bkn analysis based on the convenience and swiftness of its technical implementation, as well as its versatility for various applications in screening PG defects. We also discuss the limits of Bkn analysis applications since they are a priori limited to deficiencies in liver-expressed genes and CS biosynthetic enzymes.

Lastly, we conclude that bikunin analysis is proving to be an emerging promising asset which will significantly help clinicians and biologists that manage patients affected by inborn diseases resulting from PG biosynthesis defects.



Review

# Inherited Proteoglycan Biosynthesis Defects—Current Laboratory Tools and Bikunin as a Promising Blood Biomarker

Walid Haouari <sup>1</sup>, Johanne Dubail <sup>2,3</sup>, Christian Poüs <sup>1</sup>, Valérie Cormier-Daire <sup>2,3</sup> and Arnaud Bruneel <sup>1,4,\*</sup>

<sup>1</sup> INSERM UMR1193, Faculté de Pharmacie, Paris-Saclay University, 5 rue Jean-Baptiste Clément, 92220 Châtenay-Malabry, France; walid.haouari@universite-paris-saclay.fr (W.H.); christian.pous@u-psud.fr (C.P.)

<sup>2</sup> INSERM UMR1163, French Reference Center for Skeletal Dysplasia, Imagine Institute, Paris University, 24 Boulevard du Montparnasse, 75015 Paris, France; johanne.dubail@inserm.fr (J.D.); valerie.cormier-daire@inserm.fr (V.C.-D.)

<sup>3</sup> AP-HP, Necker Enfants Malades Hospital, 149 rue de Sèvres, 75015 Paris, France

<sup>4</sup> AP-HP, Biochimie Métabolique et Cellulaire, Hôpital Bichat-Claude Bernard, 46 rue Henri Huchard, 75018 Paris, France

\* Correspondence: arnaud.bruneel@aphp.fr

**Abstract:** Proteoglycans consist of proteins linked to sulfated glycosaminoglycan chains. They constitute a family of macromolecules mainly involved in the architecture of organs and tissues as major components of extracellular matrices. Some proteoglycans also act as signaling molecules involved in inflammatory response as well as cell proliferation, adhesion, and differentiation. Inborn errors of proteoglycan metabolism are a group of orphan diseases with severe and irreversible skeletal abnormalities associated with multiorgan impairments. Identifying the gene variants that cause these pathologies proves to be difficult because of unspecific clinical symptoms, hardly accessible functional laboratory tests, and a lack of convenient blood biomarkers. In this review, we summarize the molecular pathways of proteoglycan biosynthesis, the associated inherited syndromes, and the related biochemical screening techniques, and we focus especially on a circulating proteoglycan called bikunin and on its potential as a new biomarker of these diseases.

**Keywords:** bikunin; CDG; linkeropathies; GAG; proteoglycans; skeletal dysplasia

**Citation:** Haouari, W.; Dubail, J.; Poüs, C.; Cormier-Daire, V.; Bruneel, A. Inherited Proteoglycan Biosynthesis Defects—Current Laboratory Tools and Bikunin as a Promising Blood Biomarker. *Genes* **2021**, *12*, 1654. <https://doi.org/10.3390/genes12111654>

Academic Editors: Maurizio Scarpa and Peter Witters

Received: 27 September 2021

Accepted: 17 October 2021

Published: 20 October 2021

**Publisher's Note:** MDPI stays neutral with regard to jurisdictional claims in published maps and institutional affiliations.



**Copyright:** © 2021 by the authors. Licensee MDPI, Basel, Switzerland. This article is an open access article distributed under the terms and conditions of the Creative Commons Attribution (CC BY) license (<https://creativecommons.org/licenses/by/4.0/>).

## 1. Introduction

Proteoglycans (PGs) consist of core proteins linked to sulfated glycosaminoglycan (GAG) chains. They constitute a family of around fifty macromolecules involved in a wide variety of pathophysiological processes in humans [1]. They confer the biomechanical properties of the osteoarticular system and of the connective tissues of virtually all the organs during fetal development, growth, and aging. PGs are hydrophilic compounds mostly present in the extracellular matrices (ECM) in which they interact with each other and with hyaluronan and collagens. Such interactions are fundamental for the organization of the ECM and its viscoelastic properties [2]. PGs also mediate cell signaling through their binding to various ligands such as microbial pathogens [3], cytokines [4], and growth factors [5]. Hence, they modulate inflammatory and healing processes by promoting cell recruitment and proliferation during infections, cancers, and wound repair (Table S1).

PG biosynthesis occurs in the endoplasmic reticulum (ER) and in the Golgi apparatus and involves the interplay between numerous molecular actors along the secretory pathway. Inherited mutations causing defects in this system could result in severe orphan diseases called “PG inherited metabolic disorders” (PG-IMD). The causative variants occur in genes that encode enzymes responsible for the elongation and modifications of the GAG chains. They may also affect the proteins and transporters that regulate the synthesis and delivery of GAG assembly substrates. PG-IMD share osteoarticular malformations

and are often associated with cutaneous abnormalities, heart defects, neurological disorders, deafness, cataracts, and tooth abnormalities [6–8]. Otherwise, mucopolysaccharidoses (MPS), a group of diseases resulting from defective GAG catabolism, have very similar clinical presentations to PG-IMD. They are caused by pathogenic variants in genes encoding lysosomal GAG-degrading enzymes leading to deleterious GAG accumulation in tissues [9].

Regarding the highly variable and unspecific symptomatology of PG-IMD, convenient biochemical tests are needed to orient towards PG-IMD-causing gene variants or to ascertain the causality of the mutations unveiled by whole exome sequencing. Whatever the diagnosis route in PG-IMD, the current laboratory assays combine genetic sequencing (gene panels or whole exome sequencing) with the analysis of PG content in patient-derived fibroblasts using substrate radiolabeling, chromatography, mass spectrometry (MS), and Western blotting. Recently, a serum PG called bikunin (Bkn) has emerged as a potential new biomarker allowing the rapid detection of several PG biosynthesis deficiencies [10]. Here, we present an overview of the structure of PGs, their biosynthetic pathways, the related inherited diseases, and the current laboratory screening techniques. Furthermore, we highlight the potentials and discuss the limits of serum Bkn as a new versatile biomarker for the screening and diagnosis of PG-IMD.

## 2. Structure, Synthesis, and Modifications of Proteoglycans

As detailed in Figure 1, PGs are composed of a core protein linked to one or several highly sulfated glycosaminoglycan (GAG) chains such as chondroitin sulfate (CS), dermatan sulfate (DS), heparan sulfate (HS), heparin, or keratan sulfate (KS). Except for KSPGs, the GAG chains are linked to serine (Ser) residues of the core proteins through a common tetrasaccharide linker motif [(glucuronic acid–galactose–galactose–xylose) abbreviated as (GlcA–Gal–Gal–Xyl)]. GAG chains can then be differentiated according to distinct repeated disaccharide motifs linked to the common tetrasaccharide, i.e., [GlcA–GalNAc] for CS, [IdoA–GalNAc] for DS, [GlcA–GlcNAc] for HS, and [IdoA–GlcN] for heparin. Regarding KS, they are composed of a [GlcNAc–Gal]<sub>n</sub> backbone with three types of linkage to the core protein (Figure 1). Furthermore, several sulfate groups are branched on the sugar moieties of the GAG chains, making PGs very negatively charged, which is important for their biological functions [11].

The synthesis of the initiating tetrasaccharide linkage region starts by a serine-O-xylosylation catalyzed by xylosyltransferases (XYLT1 or XYLT2). This first reaction begins in the ER exit sites or in ER/Golgi intermediate compartments and is achieved in the *cis*-Golgi. The two following reactions, which also occur in the *cis*-Golgi, are the sequential additions of two Gal residues by the galactosyltransferases B4GALT7 and B3GALT6, respectively [12,13]. Afterwards, a GlcA is added by the glucuronyltransferase B3GAT3 in the medial-Golgi [14]. Noticeably, after the addition of the first Gal catalyzed by B4GALT7, the serine-linked Xyl residue is 2-O phosphorylated by FAM20B kinase (Figure 2). This phosphorylation is mandatory since it allows the substrate recognition by B3GALT6 and B3GAT3 for the addition of the two subsequent monosaccharides [15]. The Xyl-phosphorylation is transient since the phosphate group is removed by XYLP phosphatase after the achievement of tetrasaccharide synthesis [16]. Additionally, in CS-PGs and DS-PGs, a sulfation occurs either on the first or the second Gal residue of the linker region and may have a regulatory role for the following GAG elongation [17,18].

After the formation of the tetrasaccharide linker, the GAG chain elongation starts with the addition of the first *N*-acetyl aminosugar (i.e., GalNAc for CS/DS or GlcNAc for HS/heparin) (Figures 1 and 2). Thereafter, stepwise enzymatic additions of *n*-repeated disaccharide motifs produce the backbone of the GAG chains. For CSPGs, the *N*-acetylgalactosaminyl-transferase CSGALNACT1 or CSGALNACT2 transfers a GalNAc on the terminal GlcA of the linkage region [19]. The following polymerization of the [GlcA–GalNAc]<sub>n</sub> backbone is ensured by a chondroitin sulfate synthase complex (CHSY) composed of six enzymes, namely CHSY1, CHSY2, CHSY3, chondroitin polymerizing factor (CHPF),

CSGALNACT1, and CSGALNACT2 [20–23]. A family of glycosyltransferases called exostosins (EXT) and exostosin-like (EXTL) proteins mediates HS elongation. The GlcNAc transfer to the linkage region is catalyzed by EXTL2 or EXTL3 and the following [GlcA–GlcNAc]<sub>n</sub> polymerization is ensured by EXTL1, EXT1, and EXT2 [24–26] (Figure 1). In type-I KS, the elongation starts with the N-glycan branching of a GlcNAc residue to an asparagine (Asn) of the core protein. In type-II KS, a GalNAc is added to a Ser/Thr to form a mucin core-2 O-glycosidic linkage. Regarding type-III KS, the linkage region consists of a mannose O-linked to a Ser/Thr of the core protein. The three KS GAG-type chains consist of a sulfated [GlcNAc–Gal]<sub>n</sub> (polylactosamine) backbone that is synthesized by B3GlcNAcT7, B4GALT4, and the sulfotransferase KSGal6ST [27–29].

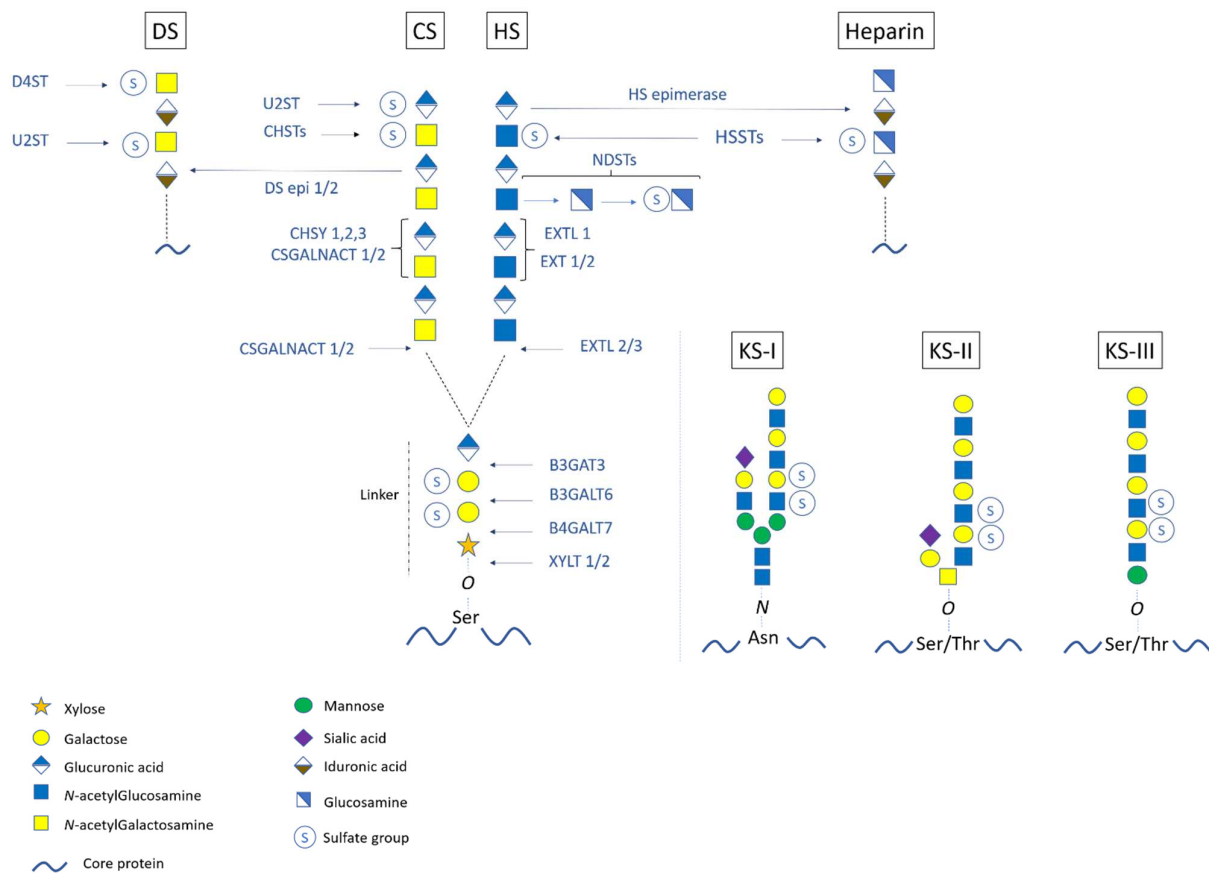


**Figure 1.** Biosynthesis and modifications of proteoglycans. Upon the core protein-linked tetrasaccharide linkage region (i.e., GlcA–Gal–Gal–Xyl), GAG chain polymerization starts with the transfer of a first amino sugar (i.e., GalNAc for CS and GlcNAc for HS) and continues with the addition of repetitive [GlcA–GalNAc] for CS and [GlcA–GlcNAc] for HS. Epimerization from CS to DS (i.e., [IdoA–GalNAc] backbone) and from HS to heparin (i.e., [IdoA–GlcNAc] backbone) could occur. The GAG chains are also modified by sulfate groups. Each pathway involves specific glycosyltransferases, sulfotransferases, and epimerases. For KS GAG chain elongation, there are three types of initiations leading to KS-I, KS-II, and KS-III GAG chains, which are composed of a polylactosamine backbone [GlcNAc–Gal]. Enzyme abbreviations: XYLT: Xylosyltransferase; B4GALT7:  $\beta$ -4-galactosyltransferase7; B3GALT6:  $\beta$ -3-galactosyltransferase6; B3GAT3:  $\beta$ -3-glucuronyltransferase3; CSGALNACT: chondroitin sulfate N-acetylgalactosaminyltransferase; CHSY: chondroitin synthase complex; CHST: chondroitin sulfotransferase; DS epi: dermatan sulfate epimerase; U2ST: uronic acid-2-sulfotransferase; D4ST: dermatan-4-sulfotransferase; EXT: exostosin family protein; EXTL: exostosin-like; NDST: N-deacetylase/N-sulfotransferase; HSST: heparan sulfotransferase; HS epimerase: heparan sulfate epimerase.

Various modifications, notably including sulfation reactions, occur on the repeated disaccharide motifs of the GAG chains (Figure 1). For the CS chains, chondroitin-4 sulfotransferases (C4ST)-1, -2, and -3 as well as C6ST-1 and -2 mediate the sulfation of several GalNAc residues [30–33]. GlcA residues can also be sulfated by the uronic acid sulfotransferase (U2ST) [34]. Furthermore, varying proportions of GlcA residues of the CS chains can be converted to IdoA by the DS epimerases (DSE)-1 and -2 to form DS chains [35,36]. Sulfations occur on both GalNAc and IdoA residues via D4ST1 (CHST14) and U2ST, respectively [34–37]. For HSPGs, several GlcNAc residues undergo *N*-deacetylation and subsequent *N*-sulfations catalyzed by bifunctional enzymes named GlcNAc *N*-deacetylase/*N*-sulfotransferases (NDSTs) [38,39]. The resulting sulfoglucosamine (GlcNS) residues can undergo an additional 6-*O* sulfation via a 6-*O* sulfotransferase to form GlcNS,6S [40]. Additionally, for the formation of heparin, some GlcA residues are converted by the HS-epimerase to IdoA residues, which are further sulfated [41]. For KSPGs, sulfations occur on both GalNAc and Gal residues composing the KS chain and are catalyzed by Gal6ST (CHST1) and GlcNAc6ST (CHST5 and/or CHST6) [42–44]. Finally, minor modifications of some GAG chains by sialic acid and fucose residues have been reported [45].

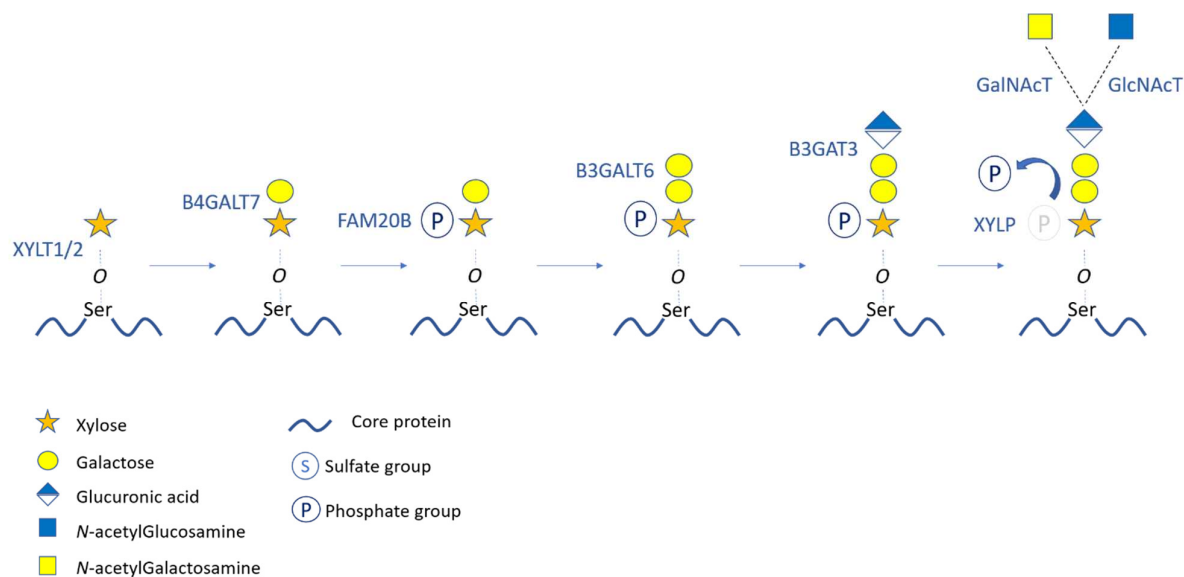


**Figure 2.** Biosynthesis and modifications of the tetrasaccharide linkage region. The successive steps of the initiating tetrasaccharide biosynthesis and modifications are represented with the corresponding enzymes. Transfer of the first aminosugar of CS or HS chains is also illustrated. The transient phosphorylation of the xylose occurs after the first Gal addition and is removed before the first aminosugar transfer. Enzyme abbreviations: XYLT: Xylosyltransferase; B4GALT7:  $\beta$ -4-galactosyltransferase7; FAM20B: Family with sequence similarity 20B; B3GALT6:  $\beta$ -3-galactosyltransferase6; B3GAT3:  $\beta$ -3-glucuronyltransferase3; XYLP: xylose phosphatase; GalNAcT: N-acetylgalactosaminyltransferase; GlcNAcT: N-acetylglucosaminyltransferase.

PG biosynthesis enzymes are transmembrane proteins having precise localization into the successive subcompartments of the Golgi apparatus according to the reaction they catalyze. This organization is maintained by a balance between the anterograde and retrograde Golgi vesicular trafficking [46]. While the molecular motors dyneins and kinesins transport cargo vesicles along microtubules, the coat protein complexes (COP 1 and COP 2) and tethering factors such as the conserved oligomeric complex (COG 1–8) participate in vesicle budding and fusion [47].

The substrates of glycosyltransferases during GAG elongation are uridine-diphosphate (UDP)-sugars. Their synthesis occurs in the cytosol and involves numerous metabolic pathways including the formation of phospho-sugars (e.g., Gal-1-P, GalNAc-1-P)



and a process frequently called “activation” consisting of the transfer of UDP to the phospho-sugars by specific UDP-sugar pyrophosphorylases [48,49]. Afterwards, the activated UDP-sugars are translocated into the lumen of the ER and the Golgi apparatus through transmembrane nucleotide-sugar transporters (NSTs). At least 31 NSTs belonging to the solute carrier 35 family (SLC35) have been described [50,51]. Glycosylation reactions release free UDP molecules, which are further converted by nucleotidases such as calcium-activated nucleotidase-1 (CANT1) to uridine-monophosphate [52], the latter being exported to the cytosol by NSTs to the benefit of new UDP-sugar molecules.

For sulfation reactions, sulfotransferases use the sulfate donor 3'-phospho-adenosine 5'-phospho-sulfate (PAPS). The biosynthesis of PAPS occurs in the cytosol and is mediated by PAPS synthases (PAPSS 1 and 2) that catalyze the transfer of phospho-adenosine-phosphate to inorganic sulfate ( $\text{SO}_4^{2-}$ ) [53]. The activated PAPS molecules are then transported into the Golgi lumen by SLC35B2 and SLC35B3 transporters [54,55]. GAG sulfation reactions release free PAP that is hydrolyzed by inositol-monophosphatase 1 (IMPAD1) into adenosine-monophosphate and inorganic phosphate [56].

### 3. Classification, Distribution, and Roles of Proteoglycans

PGs can be classified into four classes (Table S1) according to their cellular localization. The unique known intracellular PG is serglycin, which carries a heparin chain or a CS chain according to the cell type. It is involved in the storage of histamine and proteases into secretory granules in mast cells and macrophages for their delivery during inflammatory response [57].

The second class of PGs includes those embedded into the cell plasma membrane such as syndecans and glypicans. In numerous cell types including leucocytes and epithelial cells, their extracellular domain binds several ligands such as the vascular endothelial growth factor (VEGF) and inflammatory cytokines. This leads to various signal transduction pathways regulating leukocyte recruitment, angiogenesis, cell proliferation, and differentiation [58]. They also interact with ECM components such as collagens, hyaluronan, and fibronectin to form the ECM network [59]. Otherwise, the cytoplasmic domain of cell surface PGs interacts with the cytoskeleton, thereby participating in cell motility [60].

Pericellular PGs (the third class) are linked to the cell surface through adhesion molecules such as integrins and constitute a supportive matrix allowing interactions with the cellular microenvironment. For example, perlecan is a ubiquitous HSPG located in the basement membranes, which is involved in healing and angiogenesis during wound repair by interacting with collagen IV and VEGF, respectively [61].

The fourth class of PGs comprises the extracellular PGs that are composed of hyaluronan- and lectin-binding PGs (hyalectans) and the small leucine-rich proteoglycans (SLRPs). Aggrecan is a hyalectan that carries several CS, DS, and KS GAG chains and is the main PG of cartilage. It forms bulky aggregates with hyaluronan, collagen fibrils, and with other PGs to generate a hydrated gel underlying the viscoelastic consistence and the resistance of cartilage [62]. Biglycan is a CS/DS PG of the SLRPs family that is ubiquitously found in ECMs. Among the wide range of its physiological functions, biglycan is involved in bone formation by regulating osteoblast differentiation through interaction with the bone morphogenic protein (BMP) [63]. Decorin, an SLRP carrying a DS chain, is mostly present in skin ECM where it interacts with collagen I, epidermal growth factor receptor, and FGF to promote wound healing and to attenuate tumor growth [64]. In blood and urine, the inter- $\alpha$ -trypsin inhibitor proteins (IAIPs) are SLRPs carrying a unique short CS chain branched on the core protein Bkn. Their roles are described below in a dedicated section. Another circulating PG called endocan is a DSPG secreted by endothelial cells that inhibits leukocyte migration and adhesion to inflamed tissues as well as angiogenesis and cell proliferation during wound healing and tumor progression [65] (Table S1).

#### 4. Inborn Errors of Proteoglycan Metabolism

PG-IMD mostly consist of skeletal, connective tissue, and cartilage defects. The phenotypes comprise various osteoarticular manifestations including skeletal dysplasia, joint dislocations, and dysmorphisms [6]. Patients also display other symptoms including skin hyperelasticity, neurological disorders, growth retardation, heart defects, deafness, tooth abnormalities, and ocular troubles. PG-IMD can be classified according to the defective step of PG biosynthesis. Therefore, one can distinguish those caused by impaired tetrasaccharide linker formation (linkeropathies), GAG elongation, GAG sulfation, substrate supply, and by defects in Golgi homeostasis (including Golgi vesicular trafficking and ionic environment) (Table S2). Importantly, it appears that no clinical characteristic could differentiate a PG-IMD subgroup from another one.

Linkeropathies designate disorders due to the defective synthesis of the common tetrasaccharide linkage region. They arise from pathogenic variants in XYLT1, XYLT2, B4GALT7, B3GALT6, and B3GAT3, which result in Desbuquois dysplasia, spondylo-ocular syndrome, Ehlers–Danlos type 1 and type 2, and Larsen-like syndrome, respectively [12,66–69]. Otherwise, benign bone tumors called exostosis are displayed during inherited defects of HS polymerizing enzymes (i.e., EXT1 and EXT2), the resulting “hereditary multiple exostosis syndrome” (HMES) being the most frequent skeletal genetic disorder with a prevalence estimated at 1:50,000 [70,71]. GAG sulfation defects, which arise from defective sulfate uptake, activation, or linkage to the GAG chains (Table S2), lead to a range of unspecific skeletal disorders including severe achondrogenesis and spondylo-epiphyseal dysplasia [72]. Most pathogenic variants in genes encoding sugar transporters and Golgi homeostasis regulators lead to congenital disorders of glycosylation (CDG) [73]. Affected individuals mostly display impaired N- and O-glycosylation of proteins, but additional alterations of the PG metabolism have been reported in SLC35A2-CDG and SLC35A3-CDG (i.e., UDP-Gal and UDP-GlcNAc Golgi transporter defects) [74,75], in deficiencies of COG4 and GORAB (i.e., proteins regulating the Golgi retrograde trafficking) [76,77], and in TMEM165-CDG and SLC10A7-CDG (i.e., Mn<sup>2+</sup> and Ca<sup>2+</sup>-related transporter defects, respectively) [78,79]. The clinical manifestations of these CDG with PG defects remain wide and unspecific like in other CDG. Noticeably, arthrogyriposis and cutis laxa are displayed by SLC35A3-CDG and GORAB-CDG, respectively, while very severe skeletal dysplasia is associated with major osteoporosis and tooth abnormalities during TMEM165 and SLC10A7 deficiencies, respectively. Finally, a condition with severe developmental delay and epileptic seizures has been described in individuals with pathogenic variants in UGDH, a gene coding for UDP-glucose dehydrogenase that forms UDP-GlcA from UDP-glucose [80] (Table S2).

#### 5. Current Laboratory Tools and Examples of Applications

The low incidence of PG-IMD and their unspecific clinical signs make a diagnosis only based on a clinical approach difficult. As shown in Figure 3, the screening strategy benefits from the development of next-generation sequencing techniques (gene panels, whole exome/genome sequencing) classically applied to DNA from blood-derived lymphocytes for the early identification of potentially causative gene variants. However, to ascertain their pathogenicity and perform an accurate diagnosis, the implementation of tedious biochemical assays is often required. In most cases, invasive skin biopsies are performed and addressed to specialized laboratories where the overall PG content of fibroblasts is evaluated and compared to controls. The most common strategy involves fibroblasts cell culture in the presence of radiolabeled substrates (<sup>35</sup>S and <sup>3</sup>H-radiolabelled sugars) that enter the cells and are incorporated to the GAG chains of PGs. Afterwards, liquid scintillation counting is employed to quantify labeled GAGs in cell culture media or lysates (Figure 3). For example, this technique allowed the detection of decreased PG biosynthesis in XYLT1- and CANT1-deficient patient fibroblasts [66,81]. The quantification of the fibroblast PG content by immunostaining is also possible using antibodies and/or

lectins recognizing the GAG chains. Enzyme-linked immunosorbent assay using anti-CS/DS antibodies showed reduced immunostaining in CSGALNACT1-deficient patient fibroblasts [82]. Flow cytometry using anti-CS and -HS antibodies showed a significant decrease in cell surface CS and HSPG in patients with B3GAT3 linkeropathy [69]. More accurate analyses allowing the determination of GAG disaccharide composition and sulfation degree could be performed using high-performance liquid chromatography (HPLC) and mass spectrometry (MS) following specific enzymatic treatments (Figure 3). Indeed, the disaccharide units of CS/DS, HS/heparin, and KS GAG chains are obtained by treating the cell lysates with chondroitinase, heparitinase, and keratanase (i.e., GAG lyases), respectively. HPLC analysis of chondroitinase-treated fibroblast lysates from DSE-deficient patients showed decreased amounts of [IdoA–GalNAc] disaccharide (i.e., the DS backbone) compared to controls [83]. HPLC–MS coupling highlighted reduced [IdoA–GalNAc4-O-sulfate] levels in chondroitinase-treated cell fractions from D4ST1-deficient patients compared to controls [84]. Otherwise, specific PGs from skin fibroblasts such as decorin and biglycan can be used as markers, using antibody-based Western blot techniques, to highlight defective PG biosynthesis, as it has been performed for a patient with B4GALT7 linkeropathy [85].

Fibroblasts are also convenient cells for functional biochemical analyses to highlight loss of function resulting from the suspected gene variant. Indeed, decreased enzymatic activities were shown for XYLT2 [67], B4GALT7 [85], and B3GAT3 [69] in patient fibroblasts. In the case of defective UDP-sugar transporters, substrate uptake assays can be performed as shown in SLC35A3 mutated patient fibroblasts with reduced UDP-GlcNAc transport [86]. Additionally, observations of the Golgi apparatus using electron and/or fluorescence microscopy can highlight morphological alterations, impaired anterograde/retrograde trafficking balance, and the mislocalization of enzymes and transporters involved in PG biosynthesis such as in COG4 deficiency [76] (Figure 3). Less commonly, blood and urine can be used to quantify total GAG levels. Purification steps involving anion exchange chromatography and desalting allow the isolation of GAGs, which are further digested using GAG lyases (Figure 3). GAG disaccharide composition and sulfation degree can then be analyzed using HPLC or MS as it has been performed for patients with EXT1 and EXT2 deficiency where HS-related disaccharide plasma levels were decreased compared to controls [87]. Blood and urine samples can also be already treated with GAG lyases and applied to a centrifugal filter before analyzing GAG disaccharide containing filtrate by HPLC/MS. This technique showed decreased HS serum levels in EXTL3-deficient cases [88], while major hyposulfation of CS chains was detected in urine from one *CHST3* mutated patient [89]. Regarding MPS, their biochemical diagnosis is mostly based on a colorimetric method using dimethyl-methylene blue, which switches to purple when mixed with urine samples containing increased GAG concentrations. Qualitative GAG analyses from blood and urine are also performed using HPLC/MS to determine the defective GAG catabolic step [90].

The above biochemical techniques are time-consuming and often require complex technical handling and expensive material. Skin biopsies are invasive, especially for young children. Moreover, *in vitro* primary culture of skin fibroblasts can trigger phenotype changes and bias or affect the reproducibility of the results. Additionally, cell cultures are vulnerable to microbial contaminations and thus need skilled personnel able to ensure cautious handling for long-term cell viability. Blood and urine constitute more affordable biological material with easy sampling and storage. However, the complexity of blood composition and the presence of high amounts of salts in urine can hinder the following HPLC and/or MS analyses of the PG and/or GAG content. Therefore, some preliminary purification and desalting steps are frequently required [87].

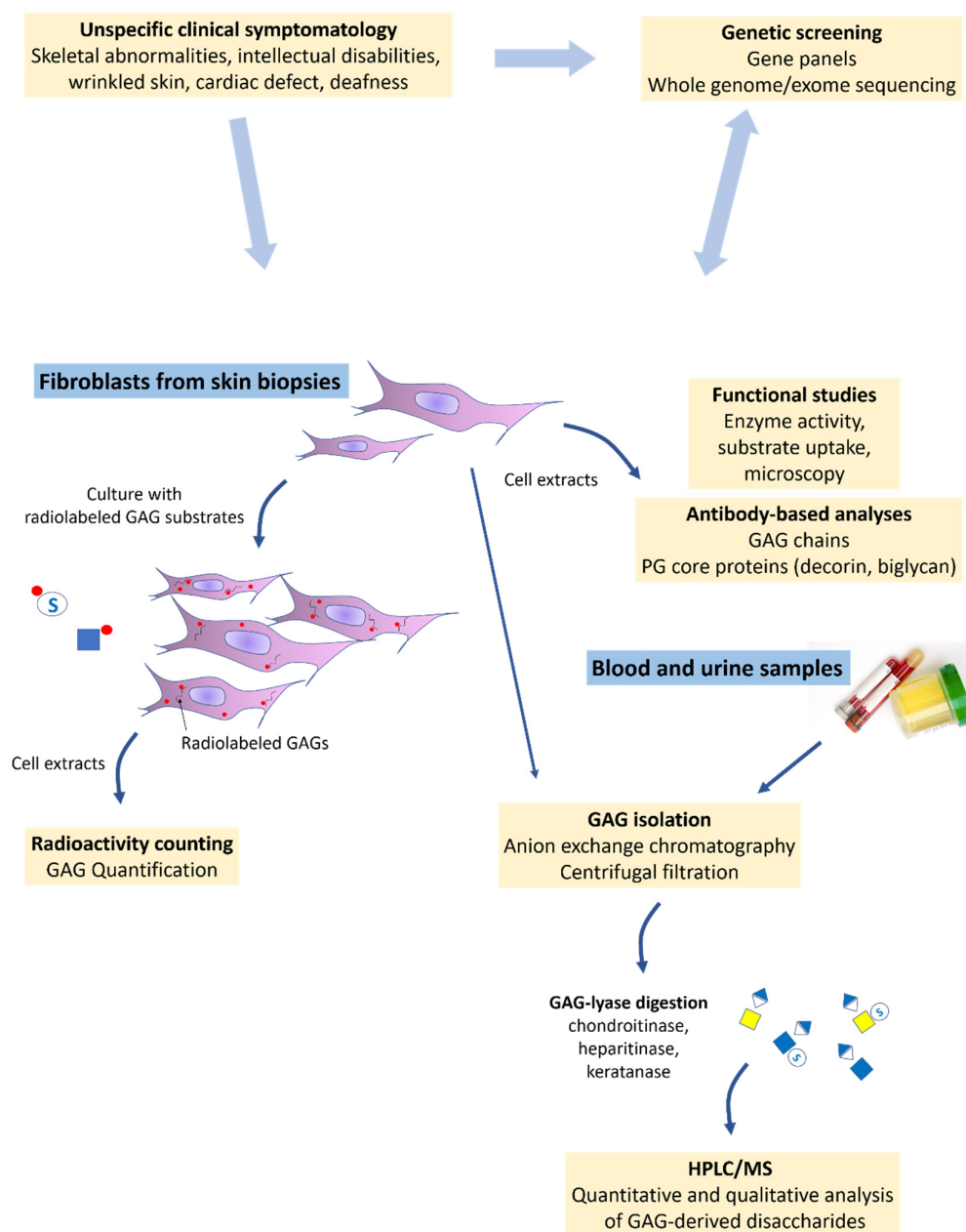


**Figure 3.** Schematic of current PG-IMD diagnosis strategy. Once PG defect is suspected clinically, genetic screening and GAG assessment are performed using patient's samples. Whole genome/exome sequencing allows the identification of possibly pathogenic variants in PG metabolism-associated genes. Fibroblasts from skin biopsies are cultured with radiolabeled substrates and the measured radioactivity in cell extracts reflects PG biosynthesis capacities. Fibroblasts are also used for functional analyses measuring the activity of the suspected defective enzyme or transporter, while microscopy could detect protein mislocalization and/or abnormal Golgi morphology. Antibody-based techniques such as Western blot and flow cytometry are useful for highlighting impaired PG biosynthesis by targeting GAG chains or PG core proteins such as decorin and biglycan. As from blood and urine, GAGs could be assessed by analyzing purified and enzymatically released disaccharides using HPLC/MS. Altogether, these laboratory analyses either orient towards a genetic deficiency or confirm the causality of the suspected gene variant.

Regarding the current lack of rapid and simple routine analyses for the screening/diagnosis of PG biosynthesis defects, the discovery and development of new blood and/or urine biomarkers are mandatory. In this context, we recently evaluated a new biochemical test based on the analysis of serum bikunin (Bkn), a CS-type PG found in the blood at high levels [10,91]. In the following sections, we describe the structure and roles of this proteoglycan and discuss its potentials and limits as a convenient blood biomarker of PG-IMD.

## 6. Bikunin Proteoglycan Isoforms

Bikunin (Bkn) is a serum protein mainly synthesized by the liver. It constitutes the core protein of a group of original CSPGs known as the inter- $\alpha$ -trypsin inhibitor proteins (IAIPs) (Figure 4). They consist of three isoforms, i.e., one light form (35 to 45 kDa) corresponding to the core Bkn linked to a short CS chain (Bkn-CS), and two heavy forms named Pro- $\alpha$ -trypsin inhibitor (P $\alpha$ I) (125 kDa) and Inter- $\alpha$ -trypsin inhibitor (ITI) (225 kDa). In ITI, the CS chain is esterified by two different heavy chain (HC1 or HC2) glycoproteins, while HC3 attachment produces P $\alpha$ I (Figure 4) [92]. CS chain elongation on the core protein involves the classical pathway of CSPG biosynthesis (described above) with the linkage of the HCs to a distal GalNAc residue in the *trans*-Golgi network (TGN). Such a “protein-GAG-protein(s)” structure has been described exclusively in IAIPs [93]. The produced isoforms are then secreted into the blood at high levels, with ITI and P $\alpha$ I being the major circulating isoforms [94]. In urine, no heavy form is normally found since they do not cross the glomerular barrier, but Bkn-CS is present in rather high amounts [95]. Note that IAIP serum and urine levels could be markedly modulated in pathological situations such as cancer, inflammation, liver diseases, and infectious diseases [96,97].

Concerning the physiological roles of IAIPs, they can be extravasated under various stimuli and then can exchange their HCs with hyaluronan to form HC-hyaluronan complexes that stabilize the ECM [98]. Such an exchange has protective effects against the degradation of joint ECM during osteoarthritis [99]. It also promotes the sequestration and inactivation of leucocytes during sepsis [100] and the protection of oocytes and of the amniotic membrane during ovulation and fetal development [101]. Additionally, the Bkn core protein carries inhibitory activity towards inflammation-associated proteases [102]. Otherwise, HCs have been shown to interact with vitronectin, a glycoprotein of the ECM involved in tissue repair [103].

## 7. Serum Bikunin Analyses in PG-IMD

The high serum levels of Bkn isoforms together with the availability of specific antibodies enable their easy, rapid, and rather cost-effective Western blot analysis for the screening of PG-IMD. Furthermore, Bkn-CS has a simple structure consisting of a unique and short CS chain branched on a small core protein not subjected to marked polymorphisms. These features facilitate the Western blot profile reading and interpretation by highlighting marked differences compared to controls in PG defects.

Western blot analysis of serum protein samples allows the detection of the three Bkn isoforms (ITI, P $\alpha$ I, and Bkn-CS) as well as the free Bkn core protein, with ITI and P $\alpha$ I being the major isoforms [10,91]. Analyses in dried blood spots and in urine have also been considered and gave encouraging results (unpublished data). In complement to classical Western blot, two-dimensional electrophoresis (2-DE) of Bkn-CS can highlight the negative charges provided by sulfate and phosphate groups [10]. However, it must be noted that 2-DE does not provide accurate structural data on GAG chains in contrast to mass spectrometry. Moreover, 2-DE technical handling could be rather delicate for inexperienced operators.

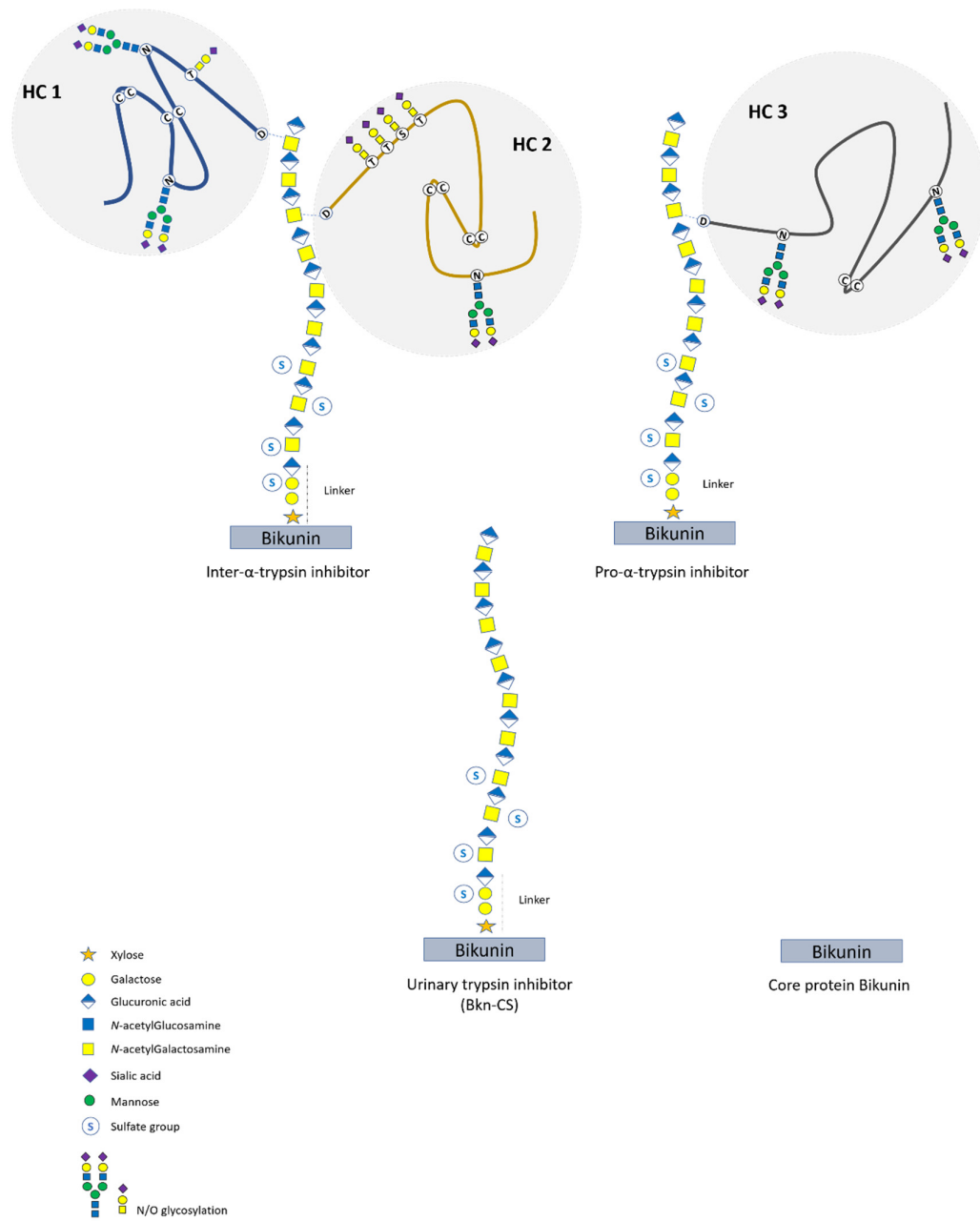


**Figure 4.** Schematic structure of bikunin isoforms (IAIP). The heavy forms ITI and PαI result from the esterification of the glycoproteins HC1, HC2, and HC3 with the CS chain of the bikunin (Bkn) core protein. The light forms correspond to UTI (Bkn-CS) and the core protein Bkn. The CS chain consists of 15 +/-3 [GlcA-GalNAc] disaccharide units and is sulfated at several GalNAc residues and at the second Gal residue of the linker region.

We addressed in Figure 5 the stepwise biosynthesis of Bkn-CS within the secretory pathway and highlighted the respective involvements of known PG-IMD-associated genes. This schematic overview points out the high diversity of the metabolic pathways engaged towards GAG elongation as well as the importance of their harmonious interplay. We also highlighted in Figure 5 the genes whose pathogenic variants impaired Bkn-CS biosynthesis and those for which Bkn analysis has not been performed yet, with anticipated potential results. We showed abnormal tetrasaccharide formation in patients with B4GALT7, B3GALT6, and B3GAT3 linkeropathies and impaired CS elongation in the CHSY1 inherited defect, with the ability to discriminate between respective deficiencies using 2-DE [10,91]. For the FAM20B kinase deficiency, it is likely that the 2-DE of serum Bkn-CS would reveal a lack of xylose phosphorylation.

In PG-IMD due to defective sugar transport and activation, we showed abnormalities in one individual with SLC35A3-CDG (impaired UDP-GlcNAc transporter) but a normal profile in one SLC35A2-CDG case (impaired UDP-Gal transporter), suggesting, at least in this individual, a preferential supply of UDP-Gal to GAG elongation rather than N-glycosylation. It would be interesting to analyze serum Bkn in CANT1 and SLC35D1 deficiencies. Otherwise, the Bkn-CS profile was clearly abnormal in TMEM165-CDG, and it would be mandatory to perform the analysis of other PG-IMD with Golgi homeostasis impairments such as COG4 and GORAB deficiencies. Finally, Bkn-CS sulfation can be assessed, notably using 2-DE, with interesting potentials in PG-IMD with impaired sulfotransferases (CHSTs), sulfate transporters (SLC26A2, SLC35B2), PAPS synthases (PAPSS1/2), and IMPAD (Figure 5). This way, we recently found altered Bkn-CS profiles in one SLC35B2-deficient individual (submitted publication).

Altogether, these features show that the Bkn-CS profile could bring a rapid evaluation of the overall functionality of PG biosynthesis in a simple screening laboratory tool. Moreover, the Bkn signature profiles displayed in some PG-IMD [10,91] suggested the ability to provide an accurate identification of some causative gene deficiencies. Nevertheless, serum Bkn-CS analysis is limited to the screening of pathological gene variants expressed by the liver. Accordingly, we observed a normal profile in XYLT1 linkeropathy (XYLT1 is not expressed in the liver) in contrast to an abnormal one detected in XYLT2 deficiency (unpublished data). Likewise, the Bkn-CS profile was normal in a patient with the CHST3 pathogenic variant (personal data) and should also be normal in CSGALNACT1 and U2ST inherited deficiencies since the liver does not express these genes. Furthermore, during specific alterations of HS or KS GAG elongation and sulfation, it is very likely that Bkn-CS may be unaffected, which remains to be tested in EXT1/2, EXTL2, CHST6, and CHST14 mutated individuals (Figure 5). Note that an isolated HS biosynthesis defect was shown during SLC10A7 deficiency [80]; the latter could therefore lead to an unaffected Bkn-CS profile. Evaluating additional circulating PGs such as PG-100, endo-can, or apolipoprotein-O could compensate such limitations of Bkn-CS isoforms as PG-IMD blood biomarkers.

## 8. Conclusions

The biosynthesis of PGs constitutes an intricate network of diverse metabolic pathways whose study proves to be a daunting task. Moreover, the severe clinical consequences of PG-IMD emphasize the major importance of PGs in pathophysiology and recall the need for improving the monitoring of these disorders. So far, the biochemical screening strategy relies on rather laborious technical implementations with a lack of routine assays to alleviate the burden of diagnosis for specialized clinicians and biologists. In this context, a single Bkn-CS isoform analysis is a promising tool that can direct the diagnosis towards numerous PG-IMD simultaneously, at least for liver-expressed gene mutants.

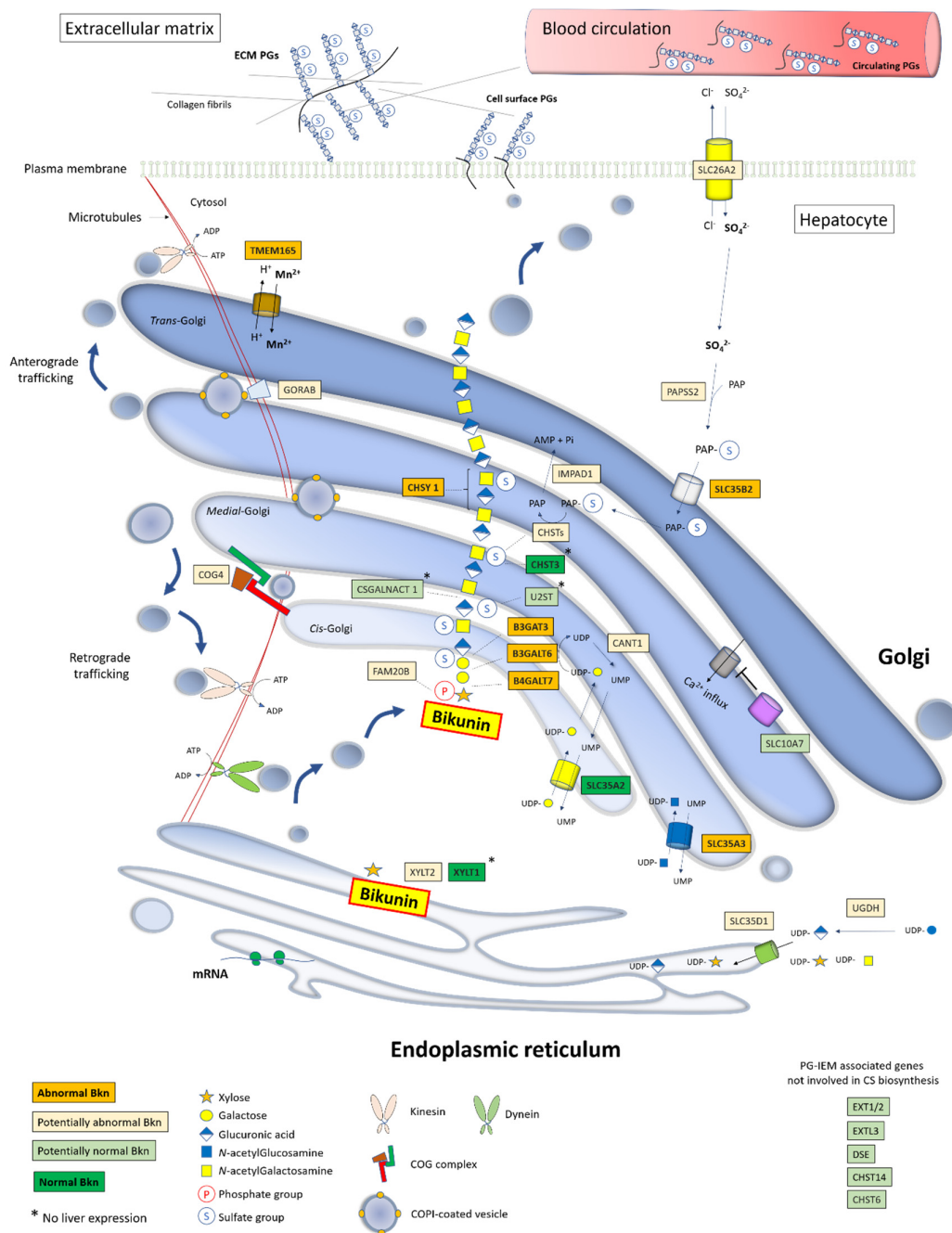


**Figure 5.** Schematic view of Bkn–CS biosynthesis into the secretory pathway and impact of PG-IMD gene deficiencies on Bkn analysis profile. The function of each PG-IMD-associated gene is depicted together with the Bkn–CS elongation, modifications, and sorting within the secretory pathway in hepatocytes. The latter include an ER-to-Golgi anterograde vesicular flow along microtubules as ensured by dynein molecular motors while retrograde trafficking within the Golgi involves tethering factors (COG complex) and Rab-GTPase-associated proteins such as GORAB. Additionally, retrograde transport to the ER involves kinesins. Golgi homeostasis is maintained by ionic equilibrium ( $H^+$ ,  $Na^+$ ,  $Mn^{2+}$ ,  $Ca^{2+}$ ) involving ion transporters such as TMEM165. UDP-sugars and PAPS are synthesized in the cytosol by specific enzymes and their uptake within the ER/Golgi lumen is ensured by nucleotide sugar transporters and PAPS transporters, respectively. Nascent PGs are sorted in the TGN and packed into cargo vesicles addressed through kinesin-dependent post-Golgi traffic to the plasma membrane and then to the ECM and/or to blood after exocytosis. Deficiencies in the highlighted genes lead to PG-IMD syndromes, the screening of which could benefit from serum Bkn analysis. Deep and light orange boxes represent gene deficiencies leading to abnormal (already investigated) and potentially abnormal (not yet investigated) Bkn–CS biosynthesis, respectively. Deep and light green boxes include genes whose deficiency results in normal (already investigated) and potentially normal (not yet investigated) Bkn profiles, respectively.



**Supplementary Materials:** The following are available online at [www.mdpi.com/article/10.3390/genes12111654/s1](http://www.mdpi.com/article/10.3390/genes12111654/s1). Table S1: Overview of some proteoglycans and their pathophysiological involvements. Table S2: Proteoglycan inherited metabolic diseases: Classification and clinical aspects.

**Author Contributions:** Conceptualization, A.B. and V.C.-D.; writing—original draft preparation, W.H., J.D., C.P., V.C.-D., and A.B.; writing—review and editing, W.H., V.C.-D., and A.B.; supervision, A.B., C.P., and V.C.-D.; funding acquisition, A.B. All authors have read and agreed to the published version of the manuscript.

**Funding:** This work was generated within the European Reference Network for Rare Hereditary Metabolic Disorders (MetabERN), co-funded by the European Union within the framework of the Third Health Programme ERN-2016—Framework Partnership Agreement 2017–2021, Project ID No. 739543.

**Institutional Review Board Statement:** Not applicable.

**Informed Consent Statement:** Not applicable.

**Data Availability Statement:** Not applicable

**Conflicts of Interest:** The authors declare no conflict of interest. The funders had no role in the design of the study; in the collection, analyses, or interpretation of data; in the writing of the manuscript, or in the decision to publish the results.

## Abbreviations

<b>2-DE</b>	two-dimensional electrophoresis
<b>AMP</b>	adenosine monophosphate
<b>Bkn</b>	bikunin
<b>B3GALT6</b>	$\beta$ -3 galactosyltransferase 6
<b>B3GAT3</b>	$\beta$ -3 glucuronyltransferase 3
<b>B4GALT7</b>	$\beta$ -4 galactosyltransferase 7
<b>CANT1</b>	calcium activated nucleotidase 1
<b>CHST</b>	chondroitin sulfotransferase
<b>CHSY1</b>	chondroitin synthase 1
<b>COG</b>	conserved oligomeric Golgi
<b>COP</b>	coated protein complex
<b>CS</b>	chondroitin sulfate
<b>CSGAL-NACT</b>	chondroitin sulfate GalNAc transferase
<b>D4ST</b>	dermatan-4-sulfotransferase
<b>DS</b>	dermatan sulfate
<b>DSE</b>	dermatan sulfate epimerase
<b>ECM</b>	extracellular matrix
<b>ER</b>	endoplasmic reticulum
<b>EXT</b>	exostosin
<b>EXTL</b>	exostosin-like
<b>FAM20B</b>	family with sequence similarity member 20B
<b>GAG</b>	glycosaminoglycan

---

<b>Gal</b>	galactose
<b>GalNAc</b>	<i>N</i> -acetylgalactosamine
<b>GlcA</b>	glucuronic acid
<b>GlcN</b>	glucosamine
<b>GlcNAc</b>	<i>N</i> -acetylglucosamine
<b>GORAB</b>	golgin Rab6-interacting protein
<b>HC protein</b>	'heavy chain' protein
<b>HMES</b>	hereditary multiple exostosis syndrome
<b>HPLC</b>	high-performance liquid chromatography
<b>HS</b>	heparan sulfate
<b>IAIP</b>	inter- $\alpha$ -trypsin inhibitor proteins
<b>IdoA</b>	iduronic acid
<b>IMPAD1</b>	inositol monophosphatase domain-containing 1
<b>ITI</b>	inter- $\alpha$ -trypsin inhibitor
<b>KS</b>	keratan sulfate
<b>MS</b>	mass spectrometry
<b>NDST</b>	<i>N</i> -deacetylase/ <i>N</i> -sulfotransferases
<b>PAP</b>	phospho-adenosine phosphate
<b>PAPS</b>	3'-phosphoadenosine 5'-phosphosulfate
<b>P<math>\alpha</math>I</b>	pro- $\alpha$ -trypsin inhibitor
<b>PG</b>	proteoglycan
<b>PG-IMD</b>	PG inherited metabolic disorders
<b>Ser</b>	serine
<b>SLC35</b>	solute carrier 35
<b>SRLP</b>	small leucin-rich proteoglycans
<b>TGN</b>	<i>trans</i> -Golgi network
<b>TMEM165</b>	transmembrane protein 165
<b>U2ST</b>	uronyl 2- <i>O</i> -sulfotransferase or uronosyl 2- <i>O</i> -sulfotransferase
<b>UTI</b>	urinary trypsin inhibitor
<b>UDP/UMP</b>	uridine di/monophosphate
<b>Xyl</b>	xylose
<b>XYLT</b>	xylosyltransferase
<b>XYLP</b>	xylose phosphatase

## References

1. Schaefer, L.; Schaefer, R.M. Proteoglycans: From structural compounds to signaling molecules. *Cell Tissue Res.* **2010**, *339*, 237–246.
2. Theocharis, A.D.; Skandalis, S.S.; Gialeli, C.; Karamanos, N.K. Extracellular matrix structure. *Adv. Drug Deliv. Rev.* **2016**, *97*, 4–27.
3. Bartlett, A.H.; Park, W. Proteoglycans in host-pathogen interactions: Molecular mechanisms and therapeutic implications. *Expert Rev. Mol. Med.* **2010**, *12*, e5.
4. Mulloy, B.; Rider, C.C. Cytokines and proteoglycans: An introductory overview. *Biochem. Soc. Trans.* **2010**, *34*, 409–413.
5. Mizumoto, S.; Yamada, S.; Sugahara, K. Molecular interactions between chondroitin–dermatan sulfate and growth factors/receptors/matrix proteins. *Curr. Opin. Struct. Biol.* **2015**, *34*, 35–42.
6. Dubail, J.; Cormier-Daire, V. Chondrodysplasias with Multiple Dislocations Caused by Defects in Glycosaminoglycan Synthesis. *Front. Genet.* **2021**, *12*, 642097.
7. Sasarman, F.; Maftai, C.; Campeau, M.; Brunel-Guitton, C.; Mitchell, G.A. Allard, Biosynthesis of glycosaminoglycans: Associated disorders and biochemical tests. *J. Inherit. Metab. Dis.* **2016**, *39*, 173–188.
8. Paganini, C.; Costantini, R.; Superti-Furga, A.; Rossi, A. Bone and connective tissue disorders caused by defects in glycosaminoglycan biosynthesis: A panoramic view. *FEBS J.* **2019**, *286*, 3008–3032.
9. Muenzer, J. Overview of the mucopolysaccharidoses. *Rheumatology* **2011**, *50*, v4–v12.
10. Haouari, W.; Dubail, J.; Lounis-Ouaras, S.; Prada, P.; Bennani, R.; Roseau, C.; Huber, C.; Afenjar, A.; Colin, E.; Vuillaumier-Barrot, S.; et al. Serum bikunin isoforms in congenital disorders of glycosylation and linkeropathies. *J. Inherit. Metab. Dis.* **2020**, *43*, 1349–1359.
11. Prydz, K.; Dalen, K.T. Synthesis and sorting of proteoglycans. *J. Cell Sci.* **2000**, *113*, 193–205.
12. Almeida, R.; Levery, S.B.; Mandel, U.; Kresse, H.; Schwientek, T.; Bennett, E.P.; and Clausen, H. Cloning and expression of a proteoglycan UDP-galactose:beta-xylose beta1,4-galactosyltransferase I. A seventh member of the human beta4-galactosyltransferase gene family. *J. Biol. Chem.* **1999**, *274*, 26165–26171.
13. Bai, X.; Zhou, D.; Brown, J.R.; Crawford, B.E.; Hennet, T.; Esko, J.D. Biosynthesis of the linkage region of glycosaminoglycans: Cloning and activity of galactosyltransferase II, the sixth member of the beta 1,3-galactosyltransferase family (beta 3GalT6). *J. Biol. Chem.* **2001**, *276*, 48189–48195.
14. Kitagawa, H.; H.; Tone, Y.; Tamura, J.; Neumann, K.W.; Ogawa, T.; Oka, S.; Kawasaki, T.; and Sugahara, K. Molecular Cloning and Expression of Glucuronyltransferase I Involved in the Biosynthesis of the Glycosaminoglycan-Protein Linkage Region of Proteoglycans. *J. Biol. Chem.* **1998**, *273*, 6615–6618.
15. Koike, T.; Izumikawa, T.; Tamura, J.I.; Kitagawa, H. FAM20B is a kinase that phosphorylates xylose in the glycosaminoglycan-protein linkage region. *Biochem. J.* **2009**, *421*, 157–162.
16. Koike, T.; Izumikawa, T.; Sato, B.; Kitagawa, H. Identification of Phosphatase That Dephosphorylates Xylose in the Glycosaminoglycan-Protein Linkage Region of Proteoglycans. *J. Biol. Chem.* **2014**, *289*, 6695–6708.
17. Gulberti, S.; Jacquinet, J.-C.; Chabel, M.; Ramalanjaona, N.; Magdalou, J.; Netter, P.; Coughtrie, M.W.H.; Ouzzine, M.; and Fournel-Gigleux, S. Chondroitin sulfate N-acetylgalactosaminyltransferase-1 (CSGalNAcT-1) involved in chondroitin sulfate initiation: Impact of sulfation on activity and specificity. *Glycobiology* **2012**, *22*, 561–571.
18. Kitagawa, H.; Tanaka, Y.; Tsuchida, K.; Goto, F.; Ogawa, T.; Lidholt, K.; Lindahl, U.; and Sugahara, K. N-acetylgalactosamine (GalNAc) transfer to the common carbohydrate-protein linkage region of sulfated glycosaminoglycans. Identification of UDP-GalNAc:chondro-oligosaccharide alpha-N-acetylgalactosaminyltransferase in fetal bovine serum. *J. Biol. Chem.* **1995**, *270*, 22190–22195.
19. Uyama, T.; Kitagawa, H.; Tamura, J.; Sugahara, K. Molecular cloning and expression of human chondroitin N-acetylgalactosaminyltransferase: The key enzyme for chain initiation and elongation of chondroitin/dermatan sulfate on the protein linkage region tetrasaccharide shared by heparin/heparan sulfate. *J. Biol. Chem.* **2002**, *277*, 8841–8846.
20. Kitagawa, H.; Uyama, T.; Sugahara, K. Molecular cloning and expression of a human chondroitin synthase. *J. Biol. Chem.* **2001**, *276*, 38721–38726.
21. Kitagawa, H.; Izumikawa, T.; Uyama, T.; Sugahara, K. Molecular Cloning of a Chondroitin Polymerizing Factor That Cooperates with Chondroitin Synthase for Chondroitin Polymerization. *J. Biol. Chem.* **2003**, *278*, 23666–23671.
22. Izumikawa, T.; Uyama, T.; Okuura, Y.; Sugahara, K.; Kitagawa, H. Involvement of chondroitin sulfate synthase-3 (chondroitin synthase-2) in chondroitin polymerization through its interaction with chondroitin synthase-1 or chondroitin-polymerizing factor. *Biochem. J.* **2007**, *403*, 545–552.
23. Izumikawa, T.; Koike, T.; Shiozawa, S.; Sugahara, K.; Tamura, J.; Kitagawa, H. Identification of chondroitin sulfate glucuronyltransferase as chondroitin synthase-3 involved in chondroitin polymerization: Chondroitin polymerization is achieved by multiple enzyme complexes consisting of chondroitin synthase family members. *J. Biol. Chem.* **2008**, *283*, 11396–11406.
24. Lind, T.; Tufaro, F.; McCormick, C.; Lindahl, U.; Lidholt, K. The putative tumor suppressors EXT1 and EXT2 are glycosyltransferases required for the biosynthesis of heparan sulfate. *J. Biol. Chem.* **1998**, *273*, 26265–26268.
25. Kim, B.T.; Kitagawa, H.; Tamura, J.; Saito, T.; Kusche-Gullberg, M.; Lindahl, U.; and Sugahara, K. Human tumor suppressor EXT gene family members EXTL1 and EXTL3 encode alpha 1,4- N-acetylglucosaminyltransferases that likely are involved in heparan sulfate/ heparin biosynthesis. *Proc. Natl. Acad. Sci. USA* **2001**, *98*, 7176–7181.

26. Kitagawa, H.; Shimakawa, H.; Sugahara, K. The tumor suppressor EXT-like gene EXTL2 encodes an alpha1, 4-N-acetylhexosaminyltransferase that transfers N-acetylgalactosamine and N-acetylglucosamine to the common glycosaminoglycan-protein linkage region. The key enzyme for the chain initiation of heparan sulfate. *J. Biol. Chem.* **1999**, *274*, 20, 13933–13937.
27. Seko, A.; Dohmae, N.; Takio, K.; Yamashita, K. Beta 1,4-galactosyltransferase (beta 4GalT)-IV is specific for GlcNAc 6-O-sulfate. Beta 4GalT-IV acts on keratan sulfate-related glycans and a precursor glycan of 6-sulfosialyl-Lewis X. *J. Biol. Chem.* **2003**, *278*, 9150–9158.
28. Seko, A.; Yamashita, K. beta1,3-N-Acetylglucosaminyltransferase-7 (beta3Gn-T7) acts efficiently on keratan sulfate-related glycans *FEBS Lett.* **2004**, *556*, 216–220.
29. Kitayama, K.; Hayashida, Y.; Nishida, K.; Akama, T.O. Enzymes responsible for synthesis of corneal keratan sulfate glycosaminoglycans. *J. Biol. Chem.* **2007**, *282*, 30085–30096.
30. Yamauchi, S.; Mita, S.; Matsubara, T.; Fukuta, M.; Habuchi, H.; Kimata, K., and Habuchi, O. Molecular cloning and expression of chondroitin 4-sulfotransferase. *J. Biol. Chem.* **2000**, *275*, 8975–8981.
31. Hiraoka, N.; Nakagawa, H.; Ong, E.; Akama, T.O.; Fukuda, M.N.; Fukuda, M. Molecular cloning and expression of two distinct human chondroitin 4-O-sulfotransferases that belong to the HNK-1 sulfotransferase gene family. *J. Biol. Chem.* **2000**, *275*, 20188–20196.
32. Kang, H.G.; Evers, M.R.; Xia, G.; Baenziger, J.U.; Schachner, M. Molecular cloning and characterization of chondroitin-4-O-sulfotransferase-3. A novel member of the HNK-1 family of sulfotransferases. *J. Biol. Chem.* **2002**, *277*, 34766–34772.
33. Fukuta, M.; Uchimura, K.; Nakashima, K.; Kato, M.; Kimata, K.; Shinomura, T.; Habuchi, O. Molecular cloning and expression of chick chondrocyte chondroitin 6-sulfotransferase. *J. Biol. Chem.* **1995**, *270*, 18575–18580.
34. Kobayashi, M.; Sugumaran, G.; Liu, J.; Shworak, N.W.; Silbert, J.E.; Rosenberg, R.D. Molecular cloning and characterization of a human uronyl 2-sulfotransferase that sulfates iduronyl and glucuronyl residues in dermatan/chondroitin sulfate. *J. Biol. Chem.* **1999**, *274*, 10474–10480.
35. Maccarana, M.; Olander, B.; Malmström, J.; Tiedemann, K.; Aebersold, R.; Lindahl, U.; Li, J.-P.; and Malmström, A. Biosynthesis of dermatan sulfate: Chondroitin-glucuronate C5-epimerase is identical to SART2. *J. Biol. Chem.* **2006**, *281*, 11560–11568.
36. Pacheco, B.; Malmström, A.; Maccarana, M. Two dermatan sulfate epimerases form iduronic acid domains in dermatan sulfate. *J. Biol. Chem.* **2009**, *284*, 9788–9795.
37. Evers, M.R.; Xia, G.; Kang, H.G.; Schachner, M.; Baenziger, J.U. Molecular cloning and characterization of a dermatan-specific N-acetylgalactosamine 4-O-sulfotransferase. *J. Biol. Chem.* **2001**, *276*, 36344–36353.
38. Hashimoto, Y.; Orellana, A.; Gil, G.; Hirschberg, C.B. Molecular cloning and expression of rat liver N-heparan sulfate sulfotransferase. *J. Biol. Chem.* **1992**, *267*, 15744–15750.
39. Eriksson, I.; Sandbäck, D.; Ek, B.; Lindahl, U.; Kjellén, L. cDNA cloning and sequencing of mouse mastocytoma glucosaminyl N-deacetylase/N-sulfotransferase, an enzyme involved in the biosynthesis of heparin. *J. Biol. Chem.* **1994**, *269*, 10438–10443.
40. Habuchi, H.; Tanaka, M.; Habuchi, O.; Yoshida, K.; Suzuki, H.; Ban, K.; and Kimata, K. The occurrence of three isoforms of heparan sulfate 6-O-sulfotransferase having different specificities for hexuronic acid adjacent to the targeted N-sulfoglucosamine. *J. Biol. Chem.* **2000**, *275*, 2859–2868.
41. Li, J.; Hagner-McWhirter, A.; Kjellén, L.; Palgi, J.; Jalkanen, M.; Lindahl, U. Biosynthesis of heparin/heparan sulfate. cDNA cloning and expression of D-glucuronyl C5-epimerase from bovine lung. *J. Biol. Chem.* **1997**, *272*, 28158–28163.
42. Fukuta, M.; Inazawa, J.; Torii, T.; Tsuzuki, K.; Shimada, E.; Habuchi, O. Molecular cloning and characterization of human keratan sulfate Gal-6-sulfotransferase. *J. Biol. Chem.* **1997**, *272*, 32321–32328.
43. Akama, T.O.; Nakayama, J.; Nishida, K.; Hiraoka, N.; Suzuki, M.; McAuliffe, J.; Hindsgaul, O.; Fukuda, M.; and Fukuda, M.N. Human corneal GlcNAc 6-O-sulfotransferase and mouse intestinal GlcNAc 6-O-sulfotransferase both produce keratan sulfate. *J. Biol. Chem.* **2001**, *276*, 16271–16278.
44. Akama, T.O.; Misra, A.K.; Hindsgaul, O.; Fukuda, M.N. Enzymatic synthesis in vitro of the disulfated disaccharide unit of corneal keratan sulfate. *J. Biol. Chem.* **2002**, *277*, 42505–42513.
45. Nilsson, J.; Noborn, F.; Gomez Toledo, A.; Nasir, W.; Sihlbom, C.; Larson, G. Characterization of Glycan Structures of Chondroitin Sulfate-Glycopeptides Facilitated by Sodium Ion-Pairing and Positive Mode LC-MS/MS. *J. Am. Soc. Mass Spectrom.* **2017**, *28*, 229–241.
46. Opat, A.S.; Van Vliet, C.; Gleason, A. Trafficking and localisation of resident Golgi glycosylation enzymes. *Biochimie* **2001**, *83*, 763–773.
47. Blackburn, J.B.; D'Souza, Z.; Lupashin, V.V. Maintaining order: COG complex controls Golgi trafficking, processing, and sorting. *FEBS Lett.* **2019**, *593*, 2466–2487.
48. Yarema, K.J.; Bertozzi, C.R. Characterizing glycosylation pathways. *Genome Biol.* **2001**, *2*, REVIEWS0004.
49. Kleczkowski, L.A.; Decker, D.; Wilczynska, M. UDP-Sugar Pyrophosphorylase: A New Old Mechanism for Sugar Activation. *Plant Physiol.* **2011**, *156*, 3–10.
50. Hirschberg, C.B. My journey in the discovery of nucleotide sugar transporters of the Golgi apparatus. *J. Biol. Chem.* **2018**, *293*, 12653–12662.
51. Song, Z. Roles of the nucleotide sugar transporters (SLC35 family) in health and disease. *Mol. Asp. Med.* **2013**, *34*, 590–600.
52. Paganini, C.; Monti, L.; Costantini, R.; Besio, R.; Lecci, S.; Biggiogera, M.; Tian, K.; Schwartz, J.-M.; Huber, C.; Cormier-Daire, V.; et al. Calcium activated nucleotidase 1 (CANT1) is critical for glycosaminoglycan biosynthesis in cartilage and endochondral ossification. *Matrix Biol.* **2019**, *81*, 70.

53. Fuda, H.; Shimizu, C.; Lee, Y.C.; Akita, H.; Strott, C.A. Characterization and expression of human bifunctional 3'-phosphoadenosine 5'-phosphosulphate synthase isoforms. *Biochem. J.* **2002**, *365*, 497–504.
54. Kamiyama, S.; Suda, T.; Ueda, R.; Suzuki, M.; Okubo, R.; Kikuchi, N.; Chiba, Y.; Goto, S.; Toyoda, H.; Saigo, K.; et al. Molecular cloning and identification of 3'-phosphoadenosine 5'-phosphosulfate transporter. *J. Biol. Chem.* **2003**, *278*, 25958–25963.
55. Kamiyama, S.; Sasaki, N.; Goda, E.; Ui-Tei, K.; Saigo, K.; Narimatsu, H.; Jigami, Y.; Kannagi, R.; Irimura, T.; and Nishihara, S. Molecular Cloning and Characterization of a Novel 3'-Phosphoadenosine 5'-Phosphosulfate Transporter, PAPST2. *J. Biol. Chem.* **2006**, *281*, 10945–10953.
56. Vissers, L.E.; Lausch, E.; Unger, S.; Campos-Xavier, A.B.; Gilissen, C.; Rossi, A.; Del Rosario, M.; Venselaar, H.; Knoll, U.; Nam-poothiri, S.; et al. Chondrodysplasia and Abnormal Joint Development Associated with Mutations in IMPAD1, Encoding the Golgi-Resident Nucleotide Phosphatase, Gpapam. *J. Hum. Genet.* **2011**, *88*, 608–615.
57. Kolset, S.O.; Tveit, H. Serglycin—Structure and biology. *Cell. Mol. Life Sci.* **2008**, *65*, 1073–1085.
58. De Rossi, G.; Evans, A.R.; Kay, E.; Woodfin, A.; McKay, T.R.; Nourshargh, S.; and Whiteford, J.R. Shed syndecan-2 inhibits angiogenesis. *J. Cell Sci.* **2014**, *127*, 4788–4799.
59. Xian, X.; Gopal, S.; Couchman, J.R. Syndecans as receptors and organizers of the extracellular matrix. *Cell Tissue Res.* **2010**, *339*, 31–46.
60. Choi, Y.; Chung, H.; Jung, H.; Couchman, J.R.; Oh, E.-S. Syndecans as cell surface receptors: Unique structure equates with functional diversity. *Matrix Biol.* **2011**, *30*, 93–99.
61. Lord, M.S.; Tang, F.; Rnjak-Kovacina, J.; Smith, J.G.W.; Melrose, J.; Whitelock, J.M. The multifaceted roles of perlecan in fibrosis. *Matrix Biol.* **2018**, *68–69*, 150–166.
62. Iozzo, R.V.; Schaefer, L. Proteoglycan form and function: A comprehensive nomenclature of proteoglycans. *Matrix Biol.* **2015**, *42*, 11–55.
63. Ye, Y.; Hu, W.; Guo, F.; Zhang, W.; Wang, J.; Chen, A. Glycosaminoglycan chains of biglycan promote bone morphogenetic protein-4-induced osteoblast differentiation. *Int. J. Mol. Med.* **2012**, *30*, 1075–1080.
64. Rühland, C.; Schönherr, E.; Robenek, H.; Hansen, U.; Iozzo, R.V.; Bruckner, P.; and Seidler, D.G. The glycosaminoglycan chain of decorin plays an important role in collagen fibril formation at the early stages of fibrillogenesis. *FEBS J.* **2007**, *274*, 4246–4255.
65. Kali, A.; Shetty, K.S.R. Endocan: A novel circulating proteoglycan. *Indian J. Pharm.* **2014**, *46*, 579–583.
66. Bui, C.; Huber, C.; Tuysuz, B.; Alanay, Y.; Bole-Feysot, C.; Leroy, J.G.; Mortier, G.; Nitschke, P.; Munnich, A.; and Cormier-Daire, V. XYLT1 Mutations in Desbuquois Dysplasia Type 2. *Am. J. Hum. Genet.* **2014**, *94*, 405–414.
67. Munns, C.F.; Fahiminiya, S.; Poudel, N.; Munteanu, M.C.; Majewski, J.; Sillence, D.O.; Metcalf, J.P.; Biggin, A.; Glorieux, F.; Fassier, F.; et al. Homozygosity for frameshift mutations in XYLT2 result in a spondylo-ocular syndrome with bone fragility, cataracts, and hearing defects. *Am. J. Hum. Genet.* **2015**, *96*, 971–978.
68. Malfait, F.; Kariminejad, A.; Van Damme, T.; Gauche, C.; Syx, D.; Merhi-Soussi, F.; Gulberti, S.; Symoens, S.; Vanhauwaert, S.; Willaert, A. et al. Defective Initiation of Glycosaminoglycan Synthesis due to B3GALT6 Mutations Causes a Pleiotropic Ehlers-Danlos-Syndrome-like Connective Tissue Disorder. *Am. J. Hum. Genet.* **2013**, *92*, 935–945.
69. Baasanjav, S.; Al-Gazali, L.; Hashiguchi, T.; Mizumoto, S.; Fischer, B.; Horn, D.; Seelow, D.; Ali, B.R.; Aziz, S.A.A.; Langer, R. et al. Faulty Initiation of Proteoglycan Synthesis Causes Cardiac and Joint Defects. *Am. J. Hum. Genet.* **2011**, *89*, 15–27.
70. Ahn, J.; Lüdecke, H.J.; Lindow, S.; Horton, W.A.; Lee, B.; Wagner, M.J.; Horsthemke, B. and Wells, D.E. Cloning of the putative tumour suppressor gene for hereditary multiple exostoses (EXT1). *Nat. Genet.* **1995**, *11*, 137–143.
71. Stickens, D.; Clines, G.; Burbee, D.; Ramos, P.; Thomas, S.; Hogue, D.; Hecht, J.T.; Lovett, M.; and Evans, G.A. The EXT2 multiple exostoses gene defines a family of putative tumour suppressor genes. *Nat. Genet.* **1996**, *14*, 25–32.
72. Soares da Costa, D.; Reis, R.L.; Pashkuleva, I. Sulfation of Glycosaminoglycans and Its Implications in Human Health and Disorders. *Annu. Rev. Biomed. Eng.* **2017**, *19*, 1–26.
73. Péanne, R.; de Lonlay, P.; Foulquier, F.; Kornak, U.; Lefeber, D.J.; Morava, E.; Pérez, B.; Seta, N.; Thiel, C.; Van Schaftingen, E.; et al. Congenital disorders of glycosylation (CDG): Quo Vadis?. *Eur. J. Med. Genet.* **2018**, *61*, 643–663.
74. Toma, L.; Pinhal, M.A.S.; Dietrich, C.P.; Nader, H.B.; Hirschberg, C.B. Transport of UDP-Galactose into the Golgi Lumen Regulates the Biosynthesis of Proteoglycans. *J. Biol. Chem.* **1996**, *271*, 3897–3901.
75. Maszczak-Seneczko, D.; Olczak, T.; Wunderlich, L.; Olczak, M. Comparative analysis of involvement of UGT1 and UGT2 splice variants of UDP-galactose transporter in glycosylation of macromolecules in MDCK and CHO cell lines. *Glycoconj. J.* **2011**, *28*, 481–492.
76. Ferreira, C.R.; Xia, Z.-J.; Clément, A.; Parry, D.A.; Davids, M.; Taylan, F.; Sharma, P.; Turgeon, C.T.; Blanco-Sánchez, B.; Ng, B.G. et al. A Recurrent De Novo Heterozygous COG4 Substitution Leads to Saul-Wilson Syndrome, Disrupted Vesicular Trafficking, and Altered Proteoglycan Glycosylation. *Am. J. Hum. Genet.* **2018**, *103*, 553–567.
77. Hennies, H.C.; Kornak, U.; Zhang, H.; Egerer, J.; Zhang, X.; Seifert, W.; Kühnisch, J.; Budde, B.; Nätebus, M.; Brancati, F. et al. Geroderma osteodysplastica is caused by mutations in SCYL1BP1, a Rab-6 interacting golgin. *Nat. Genet.* **2008**, *40*, 1410–1412.
78. Bammens, R.; Mehta, N.; Race, V.; Foulquier, F.; Jaeken, J.; Tiemeyer, M.; Steet, R.; Matthijs, G.; and Flanagan-Steet, H. Abnormal cartilage development and altered N-glycosylation in Tmem165-deficient zebrafish mirrors the phenotypes associated with TMEM165-CDG. *Glycobiology* **2015**, *25*, 669–682.
79. Dubail, J.; Huber, C.; Chantepie, S.; Sonntag, S.; Tüysüz, B.; Mihci, E.; Gordon, C.T.; Steichen-Gersdorf, E.; Amiel, J.; Nur, B. et al. SLC10A7 mutations cause a skeletal dysplasia with amelogenesis imperfecta mediated by GAG biosynthesis defects. *Nat. Commun* **2018**, *9*, 1–15.

80. Hengel, H.; Bosso-Lefèvre, C.; Grady, G.; Szenker-Ravi, E.; Li, H.; Pierce, S.; Lebigot, É.; Tan, T.-T.; Eio, M.Y.; Narayanan, G. et al. Loss-of-function mutations in UDP-Glucose 6-Dehydrogenase cause recessive developmental epileptic encephalopathy. *Nat. Commun.* **2020**, *11*, 595.
81. Nizon, M.; Huber, C.; De Leonardis, F.; Merrina, R.; Forlino, A.; Fradin, M.; Tuysuz, B.; Abu-Libdeh, B.Y.; Alanay, Y.; Albrecht, B.; et al. Further Delineation of CANT1 Phenotypic Spectrum and Demonstration of Its Role in Proteoglycan Synthesis. *Hum. Mutat.* **2012**, *33*, 1261–1266.
82. Mizumoto, S.; Janecke, A.R.; Sadeghpour, A.; Povysil, G.; McDonald, M.T.; Unger, S.; Greber-Platzer, S.; Deak, K.L.; Katsanis, N.; Superti-Furga, A.; et al. CSGALNACT1-congenital disorder of glycosylation: A mild skeletal dysplasia with advanced bone age. *Hum. Mutat.* **2020**, *41*, 655–667.
83. Müller, T.; Mizumoto, S.; Suresh, I.; Komatsu, Y.; Vodopiutz, J.; Dundar, M.; Straub, V.; Lingenhel, A.; Melmer, A.; Lechner, S.; et al. Loss of dermatan sulfate epimerase (DSE) function results in musculocontractural Ehlers–Danlos syndrome. *Hum. Mol. Genet.* **2013**, *22*, 3761–3772.
84. Dünder, M.; Müller, T.; Zhang, Q.; Pan, J.; Steinmann, B.; Vodopiutz, J.; Gruber, R.; Sonoda, T.; Krabichler, B.; Utermann, G.; et al. Loss of Dermatan-4-Sulfotransferase 1 Function Results in Adducted Thumb-Clubfoot Syndrome. *Am. J. Hum. Genet.* **2009**, *85*, 873–882.
85. Seidler, D.G.; Faiyaz-Ul-Haque, M.; Hansen, U.; Yip, G.W.; Zaidi, S.H.E.; Teebi, A.S.; Kiesel, L.; and Götte, M. Defective glycosylation of decorin and biglycan, altered collagen structure, and abnormal phenotype of the skin fibroblasts of an Ehlers–Danlos syndrome patient carrying the novel Arg270Cys substitution in galactosyltransferase I (beta4GalT-7). *J. Mol. Med.* **2006**, *84*, 583–594.
86. Edvardson, S.; Ashikov, A.; Jalas, C.; Sturiale, L.; Shaag, A.; Fedick, A.; Treff, N.R.; Garozzo, D.; Gerardy-Schahn, R.; and Elpeleg, O. Mutations in SLC35A3 cause autism spectrum disorder, epilepsy and arthrogryposis. *J. Med. Genet.* **2013**, *50*, 733–739.
87. Anower-E-Khuda, M.F.; Matsumoto, K.; Habuchi, H.; Morita, H.; Yokochi, T.; Shimizu, K.; Kimata, K. Glycosaminoglycans in the blood of hereditary multiple exostoses patients: Half reduction of heparan sulfate to chondroitin sulfate ratio and the possible diagnostic application. *Glycobiology* **2013**, *23*, 865–876.
88. Oud, M.M.; Tuijnenburg, P.; Hempel, M.; van Vlies, N.; Ren, Z.; Ferdinandusse, S.; Jansen, M.H.; Santer, R.; Johannsen, J.; Bacchelli, C.; et al. Mutations in EXTL3 Cause Neuro-immuno-skeletal Dysplasia Syndrome. *Am. J. Hum. Genet.* **2017**, *100*, 281–296.
89. Thiele, H. Loss of chondroitin 6-O-sulfotransferase-1 function results in severe human chondrodysplasia with progressive spinal involvement. *PNAS* **2004**, *101*, 10155–10160.
90. Kubaski, F.; de Oliveira Poswar, F.; Michelin-Tirelli, K.; Burin, M.G.; Rojas-Málaga, D.; Brusius-Facchin, A.C.; Leistner-Segal, S.; and Giugliani, R. Diagnosis of Mucopolysaccharidoses. *Diagnostics* **2020**, *10*, 172.
91. Bruneel, A.; Dubail, J.; Roseau, C.; Prada, P.; Haouari, W.; Huber, C.; Dupré, T.; Poüs, C.; Cormier-Daire, V.; and Seta, N. Serum bikunin is a biomarker of linkeropathies. *Clin. Chim. Acta* **2018**, *485*, 178–180.
92. Enghild, J.J.; Thøgersen, I.B.; Cheng, F.; Fransson, L.A.; Roepstorff, P.; Rahbek-Nielsen, H. Organization of the inter-alpha-inhibitor heavy chains on the chondroitin sulfate originating from Ser(10) of bikunin: Posttranslational modification of Ialpha-derived bikunin. *Biochemistry* **1999**, *38*, 11804–11813.
93. Zhuo, L.; Hascall, V.C.; Kimata, K. Inter- $\alpha$ -trypsin Inhibitor, a Covalent Protein-Glycosaminoglycan-Protein Complex. *J. Biol. Chem.* **2004**, *279*, 38079–38082.
94. Puglia, M.J.; Jortani, S.A.; Basu, M.; Sommer, R.; Kuo, H.-H.; Murphy, S.; Williamson, D.; Vranish, J.; Boyle, P.J.; Budzinski, D.; et al. Immunological evaluation of urinary trypsin inhibitors in blood and urine: Role of N- & O-linked glycoproteins. *Glycoconj. J.* **2007**, *24*, 5–15.
95. Lepedda, A.J.; Nieddu, G.; Rocchiccioli, S.; Fresu, P.; De Muro, P.; Formato, M. Development of a method for urine bikunin/urinary trypsin inhibitor (UTI) quantitation and structural characterization: Application to type 1 and type 2 diabetes. *Electrophoresis* **2013**, *34*, 3227–3233.
96. Lim, Y.-P.; Bendelja, K.; Opal, S.M.; Siryaporn, E.; Hixson, D.C.; Palardy, J.E. Correlation between mortality and the levels of inter-alpha inhibitors in the plasma of patients with severe sepsis. *J. Infect. Dis.* **2003**, *188*, 919–926.
97. Hamm, A.; Veeck, J.; Bektas, N.; Wild, P.J.; Hartmann, A.; Heindrichs, U.; Kristiansen, G.; Werbowetski-Ogilvie, T.; Del Maestro, R.; Knuechel, R.; et al. Frequent expression loss of Inter-alpha-trypsin inhibitor heavy chain (ITI<sub>H</sub>) genes in multiple human solid tumors: A systematic expression analysis. *BMC Cancer* **2008**, *8*, 1–15.
98. Briggs, D.C.; Langford-Smith, A.W.W.; Birchenough, H.L.; Jowitt, T.A.; Kieley, C.M.; Enghild, J.J.; Baldock, C.; Milner, C.M.; and Day, A.J. Inter- $\alpha$ -inhibitor heavy chain-1 has an integrin-like 3D structure mediating immune regulatory activities and matrix stabilization during ovulation. *J. Biol. Chem.* **2020**, *295*, 5278–5291.
99. Yingsung, W.; Zhuo, L.; Morgelin, M.; Yoneda, M.; Kida, D.; Watanabe, H.; Ishiguro, N.; Iwata, H.; and Kimata, K. Molecular heterogeneity of the SHAP-hyaluronan complex. Isolation and characterization of the complex in synovial fluid from patients with rheumatoid arthritis. *J. Biol. Chem.* **2003**, *278*, 32710–32718.
100. McDonald, B. Interaction of CD44 and hyaluronan is the dominant mechanism for neutrophil sequestration in inflamed liver sinusoids. *J. Exp. Med.* **2008**, *205*, 915–927.
101. Lepedda, A.J.; De Muro, P.; Capobianco, G.; Formato, M. Role of the small proteoglycan bikunin in human reproduction. *Hormones* **2019**, *19*, 123–133.

- 
102. Wisniewski, H.G.; Hua, J.C.; Poppers, D.M.; Naime, D.; Vilcek, J.; Cronstein, B.N. TNF/IL-1-inducible protein TSG-6 potentiates plasmin inhibition by inter-alpha-inhibitor and exerts a strong anti-inflammatory effect in vivo. *J. Immunol.* **1996**, *156*, 1609–1615.
  103. Adair, J.E.; Stober, V.; Sobhany, M.; Zhuo, L.; Roberts, J.D.; Negishi, M.; Kimata, K.; and Garantziotis, S. Inter- $\alpha$ -trypsin Inhibitor Promotes Bronchial Epithelial Repair after Injury through Vitronectin Binding. *J. Biol. Chem.* **2009**, *284*, 16922–16930.

## III-6 Bikunin analyses in HepG2 cells with Golgi homeostasis defects





### III-6-1 Effects of Bafilomycin A1-mediated Golgi pH defects on bikunin profile

Bafilomycin A1 targets the vacuolar-type H<sup>+</sup> -ATPase (V-ATPase) enzyme, a membrane spanning proton pump that acidifies either the extracellular environment or intracellular organelles such as the lysosome (336). Intracellularly, alkalization is expected to cause a delayed Golgi-to-ER retrograde trafficking, leading to decreased activity and mislocalization of several glyco-enzymes (337,338). Together, these perturbations might cause glycosylation defects including abnormal PG biosynthesis (339).

In this section, we present our evaluation of the potential of Bkn as a marker of V-ATPase defects in vitro using as a model the HepG2 hepatocellular carcinoma-derived cell line treated with Baf A1. We first ensured that HepG2 could efficiently secrete Bkn in normal conditions. Therefore, cells were cultivated in a fetal bovine serum-free medium for 72 h and Bkn was analyzed by Western blot in the resulting supernatant. As showed in **Figure 27**, Western blot profile displays two heavy forms corresponding to ITI (225kDa) and PaI (~ 130-200 kDa) and two light forms corresponding to Bkn-CS (~ 35-45 kDa) and free Bkn (26kDa). This result showed that HepG2 cells can produce, mature and secrete Bkn.

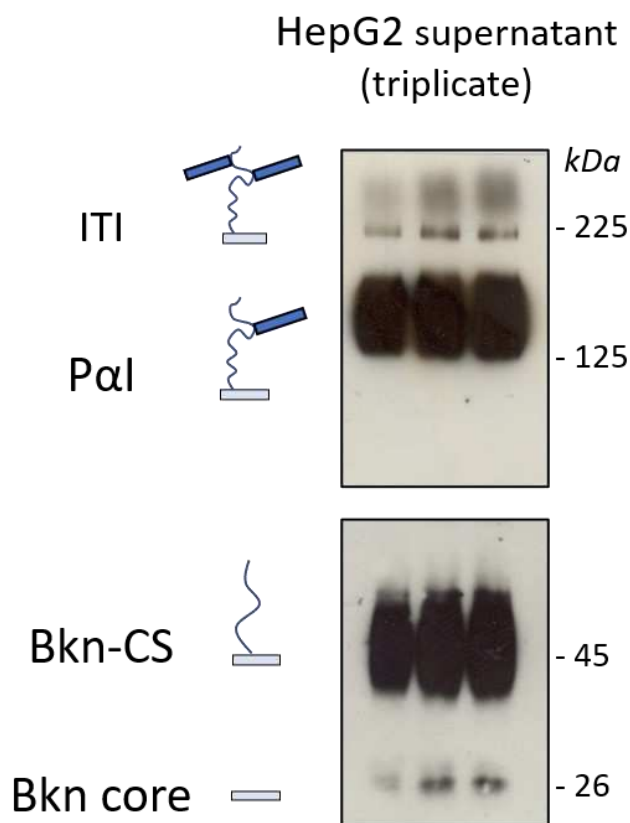


**Figure 27: Western blot profile of secreted Bkn isoforms from HepG2 cells**

Cells were cultivated in a fetal bovine serum-free medium. After 72 h, secreted Bkn was analyzed in the supernatant (40  $\mu$ L) in triplicate. Each Bkn isoform was detected.

Afterwards, we verified that Baf A1 treatment of HepG2 can efficiently trigger (i) pH increase in acidic organelles, (ii) disturbed retrograde trafficking and (iii) glycosylation defects.

To ensure that Baf A1 treatment results in pH disturbances in HepG2, we used LysoTracker (LysoT), a fluorescent probe which labels acidic organelles including the Golgi apparatus (340). Cells were pretreated with Baf A1 (50nM) for 72 h and LysoT was added into the culture medium. After 30 min, cells were fixed for fluorescence microscopy observation. In control cells, we observed various LysoT-positive intracellular regions corresponding to acidic organelles. In contrast, we found drastic fluorescence decrease in Baf A1-treated cells. This

result indicates that Baf A1 induced an efficient alkalization of intracellular organelles including most probably the Golgi apparatus (**Figure 28**).

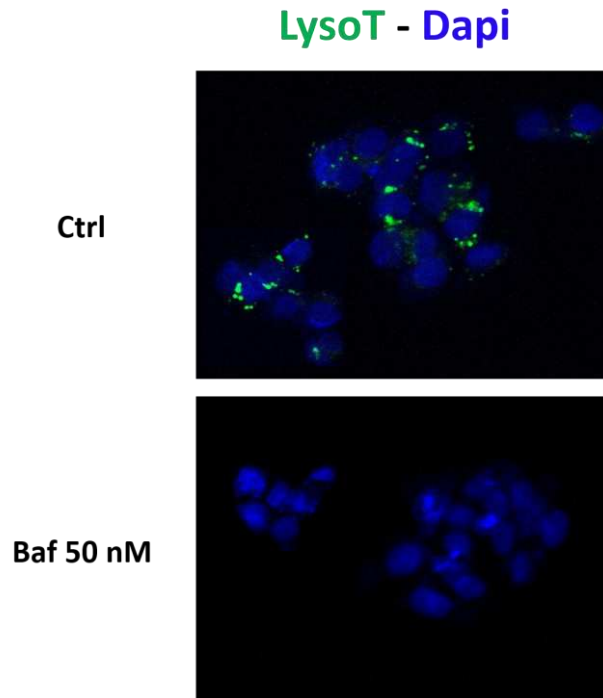


**Figure 28: Immunofluorescence analysis of LysoTracker in control and Baf A1-treated HepG2**

LysoTracker (green) and Dapi DNA marker (blue) immunofluorescent co-staining was performed in controls and 72 h Baf A1 (50nM)-treated HepG2. Magnification x40.

To determine whether such rise of pH is accompanied by impaired Golgi-to-ER retrograde trafficking, we studied the effects of BFA in Baf A1-treated HepG2. We used albumin, a protein largely routed through the ER-Golgi pathway, as a marker of the vesicular trafficking. As shown in **Figure 29 A**, albumin staining in both control and Baf A1-treated cells displayed, in absence of BFA, a compact organization consistent with a Golgi distribution. In cells treated for 4 min with BFA (10 $\mu$ M), albumin staining displayed an ER distribution indicating massive return of albumin to the ER. In contrast, albumin staining in Baf A1-treated cells exhibited several vesicular aggregates upon 4 min of BFA exposition, suggesting blockade of Golgi membrane fusion with the ER. Quantifications of cells presenting BFA-induced ER distribution of albumin

were performed upon 1, 2, and 4 minutes of BFA treatment. For each BFA treatment time, the results show that with respect to controls, only ~30% of the cells displayed an ER distribution of albumin in Baf A1-treated cells (**Figure 29 B**). Baf A1 therefore efficiently inhibits Golgi-to-ER redistribution of albumin under BFA treatment.

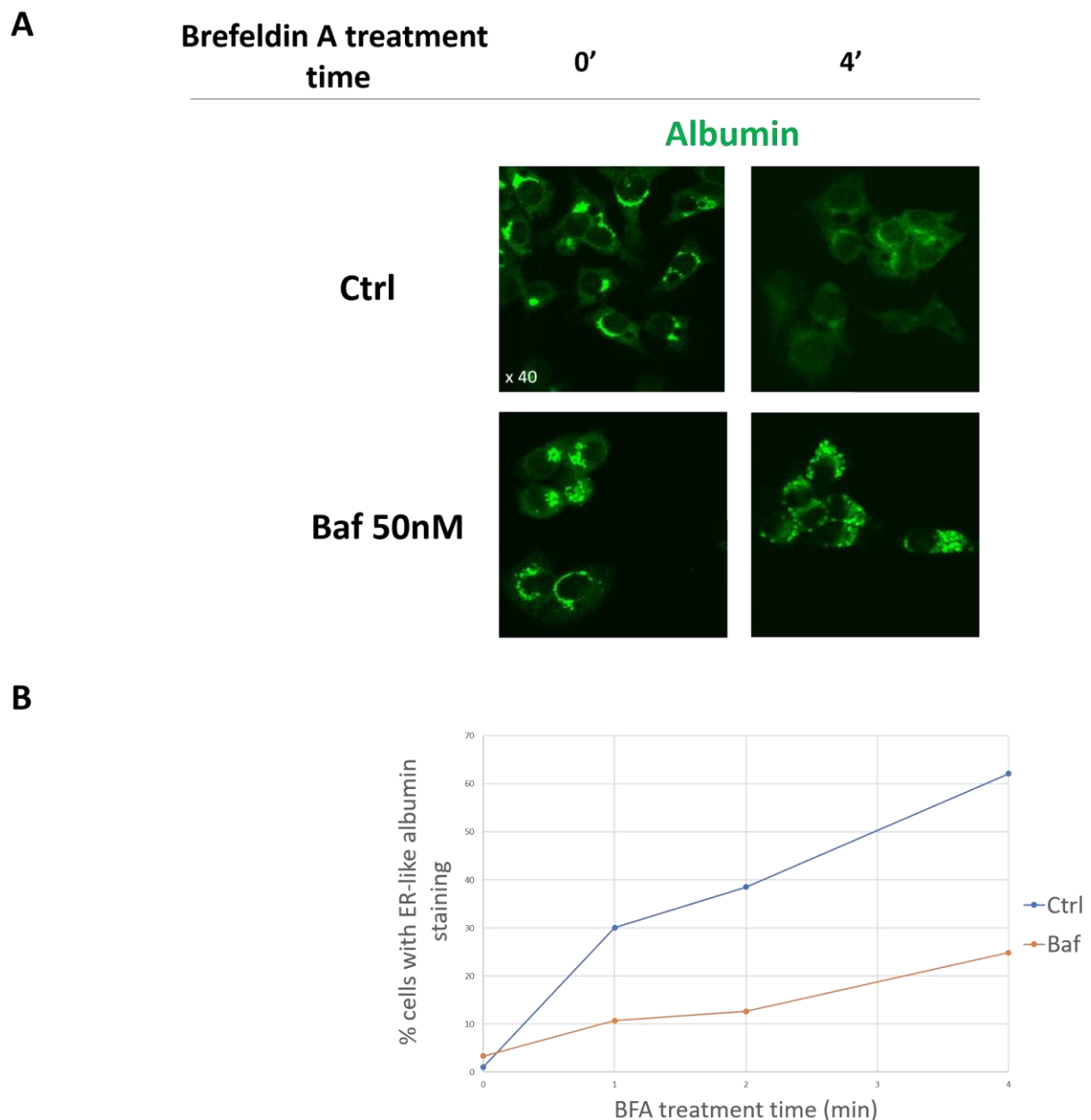


**Figure 29: Assessment of BFA-induced Golgi-to-ER retrograde trafficking in control and Baf A1-treated HepG2**

A) Albumin immunofluorescent labelling in control and Baf A1-treated cells exposed to BFA (10 $\mu$ M) for 4 minutes. Magnification x40 B) Quantification of cells presenting BFA-induced ER redistribution of albumin in control and Baf A1-treated cells incubated with BFA for 1, 2 and 4 minutes. Percentages were calculated from 200 cells in each condition.

To address the effects of Baf A1 on protein glycosylation, cells were treated with Baf (50 nM) for 72 h, and the cell culture supernatant was collected for Western blot analysis of transferrin and orosomuroid, two *N*-glycosylated proteins. As showed in **Figure 30**, the apparent molecular weight and the level of glycoprotein secretion of these two glycoproteins were clearly decreased in Baf A1-treated cells in comparison to controls. This result indicates that Baf A1 treatment triggered *N*-glycosylation defects in HepG2 cells.

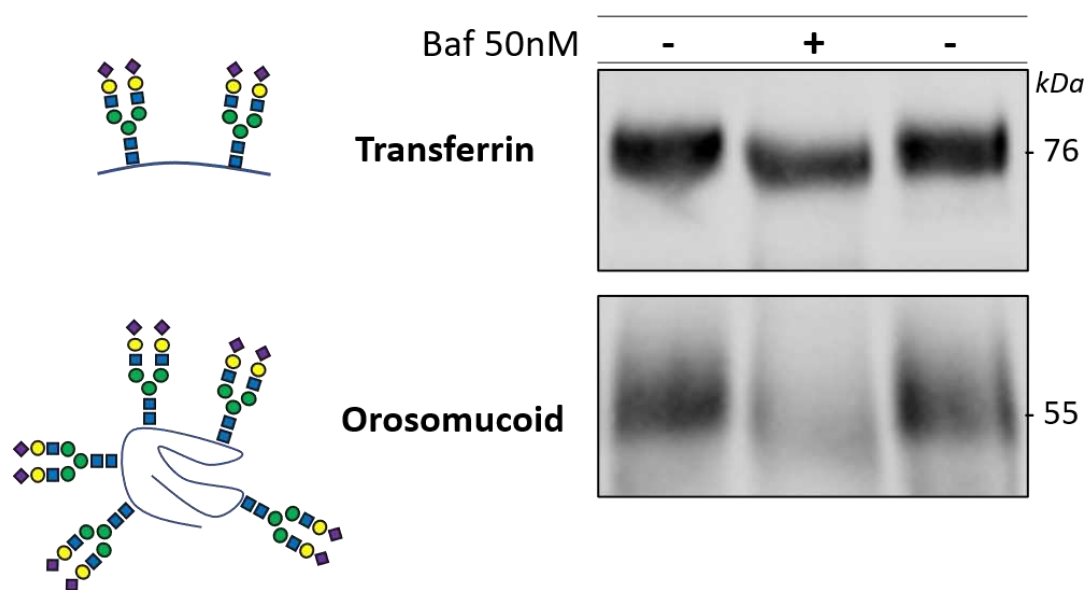


**Figure 30: Western blot analysis of transferrin and orosomuroid in Baf A1-treated HepG2**

Western blot profiles of transferrin and orosomuroid in supernatant from control and Baf A1-treated HepG2. Left schemes illustrate the *N*-glycosylation patterns of both glycoproteins

Altogether, these results indicate that HepG2 treatment with 50 nM Baf during 72 h could constitute an appropriate model to assess the potential of Bkn as an *in vitro* biomarker of Golgi homeostasis defects due to impaired V-ATPase.

HepG2 cells were incubated with Baf A1 to analyze the secreted Bkn in the resulting cell culture medium. At 48 h, Bkn Western blot profile analysis of control culture media displayed two forms corresponding to PaI (~ 130-200 kDa) and Bkn-CS (~ 35-45 kDa). In Baf A1-treated

cells, both forms were found with strikingly increased size range, together with a decreased intensity of Bkn-CS compared to controls (**Figure 31 A**). At 72 h, the Bkn profile of control cells exhibited an additional ~ 225 kDa band that is likely to correspond to ITI while P $\alpha$ I and Bkn-CS band intensities were consistently more pronounced than after 48 h of secretion. As for Baf A1 48 h-treated cells, Bkn-CS and P $\alpha$ I MW were increased, and total Bkn levels were decreased (ITI was not detected) compared to controls.

To examine whether the increased MW of Bkn isoforms in Baf A1-treated cells is due to an over-elongated Bkn-CS chain or to a defective AMBP intracellular cleavage, cell supernatants were treated by chABC to analyze Bkn resulting profile. As showed in **Figure 31 B**, chABC treatment resulted a band size consistent with the Bkn-hexasaccharide form in both control and Baf A1-treated cells. Moreover, analysis of A1MG profile showed a unique 34kDa band in both control and Baf A1- supernatants. These results indicated that the abnormally increased Bkn isoforms sizes in Baf A1-treated cells originate from an over-lengthened (and over-sulfated ?) Bkn-CS chain and not from a defective AMBP cleavage.

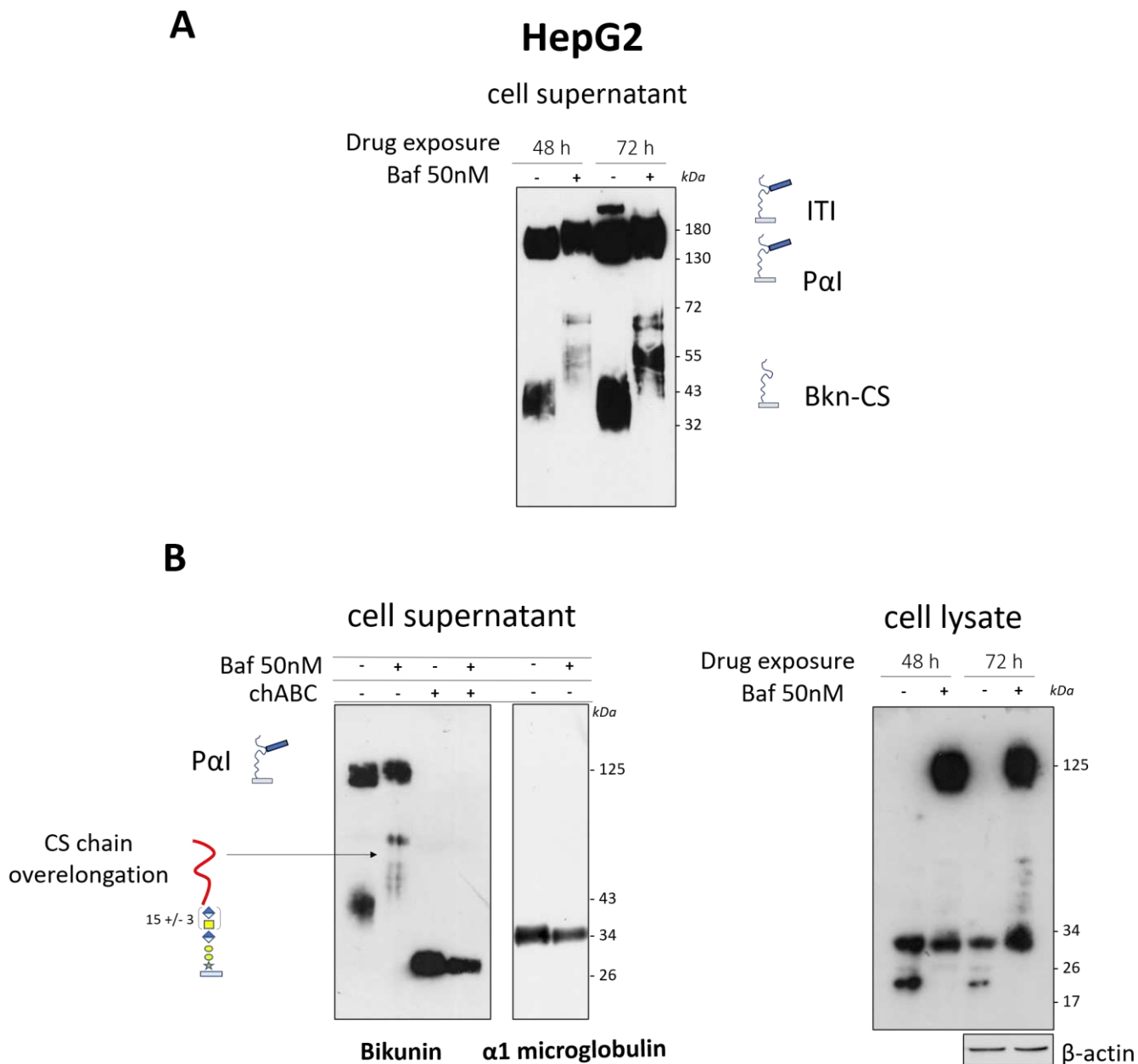


**Figure 31: Western blot profile of Bkn in supernatant and lysate of Baf A1-treated HepG2**

A) Bkn profile in supernatant of HepG2 treated with Baf A1 (50nM) during 48 and 72H compared to controls. B) Left panel shows Bkn profile in chABC treated supernatant from controls and Baf A1-treated HepG2 as well as A1MG profile in Baf A1-treated HepG2 compared to controls. Right panel shows Bkn profile in lysate from 48 h- and 72 h-Baf A1-treated HepG2. B-actin served as loading control.

To investigate whether the observed decrease of Bkn isoform levels in the supernatant of Baf A1-treated cells is due to defective synthesis or intracellular retention, we analyzed cell lysates originating from 48- and 72 h- Baf A1-treated hepG2 (**Figure 31 B**). In control cells,



Bkn displayed three light forms (~ 20, 26 and 30 kDa) that might correspond to immature biosynthetic intermediates. In Baf A1-treated cells, we observed an additional heavy Bkn form (125 kDa) that resembles P $\alpha$ I, while the 20kDa band was not detected. Together with the previously observed Bkn level decrease in the supernatant, this result indicated a Baf A1-induced intracellular retention of Bkn with possible impact on its post-translational processing.

To explore the intracellular distribution of Bkn upon Baf A1 treatment, we performed co-immunostaining against Bkn and GM130 (a *cis*-Golgi marker) in control and Baf A1-treated cells for fluorescent microscopy observation. In control cells, Bkn adopted homogeneous organization throughout the cell in contrast to GM130 which, consistently, assumed a compact Golgi distribution (**Figure 32 A**). In Baf A1-treated cells, Bkn localized in clustered structures and GM130 was slightly dispersed. Observation at high magnification (x100) of Baf-treated cells showed that Bkn clusters were localized into large-sized multivesicular bodies. Note that Baf A1-induced Bkn clusters did not colocalize with GM130 indicating that these unknown bodies are not in the *cis*-Golgi. Further work is necessary to determine which subcompartment houses such bulk structures. Nevertheless, this intracellular aggregation indicates a Baf-induced blockade of Bkn secretory route. This could lead to extended exposition of the nascent CS chain to GAG elongation and sulfation enzymes in the *trans*-Golgi/ TGN which might partially explain the over-lengthened Bkn-CS chain observed above.

To assess whether Baf A1-induced intracellular aggregation of Bkn was also encountered in other secreted proteins, we co-labelled orosomuroid and GM130 in control and Baf A1-treated HepG2 (**Figure 32 B**). As for Bkn labelling, control cells exhibited homogeneous orosomuroid distribution across the cell area. However, we observed no changes of this staining pattern in Baf A1-treated cells suggesting separate vesicular pathways for orosomuroid and Bkn upon Baf A1 treatment. This result strongly corroborates recent findings highlighting a

Golgi-stress response PG pathway which segregates the PG vesicular transport components from that of *N*-glycosylation process during Golgi homeostasis defects (84,85,341).

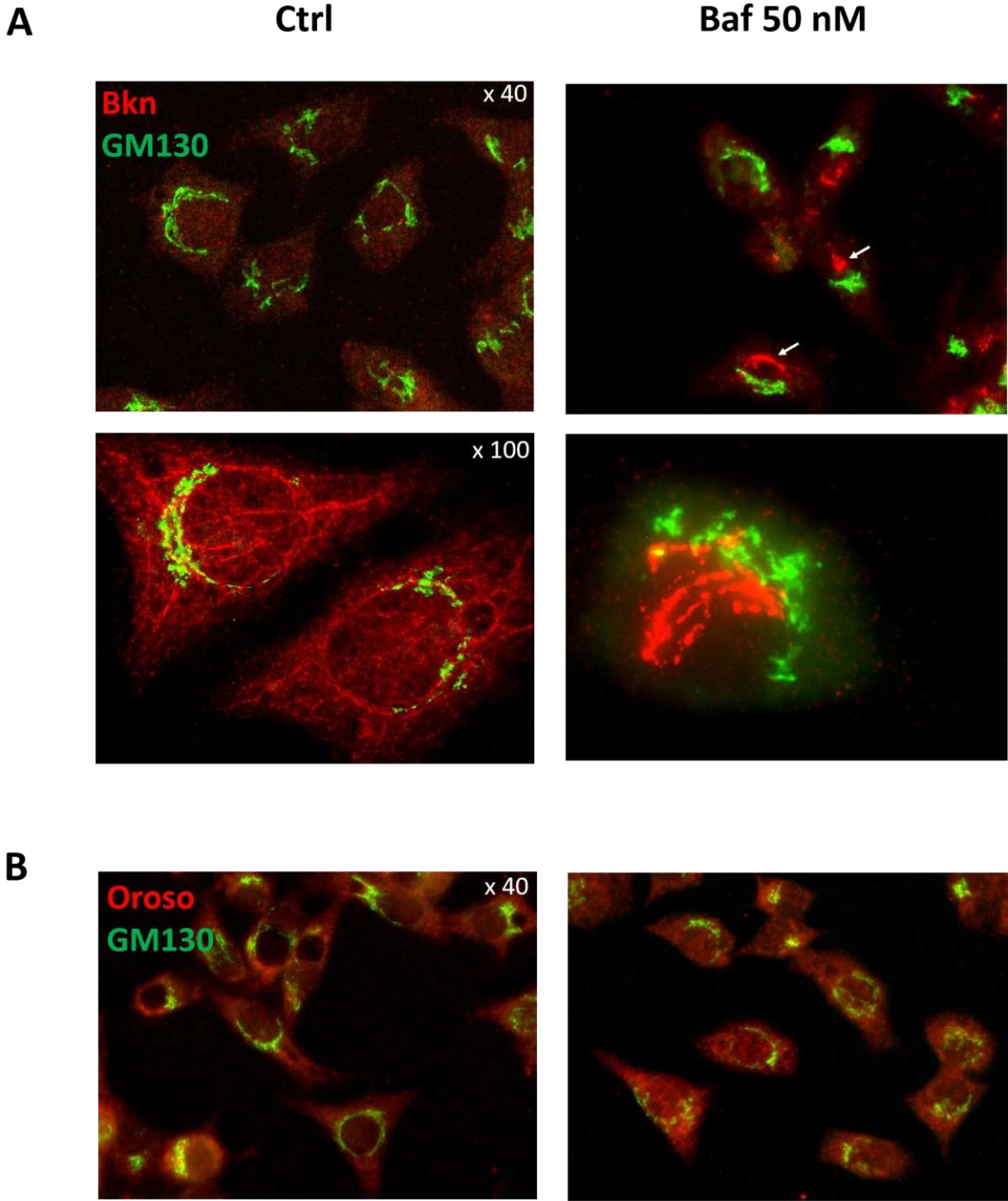


**Figure 32: Immunofluorescence analysis of Bkn in Baf A1-treated HepG2**

A) Co-immunostaining of Bkn and GM130 in control and Baf A1-treated HepG2. White arrows show Baf A1-induced Bkn clusters. Magnification x40 (up) and x100 (down). B) Co-immunostaining of orosomucoid and GM130 in control and Baf A1-treated HepG2.

In summary, we showed that Baf A1-mediated V-ATPase inhibition in HepG2 led to intracellular organelle alkalization, delayed Golgi-to-ER retrograde trafficking and *N*-glycosylation defects. Such impairments were associated to abnormal Bkn Western blot profile and intracellular retention. The observed increase of Bkn-CS chain length, the decreased Bkn secretion as well as its intracellular aggregation into compartments that remain to be identified constitute a set of arguments demonstrating that Bkn could be an *in vitro* marker of Golgi homeostasis defects at least in the context of pH disturbance.

### III-6-2 Bikunin analysis in manganese homeostasis defects

*In vitro* studies using HEK293 cells showed that  $Mn^{2+}$  supplementation of the culture medium leads to lysosomal degradation of the  $Mn^{2+}$  transporter TMEM165 (**Figure 33**) (342). Such mechanism involves a  $Mn^{2+}$ -sensitive ELGDK motif within TMEM165 polypeptide structure which confers responsiveness to  $Mn^{2+}$  variations and mediates the  $Mn^{2+}$  transport activity.

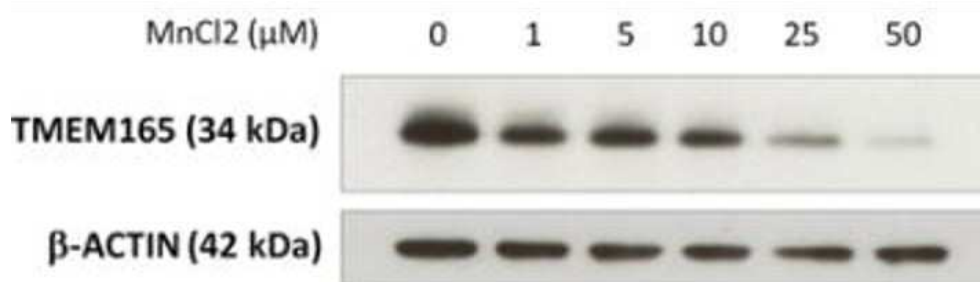


**Figure 33: High  $Mn^{2+}$  concentrations in cell culture medium result in TMEM165 degradation in HEK293 cells** (Figure from Potelle et al. 2017) (342)

We used this strategy to create a HepG2 model with Golgi  $Mn^{2+}$  homeostasis defect which could mimic the human TMEM165 deficiency. This allowed us to evaluate the potential of Bkn as a marker of Golgi  $Mn^{2+}$  defects *in vitro*.

HepG2 cells were exposed to increasing  $\text{MnCl}_2$  concentrations during 72 h and the supernatant was collected for Bkn analysis by Western blot. As showed in **Figure 34**, Bkn isoforms bands' intensities in  $\text{MnCl}_2$  treated HepG2 were decreased compared to controls proportionally to the increasing  $\text{MnCl}_2$  concentrations in the culture medium. Moreover, we observed a gradual emergence of an abnormal ~30 kDa band in  $\text{MnCl}_2$  treated HepG2 compared to controls at the expense of the usual 26 kDa Bkn core protein band.

Together, these data indicate that  $\text{MnCl}_2$ -mediated  $\text{Mn}^{2+}$  homeostasis defect triggered alteration of Bkn isoforms' biosynthesis. The observed abnormal Bkn light form in  $\text{MnCl}_2$ -treated cells is reminiscent of the previously described Bkn profiles in TMEM165 deficiency and linkeropathies which indicated an enzymatic blockade of the tetrasaccharide linkage region formation (**Figure 34**). Although further work is necessary to confirm the  $\text{MnCl}_2$ -mediated degradation of TMEM165 and glycosylation defects in HepG2, this result strongly support the reliability of Bkn as an in vitro marker of Golgi  $\text{Mn}^{2+}$  homeostasis defects which could reproduce the human TMEM165 deficiency.

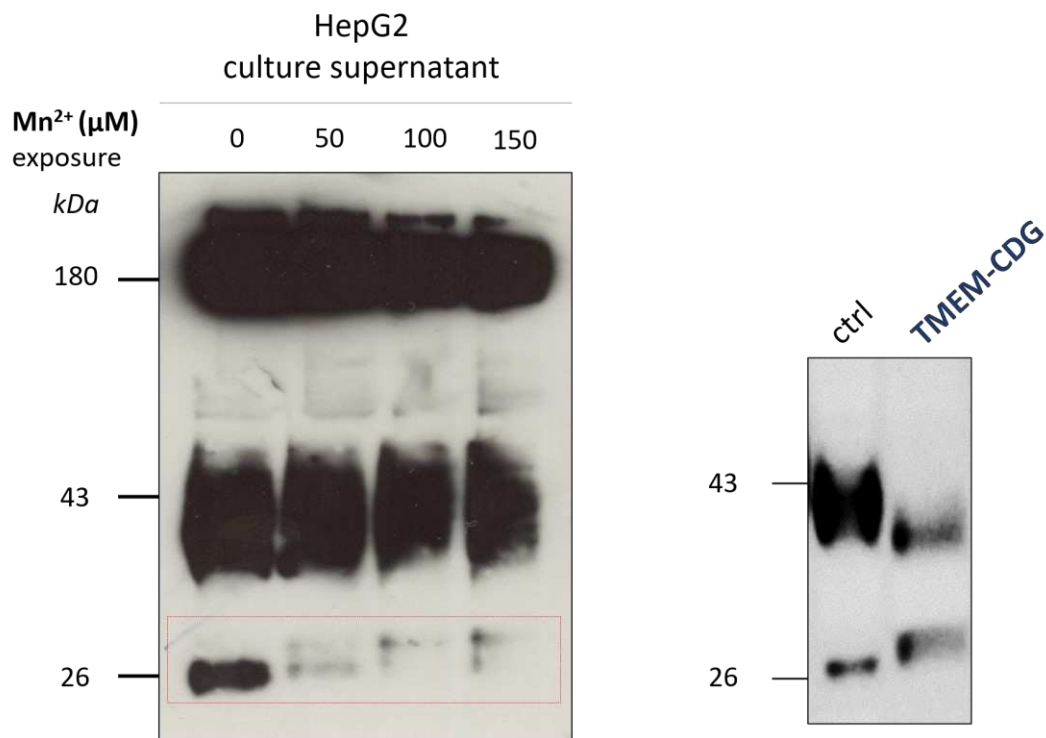


**Figure 34: Western blot analysis of Bkn in MnCl<sub>2</sub>-treated HepG2 compared to TMEM165 deficient patient**

Left panel: HepG2 cells were exposed to increasing Mn<sup>2+</sup> concentrations in the culture medium during 72h. The resulting supernatants were analyzed by Western blot for detection of bikunin isoforms. Red square shows free Bkn profile in control cells compared to Mn<sup>2+</sup>-treated cells. Right panel: Previously described Western blot profile of serum Bkn in TMEM165-CDG individual compared to control. Note the similar pattern for free Bkn in patient and in Mn<sup>2+</sup>-treated HepG2.

## General conclusion



Proteoglycans (PG) consist of a family of macromolecules composed of proteins branched to linear sulfated polysaccharides called glycosaminoglycans (GAG). According to the nature of the repeated polysaccharidic building blocks, GAG chains consist of chondroitin sulfate, dermatan sulfate, heparan sulfate and keratan sulfate. The intracellular PG biosynthetic machinery represents a complex and tightly regulated network of enzymes, membrane sugar transporters, ionic channels, and vesicular trafficking-related proteins. This “proteoglycanome” ensures the output of various types of PG playing fundamental roles in humans as reflected by the pathological consequences of a faulty inherited proteoglycan biosynthesis. Indeed, the PG inherited defects (PG-IMD) manifest themselves by skeletal malformations, cartilage defects, neurological, and other multiorgan dysfunctions. PG-IMD could be classified according to the defective PG biosynthetic steps. One can distinguish (i) linkeropathies (i.e., defective GAG initiating tetrasaccharide linker formation), (ii) GAG elongation defects, (iii) GAG sulfation defects, (iv) defective substrate supply, and (v) defective Golgi homeostasis. These inborn pathologies are rare, and their diagnosis is difficult because of unspecific symptomatology and difficult biochemical assessment. Currently, screening a PG-IMD requires the implementation of laborious biochemical assays based on GAG analyses in patients’ fibroblasts, blood and/or urine, while upstream or downstream genetic sequencing allows identification of (potentially) causative gene variants.

My thesis project focused on the development of a new biochemical test based on the analysis of bikunin, a PG produced by the liver and secreted into the blood circulation. As a so-called ‘protein-GAG-protein’ (PGP), bikunin bears a chondroitin sulfate chain that could be linked to one or two glycoproteins called heavy chains (HC) proteins through unusual ester linkage(s). We made assumption that bikunin isoforms structure would be altered during PG biosynthesis defects and could thereby represent interesting biomarkers of PG-IMD.



The analyses we developed mainly consist of a classical SDS-PAGE separation of serum proteins followed by immunodetection of bikunin isoforms (i.e., Western blot). The resulting profile was then compared to that of healthy individuals for highlighting quantitative and/or qualitative abnormalities, both suggesting defective PG biosynthesis. Regarding the qualitative alterations, complementary two-dimensional electrophoresis (2-DE) enabling charge and molecular weight separation as well as mass spectrometry analysis could be performed to better characterize the encountered Bkn abnormal forms in some cases. In this context, we found signature profiles allowing to directly suspect the causative pathogenic gene variant such as in linkeropathies. In other PG-IMD cases including GAG elongation, sulfation, substrate supply and Golgi homeostasis defects, bikunin analysis allowed to more precisely orient towards the definite diagnosis.

Moreover, we found that bikunin could be an additional biomarker of congenital disorders of glycosylation (CDG) with Golgi homeostasis defects, a group of rare genetic defects altering *N*- and mucin-type *O*-glycosylation of proteins. Indeed, in CDG due to impaired Golgi pH regulation, we found both quantitative and qualitative alterations of bikunin Western blot profile. Besides reinforcing the screening of some CDG, bikunin analysis allowed to gain novel pathophysiological insights for these diseases.

Technically, performing bikunin analysis is rather advantageous. The high serum levels of its isoforms together with the availability of specific antibodies enable easy, rapid, and cost-effective Western blot or 2-DE analysis from few microliters of serum. Bikunin analysis is currently being developed for utilization from dried blood spots, the latter being minimally invasive and allowing more convenient storage than serum.

Bikunin analysis has proven multifaceted abilities for various applications and could be considered as a biochemical “swiss army knife” (**Figure 35**) that could be deployed in the

screening arsenal of several genetic deficiencies leading to alterations of PG biosynthesis and /or Golgi homeostasis. The complexity and diversity of the post-translational modifications occurring on bikunin isoforms (i.e., glycosylation, GAG elongation, sulfation, phosphorylation, HC esterification, cleavages) allow to analyze the consequences of several genetic deficiencies related to abnormal PG and glycoprotein metabolism. Additional applications of bikunin analysis remain to be discovered such as in glycosylation and PG defects resulting from acquired pathologies including cancer, liver diseases and diabetes. Bikunin could be used as a biomarker for screening these diseases as well as for the follow-up of their progression and treatment efficacy.

The major limitation of bikunin analysis is that it misses the screening of pathologies resulting from deficiencies in genes that are not expressed by the liver since bikunin biosynthesis use the hepatocyte biosynthetic machinery. Moreover, as a CS-type PG, it is likely that specific alterations of heparan sulfate or keratan sulfate-type GAG elongation and sulfation would not be detected through bikunin analysis. Nevertheless, the resulting “false-negative” profiles may complement other data collected from the current screening strategy to help orientating the screening.

Otherwise, part of this thesis project overlapped with that of my co-worker (Dr. Samra Lounis) to evaluate in vitro the potential of bikunin as a biomarker of Golgi stresses. We used hepatic cell lines including HepG2 to create models of Golgi homeostasis defects and to analyze related bikunin profiles. I showed that bikunin isoforms biosynthesis was quantitatively and qualitatively affected during conditions with bafilomycin-mediated raised Golgi pH as well as  $Mn^{2+}$  excess, two conditions that could mimic some PG-IMD and CDG-related deficiencies. Therefore, my preliminary results suggested that bikunin patterns could be used in vitro as interesting cellular tools to detect Golgi homeostasis disturbances, at least during Golgi

alkalization and  $Mn^{2+}$  defects. Furthermore, they could provide additional insights into the pathophysiology of the related diseases in humans. Dr. Samra Louis is currently studying the effects of extracellular pH variations on bikunin profiles, and the results are very promising.

In terms of preclinical and fundamental research perspectives, bikunin analysis could be used in cellular and animal models mimicking inborn (PG-IMD, CDG) and acquired pathological conditions (cancers, liver diseases). Bikunin profiles would allow to highlight defective glycosylation, PG biosynthesis and Golgi homeostasis and provide additional insights in the pathophysiology of these diseases.



**Figure 35: Bikunin, a biological Swiss Army knife**

Bikunin isoforms display various post-translational modifications resembling the multiple blades of a swiss army knife. These post-translational modifications are altered during several diseases with glycosylation and PG defects. The analysis of Bkn-CS elongation and sulfation patterns allowed to detect abnormal PG biosynthesis in various types of PG-IMD while HC esterification-resulting heavy forms (ITI and P $\alpha$ I) were useful for screening CDG with Golgi homeostasis defects. Bkn analysis also provided interesting insights in the study of Golgi homeostasis defects using cellular models. Potential new blades remain to be uncovered for additional application of bikunin analysis such as in acquired pathologies with glycosylation, PG and Golgi homeostasis defects.

# Bibliography



1. Schjoldager KT, Narimatsu Y, Joshi HJ, Clausen H. Global view of human protein glycosylation pathways and functions. *Nat Rev Mol Cell Biol.* 2020 Dec;21(12):729–49.
2. Flynn RA, Pedram K, Malaker SA, Batista PJ, Smith BAH, Johnson AG, et al. Small RNAs are modified with N-glycans and displayed on the surface of living cells. *Cell.* 2021 Jun;184(12):3109-3124.e22.
3. Kjellén L, Lindahl U. Proteoglycans: Structures and Interactions. *Annual Review of Biochemistry.* 1991;60(1):443–75.
4. Reily C, Stewart TJ, Renfrow MB, Novak J. Glycosylation in health and disease. *Nat Rev Nephrol.* 2019 Jun;15(6):346–66.
5. Prydz K, Dalen KT. Synthesis and sorting of proteoglycans. *J Cell Sci.* 2000 Jan;113 Pt 2:193–205.
6. Iozzo RV, Schaefer L. Proteoglycan form and function: A comprehensive nomenclature of proteoglycans. *Matrix Biol.* 2015 Mar;42:11–55.
7. Schaefer L, Schaefer RM. Proteoglycans: from structural compounds to signaling molecules. *Cell Tissue Res.* 2010 Jan;339(1):237–46.
8. Paganini C, Costantini R, Superti-Furga A, Rossi A. Bone and connective tissue disorders caused by defects in glycosaminoglycan biosynthesis: a panoramic view. *The FEBS Journal.* 2019;286(15):3008–32.
9. Dubail J, Cormier-Daire V. Chondrodysplasias With Multiple Dislocations Caused by Defects in Glycosaminoglycan Synthesis. *Front Genet.* 2021;12:642097.

10. Mizumoto S, Yamada S. Congenital Disorders of Deficiency in Glycosaminoglycan Biosynthesis. *Front Genet.* 2021;12:717535.
11. Bourdon MA, Krusius T, Campbell S, Schwartz NB, Ruoslahti E. Identification and synthesis of a recognition signal for the attachment of glycosaminoglycans to proteins. *Proc Natl Acad Sci U S A.* 1987 May;84(10):3194–8.
12. Esko JD, Zhang L. Influence of core protein sequence on glycosaminoglycan assembly. *Current Opinion in Structural Biology.* 1996 Oct 1;6(5):663–70.
13. Brinkmann T, Weilke C, Kleesiek K. Recognition of acceptor proteins by UDP-D-xylose proteoglycan core protein beta-D-xylosyltransferase. *J Biol Chem.* 1997 Apr 25;272(17):11171–5.
14. Zhang L, David G, Esko JD. Repetitive Ser-Gly Sequences Enhance Heparan Sulfate Assembly in Proteoglycans. *J Biol Chem.* 1995 Nov 10;270(45):27127–35.
15. Götting C, Kuhn J, Zahn R, Brinkmann T, Kleesiek K. Molecular cloning and expression of human UDP-d-Xylose:proteoglycan core protein beta-d-xylosyltransferase and its first isoform XT-II. *J Mol Biol.* 2000 Dec 8;304(4):517–28.
16. Kearns AE, Vertel BM, Schwartz NB. Topography of glycosylation and UDP-xylose production. *J Biol Chem.* 1993 May 25;268(15):11097–104.
17. Vertel BM, Walters LM, Flay N, Kearns AE, Schwartz NB. Xylosylation is an endoplasmic reticulum to Golgi event. *J Biol Chem.* 1993 May 25;268(15):11105–12.
18. Almeida R, Lavery SB, Mandel U, Kresse H, Schwientek T, Bennett EP, et al. Cloning and expression of a proteoglycan UDP-galactose:beta-xylose beta1,4-

- galactosyltransferase I. A seventh member of the human beta4-galactosyltransferase gene family. *J Biol Chem*. 1999 Sep 10;274(37):26165–71.
19. Bai X, Zhou D, Brown JR, Crawford BE, Hennet T, Esko JD. Biosynthesis of the linkage region of glycosaminoglycans: cloning and activity of galactosyltransferase II, the sixth member of the beta 1,3-galactosyltransferase family (beta 3GalT6). *J Biol Chem*. 2001 Dec 21;276(51):48189–95.
  20. Kitagawa H, Tone Y, Tamura J, Neumann KW, Ogawa T, Oka S, et al. Molecular Cloning and Expression of Glucuronyltransferase I Involved in the Biosynthesis of the Glycosaminoglycan-Protein Linkage Region of Proteoglycans. *J Biol Chem*. 1998 Mar 20;273(12):6615–8.
  21. Caterson B, Melrose J. Keratan sulfate, a complex glycosaminoglycan with unique functional capability. *Glycobiology*. 2018 Jan 11;28(4):182–206.
  22. Koike T, Izumikawa T, Tamura J-I, Kitagawa H. FAM20B is a kinase that phosphorylates xylose in the glycosaminoglycan-protein linkage region. *Biochem J*. 2009 Jun 26;421(2):157–62.
  23. Wen J, Xiao J, Rahdar M, Choudhury BP, Cui J, Taylor GS, et al. Xylose phosphorylation functions as a molecular switch to regulate proteoglycan biosynthesis. *Proc Natl Acad Sci U S A*. 2014 Nov 4;111(44):15723–8.
  24. Gulberti S, Lattard V, Fondeur M, Jacquinet J-C, Mulliert G, Netter P, et al. Phosphorylation and sulfation of oligosaccharide substrates critically influence the activity of human beta1,4-galactosyltransferase 7 (GalT-I) and beta1,3-glucuronosyltransferase I (GlcAT-I) involved in the biosynthesis of the



- glycosaminoglycan-protein linkage region of proteoglycans. *J Biol Chem.* 2005 Jan 14;280(2):1417–25.
25. Koike T, Izumikawa T, Sato B, Kitagawa H. Identification of Phosphatase That Dephosphorylates Xylose in the Glycosaminoglycan-Protein Linkage Region of Proteoglycans. *J Biol Chem.* 2014 Mar 7;289(10):6695–708.
  26. Izumikawa T, Sato B, Mikami T, Tamura J, Igarashi M, Kitagawa H. GlcUA $\beta$ 1-3Gal $\beta$ 1-3Gal $\beta$ 1-4Xyl(2-O-phosphate) is the preferred substrate for chondroitin N-acetylgalactosaminyltransferase-1. *J Biol Chem.* 2015 Feb 27;290(9):5438–48.
  27. Kitagawa H, Tsutsumi K, Ikegami-Kuzuhara A, Nadanaka S, Goto F, Ogawa T, et al. Sulfation of the galactose residues in the glycosaminoglycan-protein linkage region by recombinant human chondroitin 6-O-sulfotransferase-1. *J Biol Chem.* 2008 Oct 10;283(41):27438–43.
  28. Lauder RM, Huckerby TN, Nieduszynski IA. Increased incidence of unsulphated and 4-sulphated residues in the chondroitin sulphate linkage region observed by high-pH anion-exchange chromatography. *Biochem J.* 2000 Apr 15;347(Pt 2):339–48.
  29. de Waard P, Vliegthart JF, Harada T, Sugahara K. Structural studies on sulfated oligosaccharides derived from the carbohydrate-protein linkage region of chondroitin 6-sulfate proteoglycans of shark cartilage. II. Seven compounds containing 2 or 3 sulfate residues. *J Biol Chem.* 1992 Mar 25;267(9):6036–43.
  30. Zhang L, Esko JD. Amino acid determinants that drive heparan sulfate assembly in a proteoglycan. *J Biol Chem.* 1994 Jul 29;269(30):19295–9.

31. Chen RL, Lander AD. Mechanisms underlying preferential assembly of heparan sulfate on glypican-1. *J Biol Chem.* 2001 Mar 9;276(10):7507–17.
32. Gulberti S, Jacquinet J-C, Chabel M, Ramalanjaona N, Magdalou J, Netter P, et al. Chondroitin sulfate N-acetylgalactosaminyltransferase-1 (CSGalNAcT-1) involved in chondroitin sulfate initiation: Impact of sulfation on activity and specificity. *Glycobiology.* 2012 Apr;22(4):561–71.
33. Uyama T, Kitagawa H, Tamura Ji J, Sugahara K. Molecular cloning and expression of human chondroitin N-acetylgalactosaminyltransferase: the key enzyme for chain initiation and elongation of chondroitin/dermatan sulfate on the protein linkage region tetrasaccharide shared by heparin/heparan sulfate. *J Biol Chem.* 2002 Mar 15;277(11):8841–6.
34. Kitagawa H, Uyama T, Sugahara K. Molecular cloning and expression of a human chondroitin synthase. *J Biol Chem.* 2001 Oct 19;276(42):38721–6.
35. Kitagawa H, Izumikawa T, Uyama T, Sugahara K. Molecular Cloning of a Chondroitin Polymerizing Factor That Cooperates with Chondroitin Synthase for Chondroitin Polymerization. *J Biol Chem.* 2003 Jun 27;278(26):23666–71.
36. Izumikawa T, Uyama T, Okuura Y, Sugahara K, Kitagawa H. Involvement of chondroitin sulfate synthase-3 (chondroitin synthase-2) in chondroitin polymerization through its interaction with chondroitin synthase-1 or chondroitin-polymerizing factor. *Biochem J.* 2007 May 1;403(Pt 3):545–52.
37. Izumikawa T, Koike T, Shiozawa S, Sugahara K, Tamura J, Kitagawa H. Identification of chondroitin sulfate glucuronyltransferase as chondroitin synthase-3 involved in chondroitin polymerization: chondroitin polymerization is achieved by multiple enzyme

- complexes consisting of chondroitin synthase family members. *J Biol Chem.* 2008 Apr 25;283(17):11396–406.
38. Mikami T, Kitagawa H. Biosynthesis and function of chondroitin sulfate. *Biochim Biophys Acta.* 2013 Oct;1830(10):4719–33.
  39. Kitagawa H, Shimakawa H, Sugahara K. The tumor suppressor EXT-like gene EXTL2 encodes an alpha1, 4-N-acetylhexosaminyltransferase that transfers N-acetylgalactosamine and N-acetylglucosamine to the common glycosaminoglycan-protein linkage region. The key enzyme for the chain initiation of heparan sulfate. *J Biol Chem.* 1999 May 14;274(20):13933–7.
  40. Kim BT, Kitagawa H, Tamura J, Saito T, Kusche-Gullberg M, Lindahl U, et al. Human tumor suppressor EXT gene family members EXTL1 and EXTL3 encode alpha 1,4- N-acetylglucosaminyltransferases that likely are involved in heparan sulfate/ heparin biosynthesis. *Proc Natl Acad Sci U S A.* 2001 Jun 19;98(13):7176–81.
  41. Lind T, Tufaro F, McCormick C, Lindahl U, Lidholt K. The putative tumor suppressors EXT1 and EXT2 are glycosyltransferases required for the biosynthesis of heparan sulfate. *J Biol Chem.* 1998 Oct 9;273(41):26265–8.
  42. Annaval T, Wild R, Créton Y, Sadir R, Vivès RR, Lortat-Jacob H. Heparan Sulfate Proteoglycans Biosynthesis and Post Synthesis Mechanisms Combine Few Enzymes and Few Core Proteins to Generate Extensive Structural and Functional Diversity. *Molecules.* 2020 Sep 14;25(18):E4215.
  43. Seko A, Dohmae N, Takio K, Yamashita K. Beta 1,4-galactosyltransferase (beta 4GalT)-IV is specific for GlcNAc 6-O-sulfate. Beta 4GalT-IV acts on keratan sulfate-related

- glycans and a precursor glycan of 6-sulfosialyl-Lewis X. *J Biol Chem.* 2003 Mar 14;278(11):9150–8.
44. Seko A, Yamashita K. beta1,3-N-Acetylglucosaminyltransferase-7 (beta3Gn-T7) acts efficiently on keratan sulfate-related glycans. *FEBS Lett.* 2004 Jan 2;556(1–3):216–20.
  45. Kitayama K, Hayashida Y, Nishida K, Akama TO. Enzymes responsible for synthesis of corneal keratan sulfate glycosaminoglycans. *J Biol Chem.* 2007 Oct 12;282(41):30085–96.
  46. Yamauchi S, Mita S, Matsubara T, Fukuta M, Habuchi H, Kimata K, et al. Molecular cloning and expression of chondroitin 4-sulfotransferase. *J Biol Chem.* 2000 Mar 24;275(12):8975–81.
  47. Hiraoka N, Nakagawa H, Ong E, Akama TO, Fukuda MN, Fukuda M. Molecular cloning and expression of two distinct human chondroitin 4-O-sulfotransferases that belong to the HNK-1 sulfotransferase gene family. *J Biol Chem.* 2000 Jun 30;275(26):20188–96.
  48. Kang H-G, Evers MR, Xia G, Baenziger JU, Schachner M. Molecular cloning and characterization of chondroitin-4-O-sulfotransferase-3. A novel member of the HNK-1 family of sulfotransferases. *J Biol Chem.* 2002 Sep 20;277(38):34766–72.
  49. Fukuta M, Uchimura K, Nakashima K, Kato M, Kimata K, Shinomura T, et al. Molecular cloning and expression of chick chondrocyte chondroitin 6-sulfotransferase. *J Biol Chem.* 1995 Aug 4;270(31):18575–80.
  50. Kobayashi M, Sugumaran G, Liu J, Shworak NW, Silbert JE, Rosenberg RD. Molecular cloning and characterization of a human uronyl 2-sulfotransferase that sulfates iduronyl

- and glucuronyl residues in dermatan/chondroitin sulfate. *J Biol Chem.* 1999 Apr 9;274(15):10474–80.
51. Maccarana M, Olander B, Malmström J, Tiedemann K, Aebersold R, Lindahl U, et al. Biosynthesis of dermatan sulfate: chondroitin-glucuronate C5-epimerase is identical to SART2. *J Biol Chem.* 2006 Apr 28;281(17):11560–8.
  52. Pacheco B, Malmström A, Maccarana M. Two dermatan sulfate epimerases form iduronic acid domains in dermatan sulfate. *J Biol Chem.* 2009 Apr 10;284(15):9788–95.
  53. Evers MR, Xia G, Kang HG, Schachner M, Baenziger JU. Molecular cloning and characterization of a dermatan-specific N-acetylgalactosamine 4-O-sulfotransferase. *J Biol Chem.* 2001 Sep 28;276(39):36344–53.
  54. Hashimoto Y, Orellana A, Gil G, Hirschberg CB. Molecular cloning and expression of rat liver N-heparan sulfate sulfotransferase. *J Biol Chem.* 1992 Aug 5;267(22):15744–50.
  55. Eriksson I, Sandbäck D, Ek B, Lindahl U, Kjellén L. cDNA cloning and sequencing of mouse mastocytoma glucosaminyl N-deacetylase/N-sulfotransferase, an enzyme involved in the biosynthesis of heparin. *J Biol Chem.* 1994 Apr 8;269(14):10438–43.
  56. Li J. Glucuronyl C5-epimerase an enzyme converting glucuronic acid to iduronic acid in heparan sulfate/heparin biosynthesis. *Prog Mol Biol Transl Sci.* 2010;93:59–78.
  57. Kobayashi M, Habuchi H, Yoneda M, Habuchi O, Kimata K. Molecular cloning and expression of Chinese hamster ovary cell heparan-sulfate 2-sulfotransferase. *J Biol Chem.* 1997 May 23;272(21):13980–5.

58. Habuchi H, Tanaka M, Habuchi O, Yoshida K, Suzuki H, Ban K, et al. The occurrence of three isoforms of heparan sulfate 6-O-sulfotransferase having different specificities for hexuronic acid adjacent to the targeted N-sulfoglucosamine. *J Biol Chem*. 2000 Jan 28;275(4):2859–68.
59. Thacker BE, Xu D, Lawrence R, Esko JD. Heparan sulfate 3-O-sulfation: A rare modification in search of a function. *Matrix Biol*. 2014 Apr;35:60–72.
60. Fukuta M, Inazawa J, Torii T, Tsuzuki K, Shimada E, Habuchi O. Molecular cloning and characterization of human keratan sulfate Gal-6-sulfotransferase. *J Biol Chem*. 1997 Dec 19;272(51):32321–8.
61. Akama TO, Nakayama J, Nishida K, Hiraoka N, Suzuki M, McAuliffe J, et al. Human corneal GlcNac 6-O-sulfotransferase and mouse intestinal GlcNac 6-O-sulfotransferase both produce keratan sulfate. *J Biol Chem*. 2001 May 11;276(19):16271–8.
62. Yarema KJ, Bertozzi CR. Characterizing glycosylation pathways. *Genome Biol*. 2001;2(5):REVIEWS0004.
63. Decker D, Kleczkowski LA. UDP-Sugar Producing Pyrophosphorylases: Distinct and Essential Enzymes With Overlapping Substrate Specificities, Providing de novo Precursors for Glycosylation Reactions. *Front Plant Sci*. 2019 Jan 4;9:1822.
64. Kleczkowski LA, Decker D, Wilczynska M. UDP-Sugar Pyrophosphorylase: A New Old Mechanism for Sugar Activation<sup>1</sup>. *Plant Physiol*. 2011 May;156(1):3–10.
65. Song Z. Roles of the nucleotide sugar transporters (SLC35 family) in health and disease. *Molecular Aspects of Medicine*. 2013 Apr 1;34(2):590–600.

66. Hirschberg CB. My journey in the discovery of nucleotide sugar transporters of the Golgi apparatus. *J Biol Chem*. 2018 Aug 17;293(33):12653–62.
67. Failer BU, Braun N, Zimmermann H. Cloning, expression, and functional characterization of a Ca(2+)-dependent endoplasmic reticulum nucleoside diphosphatase. *J Biol Chem*. 2002 Oct 4;277(40):36978–86.
68. Smith TM, Hicks-Berger CA, Kim S, Kirley TL. Cloning, expression, and characterization of a soluble calcium-activated nucleotidase, a human enzyme belonging to a new family of extracellular nucleotidases. *Arch Biochem Biophys*. 2002 Oct 1;406(1):105–15.
69. Paganini C, Monti L, Costantini R, Besio R, Lecci S, Biggiogera M, et al. Calcium activated nucleotidase 1 (CANT1) is critical for glycosaminoglycan biosynthesis in cartilage and endochondral ossification. *Matrix Biology*. 2019 Aug;81:70.
70. Fuda H, Shimizu C, Lee YC, Akita H, Strott CA. Characterization and expression of human bifunctional 3'-phosphoadenosine 5'-phosphosulphate synthase isoforms. *Biochem J*. 2002 Jul 15;365(2):497–504.
71. Kamiyama S, Sasaki N, Goda E, Ui-Tei K, Saigo K, Narimatsu H, et al. Molecular cloning and characterization of a novel 3'-phosphoadenosine 5'-phosphosulfate transporter, PAPST2. *J Biol Chem*. 2006 Apr 21;281(16):10945–53.
72. Kamiyama S, Suda T, Ueda R, Suzuki M, Okubo R, Kikuchi N, et al. Molecular cloning and identification of 3'-phosphoadenosine 5'-phosphosulfate transporter. *J Biol Chem*. 2003 Jul 11;278(28):25958–63.

73. Vissers LELM, Lausch E, Unger S, Campos-Xavier AB, Gilissen C, Rossi A, et al. Chondrodysplasia and Abnormal Joint Development Associated with Mutations in IMPAD1, Encoding the Golgi-Resident Nucleotide Phosphatase, gPAPP. *Am J Hum Genet.* 2011 May 13;88(5):608–15.
74. Kolset SO, Vuong TT, Prydz K. Apical secretion of chondroitin sulphate in polarized Madin-Darby canine kidney (MDCK) cells. *Journal of Cell Science.* 1999 Jun 1;112(11):1797–801.
75. Caplan MJ, Stow JL, Newman AP, Madri J, Anderson HC, Farquhar MG, et al. Dependence on pH of polarized sorting of secreted proteins. *Nature.* 1987 Oct 15;329(6140):632–5.
76. Mertens G, Van der Schueren B, van den Berghe H, David G. Heparan sulfate expression in polarized epithelial cells: the apical sorting of glypican (GPI-anchored proteoglycan) is inversely related to its heparan sulfate content. *J Cell Biol.* 1996 Feb;132(3):487–97.
77. Mihov D, Raja E, Spiess M. Chondroitin Sulfate Accelerates Trans-Golgi-to-Surface Transport of Proteoglycan Amyloid Precursor Protein. *Traffic.* 2015 Aug;16(8):853–70.
78. Kobialka S, Beuret N, Ben-Tekaya H, Spiess M. Glycosaminoglycan Chains Affect Exocytic and Endocytic Protein Traffic. *Traffic.* 2009 Dec 1;10(12):1845–55.
79. Biederbick A, Licht A, Kleene R. Serglycin proteoglycan is sorted into zymogen granules of rat pancreatic acinar cells. *Eur J Cell Biol.* 2003 Jan;82(1):19–29.
80. Simons K, Ikonen E. Functional rafts in cell membranes. *Nature.* 1997 Jun;387(6633):569–72.



81. Nickel W, Kipper N, Barthel A, Kahn RA, FABHAUER D, Söling H-D. ARF and VAPP14: Two Proteins Involved in the Delivery of Heparan Sulfate Proteoglycan from the trans-Golgi Network to the Plasma Membrane. *Annals of the New York Academy of Sciences*. 1994;733(1):344–56.
82. Polishchuk EV, Di Pentima A, Luini A, Polishchuk RS. Mechanism of constitutive export from the golgi: bulk flow via the formation, protrusion, and en bloc cleavage of large trans-golgi network tubular domains. *Mol Biol Cell*. 2003 Nov;14(11):4470–85.
83. Yano H, Yamamoto-Hino M, Abe M, Kuwahara R, Haraguchi S, Kusaka I, et al. Distinct functional units of the Golgi complex in *Drosophila* cells. *Proc Natl Acad Sci U S A*. 2005 Sep 20;102(38):13467–72.
84. Sasaki K, Yoshida H. Golgi stress response and organelle zones. *FEBS Letters*. 2019;593(17):2330–40.
85. Sasaki K, Yoshida H. Organelle Zones. *Cell Struct Funct*. 2019 Aug 21;44(2):85–94.
86. Vynios DH. Metabolism of Cartilage Proteoglycans in Health and Disease. *Biomed Res Int* [Internet]. 2014 [cited 2019 Nov 25];2014. Available from: <https://www.ncbi.nlm.nih.gov/pmc/articles/PMC4106107/>
87. Muenzer J. Overview of the mucopolysaccharidoses. *Rheumatology (Oxford)*. 2011 Dec 1;50(suppl\_5):v4–12.
88. Kellokumpu S. Golgi pH, Ion and Redox Homeostasis: How Much Do They Really Matter? *Frontiers in Cell and Developmental Biology*. 2019;7:93.

89. Dick G, Akslen-Hoel LK, Grøndahl F, Kjos I, Prydz K. Proteoglycan Synthesis and Golgi Organization in Polarized Epithelial Cells. *J Histochem Cytochem.* 2012 Dec;60(12):926–35.
90. Opat AS, van Vliet C, Gleeson PA. Trafficking and localisation of resident Golgi glycosylation enzymes. *Biochimie.* 2001 Aug 1;83(8):763–73.
91. Blackburn JB, D’Souza Z, Lupashin VV. Maintaining order: COG complex controls Golgi trafficking, processing, and sorting. *FEBS Lett.* 2019 Sep;593(17):2466–87.
92. Stenmark H. Rab GTPases as coordinators of vesicle traffic. *Nat Rev Mol Cell Biol.* 2009 Aug;10(8):513–25.
93. Sugumaran G, Katsman M, Silbert JE. Effects of brefeldin A on the localization of chondroitin sulfate-synthesizing enzymes. Activities in subfractions of the Golgi from chick embryo epiphyseal cartilage. *J Biol Chem.* 1992 May 5;267(13):8802–6.
94. Spiro RC, Freeze HH, Sampath D, Garcia JA. Uncoupling of chondroitin sulfate glycosaminoglycan synthesis by brefeldin A. *J Cell Biol.* 1991 Dec;115(5):1463–73.
95. Mason RM, Lancaster CA. Effects of cyclofenil diphenol, an agent which disrupts Golgi structure, on proteoglycan synthesis in chondrocytes. *Biochem J.* 1992 Jan 15;281(Pt 2):525–31.
96. Wu MM, Llopis J, Adams S, McCaffery JM, Kulomaa MS, Machen TE, et al. Organelle pH studies using targeted avidin and fluorescein-biotin. *Chem Biol.* 2000 Mar;7(3):197–209.
97. Demarex N, Furuya W, D’Souza S, Bonifacino JS, Grinstein S. Mechanism of acidification of the trans-Golgi network (TGN). In situ measurements of pH using

- retrieval of TGN38 and furin from the cell surface. *J Biol Chem*. 1998 Jan 23;273(4):2044–51.
98. Dick G, Akslen-Hoel LK, Grøndahl F, Kjos I, Prydz K. Proteoglycan Synthesis and Golgi Organization in Polarized Epithelial Cells. *J Histochem Cytochem*. 2012 Dec;60(12):926–35.
  99. Prydz K. Determinants of Glycosaminoglycan (GAG) Structure. *Biomolecules*. 2015 Aug 21;5(3):2003–22.
  100. Grøndahl F, Tveit H, Prydz K. Neutralization of endomembrane compartments in epithelial MDCK cells affects proteoglycan synthesis in the apical secretory pathway. *Biochemical Journal*. 2009 Mar 15;418(3):517–28.
  101. Marshansky V, Rubinstein JL, Grüber G. Eukaryotic V-ATPase: Novel structural findings and functional insights. *Biochimica et Biophysica Acta (BBA) - Bioenergetics*. 2014 Jun 1;1837(6):857–79.
  102. Maeda Y, Ide T, Koike M, Uchiyama Y, Kinoshita T. GPHR is a novel anion channel critical for acidification and functions of the Golgi apparatus. *Nat Cell Biol*. 2008 Oct;10(10):1135–45.
  103. Kornak U, Reynders E, Dimopoulou A, van Reeuwijk J, Fischer B, Rajab A, et al. Impaired glycosylation and cutis laxa caused by mutations in the vesicular H<sup>+</sup>-ATPase subunit ATP6V0A2. *Nat Genet*. 2008 Jan;40(1):32–4.
  104. Jansen EJR, Timal S, Ryan M, Ashikov A, van Scherpenzeel M, Graham LA, et al. ATP6AP1 deficiency causes an immunodeficiency with hepatopathy, cognitive impairment and abnormal protein glycosylation. *Nat Commun*. 2016 27;7:11600.

105. Jansen JC, Cirak S, van Scherpenzeel M, Timal S, Reunert J, Rust S, et al. *CCDC115 Deficiency Causes a Disorder of Golgi Homeostasis with Abnormal Protein Glycosylation*. *Am J Hum Genet*. 2016 Feb 4;98(2):310–21.
106. Spiro RC, Parsons WG, Perry SK, Caulfield JP, Hein A, Reisfeld RA, et al. *Inhibition of post-translational modification and surface expression of a melanoma-associated chondroitin sulfate proteoglycan by diethylcarbamazine or ammonium chloride*. *Journal of Biological Chemistry*. 1986 Apr 15;261(11):5121–9.
107. Vadaie N, Hulinsky RS, Jarvis DL. *Identification and characterization of a Drosophila melanogaster ortholog of human beta1,4-galactosyltransferase VII*. *Glycobiology*. 2002 Oct;12(10):589–97.
108. Liu AC-H, Heinrichs BS, Leach RM. *Influence of Manganese Deficiency on the Characteristics of Proteoglycans of Avian Epiphyseal Growth Plate Cartilage*. *Poultry Science*. 1994 May 1;73(5):663–9.
109. Bouakka M, Legendre P, Jouis V, Langris M, Béliard R, Loyau G, et al. *Calcium ionophore and phorbol myristate acetate synergistically inhibited proteoglycan biosynthesis in articular chondrocytes by prostaglandin independent mechanism*. *Biochem Biophys Res Commun*. 1988 Jun 16;153(2):690–8.
110. Takeuchi Y, Sakaguchi K, Yanagishita M, Aurbach GD, Hascall VC. *Extracellular calcium regulates distribution and transport of heparan sulfate proteoglycans in a rat parathyroid cell line*. *J Biol Chem*. 1990 Aug 15;265(23):13661–8.
111. Kolset SO, Tveit H. *Serglycin – Structure and biology*. *Cell Mol Life Sci*. 2008 Apr 1;65(7):1073–85.

112. Alexopoulou AN, Multhaupt HAB, Couchman JR. Syndecans in wound healing, inflammation and vascular biology. *The International Journal of Biochemistry & Cell Biology*. 2007 Jan 1;39(3):505–28.
113. De Rossi G, Evans AR, Kay E, Woodfin A, McKay TR, Nourshargh S, et al. Shed syndecan-2 inhibits angiogenesis. *J Cell Sci*. 2014 Nov 1;127(Pt 21):4788–99.
114. Song HH, Filmus J. The role of glypicans in mammalian development. *Biochimica et Biophysica Acta (BBA) - General Subjects*. 2002 Dec 19;1573(3):241–6.
115. Filmus J. Glypicans in growth control and cancer. *Glycobiology*. 2001 Mar 1;11(3):19R-23R.
116. Xian X, Gopal S, Couchman JR. Syndecans as receptors and organizers of the extracellular matrix. *Cell Tissue Res*. 2010 Jan;339(1):31–46.
117. Choi Y, Chung H, Jung H, Couchman JR, Oh E-S. Syndecans as cell surface receptors: Unique structure equates with functional diversity. *Matrix Biol*. 2011 Mar;30(2):93–9.
118. Lord MS, Tang F, Rnjak-Kovacina J, Smith JGW, Melrose J, Whitelock JM. The multifaceted roles of perlecan in fibrosis. *Matrix Biol*. 2018 Aug;68–69:150–66.
119. Kiani C, Chen L, Wu YJ, Yee AJ, Yang BB. Structure and function of aggrecan. *Cell Res*. 2002 Mar;12(1):19–32.
120. Ye Y, Hu W, Guo F, Zhang W, Wang J, Chen A. Glycosaminoglycan chains of biglycan promote bone morphogenetic protein-4-induced osteoblast differentiation. *Int J Mol Med*. 2012 Nov;30(5):1075–80.

121. Reed CC, Iozzo RV. The role of decorin in collagen fibrillogenesis and skin homeostasis. *Glycoconj J*. 2002 Jun;19(4–5):249–55.
122. Nikitovic D, Aggelidakis J, Young MF, Iozzo RV, Karamanos NK, Tzanakakis GN. The Biology of Small Leucine-rich Proteoglycans in Bone Pathophysiology. *J Biol Chem*. 2012 Oct 5;287(41):33926–33.
123. Takeuchi Y, Kodama Y, Matsumoto T. Bone matrix decorin binds transforming growth factor-beta and enhances its bioactivity. *J Biol Chem*. 1994 Dec 23;269(51):32634–8.
124. Riquelme C, Larrain J, Schonherr E, Henriquez JP, Kresse H, Brandan E. Antisense inhibition of decorin expression in myoblasts decreases cell responsiveness to transforming growth factor beta and accelerates skeletal muscle differentiation. *J Biol Chem*. 2001 Feb 2;276(5):3589–96.
125. Kali A, Shetty KSR. Endocan: A novel circulating proteoglycan. *Indian J Pharmacol*. 2014;46(6):579–83.
126. Pacifici M, Shimo T, Gentili C, Kirsch T, Freeman TA, Enomoto-Iwamoto M, et al. Syndecan-3: a cell-surface heparan sulfate proteoglycan important for chondrocyte proliferation and function during limb skeletogenesis. *J Bone Miner Metab*. 2005;23(3):191–9.
127. Fawcett JW, Oohashi T, Pizzorusso T. The roles of perineuronal nets and the perinodal extracellular matrix in neuronal function. *Nat Rev Neurosci*. 2019 Aug;20(8):451–65.
128. Jan AT, Lee EJ, Choi I. Fibromodulin: A regulatory molecule maintaining cellular architecture for normal cellular function. *The International Journal of Biochemistry & Cell Biology*. 2016 Nov 1;80:66–70.

129. Rühland C, Schönherr E, Robenek H, Hansen U, Iozzo RV, Bruckner P, et al. The glycosaminoglycan chain of decorin plays an important role in collagen fibril formation at the early stages of fibrillogenesis. *FEBS J.* 2007 Aug;274(16):4246–55.
130. Csordás G, Santra M, Reed CC, Eichstetter I, McQuillan DJ, Gross D, et al. Sustained down-regulation of the epidermal growth factor receptor by decorin. A mechanism for controlling tumor growth in vivo. *J Biol Chem.* 2000 Oct 20;275(42):32879–87.
131. Kram V, Shainer R, Jani P, Meester JAN, Loeys B, Young MF. Biglycan in the Skeleton. *J Histochem Cytochem.* 2020 Nov 1;68(11):747–62.
132. Seppinen L, Pihlajaniemi T. The multiple functions of collagen XVIII in development and disease. *Matrix Biology.* 2011 Mar 1;30(2):83–92.
133. Izu Y, Sun M, Zwolanek D, Veit G, Williams V, Cha B, et al. Type XII collagen regulates osteoblast polarity and communication during bone formation. *J Cell Biol.* 2011 Jun 13;193(6):1115–30.
134. McNeill EP, Zeitouni S, Pan S, Haskell A, Cesarek M, Tahan D, et al. Characterization of a pluripotent stem cell-derived matrix with powerful osteoregenerative capabilities. *Nat Commun.* 2020 Jun 15;11:3025.
135. Izu Y, Adams SM, Connizzo BK, Beason DP, Soslowsky LJ, Koch M, et al. Collagen XII mediated cellular and extracellular mechanisms regulate establishment of tendon structure and function. *Matrix Biol.* 2021 Jan;95:52–67.
136. Melrose J. Perlecan, a modular instructive proteoglycan with diverse functional properties. *The International Journal of Biochemistry & Cell Biology.* 2020 Nov 1;128:105849.

137. Lord MS, Melrose J, Day AJ, Whitelock JM. The Inter- $\alpha$ -Trypsin Inhibitor Family: Versatile Molecules in Biology and Pathology. *J Histochem Cytochem.* 2020 Dec 1;68(12):907–27.
138. Partenheimer A, Schwarz K, Wrocklage C, Kölsch E, Kresse H. Proteoglycan form of colony-stimulating factor-1 (proteoglycan-100). Stimulation of activity by glycosaminoglycan removal and proteolytic processing. *The Journal of Immunology.* 1995 Dec 15;155(12):5557–65.
139. Chang MY, Olin KL, Tsoi C, Wight TN, Chait A. Human monocyte-derived macrophages secrete two forms of proteoglycan-macrophage colony-stimulating factor that differ in their ability to bind low density lipoproteins. *J Biol Chem.* 1998 Jun 26;273(26):15985–92.
140. Lamant M, Smih F, Harmancey R, Philip-Couderc P, Pathak A, Roncalli J, et al. ApoO, a novel apolipoprotein, is an original glycoprotein up-regulated by diabetes in human heart. *J Biol Chem.* 2006 Nov 24;281(47):36289–302.
141. Weijler AM, Schmidinger B, Kapiotis S, Laggner H, Hermann M. Oleic acid induces the novel apolipoprotein O and reduces mitochondrial membrane potential in chicken and human hepatoma cells. *Biochimie.* 2018 Apr 1;147:136–42.
142. Bui C, Huber C, Tuysuz B, Alanay Y, Bole-Feysot C, Leroy JG, et al. XYLT1 Mutations in Desbuquois Dysplasia Type 2. *The American Journal of Human Genetics.* 2014 Mar 6;94(3):405–14.
143. Munns CF, Fahiminiya S, Poudel N, Munteanu MC, Majewski J, Sillence DO, et al. Homozygosity for frameshift mutations in XYLT2 result in a spondylo-ocular syndrome



- with bone fragility, cataracts, and hearing defects. *Am J Hum Genet.* 2015 Jun 4;96(6):971–8.
144. Malfait F, Kariminejad A, Van Damme T, Gauche C, Syx D, Merhi-Soussi F, et al. Defective Initiation of Glycosaminoglycan Synthesis due to B3GALT6 Mutations Causes a Pleiotropic Ehlers-Danlos-Syndrome-like Connective Tissue Disorder. *Am J Hum Genet.* 2013 Jun 6;92(6):935–45.
145. Baasanjav S, Al-Gazali L, Hashiguchi T, Mizumoto S, Fischer B, Horn D, et al. Faulty Initiation of Proteoglycan Synthesis Causes Cardiac and Joint Defects. *Am J Hum Genet.* 2011 Jul 15;89(1):15–27.
146. Kuroda Y, Murakami H, Enomoto Y, Tsurusaki Y, Takahashi K, Mitsuzuka K, et al. A novel gene (FAM20B encoding glycosaminoglycan xylosylkinase) for neonatal short limb dysplasia resembling Desbuquois dysplasia. *Clinical Genetics.* 2019;95(6):713–7.
147. Vodopituz J, Mizumoto S, Lausch E, Rossi A, Unger S, Janocha N, et al. Chondroitin Sulfate N-acetylgalactosaminyltransferase-1 (CSGalNAcT-1) Deficiency Results in a Mild Skeletal Dysplasia and Joint Laxity. *Hum Mutat.* 2017;38(1):34–8.
148. Li Y, Laue K, Temtamy S, Aglan M, Kotan LD, Yigit G, et al. Temtamy preaxial brachydactyly syndrome is caused by loss-of-function mutations in chondroitin synthase 1, a potential target of BMP signaling. *Am J Hum Genet.* 2010 Dec 10;87(6):757–67.
149. Volpi S, Yamazaki Y, Brauer PM, van Rooijen E, Hayashida A, Slavotinek A, et al. EXTL3 mutations cause skeletal dysplasia, immune deficiency, and developmental delay. *J Exp Med.* 2017 Mar 6;214(3):623–37.

150. Ahn J, Lüdecke HJ, Lindow S, Horton WA, Lee B, Wagner MJ, et al. Cloning of the putative tumour suppressor gene for hereditary multiple exostoses (EXT1). *Nat Genet.* 1995 Oct;11(2):137–43.
151. Stickens D, Clines G, Burbee D, Ramos P, Thomas S, Hogue D, et al. The EXT2 multiple exostoses gene defines a family of putative tumour suppressor genes. *Nat Genet.* 1996 Sep;14(1):25–32.
152. Müller T, Mizumoto S, Suresh I, Komatsu Y, Vodopiutz J, Dunder M, et al. Loss of dermatan sulfate epimerase (DSE) function results in musculocontractural Ehlers–Danlos syndrome. *Hum Mol Genet.* 2013 Sep 15;22(18):3761–72.
153. Superti-Furga A, Hästbacka J, Wilcox WR, Cohn DH, van der Harten HJ, Rossi A, et al. Achondrogenesis type IB is caused by mutations in the diastrophic dysplasia sulphate transporter gene. *Nat Genet.* 1996 Jan;12(1):100–2.
154. Hästbacka J, Superti-Furga A, Wilcox WR, Rimoin DL, Cohn DH, Lander ES. Atelosteogenesis type II is caused by mutations in the diastrophic dysplasia sulfate-transporter gene (DTDST): evidence for a phenotypic series involving three chondrodysplasias. *Am J Hum Genet.* 1996 Feb;58(2):255–62.
155. Rossi A, Superti-Furga A. Mutations in the diastrophic dysplasia sulfate transporter (DTDST) gene (SLC26A2): 22 novel mutations, mutation review, associated skeletal phenotypes, and diagnostic relevance. *Hum Mutat.* 2001 Mar;17(3):159–71.
156. Thiele H, Sakano M, Kitagawa H, Sugahara K, Rajab A, Höhne W, et al. Loss of chondroitin 6-O-sulfotransferase-1 function results in severe human chondrodysplasia with progressive spinal involvement. *Proc Natl Acad Sci U S A.* 2004 Jul 6;101(27):10155–60.

157. Akama TO, Nishida K, Nakayama J, Watanabe H, Ozaki K, Nakamura T, et al. Macular corneal dystrophy type I and type II are caused by distinct mutations in a new sulphotransferase gene. *Nat Genet.* 2000 Oct;26(2):237–41.
158. Guo Y, Zhou Y, Yan S, Qu C, Wang L, Guo X, et al. Decreased Expression of CHST-12, CHST-13, and UST in the Proximal Interphalangeal Joint Cartilage of School-Age Children with Kashin-Beck Disease: an Endemic Osteoarthritis in China Caused by Selenium Deficiency. *Biol Trace Elem Res.* 2019 Oct;191(2):276–85.
159. Dündar M, Müller T, Zhang Q, Pan J, Steinmann B, Vodopiutz J, et al. Loss of dermatan-4-sulfotransferase 1 function results in adducted thumb-clubfoot syndrome. *Am J Hum Genet.* 2009 Dec;85(6):873–82.
160. Miyake N, Kosho T, Mizumoto S, Furuichi T, Hatamochi A, Nagashima Y, et al. Loss-of-function mutations of CHST14 in a new type of Ehlers-Danlos syndrome. *Human Mutation.* 2010;31(8):966–74.
161. Haque MF ul, King LM, Krakow D, Cantor RM, Rusiniak ME, Swank RT, et al. Mutations in orthologous genes in human spondyloepimetaphyseal dysplasia and the brachymorphic mouse. *Nature Genetics.* 1998 Oct;20(2):157–62.
162. Miyake N, Elcioglu NH, Iida A, Isguven P, Dai J, Murakami N, et al. PAPSS2 mutations cause autosomal recessive brachyolmia. *J Med Genet.* 2012 Aug;49(8):533–8.
163. Oostdijk W, Idkowiak J, Mueller JW, House PJ, Taylor AE, O'Reilly MW, et al. PAPSS2 deficiency causes androgen excess via impaired DHEA sulfation--in vitro and in vivo studies in a family harboring two novel PAPSS2 mutations. *J Clin Endocrinol Metab.* 2015 Apr;100(4):E672-680.

164. Nizon M, Alanay Y, Tuysuz B, Kiper POS, Geneviève D, Sillence D, et al. IMPAD1 mutations in two Catel-Manzke like patients. *American Journal of Medical Genetics Part A*. 2012;158A(9):2183–7.
165. Furuichi T, Kayserili H, Hiraoka S, Nishimura G, Ohashi H, Alanay Y, et al. Identification of loss-of-function mutations of SLC35D1 in patients with Schneckenbecken dysplasia, but not with other severe spondylodysplastic dysplasias group diseases. *J Med Genet*. 2009 Aug;46(8):562–8.
166. Hiraoka S, Furuichi T, Nishimura G, Shibata S, Yanagishita M, Rimoin DL, et al. Nucleotide-sugar transporter SLC35D1 is critical to chondroitin sulfate synthesis in cartilage and skeletal development in mouse and human. *Nat Med*. 2007 Nov;13(11):1363–7.
167. Edvardson S, Ashikov A, J alas C, Sturiale L, Shaag A, Fedick A, et al. Mutations in SLC35A3 cause autism spectrum disorder, epilepsy and arthrogyriposis. *J Med Genet*. 2013 Nov;50(11):733–9.
168. Ng BG, Buckingham KJ, Raymond K, Kircher M, Turner EH, He M, et al. Mosaicism of the UDP-Galactose Transporter SLC35A2 Causes a Congenital Disorder of Glycosylation. *Am J Hum Genet*. 2013 Apr 4;92(4):632–6.
169. Ng BG, Sosicka P, Agadi S, Almannai M, Bacino CA, Barone R, et al. SLC35A2-CDG: Functional Characterization, Expanded Molecular, Clinical, and Biochemical Phenotypes of 30 Unreported Individuals. *Hum Mutat*. 2019 Feb 28;
170. Huber C, Oulès B, Bertoli M, Chami M, Fradin M, Alanay Y, et al. Identification of CANT1 Mutations in Desbuquois Dysplasia. *American Journal of Human Genetics*. 2009 Nov 13;85(5):706.

171. Faden M, Al-Zahrani F, Arafah D, Alkuraya FS. Mutation of CANT1 causes Desbuquois dysplasia. *Am J Med Genet A*. 2010 May;152A(5):1157–60.
172. Dai J, Kim O-H, Cho T-J, Miyake N, Song H-R, Karasugi T, et al. A founder mutation of CANT1 common in Korean and Japanese Desbuquois dysplasia. *J Hum Genet*. 2011 May;56(5):398–400.
173. Furuichi T, Dai J, Cho T-J, Sakazume S, Ikema M, Matsui Y, et al. CANT1 mutation is also responsible for Desbuquois dysplasia, type 2 and Kim variant. *J Med Genet*. 2011 Jan;48(1):32–7.
174. Nizon M, Huber C, De Leonardis F, Merrina R, Forlino A, Fradin M, et al. Further Delineation of CANT1 Phenotypic Spectrum and Demonstration of Its Role in Proteoglycan Synthesis. *Hum Mutat*. 2012 Aug;33(8):1261–6.
175. Foulquier F, Amyere M, Jaeken J, Zeevaert R, Schollen E, Race V, et al. TMEM165 Deficiency Causes a Congenital Disorder of Glycosylation. *Am J Hum Genet*. 2012 Jul 13;91(1):15–26.
176. Ferreira CR, Xia Z-J, Clément A, Parry DA, Davids M, Taylan F, et al. A Recurrent De Novo Heterozygous COG4 Substitution Leads to Saul-Wilson Syndrome, Disrupted Vesicular Trafficking, and Altered Proteoglycan Glycosylation. *Am J Hum Genet*. 2018 Oct 4;103(4):553–67.
177. Laugel-Haushalter V, Bär S, Schaefer E, Stoetzel C, Geoffroy V, Alembik Y, et al. A New SLC10A7 Homozygous Missense Mutation Responsible for a Milder Phenotype of Skeletal Dysplasia With Amelogenesis Imperfecta. *Front Genet*. 2019;10:504.

178. Dubail J, Huber C, Chantepie S, Sonntag S, Tüysüz B, Mihci E, et al. SLC10A7 mutations cause a skeletal dysplasia with amelogenesis imperfecta mediated by GAG biosynthesis defects. *Nat Commun* [Internet]. 2018 Aug 6 [cited 2020 May 10];9. Available from: <https://www.ncbi.nlm.nih.gov/pmc/articles/PMC6078967/>
179. Rajab A, Kornak U, Budde BS, Hoffmann K, Jaeken J, Nürnberg P, et al. Geroderma osteodysplasticum hereditaria and wrinkly skin syndrome in 22 patients from Oman. *Am J Med Genet A*. 2008 Apr 15;146A(8):965–76.
180. Guo L, Elcioglu NH, Iida A, Demirkol YK, Aras S, Matsumoto N, et al. Novel and recurrent XYLT1 mutations in two Turkish families with Desbuquois dysplasia, type 2. *J Hum Genet*. 2017 Mar;62(3):447–51.
181. Schreml J, Durmaz B, Cogulu O, Keupp K, Beleggia F, Pohl E, et al. The missing “link”: an autosomal recessive short stature syndrome caused by a hypofunctional XYLT1 mutation. *Hum Genet*. 2014 Jan 1;133(1):29–39.
182. Munns CF, Fahiminiya S, Poudel N, Munteanu MC, Majewski J, Silience DO, et al. Homozygosity for Frameshift Mutations in XYLT2 Result in a Spondylo-Ocular Syndrome with Bone Fragility, Cataracts, and Hearing Defects. *The American Journal of Human Genetics*. 2015 Jun 4;96(6):971–8.
183. Taylan F, Mäkitie O. Abnormal Proteoglycan Synthesis Due to Gene Defects Causes Skeletal Diseases with Overlapping Phenotypes. *Horm Metab Res*. 2016 Nov;48(11):745–54.
184. Taylan F, Costantini A, Coles N, Pekkinen M, Héon E, Şıklar Z, et al. Spondyloocular Syndrome: Novel Mutations in XYLT2 Gene and Expansion of the Phenotypic Spectrum. *Journal of Bone and Mineral Research*. 2016;31(8):1577–85.

185. Kausar M, Chew EGY, Ullah H, Anees M, Khor CC, Foo JN, et al. A Novel Homozygous Frameshift Variant in XYLT2 Causes Spondyloocular Syndrome in a Consanguineous Pakistani Family. *Front Genet* [Internet]. 2019 [cited 2020 Apr 10];10. Available from: <https://www.frontiersin.org/articles/10.3389/fgene.2019.00144/full>
186. Umair M, Eckstein G, Rudolph G, Strom T, Graf E, Hendig D, et al. Homozygous XYLT2 variants as a cause of spondyloocular syndrome. *Clin Genet*. 2018 Apr;93(4):913–8.
187. Okajima T, Yoshida K, Kondo T, Furukawa K. Human homolog of *Caenorhabditis elegans* sqv-3 gene is galactosyltransferase I involved in the biosynthesis of the glycosaminoglycan-protein linkage region of proteoglycans. *J Biol Chem*. 1999 Aug 13;274(33):22915–8.
188. Guo MH, Stoler J, Lui J, Nilsson O, Bianchi DW, Hirschhorn JN, et al. Redefining the progeroid form of Ehlers-Danlos syndrome: report of the fourth patient with B4GALT7 deficiency and review of the literature. *Am J Med Genet A*. 2013 Oct;161A(10):2519–27.
189. Salter CG, Davies JH, Moon RJ, Fairhurst J, Bunyan D, DDD Study, et al. Further defining the phenotypic spectrum of B4GALT7 mutations. *Am J Med Genet A*. 2016;170(6):1556–63.
190. Ritelli M, Dordoni C, Cinquina V, Venturini M, Calzavara-Pinton P, Colombi M. Expanding the clinical and mutational spectrum of B4GALT7-spondylodysplastic Ehlers-Danlos syndrome. *Orphanet J Rare Dis*. 2017 Sep 7;12(1):153.

191. Quentin E, Gladen A, Rodén L, Kresse H. A genetic defect in the biosynthesis of dermatan sulfate proteoglycan: galactosyltransferase I deficiency in fibroblasts from a patient with a progeroid syndrome. *Proc Natl Acad Sci U S A*. 1990 Feb;87(4):1342–6.
192. Seidler DG, Faiyaz-Ul-Haque M, Hansen U, Yip GW, Zaidi SHE, Teebi AS, et al. Defective glycosylation of decorin and biglycan, altered collagen structure, and abnormal phenotype of the skin fibroblasts of an Ehlers–Danlos syndrome patient carrying the novel Arg270Cys substitution in galactosyltransferase I ( $\beta$ 4GalT-7). *J Mol Med*. 2006 Jul 1;84(7):583–94.
193. Götte M, Spillmann D, Yip GW, Versteeg E, Echtermeyer FG, van Kuppevelt TH, et al. Changes in heparan sulfate are associated with delayed wound repair, altered cell migration, adhesion and contractility in the galactosyltransferase I ( $\beta$ 4GalT-7) deficient form of Ehlers-Danlos syndrome. *Hum Mol Genet*. 2008 Apr 1;17(7):996–1009.
194. Delbaere S, De Clercq A, Mizumoto S, Noborn F, Bek JW, Alluyn L, et al.  $\beta$ 3galT6 Knock-Out Zebrafish Recapitulate  $\beta$ 3GalT6-Deficiency Disorders in Human and Reveal a Trisaccharide Proteoglycan Linkage Region. *Front Cell Dev Biol*. 2020;8:597857.
195. Nakajima M, Mizumoto S, Miyake N, Kogawa R, Iida A, Ito H, et al. Mutations in B3GALT6, which Encodes a Glycosaminoglycan Linker Region Enzyme, Cause a Spectrum of Skeletal and Connective Tissue Disorders. *Am J Hum Genet*. 2013 Jun 6;92(6):927–34.
196. Ritelli M, Chiarelli N, Zoppi N, Dordoni C, Quinzani S, Traversa M, et al. Insights in the etiopathology of galactosyltransferase II (GalT-II) deficiency from transcriptome-wide



- expression profiling of skin fibroblasts of two sisters with compound heterozygosity for two novel B3GALT6 mutations. *Mol Genet Metab Rep*. 2015 Mar;2:1–15.
197. Ritelli M, Cinquina V, Giacomuzzi E, Venturini M, Chiarelli N, Colombi M. Further Defining the Phenotypic Spectrum of B3GAT3 Mutations and Literature Review on Linkeropathy Syndromes. *Genes*. 2019 Sep;10(9):631.
198. Byrne AB, Mizumoto S, Arts P, Yap P, Feng J, Schreiber AW, et al. Pseudodiastrophic dysplasia expands the known phenotypic spectrum of defects in proteoglycan biosynthesis. *J Med Genet*. 2020 Jul;57(7):454–60.
199. Budde BS, Mizumoto S, Kogawa R, Becker C, Altmüller J, Thiele H, et al. Skeletal dysplasia in a consanguineous clan from the island of Nias/Indonesia is caused by a novel mutation in B3GAT3. *Hum Genet*. 2015 Jul;134(7):691–704.
200. Ma P, Yan W, Tian Y, Wang J, Feng JQ, Qin C, et al. Inactivation of Fam20B in Joint Cartilage Leads to Chondrosarcoma and Postnatal Ossification Defects. *Sci Rep* [Internet]. 2016 Jul 13 [cited 2020 Apr 11];6. Available from: <https://www.ncbi.nlm.nih.gov/pmc/articles/PMC4942823/>
201. Mizumoto S, Janecke AR, Sadeghpour A, Povysil G, McDonald MT, Unger S, et al. CSGALNACT1-congenital disorder of glycosylation: A mild skeletal dysplasia with advanced bone age. *Hum Mutat*. 2020 Mar;41(3):655–67.
202. Watanabe Y, Takeuchi K, Higa Onaga S, Sato M, Tsujita M, Abe M, et al. Chondroitin sulfate N-acetylgalactosaminyltransferase-1 is required for normal cartilage development. *Biochem J*. 2010 Nov 15;432(1):47–55.

203. Tian J, Ling L, Shboul M, Lee H, O'Connor B, Merriman B, et al. Loss of CHSY1, a Secreted FRINGE Enzyme, Causes Syndromic Brachydactyly in Humans via Increased NOTCH Signaling. *Am J Hum Genet.* 2010 Dec 10;87(6):768–78.
204. Sher G, Naeem M. A novel CHSY1 gene mutation underlies Temtamy preaxial brachydactyly syndrome in a Pakistani family. *European Journal of Medical Genetics.* 2014 Jan 1;57(1):21–4.
205. Oud MM, Tuijnenburg P, Hempel M, van Vlies N, Ren Z, Ferdinandusse S, et al. Mutations in EXTL3 Cause Neuro-immuno-skeletal Dysplasia Syndrome. *Am J Hum Genet.* 2017 Feb 2;100(2):281–96.
206. Oud MM, Tuijnenburg P, Hempel M, van Vlies N, Ren Z, Ferdinandusse S, et al. Mutations in EXTL3 Cause Neuro-immuno-skeletal Dysplasia Syndrome. *The American Journal of Human Genetics.* 2017 Feb 2;100(2):281–96.
207. Wuyts W, Van Hul W. Molecular basis of multiple exostoses: mutations in the EXT1 and EXT2 genes. *Hum Mutat.* 2000;15(3):220–7.
208. Anower-E-Khuda MdF, Matsumoto K, Habuchi H, Morita H, Yokochi T, Shimizu K, et al. Glycosaminoglycans in the blood of hereditary multiple exostoses patients: Half reduction of heparan sulfate to chondroitin sulfate ratio and the possible diagnostic application. *Glycobiology.* 2013 Jul 1;23(7):865–76.
209. Trebicz-Geffen M, Robinson D, Evron Z, Glaser T, Fridkin M, Kollander Y, et al. The molecular and cellular basis of exostosis formation in hereditary multiple exostoses. *Int J Exp Pathol.* 2008 Oct;89(5):321–31.

210. Pacifici M. The pathogenic roles of heparan sulfate deficiency in hereditary multiple exostoses. *Matrix Biol.* 2018;71–72:28–39.
211. Bovée JVMG. Multiple osteochondromas. *Orphanet J Rare Dis.* 2008 Feb 13;3:3.
212. Müller T, Mizumoto S, Suresh I, Komatsu Y, Vodopiutz J, Dunder M, et al. Loss of dermatan sulfate epimerase (DSE) function results in musculocontractural Ehlers–Danlos syndrome. *Human Molecular Genetics.* 2013 Sep 15;22(18):3761–72.
213. Syx D, Van Damme T, Symoens S, Maiburg MC, van de Laar I, Morton J, et al. Genetic heterogeneity and clinical variability in musculocontractural Ehlers-Danlos syndrome caused by impaired dermatan sulfate biosynthesis. *Hum Mutat.* 2015 May;36(5):535–47.
214. Villena J, Brandan E. Dermatan sulfate exerts an enhanced growth factor response on skeletal muscle satellite cell proliferation and migration. *J Cell Physiol.* 2004 Feb;198(2):169–78.
215. Soares da Costa D, Reis RL, Pashkuleva I. Sulfation of Glycosaminoglycans and Its Implications in Human Health and Disorders. *Annu Rev Biomed Eng.* 2017 Jun 21;19:1–26.
216. Unger S, Lausch E, Rossi A, Mégarbané A, Sillence D, Alcausin M, et al. Phenotypic features of carbohydrate sulfotransferase 3 (CHST3) deficiency in 24 patients: congenital dislocations and vertebral changes as principal diagnostic features. *Am J Med Genet A.* 2010 Oct;152A(10):2543–9.
217. Hermanns P, Unger S, Rossi A, Perez-Aytes A, Cortina H, Bonafé L, et al. Congenital joint dislocations caused by carbohydrate sulfotransferase 3 deficiency in recessive

- Larsen syndrome and humero-spinal dysostosis. *Am J Hum Genet.* 2008 Jun;82(6):1368–74.
218. Malfait F, Syx D, Vlummens P, Symoens S, Nampoothiri S, Hermanns-Lê T, et al. Musculocontractural Ehlers-Danlos Syndrome (former EDS type VIB) and adducted thumb clubfoot syndrome (ATCS) represent a single clinical entity caused by mutations in the dermatan-4-sulfotransferase 1 encoding CHST14 gene. *Hum Mutat.* 2010 Nov;31(11):1233–9.
219. Dündar M, Müller T, Zhang Q, Pan J, Steinmann B, Vodopiutz J, et al. Loss of Dermatan-4-Sulfotransferase 1 Function Results in Adducted Thumb-Clubfoot Syndrome. *Am J Hum Genet.* 2009 Dec 11;85(6):873–82.
220. Kosho T. CHST14/D4ST1 deficiency: New form of Ehlers–Danlos syndrome. *Pediatrics International.* 2016;58(2):88–99.
221. Hästbacka J, de la Chapelle A, Mahtani MM, Clines G, Reeve-Daly MP, Daly M, et al. The diastrophic dysplasia gene encodes a novel sulfate transporter: positional cloning by fine-structure linkage disequilibrium mapping. *Cell.* 1994 Sep 23;78(6):1073–87.
222. Rossi A, Kaitila I, Wilcox WR, Rimoin DL, Steinmann B, Cetta G, et al. Proteoglycan sulfation in cartilage and cell cultures from patients with sulfate transporter chondrodysplasias: relationship to clinical severity and indications on the role of intracellular sulfate production. *Matrix Biol.* 1998 Oct;17(5):361–9.
223. Noordam C, Dhir V, McNelis JC, Schlereth F, Hanley NA, Krone N, et al. Inactivating PAPSS2 mutations in a patient with premature pubarche. *N Engl J Med.* 2009 May 28;360(22):2310–8.

224. Sugahara K, Schwartz NB. Defect in 3'-phosphoadenosine 5'-phosphosulfate formation in brachymorphic mice. *Proc Natl Acad Sci U S A*. 1979 Dec;76(12):6615–8.
225. Sohaskey ML, Yu J, Diaz MA, Plaas AH, Harland RM. JAWS coordinates chondrogenesis and synovial joint positioning. *Development*. 2008 Jul;135(13):2215–20.
226. Frederick JP, Tafari AT, Wu S-M, Megosh LC, Chiou S-T, Irving RP, et al. A role for a lithium-inhibited Golgi nucleotidase in skeletal development and sulfation. *Proc Natl Acad Sci USA*. 2008 Aug 19;105(33):11605–12.
227. Rautengarten C, Quarrell OW, Stals K, Caswell RC, De Franco E, Baple E, et al. A hypomorphic allele of SLC35D1 results in Schneckenbecken-like dysplasia. *Hum Mol Genet*. 2019 Nov 1;28(21):3543–51.
228. Furuichi T, Kayserili H, Hiraoka S, Nishimura G, Ohashi H, Alanay Y, et al. Identification of loss-of-function mutations of SLC35D1 in patients with Schneckenbecken dysplasia, but not with other severe spondylodysplastic dysplasias group diseases. *J Med Genet*. 2009 Aug;46(8):562–8.
229. Borochowitz Z, Jones KL, Silbey R, Adomian G, Lachman R, Rimoin DL. A distinct lethal neonatal chondrodysplasia with snail-like pelvis: Schneckenbecken dysplasia. *Am J Med Genet*. 1986 Sep;25(1):47–59.
230. Edmondson AC, Bedoukian EC, Deardorff MA, McDonald-McGinn DM, Li X, He M, et al. A human case of SLC35A3-related skeletal dysplasia. *American Journal of Medical Genetics Part A*. 2017;173(10):2758–62.

231. Marini C, Hardies K, Pisano T, May P, Weckhuysen S, Cellini E, et al. Recessive mutations in SLC35A3 cause early onset epileptic encephalopathy with skeletal defects. *Am J Med Genet A*. 2017 Apr;173(4):1119–23.
232. Maszczak-Seneczko D, Sosicka P, Olczak T, Jakimowicz P, Majkowski M, Olczak M. UDP-N-acetylglucosamine transporter (SLC35A3) regulates biosynthesis of highly branched N-glycans and keratan sulfate. *J Biol Chem*. 2013 Jul 26;288(30):21850–60.
233. Ng BG, Sosicka P, Agadi S, Almannai M, Bacino CA, Barone R, et al. SLC35A2-CDG: Functional characterization, expanded molecular, clinical, and biochemical phenotypes of 30 unreported Individuals. *Hum Mutat*. 2019;40(7):908–25.
234. Yates TM, Suri M, Desurkar A, Lesca G, Wallgren-Pettersson C, Hammer TB, et al. SLC35A2-related congenital disorder of glycosylation: Defining the phenotype. *Eur J Paediatr Neurol*. 2018 Nov;22(6):1095–102.
235. Toma L, Pinhal MAS, Dietrich CP, Nader HB, Hirschberg CB. Transport of UDP-Galactose into the Golgi Lumen Regulates the Biosynthesis of Proteoglycans. *J Biol Chem*. 1996 Feb 16;271(7):3897–901.
236. Maszczak-Seneczko D, Olczak T, Wunderlich L, Olczak M. Comparative analysis of involvement of UGT1 and UGT2 splice variants of UDP-galactose transporter in glycosylation of macromolecules in MDCK and CHO cell lines. *Glycoconj J*. 2011 Oct;28(7):481–92.
237. Ungar D, Oka T, Brittle EE, Vasile E, Lupashin VV, Chatterton JE, et al. Characterization of a mammalian Golgi-localized protein complex, COG, that is required for normal Golgi morphology and function. *J Cell Biol*. 2002 Apr 29;157(3):405–15.

238. Peanne R, Legrand D, Duvet S, Mir A-M, Matthijs G, Rohrer J, et al. Differential effects of lobe A and lobe B of the Conserved Oligomeric Golgi complex on the stability of  $\beta$ 1,4-galactosyltransferase 1 and  $\alpha$ 2,6-sialyltransferase 1. *Glycobiology*. 2011 Jul 1;21(7):864–76.
239. Witkos TM, Chan WL, Joensuu M, Rhiel M, Pallister E, Thomas-Oates J, et al. GORAB scaffolds COPI at the trans -Golgi for efficient enzyme recycling and correct protein glycosylation. *Nature Communications*. 2019 Jan 10;10(1):1–18.
240. Hennies HC, Kornak U, Zhang H, Egerer J, Zhang X, Seifert W, et al. Geroderma osteodysplastica is caused by mutations in SCYL1BP1, a Rab-6 interacting golgin. *Nat Genet*. 2008 Dec;40(12):1410–2.
241. Takeda R, Takagi M, Shinohara H, Futagawa H, Narumi S, Hasegawa T, et al. Novel compound heterozygous mutations identified by whole exome sequencing in a Japanese patient with geroderma osteodysplastica. *Eur J Med Genet*. 2017 Dec;60(12):635–8.
242. Chan WL, Steiner M, Witkos T, Egerer J, Busse B, Mizumoto S, et al. Impaired proteoglycan glycosylation, elevated TGF- $\beta$  signaling, and abnormal osteoblast differentiation as the basis for bone fragility in a mouse model for geroderma osteodysplastica. *PLoS Genet*. 2018 Mar;14(3):e1007242.
243. Lebretonchel E, Houdou M, Potelle S, de Bettignies G, Schulz C, Krzewinski Recchi M-A, et al. Dissection of TMEM165 function in Golgi glycosylation and its Mn<sup>2+</sup> sensitivity. *Biochimie*. 2019 Oct;165:123–30.
244. Foulquier F, Amyere M, Jaeken J, Zeevaert R, Schollen E, Race V, et al. TMEM165 deficiency causes a congenital disorder of glycosylation. *Am J Hum Genet*. 2012 Jul 13;91(1):15–26.

245. Potelle S, Morelle W, Dulary E, Duvet S, Vicogne D, Spriet C, et al. Glycosylation abnormalities in Gdt1p/TMEM165 deficient cells result from a defect in Golgi manganese homeostasis. *Hum Mol Genet.* 2016 Apr 15;25(8):1489–500.
246. Bammens R, Mehta N, Race V, Foulquier F, Jaeken J, Tiemeyer M, et al. Abnormal cartilage development and altered N-glycosylation in Tmem165-deficient zebrafish mirrors the phenotypes associated with TMEM165-CDG. *Glycobiology.* 2015 Jun;25(6):669–82.
247. Faden M, Al-Zahrani F, Arafah D, Alkuraya FS. Mutation of CANT1 causes Desbuquois dysplasia. *Am J Med Genet A.* 2010 May;152A(5):1157–60.
248. Laccone F, Schoner K, Krabichler B, Kluge B, Schwerdtfeger R, Schulze B, et al. Desbuquois dysplasia type I and fetal hydrops due to novel mutations in the CANT1 gene. *Eur J Hum Genet.* 2011 Nov;19(11):1133–7.
249. Menzies L, Cullup T, Calder A, Wilson L, Faravelli F. A novel homozygous variant in CANT1 in a patient with Kim-type Desbuquois dysplasia. *Clin Dysmorphol.* 2019 Oct;28(4):219–23.
250. Karakus E, Wannowius M, Müller SF, Leiting S, Leidolf R, Noppes S, et al. The orphan solute carrier SLC10A7 is a novel negative regulator of intracellular calcium signaling. *Sci Rep.* 2020 Apr 29;10(1):7248.
251. Ashikov A, Abu Bakar N, Wen X-Y, Niemeijer M, Rodrigues Pinto Osorio G, Brand-Arzamendi K, et al. Integrating glycomics and genomics uncovers SLC10A7 as essential factor for bone mineralization by regulating post-Golgi protein transport and glycosylation. *Hum Mol Genet.* 2018 Sep 1;27(17):3029–45.



252. Mizumoto S, Janecke AR, Sadeghpour A, Povysil G, McDonald MT, Unger S, et al. CSGALNACT1-congenital disorder of glycosylation: A mild skeletal dysplasia with advanced bone age. *Hum Mutat.* 2020 Mar;41(3):655–67.
253. Kubaski F, de Oliveira Poswar F, Michelin-Tirelli K, Burin MG, Rojas-Málaga D, Brusius-Facchin AC, et al. Diagnosis of Mucopolysaccharidoses. *Diagnostics (Basel).* 2020 Mar 22;10(3):172.
254. McKeehan WL, Sakagami Y, Hoshi H, McKeehan KA. Two apparent human endothelial cell growth factors from human hepatoma cells are tumor-associated proteinase inhibitors. *J Biol Chem.* 1986 Apr 25;261(12):5378–83.
255. Thøgersen IB, Enghild JJ. Biosynthesis of bikunin proteins in the human carcinoma cell line HepG2 and in primary human hepatocytes. Polypeptide assembly by glycosaminoglycan. *J Biol Chem.* 1995 Aug 4;270(31):18700–9.
256. Bost F, Diarra-Mehrpour M, Martin J-P. Inter- $\alpha$ -trypsin inhibitor proteoglycan family. *European Journal of Biochemistry.* 1998;252(3):339–46.
257. Enghild JJ, Thøgersen IB, Pizzo SV, Salvesen G. Analysis of inter-alpha-trypsin inhibitor and a novel trypsin inhibitor, pre-alpha-trypsin inhibitor, from human plasma. Polypeptide chain stoichiometry and assembly by glycan. *J Biol Chem.* 1989 Sep 25;264(27):15975–81.
258. Kaczmarczyk A, Thuveson M, Fries E. Intracellular coupling of the heavy chain of pre-alpha-inhibitor to chondroitin sulfate. *J Biol Chem.* 2002 Apr 19;277(16):13578–82.

259. Mizon C, Piva F, Queyrel V, Balduyck M, Hachulla E, Mizon J. Urinary bikunin determination provides insight into proteinase/proteinase inhibitor imbalance in patients with inflammatory diseases. *Clin Chem Lab Med*. 2002 Jun;40(6):579–86.
260. Pugia MJ, Jortani SA, Basu M, Sommer R, Kuo H-H, Murphy S, et al. Immunological evaluation of urinary trypsin inhibitors in blood and urine: Role of N- & O-linked glycoproteins. *Glycoconj J*. 2007 Jan 1;24(1):5–15.
261. Lapedda AJ, Nieddu G, Rocchiccioli S, Fresu P, De Muro P, Formato M. Development of a method for urine bikunin/urinary trypsin inhibitor (UTI) quantitation and structural characterization: Application to type 1 and type 2 diabetes. *Electrophoresis*. 2013 Dec;34(22–23):3227–33.
262. Lim Y-P, Bendelja K, Opal SM, Siryaporn E, Hixson DC, Palardy JE. Correlation between mortality and the levels of inter-alpha inhibitors in the plasma of patients with severe sepsis. *J Infect Dis*. 2003 Sep 15;188(6):919–26.
263. Hamm A, Veeck J, Bektas N, Wild PJ, Hartmann A, Heindrichs U, et al. Frequent expression loss of Inter-alpha-trypsin inhibitor heavy chain (ITIH) genes in multiple human solid tumors: a systematic expression analysis. *BMC Cancer*. 2008 Jan 28;8:25.
264. Diarra-Mehrpour M, Bourguignon J, Sesboué R, Mattei MG, Passage E, Salier JP, et al. Human plasma inter-alpha-trypsin inhibitor is encoded by four genes on three chromosomes. *Eur J Biochem*. 1989 Jan 15;179(1):147–54.
265. Kaumeyer JF, Polazzi JO, Kotick MP. The mRNA for a proteinase inhibitor related to the HI-30 domain of inter- $\alpha$ -trypsin inhibitor also encodes  $\alpha$ -1-microglobulin (protein HC). *Nucleic Acids Res*. 1986 Oct 1;14(20):7839–50.

266. Chan P, Salier JP. Mouse alpha-1-microglobulin/bikunin precursor: cDNA analysis, gene evolution and physical assignment of the gene next to the orosomucoid locus. *Biochim Biophys Acta*. 1993 Aug 19;1174(2):195–200.
267. Hanley S, McInerney JO, Powell R. Sequence analysis and evolutionary aspects of piscine alpha-1-microglobulin/bikunin mRNA transcripts. *Mol Marine Biol Biotechnol*. 1995 Jun;4(2):105–9.
268. Vetr H, Gebhard W. Structure of the human alpha 1-microglobulin-bikunin gene. *Biol Chem Hoppe-Seyler*. 1990 Dec;371(12):1185–96.
269. Rouet P, Raguenez G, Tronche F, Yaniv M, N’Guyen C, Salier JP. A potent enhancer made of clustered liver-specific elements in the transcription control sequences of human alpha 1-microglobulin/bikunin gene. *J Biol Chem*. 1992 Oct 15;267(29):20765–73.
270. Rouet P, Raguenez G, Tronche F, Mfou’ou V, Salier JP. Hierarchy and positive/negative interplays of the hepatocyte nuclear factors HNF-1, -3 and -4 in the liver-specific enhancer for the human alpha-1-microglobulin/bikunin precursor. *Nucleic Acids Res*. 1995 Feb 11;23(3):395–404.
271. Mizushima S, Nii A, Kato K, Uemura A. Gene expression of the two heavy chains and one light chain forming the inter-alpha-trypsin-inhibitor in human tissues. *Biol Pharm Bull*. 1998 Feb;21(2):167–9.
272. Itoh H, Tomita M, Kobayashi T, Uchino H, Maruyama H, Nawa Y. Expression of inter-alpha-trypsin inhibitor light chain (bikunin) in human pancreas. *J Biochem*. 1996 Aug;120(2):271–5.

273. Bourguignon J, Borghi H, Sesboüé R, Diarra-Mehrpour M, Bernaudin J-F, Josette M, et al. Immunohistochemical Distribution of Inter- $\alpha$ -trypsin Inhibitor Chains in Normal and Malignant Human Lung Tissue. *J Histochem Cytochem*. 1999 Dec 1;47(12):1625–32.
274. Chang-Yi C, Aragane Y, Maeda A, Yu-Lan P, Takahashi M, Lee-Hwa K, et al. Bikunin, a Serine Protease Inhibitor, is Present on the Cell Boundary of Epidermis. *Journal of Investigative Dermatology*. 1999 Aug 1;113(2):182–8.
275. Khan SR. Role of renal epithelial cells in the initiation of calcium oxalate stones. *Nephron Exp Nephrol*. 2004;98(2):e55-60.
276. Grewal JS, Tsai JY, Khan SR. Oxalate-inducible AMBP gene and its regulatory mechanism in renal tubular epithelial cells. *Biochem J*. 2005 May 1;387(Pt 3):609–16.
277. Salier JP, Simon D, Rouet P, Raguenez G, Muscatelli F, Gebhard W, et al. Homologous chromosomal locations of the four genes for inter-alpha-inhibitor and pre-alpha-inhibitor family in human and mouse: assignment of the ancestral gene for the lipocalin superfamily. *Genomics*. 1992 Sep;14(1):83–8.
278. Diarra-Mehrpour M, Bourguignon J, Sarafan N, Bost F, Sesboüé R, Muschio-Bonnet F, et al. Tandem orientation of the inter-alpha-trypsin inhibitor heavy chain H1 and H3 genes. *Biochim Biophys Acta*. 1994 Oct 18;1219(2):551–4.
279. Bost F, Bourguignon J, Martin JP, Sesboüé R, Thiberville L, Diarra-Mehrpour M. Isolation and characterization of the human inter-alpha-trypsin inhibitor heavy-chain H1 gene. *Eur J Biochem*. 1993 Dec 1;218(2):283–91.

280. Gebhard W, Schreitmüller T, Hochstrasser K, Wachter E. Complementary DNA and derived amino acid sequence of the precursor of one of the three protein components of the inter- $\alpha$ -trypsin inhibitor complex. *FEBS Letters*. 1988;229(1):63–7.
281. Zhuo L, Kimata K. Structure and function of inter-alpha-trypsin inhibitor heavy chains. *Connect Tissue Res*. 2008;49(5):311–20.
282. Salier JP, Diarra-Mehrpour M, Sesboue R, Bourguignon J, Benarous R, Ohkubo I, et al. Isolation and characterization of cDNAs encoding the heavy chain of human inter-alpha-trypsin inhibitor (I alpha TI): unambiguous evidence for multipolypeptide chain structure of I alpha TI. *Proc Natl Acad Sci USA*. 1987 Dec;84(23):8272–6.
283. Salier JP, Chan P, Raguenez G, Zwingman T, Erickson RP. Developmentally regulated transcription of the four liver-specific genes for inter-alpha-inhibitor family in mouse. *Biochem J*. 1993 Nov 15;296 ( Pt 1):85–91.
284. Daveau M, Rouet P, Scotte M, Faye L, Hiron M, Lebreton JP, et al. Human inter-alpha-inhibitor family in inflammation: simultaneous synthesis of positive and negative acute-phase proteins. *Biochem J*. 1993 Jun 1;292 ( Pt 2):485–92.
285. Bratt T, Olsson H, Sjöberg EM, Jergil B, Akerström B. Cleavage of the alpha 1-microglobulin-bikunin precursor is localized to the Golgi apparatus of rat liver cells. *Biochim Biophys Acta*. 1993 Jun 11;1157(2):147–54.
286. Toledo AG, Nilsson J, Noborn F, Sihlbom C, Larson G. Positive Mode LC-MS/MS Analysis of Chondroitin Sulfate Modified Glycopeptides Derived from Light and Heavy Chains of The Human Inter- $\alpha$ -Trypsin Inhibitor Complex. *Molecular & Cellular Proteomics : MCP*. 2015 Dec;14(12):3118.

287. Tyagi S, Salier J-P, Lal SK. The liver-specific human alpha(1)-microglobulin/bikunin precursor (AMBP) is capable of self-association. *Arch Biochem Biophys*. 2002 Mar 1;399(1):66–72.
288. Sjöberg EM, Fries E. Biosynthesis of bikunin (urinary trypsin inhibitor) in rat hepatocytes. *Arch Biochem Biophys*. 1992 Jun;295(2):217–22.
289. Bergwik J, Kristiansson A, Welinder C, Göransson O, Hansson SR, Gram M, et al. Knockout of the radical scavenger  $\alpha$ 1-microglobulin in mice results in defective bikunin synthesis, endoplasmic reticulum stress and increased body weight. *Free Radical Biology and Medicine* [Internet]. 2020 Feb 21 [cited 2020 Mar 9]; Available from: <http://www.sciencedirect.com/science/article/pii/S0891584919323512>
290. Yuki Y, Nakagawa T, Kato K. Amino acid sequences for human urinary bikunin (trypsin inhibitor) isomers. *Biol Pharm Bull*. 1995 Nov;18(11):1599–601.
291. Toyoda H, Ikei T, Demachi Y, Toida T, Imanari T. Structural analysis of the N-linked oligosaccharides from human urinary trypsin inhibitor. *Chem Pharm Bull*. 1992 Oct;40(10):2882–4.
292. Enghild JJ, Thøgersen IB, Cheng F, Fransson LA, Roepstorff P, Rahbek-Nielsen H. Organization of the inter-alpha-inhibitor heavy chains on the chondroitin sulfate originating from Ser(10) of bikunin: posttranslational modification of IalphaI-derived bikunin. *Biochemistry*. 1999 Sep 7;38(36):11804–13.
293. Xu Y, Carr PD, Guss JM, Ollis DL. The crystal structure of bikunin from the inter-alpha-inhibitor complex: a serine protease inhibitor with two Kunitz domains. *J Mol Biol*. 1998 Mar 13;276(5):955–66.

294. Atmani F, Mizon J, Khan SR. Inter-alpha-inhibitor: a protein family involved in the inhibition of calcium oxalate crystallization. *Scanning Microsc.* 1996;10(2):425–33; discussion 433-434.
295. Pönighaus C, Ambrosius M, Casanova JC, Prante C, Kuhn J, Esko JD, et al. Human Xylosyltransferase II Is Involved in the Biosynthesis of the Uniform Tetrasaccharide Linkage Region in Chondroitin Sulfate and Heparan Sulfate Proteoglycans. *J Biol Chem.* 2007 Feb 23;282(8):5201–6.
296. Casanova JC, Roch C, Kuhn J, Kleesiek K, Götting C. First in-gel detection and purification of human xylosyltransferase II. *Biochem Biophys Res Commun.* 2009 Feb 6;379(2):243–8.
297. Ouzzine M, Gulberti S, Netter P, Magdalou J, Fournel-Gigleux S. Structure/function of the human Galbeta1,3-glucuronosyltransferase. Dimerization and functional activity are mediated by two crucial cysteine residues. *J Biol Chem.* 2000 Sep 8;275(36):28254–60.
298. van Kuppevelt TH, Oosterhof A, Versteeg EMM, Podhumljak E, van de Westerlo EMA, Daamen WF. Sequencing of glycosaminoglycans with potential to interrogate sequence-specific interactions. *Sci Rep.* 2017 01;7(1):14785.
299. Chi L, Wolff JJ, Laremore TN, Restaino OF, Xie J, Schiraldi C, et al. Structural Analysis of Bikunin Glycosaminoglycan. *J Am Chem Soc.* 2008 Feb 27;130(8):2617–25.
300. Laremore TN, Leach FE, Amster IJ, Linhardt RJ. Electrospray ionization Fourier transform mass spectrometric analysis of intact bikunin glycosaminoglycan from normal human plasma. *Int J Mass Spectrom.* 2011 Aug 15;305(2–3):109–15.

301. Mizon C, Mairie C, Balduyck M, Hachulla E, Mizon J. The chondroitin sulfate chain of bikunin-containing proteins in the inter-alpha-inhibitor family increases in size in inflammatory diseases. *Eur J Biochem.* 2001 May;268(9):2717–24.
302. Nilsson J, Noborn F, Gomez Toledo A, Nasir W, Sihlbom C, Larson G. Characterization of Glycan Structures of Chondroitin Sulfate-Glycopeptides Facilitated by Sodium Ion-Pairing and Positive Mode LC-MS/MS. *J Am Soc Mass Spectrom.* 2017;28(2):229–41.
303. Yamada S, Oyama M, Kinugasa H, Nakagawa T, Kawasaki T, Nagasawa S, et al. The sulphated carbohydrate-protein linkage region isolated from chondroitin 4-sulphate chains of inter-alpha-trypsin inhibitor in human plasma. *Glycobiology.* 1995 May;5(3):335–41.
304. Yamada S, Oyama M, Yuki Y, Kato K, Sugahara K. The Uniform Galactose 4-Sulfate Structure in the Carbohydrate-Protein Linkage Region of Human Urinary Trypsin Inhibitor. *European Journal of Biochemistry.* 1995;233(2):687–93.
305. Sugumaran G, Silbert JE. Relationship of sulfation to ongoing chondroitin polymerization during biosynthesis of chondroitin 4-sulfate by microsomal preparations from cultured mouse mastocytoma cells. *J Biol Chem.* 1990 Oct 25;265(30):18284–8.
306. Toyoda H, Kobayashi S, Sakamoto S, Toida T, Imanari T. Structural analysis of a low-sulfated chondroitin sulfate chain in human urinary trypsin inhibitor. *Biol Pharm Bull.* 1993 Sep;16(9):945–7.
307. Ly M, Leach FE, Laremore TN, Toida T, Amster IJ, Linhardt RJ. The proteoglycan bikunin has a defined sequence. *Nat Chem Biol.* 2011 Oct 9;7(11):827–33.



308. Bourguignon J, Diarra-Mehrpour M, Thiberville L, Bost F, Sesboüé R, Martin JP. Human pre-alpha-trypsin inhibitor-precursor heavy chain. cDNA and deduced amino-acid sequence. *Eur J Biochem.* 1993 Mar 15;212(3):771–6.
309. Thuveson M, Fries E. Intracellular proteolytic processing of the heavy chain of rat pre-alpha-inhibitor. The COOH-terminal propeptide is required for coupling to bikunin. *J Biol Chem.* 1999 Mar 5;274(10):6741–6.
310. Olsen EH, Rahbek-Nielsen H, Thøgersen IB, Roepstorff P, Enghild JJ. Posttranslational modifications of human inter-alpha-inhibitor: identification of glycans and disulfide bridges in heavy chains 1 and 2. *Biochemistry.* 1998 Jan 6;37(1):408–16.
311. Flahaut C, Capon C, Balduyck M, Ricart G, Sautiere P, Mizon J. Glycosylation pattern of human inter-alpha-inhibitor heavy chains. *Biochem J.* 1998 Aug 1;333 ( Pt 3):749–56.
312. Flahaut C, Mizon C, Aumercier-Maes P, Colson P, Bailly C, Sautiere P, et al. Disulphide bonds assignment in the inter-alpha-inhibitor heavy chains--structural and functional implications. *Eur J Biochem.* 1998 Jul 1;255(1):107–15.
313. Thuveson M, Fries E. The low pH in trans-Golgi triggers autocatalytic cleavage of pre-alpha-inhibitor heavy chain precursor. *J Biol Chem.* 2000 Oct 6;275(40):30996–1000.
314. Enghild JJ, Salvesen G, Hefta SA, Thøgersen IB, Rutherford S, Pizzo SV. Chondroitin 4-sulfate covalently cross-links the chains of the human blood protein pre-alpha-inhibitor. *J Biol Chem.* 1991 Jan 15;266(2):747–51.

315. Morelle W, Capon C, Balduyck M, Sautiere P, Kouach M, Michalski C, et al. Chondroitin sulphate covalently cross-links the three polypeptide chains of inter- $\alpha$ -trypsin inhibitor. *European Journal of Biochemistry*. 1994;221(2):881–8.
316. Fries E, Kaczmarczyk A. Inter-alpha-inhibitor, hyaluronan and inflammation. *Acta Biochim Pol*. 2003;50(3):735–42.
317. Zhao M, Yoneda M, Ohashi Y, Kurono S, Iwata H, Ohnuki Y, et al. Evidence for the Covalent Binding of SHAP, Heavy Chains of Inter- $\alpha$ -Trypsin Inhibitor, to Hyaluronan. *J Biol Chem*. 1995 Nov 3;270(44):26657–63.
318. Lepadda AJ, De Muro P, Capobianco G, Formato M. Role of the small proteoglycan bikunin in human reproduction. *Hormones (Athens)*. 2019 Nov 14;
319. Fülöp C, Szántó S, Mukhopadhyay D, Bárdos T, Kamath RV, Rugg MS, et al. Impaired cumulus mucification and female sterility in tumor necrosis factor-induced protein-6 deficient mice. *Development*. 2003 May;130(10):2253–61.
320. Rugg MS, Willis AC, Mukhopadhyay D, Hascall VC, Fries E, Fülöp C, et al. Characterization of Complexes Formed between TSG-6 and Inter- $\alpha$ -inhibitor That Act as Intermediates in the Covalent Transfer of Heavy Chains onto Hyaluronan. *J Biol Chem*. 2005 Jul 8;280(27):25674–86.
321. Briggs DC, Langford-Smith AWW, Birchenough HL, Jowitt TA, Kielty CM, Enghild JJ, et al. Inter- $\alpha$ -inhibitor heavy chain-1 has an integrin-like 3D structure mediating immune regulatory activities and matrix stabilization during ovulation. *J Biol Chem*. 2020 Mar 6;

322. Milner CM, Tongsoongnoen W, Rugg MS, Day AJ. The molecular basis of inter-alpha-inhibitor heavy chain transfer on to hyaluronan. *Biochem Soc Trans.* 2007 Aug;35(Pt 4):672–6.
323. Sanggaard KW, Karring H, Valnickova Z, Thøgersen IB, Enghild JJ. The TSG-6 and I alpha I interaction promotes a transesterification cleaving the protein-glycosaminoglycan-protein (PGP) cross-link. *J Biol Chem.* 2005 Mar 25;280(12):11936–42.
324. Yingsung W, Zhuo L, Morgelin M, Yoneda M, Kida D, Watanabe H, et al. Molecular heterogeneity of the SHAP-hyaluronan complex. Isolation and characterization of the complex in synovial fluid from patients with rheumatoid arthritis. *J Biol Chem.* 2003 Aug 29;278(35):32710–8.
325. McDonald B, McAvoy EF, Lam F, Gill V, de la Motte C, Savani RC, et al. Interaction of CD44 and hyaluronan is the dominant mechanism for neutrophil sequestration in inflamed liver sinusoids. *J Exp Med.* 2008 Apr 14;205(4):915–27.
326. Wisniewski HG, Hua JC, Poppers DM, Naime D, Vilcek J, Cronstein BN. TNF/IL-1-inducible protein TSG-6 potentiates plasmin inhibition by inter-alpha-inhibitor and exerts a strong anti-inflammatory effect in vivo. *J Immunol.* 1996 Feb 15;156(4):1609–15.
327. Adair JE, Stober V, Sobhany M, Zhuo L, Roberts JD, Negishi M, et al. Inter- $\alpha$ -trypsin Inhibitor Promotes Bronchial Epithelial Repair after Injury through Vitronectin Binding. *J Biol Chem.* 2009 Jun 19;284(25):16922–30.

328. Okroj M, Holmquist E, Sjölander J, Corrales L, Saxne T, Wisniewski H-G, et al. Heavy chains of inter alpha inhibitor ( $I\alpha I$ ) inhibit the human complement system at early stages of the cascade. *J Biol Chem*. 2012 Jun 8;287(24):20100–10.
329. Candiano G, Bruschi M, Musante L, Santucci L, Ghiggeri GM, Carnemolla B, et al. Blue silver: a very sensitive colloidal Coomassie G-250 staining for proteome analysis. *Electrophoresis*. 2004 May;25(9):1327–33.
330. Lim MD. Dried Blood Spots for Global Health Diagnostics and Surveillance: Opportunities and Challenges. *Am J Trop Med Hyg*. 2018 Aug;99(2):256–65.
331. Sharma A, Jaiswal S, Shukla M, Lal J. Dried blood spots: concepts, present status, and future perspectives in bioanalysis. *Drug Test Anal*. 2014 May;6(5):399–414.
332. Reeder BJ, Wilson MT. Hemoglobin and myoglobin associated oxidative stress: from molecular mechanisms to disease States. *Curr Med Chem*. 2005;12(23):2741–51.
333. Marquardt T, Bzduch V, Högbe M, Rust S, Reunert J, Grüneberg M, et al. SLC37A4-CDG: Mislocalization of the glucose-6-phosphate transporter to the Golgi causes a new congenital disorder of glycosylation. *Mol Genet Metab Rep* [Internet]. 2020 Aug 21 [cited 2021 Apr 26];25. Available from: <https://www.ncbi.nlm.nih.gov/pmc/articles/PMC7451446/>
334. Wilson MP, Quelhas D, Leão-Teles E, Sturiale L, Rymen D, Keldermans L, et al. SLC37A4-CDG: Second patient. *JIMD Rep*. 2021 Mar;58(1):122–8.
335. Ng BG, Sosicka P, Fenaille F, Harroche A, Vuillaumier-Barrot S, Porterfield M, et al. A mutation in SLC37A4 causes a dominantly inherited congenital disorder of glycosylation characterized by liver dysfunction. *Am J Hum Genet*. 2021 Jun 3;108(6):1040–52.

336. Hanada H, Moriyama Y, Maeda M, Futai M. Kinetic studies of chromaffin granule H<sup>+</sup>-ATPase and effects of bafilomycin A1. *Biochem Biophys Res Commun.* 1990 Jul 31;170(2):873–8.
337. Moriyama Y, Nelson N. H<sup>+</sup>-translocating ATPase in Golgi apparatus. Characterization as vacuolar H<sup>+</sup>-ATPase and its subunit structures. *J Biol Chem.* 1989 Nov 5;264(31):18445–50.
338. Palokangas H, Ying M, Väänänen K, Saraste J. Retrograde transport from the pre-Golgi intermediate compartment and the Golgi complex is affected by the vacuolar H<sup>+</sup>-ATPase inhibitor bafilomycin A1. *Mol Biol Cell.* 1998 Dec;9(12):3561–78.
339. Axelsson MAB, Karlsson NG, Steel DM, Ouwendijk J, Nilsson T, Hansson GC. Neutralization of pH in the Golgi apparatus causes redistribution of glycosyltransferases and changes in the O-glycosylation of mucins. *Glycobiology.* 2001 Aug 1;11(8):633–44.
340. Moreno RD, Ramalho-Santos J, Chan EKL, Wessel GM, Schatten G. The Golgi Apparatus Segregates from the Lysosomal/Acrosomal Vesicle during Rhesus Spermiogenesis: Structural Alterations. *Developmental Biology.* 2000 Mar 15;219(2):334–49.
341. Sasaki K, Komori R, Taniguchi M, Shimaoka A, Midori S, Yamamoto M, et al. PGSE Is a Novel Enhancer Regulating the Proteoglycan Pathway of the Mammalian Golgi Stress Response. *Cell Struct Funct.* 2019 Jan 11;44(1):1–19.
342. Potelle S, Dulary E, Duvet S, Morelle W, Vicogne D, Spriet C, et al. Manganese-induced trafficking and turnover of TMEM165. *Biochem J.* 2017 Apr 19;474(9):1481–93.

# Material & Methods



## Mass spectrometry analyses

### Gel collection procedure

10  $\mu\text{L}$  of each serum from healthy individuals was treated with 5 $\mu\text{L}$  of Chondroitinase ABC (chABC) 5 U from *Proteus vulgaris* (Sigma-Aldrich) (reconstituted in 300 $\mu\text{L}$  BSA 0.01 %) in 20  $\mu\text{L}$  of sodium acetate buffer pH 7.9. The final 35 $\mu\text{L}$  solution was incubated overnight at 37°C under stirring and stored at -20°C. After rapid centrifugation, each digested sample was mixed with rehydration sample buffer (pH 4-7) in a final volume of 155  $\mu\text{L}$ . For patient, 10  $\mu\text{L}$  of serum was directly mixed with rehydration buffer. After 2-DE, second dimension gels were fixed for 1 h in a fixation solvent (30% ETOH / 7% acetic acid / 63 % H<sub>2</sub>O) and stained for 24 – 48 h under gentle shaking with colloidal G-250 Blue Silver dye consisting of 0.12% G-250 dye, 10% ammonium sulfate, 10% phosphoric acid, and 20% methanol. Stained gels were washed 48 – 72 h in regularly changed deionized water baths under gentle shaking. Gel pieces of interest were carefully removed from the whole gel and stored at -20°C in 1% acetic acid aqueous solution.

### Protein In-Gel Digestion

Gel pieces were washed with a succession of ammonium bicarbonate (NH<sub>4</sub>HCO<sub>3</sub>) and acetonitrile baths to eliminate dye residues. A reduction/alkylation step was performed using dithiothreitol (DTT) 10 mM and iodoacetamide 55 mM. Gel pieces were then rehydrated at 4°C in 12 ng/ $\mu\text{L}$  sequencing grade modified trypsin (Promega, France) solubilized in 25 mM NH<sub>4</sub>HCO<sub>3</sub> during 1 h and then digested at 37°C overnight. After tryptic digestion, peptides were extracted by incubating gel pieces in extraction solvent (70% ACN / 30% H<sub>2</sub>O / 0.5 % AF).



## Liquid Chromatography - Tandem Mass Spectrometry (LC-MS/MS)

Samples were analyzed on an Acquity UPLC M-Class coupled with a high-resolution mass spectrometer Xevo® G2-XS QToF (Waters™) run by Masslynx 4.1 Software. The ionization interface consisted of a nanoelectrospray used in positive polarity mode. For the sample's analysis, 2 to 4  $\mu\text{L}$  of protein digest were loaded onto a C18 trap column (Waters™) (NanoE MZ Sym C18 – 5  $\mu\text{m}$  – 180  $\mu\text{m}$  x 20 mm), at 20  $\mu\text{L min}^{-1}$  and desalted with 0.1% (v/v) formic acid and 5% (v/v) Acetonitrile. After 4 min, the precolumn was connected to a C18 nanocolumn (nanoEASE™ M/Z HSS C18 T3 – 100  $\text{Å}$  – 1.8  $\mu\text{m}$  1/PK – 75  $\mu\text{m}$  x 100 mm Column - Waters™).

Electrospray ionization (ESI) was performed at 2.5 kV, with a source temperature of 120°C, a desolvation temperature of 250°C, and a cone gas flow at 80L/Hr. Buffers were 0.1% formic acid in 100 % Water (A) and 0.1% formic acid in 100% ACN (B). Peptides were separated using a linear gradient from 5% to 95% buffer B for 80 min at 300  $\text{nL min}^{-1}$ . One run took 90 min, including the regeneration step at 95% buffer B and the equilibration step at 95% buffer A.

Two analyses were performed for each sample: one in data independent acquisition mode ( $\text{MS}^{\circ}$ ). The other was a MS/MS run designed to acquire fragmentation data for specified m/z ions, using positive / sensitivity mode, a scan time of 0.5 seconds, a cone voltage override of 40 V and a collision energy ramp from 18 to 40 V.

## **Mass spectrum and data processing parameters**

Mass spectrometric data were investigated with Progenesis QI for proteomic and Masslynx 4.1.

The Human and AMBP protein databanks used for identification in Progenesis originated from Uniprot KB/SwissProt. They were concatenated with a cRAP (common Repository of Adventitious Proteins) to acknowledge possible contaminants. Parameters used for the processing included: missed cleavage (1), fixed modification (Carbamidomethyl [C] – 57.0215), variable modifications (Oxydation [M] – 15.9949), FDR (4%) and ion matching requirements (3/7/1).

For Masslynx 4.1, the MS/MS data collected for the m/z of interest were screened manually, searching for correlated chromatographic data, MS spectrum and fragmentation profiles, to assess the presence of a possible peptide and his modified linker.

## **2-DE analysis of chondroitinase treated serum samples**

5  $\mu$ L of crude serum samples were incubated in a solution containing 2.5  $\mu$ L of chABC (5U) and 20  $\mu$ L of acetate buffer pH 7.9 overnight at 37 °C under stirring. The next day, chABC-treated samples were mixed with 125  $\mu$ L of rehydration buffer pH 4-7. Samples were introduced into ZOOM IPG runner cassettes (ThermoFisher) for overnight rehydration of ZOOM strip pH 4-7 (ThermoFisher). Isoelectric focusing program was performed using BioRad Power Pac as follows: S1 100V 1h; S2  $\rightarrow$  2000V 1h30; S3 2000V 1h45. ZOOM strips were then incubated for 10 min in a solution containing NuPAGE LDS sample buffer 1X and sample reducing agent 10X (9v/1v) then 10 min in NuPAGE LDS sample buffer containing 2% iodoacetamide. Second dimension was performed using 4% - 12% Nu-PAGE bis-tris gel (ThermoFisher). Separated proteins were transferred (90minutes, 100 V) to nitrocellulose sheets. After incubation in

blocking solution (PBS/milk 10%) overnight, anti-Bkn immunoblotting was performed as described above (see Materiel & Methods in Haouari et al 2020, JIMD).

## **Hemoglobin depletion from dried blood spots for Bkn analysis**

### **(Manufacturer protocol)**

1. Extraction of dried protein from the card. Punch out the dried blood section from the card into a microfuge tube. Add 400  $\mu$ l PEB buffer. Shake for 30 minutes at room temperature. Centrifuge at 5000 rpm for 4 minutes. This is the Sample used for Step #5.

2. Weigh out 50 mg of HemoVoid™ matrix into the supplied SpinX filter.

3. Add 400  $\mu$ l of Binding Buffer HVBB to the SpinX filter. Vortex or mix well for 5 minutes at room temperature followed by centrifugation at 3000 rpm. Discard the supernatant.

4. Repeat step 3.

5. Add 200  $\mu$ l of Binding Buffer HVBB to the SpinX filter. Add 300  $\mu$ l of the Sample prepared in step 1 to the same SpinX filter. Vortex for 10 min and then centrifuge for 2 minutes at 5000 rpm.

6. Discard the hemoglobin containing filtrate.

7. To the pellet, add 500  $\mu$ l of Wash Buffer HVWB. Vortex or mix well for 5 min and centrifuge for 2 minutes at 5000 rpm. Discard the filtrate.

8. Repeat Step 7, twice.

9. To the pellet, add 200  $\mu$ l of Elution Buffer HVEB. Vortex or mix well for 10 min and centrifuge for 2 minutes at 5000 rpm. Analyze the hemoglobin depleted eluate proteome

For Western blot, crude hemoglobin-depleted samples were analyzed as serum samples (Material and methods in Haouari et al 2020, JIMD).

## **Bkn analyses in HepG2**

### **Cell culture and treatments**

HepG2 were incubated in 6 well plates with or without coverslips 18 mm and containing, per well, 2 mL of Dulbecco's Modified Eagle Medium (DMEM - from Thermo Fisher) + 10% fetal bovine serum (FBS) supplemented with 100 UI/mL penicillin and 0,23 µg/ml de streptomycin and incubated at 37°C with 5% CO<sub>2</sub>. Until 75% confluence, cells were briefly washed with PBS and the DMEM 10% FBS was replaced by OPTIMEM FBS free containing the desired drug concentration (BafA1 was purchased from Merck, MnCl<sub>2</sub> from Sigma and Brefeldin A from Sigma). For lysotracker-related experiments, LysoTracker Red DND-99 (Molecular probes) was added in the cell culture medium for 30 min incubation upon classical cell culture condition.

### **Western blot analysis**

For coverslip-free wells, supernatants were collected at the end of treatments in Eppendorf tubes. Cells were washed with PBS and lysates were obtained by treating cells with hot (100°C) lysis buffer (Tris pH 6,8, SDS, glycerol, HCl) for 10 min before scraping, collection in Eppendorf tubes, and ultrasonic homogenization. 40µL of crude supernatant and 1/10<sup>th</sup> diluted lysate were treated with NuPAGE LDS sample buffer (1X) + sample reducing agent (1X) (ThermoFisher) and heated at 100°C for 10 minutes. Polyacrylamide gel electrophoresis, with 50 µg of treated sample loaded per well, was conducted using Nu-PAGE 4% to 12% bis-Tris gels (ThermoFisher), as recommended by the manufacturer. After transfer to nitrocellulose (70 minutes, 100 V), antibody incubations were performed for 90 min in TTBS-5% milk with the

corresponding dilutions: rabbit anti-bikunin (Merck-Millipore) 1/5000; rabbit anti-alpha-1microglobulin (Siemens) 1/5000; rabbit anti-transferrin 1/5000 (Thermo Fisher); rabbit anti-orosomuroid (Sigma) 1/5000. HRP-linked anti-rabbit secondary antibodies (Cell Signaling Technologies) were used (1/5000 in TTBS-5% milk for 60 min). ECL revelation was conducted using Clarity Western ECL Substrate (ThermoFisher) and HyperFilm (GE).

### **Immunofluorescence**

For coverslip-containing wells, cells were fixed and permeabilized with methanol (1mL) for 5min at -20°C. After 3 x 5 min PBS washes at room temperature, cells were incubated for 90 min at 37 °C with primary antibodies at the corresponding dilutions in PBS 1%BSA: rabbit anti-Bikunin (CP6) polyclonal antibody (Merck-Millipore) 1/1000; mouse anti-GM130 (BD Biosciences) 1/500; rabbit anti-albumin (Sigma) 1/1000; rabbit anti-orosomuroid (Sigma) 1/1000. After 3 x 5 min PBS washes at room temperature, incubation with secondary antibodies were performed for 60 min at 37°C with the corresponding dilutions: Goat anti-mouse 488 (Molecular probes) 1/500; Goat anti-rabbit 555 and 488 (Molecular probes) 1/1000. After 3 x 5 min PBS washes, coverslips were mounted onto StarFrost microscope slides (Knittel GLASS) with a drop of mounting medium (Prolong Gold antifade reagent +/- Dapi Invitrogen). Observations were performed with fluorescent microscope (Leica) and Clara Vision camera (Scion Corporation). Data acquisition and image treatments were performed with Imager 5.3 and ImageJ63 software's.

*Résumé en français*



Les protéoglycanes constituent une famille de macromolécules composées de protéines liées à des chaînes polysaccharidiques sulfatées appelées glycosaminoglycanes (GAG). Il existe plusieurs types de chaînes GAG : chondroïtine sulfate (CS), héparane sulfate (HS), dermatane sulfate (DS) et kératane sulfate (KS). La biosynthèse des protéoglycanes est un processus métabolique complexe ayant lieu dans plusieurs types cellulaires, essentiellement dans l'appareil de Golgi, et faisant intervenir de nombreux acteurs moléculaires. Des glycosyltransférases catalysent le transfert de résidus monosaccharidiques sur les protéines et sur la chaîne GAG tandis que des sulfotransférases catalysent l'ajout de groupement sulfates. Des transporteurs de sucres et de sulfate sont présents à la membrane de l'appareil de Golgi et permettent l'entrée de ces substrats, tandis que des protéines régulatrices de l'homéostasie golgienne (pompes à proton, canaux ioniques) assurent un environnement adéquat pour les réactions de biosynthèse. Enfin, des protéines régulant le trafic vésiculaire permettent la localisation correcte des acteurs moléculaires et des substrats pour la biosynthèse des protéoglycanes.

Selon leur nature, les protéoglycanes peuvent être adressés vers les membranes plasmiques des cellules, les matrices extracellulaires, ou la circulation sanguine. Concernant leurs rôles physiologiques, ils participent à l'architecture des matrices extracellulaires et confèrent, entre autres, les propriétés lubrifiantes du liquide synovial articulaire, la rigidité du cartilage et l'élasticité de la peau. De plus, en interagissant avec de nombreux facteurs de croissance et cytokines, les protéoglycanes sont impliqués dans le développement osseux, la réponse inflammatoire et la prolifération cellulaire.

La genèse de ce travail résulte de notre collaboration avec les cliniciens de l'hôpital Necker (Paris - France) qui prennent en charge des patients atteints de maladies génétiques dues à des altérations de la biosynthèse des protéoglycanes. Ces maladies métaboliques héréditaires



appelées PG-IMD (proteoglycan inherited metabolic diseases) sont dues à des mutations sur les gènes codant pour des protéines impliquées dans l'élongation des GAG comme les glycosyl/sulfotransférases et les transporteurs de sucres/sulfates, ou pour des protéines régulant l'homéostasie de l'appareil de Golgi, comme les canaux ioniques et les régulateurs du trafic vésiculaire.

Les manifestations cliniques des PG-IMD comprennent de graves troubles ostéoarticulaires qui peuvent être associés à des pathologies multiples telles que des désordres neurologiques, des anomalies cardiaques et des affections cutanées. En raison de cette symptomatologie peu spécifique, il est difficile d'établir un diagnostic pour ces syndromes. De plus, le dépistage biologique manque de biomarqueurs pratiques et repose sur des tests de laboratoire difficilement accessibles comme la quantification de GAG dans les fibroblastes cutanés de patients. Par ailleurs, les analyses par séquençage d'ADN peuvent retrouver des mutations sur des gènes impliqués dans la synthèse des protéoglycanes sans permettre d'affirmer formellement leur causalité.

Dans ce contexte, nous nous sommes intéressés au développement d'un test biochimique basé sur l'analyse de la bikunine, un protéoglycane de type CS synthétisé par le foie et sécrété dans la circulation sanguine. Ce protéoglycane original se présente sous quatre isoformes sériques : deux formes légères correspondant à la bikunine libre et à la bikunine liée à une chaîne CS (Bkn-CS), et deux formes lourdes appelées ITI et PaI correspondant à la Bkn-CS liée, respectivement, à une ou deux glycoprotéines appelées « heavy chains » (HC).

Nous avons évalué le potentiel de la bikunine en tant que biomarqueur des PG-IMD en analysant son profil par Western blot, électrophorèse bidimensionnelle et spectrométrie de masse à partir de sérum de patients atteints en comparaison à des individus sains. Les analyses ont montré des anomalies quantitatives et qualitatives des isoformes la bikunine chez plusieurs

patients et ont mis en évidence des profils « signatures » permettant d'orienter précisément le diagnostic de certains PG-IMD.

Par ailleurs, en analysant la bikunine chez des patients atteints de désordres congénitaux de la glycosylation (CDG) avec altération de l'homéostasie golgienne, nous avons mis en évidence des profils anormaux notamment pour les formes lourdes ITI et PaI de la bikunine. Bien que le diagnostic des CDG bénéficie actuellement de techniques de dépistage relativement performantes, l'analyse du profil de la bikunine a permis d'enrichir la compréhension de la physiopathologie de certains CDG avec troubles de l'homéostasie golgienne.

Enfin, nous avons analysé les profils de la bikunine dans un modèle de lignée cellulaire issue de carcinome hépatique (cellules HepG2) présentant des altérations de l'homéostasie golgienne. En perturbant le pH et les équilibres ioniques dans l'appareil de Golgi, nous avons montré des altérations significative de la biosynthèse de la bikunine. Ces résultats ont montré que la bikunine peut être un marqueur in vitro pour l'analyse des troubles de l'homéostasie golgienne.

Les résultats de nos travaux ont fait l'objet de quatre publications qui sont présentées dans ce manuscrit : une lettre à l'éditeur publiée dans *Clinica Chimica Acta*, un article de recherche publié dans *Journal of Inherited Metabolic Disease*, un article de recherche publié dans *Clinica Chimica Acta* et une revue publiée dans *Genes*. Ces articles sont complétés par d'autres résultats non-encore publiés.

En conclusion ce travail a permis de mettre en évidence l'utilité de l'analyse de la bikunine dans le dépistage de troubles innés de la synthèse des protéoglycanes avec d'éventuels profils « signature » pour certaines maladies. Par ailleurs, il a montré le potentiel de la bikunine comme biomarqueur de seconde intention dans le cadre du dépistage de certains CDG avec troubles de

l'homéostasie golgienne. Enfin, la bikunine pourrait potentiellement être utilisée comme marqueur de stress golgien dans des cellules hépatiques en culture.

Ce travail a également ouvert des perspectives intéressantes. Les profils de la bikunine seront étudiés dans le cadre de maladies acquises pour lesquels des troubles de la glycosylation et de synthèse des protéoglycanes ont été observés (cancers, maladies hépatiques, diabète). L'analyse de la bikunine pourrait permettre de suivre leur évolution ainsi que la réponse à leurs traitements. Dans un contexte préclinique voir fondamental, l'analyse de la bikunine pourrait être appliquée à des modèles cellulaires et/ou animaux mimant des situations pathologiques innées (PG-IMD, CDG) et/ou acquises (cancers, maladies hépatiques). Les profils de la bikunine pourraient permettre de mettre en évidence des troubles de la glycosylation, de la synthèse des protéoglycanes et de l'homéostasie de l'appareil de Golgi dans ces situations et ainsi enrichir la compréhension de leur physiopathologie.

**Titre :** La bikunine : un biomarqueur des troubles innés de la synthèse des protéoglycanes et de l'homéostasie de l'appareil de Golgi

**Mots clés :** Bikunine, Protéoglycanes, Glycosaminoglycanes, Homéostasie Golgienne, Glycosylation

**Résumé :**

Les protéoglycanes (PG) sont des macromolécules composées de protéines liées à des chaînes polysaccharidiques appelées glycosaminoglycanes. Leur synthèse intracellulaire a lieu essentiellement dans l'appareil de Golgi et met en jeu un réseau complexe d'enzymes, de transporteurs, de canaux ioniques et de protéines liées au trafic vésiculaire. Ce "protéoglycanome" assure la synthèse de divers types de PG jouant des rôles fondamentaux chez l'homme, comme en témoignent les conséquences pathologiques des troubles innés de la biosynthèse des PG. Ces maladies héréditaires rares (PG-IMD) se manifestent par des malformations ostéoarticulaires associées à des pathologies multiples. Leur diagnostic est difficile en raison d'une clinique peu spécifique et d'un dépistage biologique nécessitant des techniques assez laborieuses

Nous avons développé un test biochimique basé sur l'analyse de la bikunine, un PG circulant synthétisé par le foie. Grâce à des techniques relativement simples et rapides, nous avons montré chez certains patients des profils « signatures » permettant de suspecter le déficit génétique causant la maladie et ainsi orienter le diagnostic. De plus, nous avons découvert que la bikunine pouvait être un biomarqueur additionnel pour le dépistage des désordres congénitaux de la glycosylation (CDG) avec troubles de l'homéostasie Golgienne, un autre groupe de maladies génétiques rares altérant la *N*- et la *O*-glycosylation des protéines. Enfin, nous avons analysé la bikunine dans des cellules hépatiques en culture et avons montré son potentiel en tant que marqueur *in vitro* de troubles de l'homéostasie Golgienne.

**Title :** Serum bikunin: a biomarker of inborn errors of proteoglycan biosynthesis and Golgi homeostasis

**Keywords :** Bikunin, Proteoglycans, Glycosaminoglycans, Golgi homeostasis, Glycosylation

**Abstract :**

Proteoglycans (PG) are a family of macromolecules consisting of proteins linked to polysaccharidic chains called glycosaminoglycans. Their intracellular synthesis takes place mainly in the Golgi apparatus and involves a complex network of enzymes, transporters, ion channels and vesicular trafficking-related proteins. This "proteoglycanome" ensures the synthesis of various types of PG which play fundamental roles in humans, as evidenced by the pathological consequences of inborn errors of PG biosynthesis (PG-IMD). These rare inherited diseases manifest by osteoarticular malformations associated to multiple pathologies. Their diagnosis is difficult due to unspecific symptomatology and a biological screening requiring rather laborious techniques

We developed a biochemical test based on the analysis of bikunin, a circulating PG synthesized by the liver. Using rather convenient techniques, we found "signature" profiles in some patients allowing to suspect the causative genetic deficiency and thereby to orient the diagnosis. Furthermore, we found that bikunin could be an additional biomarker for the screening of congenital disorders of glycosylation (CDG) with Golgi homeostasis defects, another group of rare genetic diseases altering *N*- and *O*-glycosylation of proteins. Lastly, we analyzed bikunin in cultured hepatic cell lines and showed its potential as an *in vitro* marker of Golgi homeostasis defects.